INFORMATION TO USERS

This manuscript has been reproduced from the microfilm master. UMI films the text directly from the original or copy submitted. Thus, some thesis and dissertation copies are in typewriter face, while others may be from any type of computer printer.

The quality of this reproduction is dependent upon the quality of the copy submitted. Broken or indistinct print, colored or poor quality illustrations and photographs, print bleedthrough, substandard margins, and improper alignment can adversely affect reproduction.

In the unlikely event that the author did not send UMI a complete manuscript and there are missing pages, these will be noted. Also, if unauthorized copyright material had to be removed, a note will indicate the deletion.

Oversize materials (e.g., maps, drawings, charts) are reproduced by sectioning the original, beginning at the upper left-hand corner and continuing from left to right in equal sections with small overlaps.

Photographs included in the original manuscript have been reproduced xerographically in this copy. Higher quality 6" x 9" black and white photographic prints are available for any photographs or illustrations appearing in this copy for an additional charge. Contact UMI directly to order.

Bell & Howell Information and Learning
300 North Zeeb Road, Ann Arbor, MI 48106-1346 USA
800-521-0600

Université d'Ottawa · University of Ottawa

Was man an der Natur Geheimnisvolles pries,
Das wagen wir verständig zu probieren,
Und was sie sonst organisieren ließ,
Das lassen wir kristallisieren.

J.W.V. Goethe
Gesammelte Werke
Band 4 - Faust: Eine Tragödie
Der Tragödie Zweiter Teil
Zweiter Akt: Laboratorium

Gewidmet an Oma Wanda,

Mami, Papi,

Samira, Layla und Karim

Aziz,

Myriam und Tarik.

Abstract

This thesis has been divided into four major sections. The first section deals with the reactions of CrR_4 (R is neopentyl or trimethylsilylmethyl) with the surfaces of partially dehydroxylated silicas, leading to the formation of discrete mononuclear surface organometallic fragments. The reaction stoichiometry was found to depend on the density of surface hydroxyl groups. On silica subjected to prior dehydroxylation at 500°C, one Cr is grafted per hydroxyl group and one equiv. of alkane is evolved, leaving $\equiv SiOCrR_3$ on the surface. On silica dehydroxylated at 200°C, each Cr is grafted onto two hydroxyl groups and two equiv. of alkane are evolved, giving $(\equiv SiO)_2CrR_2$. When CrR_4 reacts with deuterated hydroxyl groups, monodeuteroalkane is liberated. The chemisorbed Cr species retain the oxidation state (IV) and nuclearity (mono-) of their parent molecular precursors.

The second section examines the thermal transformations of silica-supported $(\equiv SiO)_2Cr(CH_2CMe_3)_2$, which undergoes a clean reaction at 69°C to generate a supported alkylidene complex, $(\equiv SiO)_2Cr{=}CHCMe_3$, with concurrent liberation of CMe_4. The reaction is quantitative and kinetically first-order. Isotope-labeling and kinetics experiments support a mechanistic assignment of intramolecular α-H abstraction. The temperature dependence of the first-order rate constants is consistent with a two-step mechanism of reversible (alkyl)(alkylidene)Cr(VI) hydride formation followed by reductive elimination of alkane. Reactions with acetone and Br_2 are consistent with the alkylidene formulation. A related alkylidene complex was prepared by thermolysis of silica-supported $(\equiv SiO)_2Cr(CH_2SiMe_3)_2$ at 150°C.

The third section describes the reactions of supported alkylidenes with various olefins. In contrast to silica-supported bis(neopentyl)Cr(IV), the surface alkylidene complexes are efficient room temperature α-olefin polymerization catalysts. Based on kinetic and isotope effects, a mechanism of agostic-assisted migratory insertion is proposed for the propagation step. The overall oxidation state of the Cr remains (IV) during the reaction.

The last part of this thesis deals with the study of silica-supported amido and alkoxo chromium complexes. The reactions of $Cr(NEt_2)_4$ and $Cr(O^tBu)_4$ with the partially dehydroxylated silica surface at 200°C give exclusively $(\equiv SiO)_2Cr(NEt_2)_2$ and $(\equiv SiO)_2Cr(O^tBu)_2$, respectively. Both surface organometallic complexes undergo ligand exchange reactions with alcohols. Thermal treatment of $(\equiv SiO)_2Cr(O^tBu)_2$ followed by addition of benzyl alcohol shows evidence for oxidation to benzoic acid. However, the "Cr=O" intermediate has yet to be detected.

Acknowledgements

The completion of this work would not have been possible without a number of people to whom I am very grateful. First, I would like to thank my dear supervisor Dr. Susannah L. Scott for giving me the opportunity to work in her lab. I offer her my sincere appreciation for her support, advice, and most of all her willingness to debate chemistry problems, also for being a very understanding person.

I would like to thank the University of Ottawa for an Admission Scholarship and NSERC (Canada) for a postgraduate scholarship.

All my friendship is extended to the members of the laboratory whom I had the pleasure of working with over the years, undergraduates, fellow graduate students and postdocs. There are far too many of you to mention but I would particularly like to thank Valérie Paquet, Dr. Carmen Roveda, Dr. Gordon Rice, Marcel Beaudoin and Abdillahi Omar Bouh.

My thanks go also to the entire Chemistry Department staff, particularly John Hopkins, Don Hopkins and Lee Sorensen, Dr. Glenn Facey for his help with running the NMR spectra, Dr. Anne-Marie Lamarche for recording the EPR spectra, Andrew Zlotorzynski for some of the GC-MS analyses, and Prof. Tito Scaiano for use of the UV-visible spectrometer.

I would like to acknowledge also Dr. Scott Tripp at Quantum Design (San Diego), and Dr. Laurie Thompson at Memorial University (Newfoundland), for the magnetic susceptibility measurements, Dr. Tim Wenzel at Union Carbide (West Virginia) and Dr. Qinyan Wang at Nova Chemicals (Calgary) for ethylene polymerization studies.

I would like to thank deeply my dear and affectionate husband Dr. Abdelaziz Nait Ajjou for all his help and guidance, my lovely daughter Myriam and my wonderful son Tarik.

I would like to thank my family whom I love very much, my mother Inge Amor, my father Dipl. Ing. Abdelmalek Amor, my sisters Layla, Samira and her little family, my brother Karim, my aunt Nicole Parent-Zahri and my uncle Ali Zahri. You have always been there for me whenever I needed you, particularly towards the end of my thesis.

I would like to thank my best friends Dr. Carmen Roveda, Hafida El Bilali, Dr. Marcello Piotti, Dr. Raluca Aldea and Dr. Gary Jefferson for their support and encouragement.

Table of Contents

	Page
Abstract	ii
Acknowledgements	iv
Table of Contents	vi
List of Figures	xii
List of Schemes	xxi
List of Tables	xxiv

Chapter 1. Introduction

1.1 Chromium-based Processes	1
1.2 Metal-catalyzed Ethylene Polymerization	1
1.2.1 Ziegler-Natta Catalysts	2
1.2.2 Supported Chromium Catalysts	5
1.2.2.1 Phillips-type Catalysts	5
1.2.2.2 Organochromium Catalysts	8
1.2.3 Catalyst Comparisons	9
1.3 Proposed Mechanism of Initiation of Ethylene Polymerization by Supported Chromium Catalysts	11
1.4 Homogeneous Model Systems for Ethylene Polymerization Catalysts	15
1.5 Surface Chemistry of Silica	18
1.6 Surface Organometallic Chemistry	25
1.7 References	28

Page

Chapter 2. Experimental Techniques

2.1 Reagents 32

2.1.1 Solid Support for Surface Metal Complexes 32

2.1.2 Gases 32

2.1.3 Commercial Liquids, Solid Reagents and Solvents 33

2.1.4 Molecular Chromium Complexes 34

2.1.4.1 Tetraalkylchromium(IV) Complexes 34

2.1.4.1.1 $Cr(CH_2C(CH_3)_3)_4$ 35

* Synthesis of $(CH_3)_3CCH_2MgBr$ 35

* Synthesis of $Cr(CH_2C(CH_3)_3)_4$ 35

2.1.4.1.2 $Cr(CH_2Si(CH_3)_3)_4$ 37

2.1.4.1.3 $Cr(CD_2C(CH_3)_3)_4$ 37

* Synthesis of $(CH_3)_3CCD_2OH$ 37

* Synthesis of $(CH_3)_3CCD_2Br$ 38

* Synthesis of $(CH_3)_3CCD_2MgBr$ 39

* Synthesis of $Cr(CD_2C(CH_3)_3)_4$ 40

2.1.4.2 Tetrakis(diethylamido)chromium(IV) 40

2.1.4.3 Tetra-t-butoxochromium(IV) 41

2.2 Preparation of Supported Chromium Complexes 42

2.2.1 Pretreatment of Silica 42

2.2.2 Breakseal Techniques 43

2.2.3 Grafting of Organometallic Complexes 44

2.3 Characterization of Silica-Supported Chromium Complexes 44

2.3.1 Infrared Spectroscopy 44

2.3.2 EPR Spectroscopy 46

2.3.3 Solid State NMR Spectroscopy 47

Page

2.3.4 Diffuse Reflectance UV-visible Spectroscopy 48

2.3.5 Elemental Analysis 48

2.3.6 Magnetic Susceptibility 50

2.4 Analysis of Volatile Reaction Products 54

2.4.1 Qualitative Analysis 54

2.4.2 Isotopomer Analysis 55

2.4.3 Quantitative Analysis 57

2.4.3.1 Volumetric Analysis 57

2.4.3.2 IR Spectroscopy 57

2.5 Kinetic Studies 58

2.6 Ethylene Polymerization Studies 63

2.6.1 Nova Chemicals Catalyst Testing Protocol 63

2.6.2 Union Carbide Catalyst Testing Protocol 63

2.7 Polymer Characterization 64

2.7.1 Molecular Weight and Polydispersity 64

2.7.2 NMR Spectroscopy 65

2.7.3 Thermal Analysis 68

2.8 References 70

Chapter 3. Reactions of Tetraalkylchromium(IV) Complexes with Silica Surfaces

3.1 Introduction 72

3.2 Synthesis of Surface Organometallic Complexes 73

3.3 Characterization of Surface Organometallic Complexes 74

3.3.1 Infrared Spectroscopy 74

3.3.2 Electronic Spectroscopy 78

Page

3.3.3 Nuclearity and Oxidation State of Grafted Complexes 78

3.3.3.1 Electron Paramagnetic Resonance 80

3.3.3.2 Magnetic Susceptibility 83

3.4 Stoichiometry of the Reaction of CrR_4 with Silica 83

3.4.1 On Silica-500 83

3.4.2 On Silica-200 87

3.5 Molecular Modeling 91

3.6 Mechanism of Grafting 98

3.7 Reactivity Survey of Supported Alkylchromium(IV) Fragments 102

3.7.1 Reaction with Water 103

3.7.2 Reaction with O_2 103

3.7.3 Reactions with CO and Ethylene 103

3.7.4 Reaction with NO 103

3.8 Conclusion 104

3.9 References 106

Chapter 4. Silica-Supported Chromium(IV) Alkylidene Complexes

4.1 Introduction 108

4.2 Thermolysis of the Grafted Complexes 111

4.2.1 IR Spectroscopic Evidence 112

4.2.2 Post-thermolysis Magnetic Susceptibility 117

4.3 Composition of Supported Cr Complexes Formed upon Thermolysis 117

4.4 α-Deuterium-Labeling Experiments 126

4.5 Kinetics Studies of Thermolysis Reactions 132

4.6 Uniformity of Supported Organochromium Complexes 141

4.7 Reactivity of Chromium(IV) Alkylidenes 143

Page

4.7.1 Reaction with Water 144

4.7.2 Reaction with Bromine 144

4.7.3 Reaction with Acetone 144

4.7.4 Reaction with Styrene 145

4.8 Conclusion 145

4.9 References 148

Chapter 5. Mechanism of Olefin Polymerization Catalyzed by Silica-supported Chromium(IV) Alkylidene Complexes

5.1 Introduction 151

5.2 Reactivity of Silica-supported Chromium(IV) Alkylidenes 154

5.2.1 Towards Norbornene 154

5.2.2 Towards Styrene 155

5.2.3 Towards Ethylene 157

5.2.4 Towards Propylene 160

5.2.5 Towards 1-Hexene 160

5.3 Number of Active Sites 163

5.4 Active Oxidation State 167

5.5 Kinetics of Ethylene Polymerization 168

5.6 Kinetics of C_2D_4 Polymerization 179

5.7 Polymerization Induced by $(\equiv SiO)_2Cr(CH_2C(CH_3)_3)_2$ 183

5.8 Catalyst Recycling 184

5.9 Effect of H_2 186

5.10 Kinetics of 1-Hexene Polymerization 189

5.11 Kinetics of Ethylene-1-Hexene Copolymerization 193

5.12 Catalytic Activity 201

Page

5.13 Polyethylene Characterization 204
5.13.1 Infrared Spectroscopy 204
5.13.2 NMR Spectroscopy 208
5.13.3 Gel Permeation Chromatography (GPC) Analysis 209
5.13.4 Thermal Analysis 209
5.14 Polypropylene Characterization 212
5.14.1 Infrared Spectroscopy 212
5.14.2 NMR Spectroscopy 212
5.15 Polystyrene Characterization 215
5.15.1 Infrared Spectroscopy 215
5.15.2 NMR Spectroscopy 215
5.16 Poly-1-hexene Characterization 216
5.16.1 Infrared Spectroscopy 216
5.16.2 NMR Spectroscopy 216
5.17 Proposed Mechanism for Polymerization of Ethylene 219
5.18 Proposed Mechanism for Polymerization of Propylene 228
5.19 Conclusion 232
5.20 References 233

Chapter 6. Synthesis of Silica-supported Amido and Alkoxo Complexes of Chromium(IV)

6.1 Introduction 236
6.2 Reaction of $Cr(NEt_2)_4$ with Silica-200 240
6.2.1 Infrared Spectroscopy Characterization 240
6.2.2 Electronic Spectroscopy 240
6.2.3 Stoichiometry of the Reaction of $Cr(NEt_2)_4$ with Silica 242

Page

6.2.4 Reactions of $(\equiv SiO)_2Cr(NEt_2)_2$ with Alcohols 244

6.2.4.1 With *tert*-Butanol 244

6.2.4.2 With Trimethylsilanol 249

6.3 Direct Reaction of $Cr(O^tBu)_4$ with Silica 249

6.3.1 Infrared Spectroscopy Characterization 250

6.3.2 Stoichiometry of the Reaction of $Cr(O^tBu)_4$ with Silica 252

6.3.3 Electonic Spectroscopy 254

6.4 Thermolysis of Supported Alkoxo/Siloxo Chromium Complexes 254

6.4.1 Thermolysis of $(\equiv SiO)_2Cr(O^tBu)_2$ 254

6.4.2 Thermolysis of $(\equiv SiO)_2Cr(OSi(CH_3)_3)_2$ 256

6.4.3 Reactivity towards Various Alcohols 256

6.2.4.1 Towards Allylic Alcohol 256

6.2.4.2 Towards Benzyl Alcohol 256

6.5 Conclusions 258

6.6 References 259

Chapter 7. General Conclusions 261

List of Publications 263

Claims to Original Research 264

List of Figures

Chapter 1		Page
Figure 1.1	Types of hydroxyl groups on the silica surface	20
Figure 1.2	Infrared spectra of self-supporting disks of silica showing the effect of temperature on the hydroxyl group distribution.	21
Figure 1.3	Model of the (111) face of β-cristobalite proposed by DeBoer and Vleeskins.	22
Figure 1.4	Geometry of the (100) face of β-cristobalite.	24
Figure 1.5	Mixed-surface model proposed by Maciel and Sindorf showing the reversible dehydration of the silica surface.	26

Chapter 2		
Figure 2.1	Schematic of a breakseal reactor.	43
Figure 2.2	Schematic of an in situ IR cell.	45
Figure 2.3	Schematic of an EPR reactor.	47
Figure 2.4	Calibration curve for chromium analysis.	49
Figure 2.5	Schematic of a magnetic susceptibility reactor.	51
Figure 2.6	Calibration curves for (a) neopentane; (b) tetramethylsilane; (c) $HNEt_2$; (d) ^tBuOH.	59-60
Figure 2.7	Schematic of a reactor for preparing large quantities of Cr/silica used in kinetics studies	61
Figure 2.8	Carbon labeling in ethylene-1-olefin copolymers.	66

Chapter 3

Page

Figure 3.1	Transmission infrared spectra of (a) a self-supporting disk of silica, partially dehydroxylated at 200°C; (b) after reaction with $Cr(CH_2CCH_3)_3)_4$.	75
Figure 3.2	Transmission infrared spectra of (a) a self-supporting disk of silica, partially dehydroxylated at 200°C; (b) after reaction with $Cr(CH_2SiCH_3)_3)_4$.	76
Figure 3.3	Diffuse reflectance UV-visible spectra of silica-500 modified with (a) $Cr(CH_2C(CH_3)_3)_4$, **1a**, and (b) $Cr(CH_2Si(CH_3)_3)_4$, **1b**.	79
Figure 3.4	EPR spectrum of silica-200 modified by $Cr(CH_2C(CH_3)_3)_4$, at 88K.	81
Figure 3.5	EPR spectra of $Cr(CH_2C(CH_3)_3)_4$, **1a**, (a) at 180 K in hexane (b) at 147 K in hexane.	82
Figure 3.6	Temperature-dependence of the magnetic moment of 21 mg $CrNp_4$/silica-500 with 1.02 wt.% Cr loading.	84
Figure 3.7	Model of $(HO)_3SiOCr(CH_2C(CH_3)_3)_3$.	92
Figure 3.8	Model of $(\mu\text{-}O)[(HO)_2SiO]_2Cr(CH_2C(CH_3)_3)_2$.	93
Figure 3.9	Molecular modeling of $(HO)_3SiOCr(CH_2C(CH_3)_3)_3$ (a) side view ball-stick representation; (b) top view, space-filling representation.	94-95
Figure 3.10	Molecular modeling of $(\mu\text{-}O)[(HO)_2SiO]_2Cr(CH_2CMe_3)_2$ (a) side view ball-stick representation; (b) top view, space-filling representation.	96-97

Chapter 4

Page

Figure 4.1	Transmission infrared spectra of (a) $(\equiv SiO)_2Cr(CH_2C(CH_3)_3)_2$, 1.94 wt.% Cr, at room temperature, and (b) after heating in vacuum at 69°C for 4 hours.	115
Figure 4.2	Thermal evolution of $(\equiv SiO)_2Cr(CH_2C(CH_3)_3)_2$ and $(\equiv SiO)_2Cr(CH_2Si(CH_3)_3)_2$ in vacuum.	116
Figure 4.3	Temperature-dependent magnetic susceptibility after thermolysis of $(\equiv SiO)_2Cr(CH_2C(CH_3)_3)_2$.	118
Figure 4.4	Transmission infrared spectra of (a) $(\equiv SiO)_2Cr(CD_2C(CH_3)_3)_2$ at room temperature, and (b) after heating in vacuum at 69°C for 10 hours.	128
Figure 4.5	Time-resolved evolution of $C(CH_3)_4$ from $(\equiv SiO)_2Cr(CH_2C(CH_3)_3)_2$, and $(\equiv SiO)_2Cr(CD_2C(CH_3)_3)_2$ at 69°C.	135
Figure 4.6	(a) Time-resolved evolution of $C(CH_3)_4$ from $(\equiv SiO)_2Cr(CH_2C(CH_3)_3)_2$ at various temperatures. (b) Eyring plot of the temperature-dependence of rate constants for the thermolysis of $(\equiv SiO)_2Cr(CH_2C(CH_3)_3)_2$.	138
Figure 4.7	(a) Time-resolved evolution of $Si(CH_3)_4$ from $(\equiv SiO)_2Cr(CH_2Si(CH_3)_3)_2$ at various temperatures. (b) Eyring plot of the temperature-dependence of rate constants for the thermolysis of $(\equiv SiO)_2Cr(CH_2Si(CH_3)_3)_2$.	139

Chapter 5 Page

Figure 5.1	Transmission infrared spectra of (a) $(\equiv SiO)_2Cr=CHC(CH_3)_3$ at room temperature; (b) after addition of norbornene; (c) difference spectrum, obtained by subtraction of (a) from (b).	156
Figure 5.2	Transmission infrared spectra of (a) $(\equiv SiO)_2Cr=CHC(CH_3)_3$ and (b) after addition of styrene at room temperature.	158
Figure 5.3	Transmission infrared difference spectrum obtained by subtraction of the spectrum of $(\equiv SiO)_2Cr=CHC(CH_3)_3$ from the spectrum of $(\equiv SiO)_2Cr=CHC(CH_3)_3$ after addition of ethylene at room temperature.	159
Figure 5.4	Transmission infrared difference spectrum obtained by subtraction of the spectrum of $(\equiv SiO)_2Cr=CHC(CH_3)_3$ from the spectrum of $(\equiv SiO)_2Cr=CHC(CH_3)_3$ after addition of propylene at room temperature.	161
Figure 5.5	Transmission infrared difference spectrum obtained by subtraction of the spectrum of $(\equiv SiO)_2Cr=CHC(CH_3)_3$ from the spectrum of $(\equiv SiO)_2Cr=CHC(CH_3)_3$ after addition of 1-hexene at room temperature.	162
Figure 5.6	Temperature-dependent magnetic susceptibility of 10 mg $(\equiv SiO)_2Cr=CHC(CH_3)_3$ (0.5 wt.% Cr) after polymerization of ethylene.	169
Figure 5.7	Time resolved consumption of ethylene during polymerization with $(\equiv SiO)_2Cr=CHC(CH_3)_3$, 4a, at 21°C. (a) 0.45 (b) 0.62 and (c) 0.78 wt.% Cr loading.	170

		Page
Figure 5.8	Dependence of the observed rate constant k_{app} for ethylene polymerization catalyzed by $(SiO)_2Cr=CHCMe_3$ on the quantity of Cr, in the range 0.35 - 0.78 wt.% Cr loading.	172
Figure 5.9	Time-resolved consumption of ethylene during polymerization with $(\equiv SiO)_2Cr=CHC(CH_3)_3$, **4a**, at 48°C. (a) 0.35 (b) 0.62 and (c) 0.78 wt.% Cr loading.	175
Figure 5.10	Time-resolved consumption of ethylene during polymerization with $(\equiv SiO)_2Cr=CHC(CH_3)_3$, **4a**, at 80°C. (a) 0.35 (b) 0.62 and (c) 0.78 wt.% Cr loading.	176
Figure 5.11	Eyring plot of temperature-dependence of rate constants for ethylene polymerisation catalyzed by $(SiO)_2Cr=CHCMe_3$.	177
Figure 5.12	Time-resolved consumption of D-labeled ethylene during polymerization with $(\equiv SiO)_2Cr=CHC(CH_3)_3$, **4a**, at 21°C. (a) 0.52 (b) 0.77 and (c) 0.99 wt.% Cr loading.	180
Figure 5.13	Dependence of the observed rate constant k_{app} at 21°C for polymerization of ethylene, and D-labeled ethylene catalyzed by $(SiO)_2Cr=CHCMe_3$ on the quantity of Cr. Cr loadings range from 0.35-0.99 wt.%.	182
Figure 5.14	Time-resolved consumption of C_2H_4 during polymerization starting with $(\equiv SiO)_2Cr(CH_2C(CH_3)_3)_2$, at 0.89 wt.% Cr loading.	183
Figure 5.15	Time-resolved consumption of ethylene in three subsequent additions (a) 67, (b) 69 and (c) 65 Torr ethylene. The catalyst was $(\equiv SiO)_2Cr=CHC(CH_3)_3$, with 0.99 wt.% Cr loading at 21°C.	185

Page

Figure 5.16 Time-resolved consumption of C_2H_4 during polymerization in the presence of H_2 with $(\equiv SiO)_2Cr=CHC(CH_3)_3$, at 21°C. (a) 0.56 (b) 0.89 and (c) 1.27 wt.% Cr loading. 187

Figure 5.17 Dependence of k_{app} for ethylene polymerization catalyzed by $(SiO)_2Cr=CHCMe_3$ in the presence of H_2 at 21°C on the quantity of Cr. 188

Figure 5.18 Time-resolved consumption of 1-hexene during polymerization with $(\equiv SiO)_2Cr=CHC(CH_3)_3$, at 21°C. (a) 0.52 (b) 0.77 (c) 0.81 (d) 0.99 wt.% Cr loading. 190-191

Figure 5.19 Dependence of the observed rate constant k_{app} for 1-hexene polymerization catalyzed by $(SiO)_2Cr=CHCMe_3$ on the quantity of Cr, in the range 0.52 - 0.99 wt.% Cr loading. 192

Figure 5.20 Time-resolved consumption of C_2D_4 during copolymerization with 1-hexene with $(\equiv SiO)_2Cr=CHC(CH_3)_3$, at 21°C. (a) 0.56 (b) 0.89 and (c) 0.99 wt.% Cr loadings. 194

Figure 5.21 Time-resolved consumption of 1-hexene during copolymerization with C_2D_4 with $(\equiv SiO)_2Cr=CHC(CH_3)_3$, at 21°C. (a) 0.56 (b) 0.89 and (c) 0.99 wt.% Cr loadings. 195

Figure 5.22 Dependence of the observed rate constant k_{app} for copolymerization of C_2D_4 and 1-hexene catalyzed by $(SiO)_2Cr=CHCMe_3$ on the quantity of Cr, in the range 0.56 - 0.99 wt % Cr loading. 198

Page

Figure 5.23	Dependence of the observed rate constants k_{app} for polymerization of (a) $C_2H_4 + H_2$, (b) C_2H_4, (c) C_2D_4, (d) C_2D_4 in the presence of 1-hexene, catalyzed by $(SiO)_2Cr=CHCMe_3$, on the quantity of Cr, in the range 0.33 - 1.27 wt.% Cr loading at 21°C.	200
Figure 5.24	Transmission infrared spectrum of $(\equiv SiO)_2Cr=CH_2C(CH_3)_3$ after addition of C_2D_4 at room temperature.	206
Figure 5.25	Transmission IR spectrum of polyethylene film showing bands due to methyl and vinyl end groups at 1377 and 908 cm^{-1}, respectively.	207
Figure 5.26	DSC of polyethylene produced by $(\equiv SiO)_2Cr=CHC(CH_3)_3)_2$.	211
Figure 5.27	^{13}C NMR of polypropylene produced by $(\equiv SiO)_2Cr=CHC(CH_3)_3)_2$ (a) CH_2, CH, CH_3 regions; (b) CH_3 region with [mmmm] = 53%.	214
Figure 5.28	^{13}C NMR of polystyrene produced by $(\equiv SiO)_2Cr=CHC(CH_3)_3)_2$.	217
Figure 5.29	^{13}C NMR of poly-1-hexene produced by $(\equiv SiO)_2Cr=CHC(CH_3)_3)_2$.	218
Figure 5.30	GC-MS of volatile reaction products upon treatment of **4a** with 0.1 Torr ethylene.	220
Figure 5.31	GC-MS of volatile reaction products upon treatment of **4a** with 48 Torr ethylene.	223
Figure 5.32	Mass spectra of 4,4-dimethyl-2-pentene formed by reaction of **4a** with (a) C_2H_4, and (b) C_2D_4.	227
Figure 5.33	GC-MS of volatile reaction products upon treatment of **4a** with 10 Torr propylene.	229

Chapter 6 Page

Figure 6.1	In situ IR difference spectra of a self-supporting disk of silica-200 treated with $Cr(NEt_2)_4$. (a) Region 4000 - 1300 cm^{-1}, and (b) region 1000 - 800 cm^{-1}.	241
Figure 6.2	UV-visible spectrum of silica-200 modified with $Cr(NEt_2)_4$.	243
Figure 6.3	In situ IR difference spectra of a self-supporting disk of (a) $(\equiv SiO)_2Cr(NEt_2)_2$, followed by (b) addition of $(CD_3)_3COD$ to give $(\equiv SiO)_2Cr(O^tBu\text{-}d_9)_2$, followed by (c) addition of $(CH_3)_3COH$ to give $(\equiv SiO)_2Cr(O^tBu)_2$.	247
Figure 6.4	(a) ^2H MAS NMR spectrum at a spin rate of 4 kHz, and (b) stationary ^2H NMR spectrum of $(\equiv SiO)_2Cr(O^tBu)_2$.	248
Figure 6.5	In situ IR difference spectra of a self-supporting disk of silica-200 treated with $Cr(O^tBu)_4$. (a) Region 4000 - 1300 cm^{-1}, and (b) region 1000 - 800 cm^{-1}.	251
Figure 6.6	UV-visible spectrum of silica-200 modified with $Cr(O^tBu)_4$.	255
Figure 6.7	In situ IR difference spectra of a self-supporting disk of (a) thermolyzed $(\equiv SiO)_2Cr(O^tBu)_2$, followed by (b) the reaction with benzyl alcohol.	257

List of Schemes

Chapter 1		Page
Scheme 1.1	Protonation of silica-supported chromous ions to initiate ethylene polymerization.	12
Scheme 1.2	Ethylene-induced migration of silanol protons to chromium.	12
Scheme 1.3	Metallacyclopentane/metal carbene mechanisms for initiation of ethylene polymerization.	13
Scheme 1.4	Metal carbene/metallacycle mechanism on adjacent active sites.	14
Chapter 2		
Scheme 2.1	Neopentane-d_n isotopomer fragmentation.	55
Chapter 3		
Scheme 3.1	Mechanism for reaction of $Cr(CH_2EMe_3)_4$ on deuterated silica-500.	101
Scheme 3.2	Mechanism for reaction of $Cr(CH_2EMe_3)_4$ with deuterated silica-200.	102

Chapter 4

		Page
Scheme 4.1	Intramolecular and intermolecular mechanisms for α-hydrogen abstraction in transition-metal alkyl complexes.	110
Scheme 4.2	Possible structures for $(\equiv SiO)_2Cr(C_4EH_{10})$, where E = C or Si.	122
Scheme 4.3	Predicted isotopomer distribution from thermolysis of 90% α-D_2-labeled $CrNp_4$.	131
Scheme 4.4	Mechanism of thermolysis of silica-supported bis(neopentyl)chromium(IV) involving α-hydrogen abstraction.	140
Scheme 4.5	Stabilization of chromium(IV) alkylidene surface species through reversible coordination of a surface siloxane oxygen.	143

Chapter 5

Scheme 5.1	Cossee mechanism.	151
Scheme 5.2	Green-Rooney mechanism.	152
Scheme 5.3	Green-Rooney-Brookhart mechanism.	152
Scheme 5.4	Analogy between hyperconjugation and α-agostic interactions.	153
Scheme 5.5	Termination mechanism for ethylene polymerization.	154
Scheme 5.6	Transition state for ethylene insertion, showing α-agostic interaction.	179

		Page
Scheme 5.7	The ten possible stereochemical pentads of polypropylene.	213
Scheme 5.8	Carbon numbering in poly-1-hexene for ^{13}C NMR.	216
Scheme 5.9	Proposed origin of heptene isomers during early stages of ethylene polymerization.	225
Scheme 5.10	Mechanism for initiation of propylene polymerization.	231

Chapter 6

Scheme 6.1	A proposed structure for the active site of the Ti(IV)/SiO_2 catalyst developed by Shell.	238
Scheme 6.2	Peroxometal and oxometal pathways for catalytic oxidation reactions.	239

List of Tables

Chapter 1		Page
Table 1.1	Comparison of three catalysts for ethylene polymerization.	10
Chapter 2		
Table 2.1	Polyethylene backbone and side-chain chemical shifts in ppm from TMS as a function of branch length.	67
Table 2.2	Various spectral regions in the ^{13}C NMR spectrum of ethylene-1-olefin copolymer.	68
Chapter 3		
Table 3.1	Infrared frequencies (cm^{-1}) of silica modified by $Cr((CH_2C(CH_3)_3)_4$ and $Cr((CH_2Si(CH_3)_3)_4$.	77
Table 3.2	Quantitative product analysis for the reaction of CrR_4 with silica-500.	86
Table 3.3	Quantitative product analysis for the reaction of $Cr(CH_2C(CH_3)_3)_4$ with silica-200.	89
Table 3.4	Quantitative product analysis for the reaction of $Cr(CH_2Si(CH_3)_3)_4$ with silica-200.	90
Table 3.5	Isotopomer distribution in volatile products from grafting of CrR_4 on deuterated silica-500.	99

		Page
Table 3.6	Isotopomer distribution in volatile products from grafting of CrR_4 on deuterated silica-200.	100

Chapter 4

Table 4.1	Quantitative IR analyses of *in vacuo* thermolysis of $(\equiv SiO)_2Cr(CH_2C(CH_3)_3)_2$.	113
Table 4.2	Quantitative IR analyses of *in vacuo* thermolysis of $(\equiv SiO)_2Cr(CH_2Si(CH_3)_3)_2$.	114
Table 4.3	Quantitative analysis of volatile products in the thermolysis of $(\equiv SiO)_2Cr(CH_2C(CH_3)_3)_2$ and subsequent protonolysis.	119-121
Table 4.4	Quantitative analysis of volatile products in the thermolysis of $(\equiv SiO)_2Cr(CH_2Si(CH_3)_3)_2$ and subsequent protonolysis.	124-125
Table 4.5	Quantitative and isotope analysis of the reaction of $Cr(CD_2C(CH_3)_3)_4$ with silica-200.	129
Table 4.6	Quantitative and isotope analysis of the thermolysis of $(\equiv SiO)_2Cr(CD_2C(CH_3)_3)_2$.	130
Table 4.7	Quantitative and isotope analysis of subsequent protonolysis of $(\equiv SiO)_2Cr(CD_2C(CH_3)_3)_2$.	133
Table 4.8	First-order rate constants for alkane elimination.	136

Chapter 5

Page

Table 5.1	Determination of the fraction of active sites in polymerization of ca. 50 Torr C_2H_4 by partial poisoning of $(\equiv SiO)_2Cr=CHC(CH_3)_3$ with O_2.	166
Table 5.2	Determination of the fraction of active sites in polymerization of ca. 250 Torr C_2H_4 by partial poisoning of $(\equiv SiO)_2Cr=CHC(CH_3)_3$ with O_2.	167
Table 5.3	Apparent first-order rate constants for C_2H_4 polymerization catalyzed by $(SiO)_2Cr=CHCMe_3$.	171
Table 5.4	Observed second-order rate constants for C_2H_4 polymerization catalyzed by $(SiO)_2Cr=CHCMe_3$ at different temperatures.	177
Table 5.5	Apparent first-order rate constants for C_2D_4 polymerization catalyzed by $(SiO)_2Cr=CHCMe_3$ at 21°C.	181
Table 5.6	Apparent first-order rate constants for C_2H_4 polymerization catalyzed by $(SiO)_2Cr=CHCMe_3$, in successive additions of C_2H_4 at 21°C.	184
Table 5.7	Apparent first-order rate constants for C_2H_4 polymerization catalyzed by $(SiO)_2Cr=CHCMe_3$ in the presence of H_2 at 21°C.	186
Table 5.8	Apparent first-order rate constants for 1-hexene polymerization catalyzed by $(SiO)_2Cr=CHCMe_3$ at 21°C.	189
Table 5.9	Apparent first-order rate constants for copolymerization of C_2D_4/1-hexene mixtures, catalyzed by $(SiO)_2Cr=CHCMe_3$ at 21°C.	196

		Page
Table 5.10	Summary of composite second-order rate constants for olefin polymerization catalyzed by $(SiO)_2Cr=CHCMe_3$ at 21°C.	199
Table 5.11	Activity tests for batch polymerization of ethylene and analysis of the resulting polymer performed at Nova Chemicals.	202
Table 5.12	Batch polymerization of ethylene with $(\equiv SiO)_2Cr=CHC(CH_3)_3$ and analysis of the resulting polymer performed at Union Carbide.	203
Table 5.13	Determination of short chain branching by ^{13}C NMR.	209
Table 5.14	DSC analysis of polyethylene produced by $(\equiv SiO)_2Cr=CHC(CH_3)_3$.	212
Table 5.15	Volatiles formed upon reaction of $(\equiv SiO)_2Cr=CHC(CH_3)_3$ with 0.1 Torr ethylene.	221
Table 5.16	Volatile reaction products upon treatment of $(\equiv SiO)_2Cr=CHC(CH_3)_3$ with 48 Torr ethylene.	224
Table 5.17	Volatile reaction products upon treatment of $(\equiv SiO)_2Cr=CHC(CH_3)_3$ with 10 Torr propylene.	230

Chapter 6

Table 6.1	Infrared frequencies (cm^{-1}) of silica modified by $Cr(NEt_2)_4$.	242
Table 6.2	Quantitative product analysis for the reaction of $Cr(NEt_2)_4$ with SiO_2-200.	245

Page

Table 6.3 Infrared frequencies (cm^{-1}) of silica modified by $Cr(O^tBu)_4$. 250

Table 6.4 Quantitative product analysis for the reaction of $Cr(O^tBu)_4$ with SiO_2-200. 253

Chapter 1

Introduction

1.1 Chromium-based Processes

The metal chromium and its derivatives are used in industries such as leather tanning, electroplating, pigment production and synthesis of various chemicals. Not surprisingly, large quantities of chromium have found their way into solid and liquid wastes. Despite the metal's usefulness, the high toxicity of chromium makes its release highly undesirable.

In chemistry, chromium complexes react readily with various organic and inorganic substrates. These properties make chromium an excellent catalyst for important reactions such as the oxidation of alcohols[1] and the polymerization of ethylene,[2,3] in both homogeneous and heterogeneous processes. One major advantage of heterogeneous catalyst formulations is the minimization of soluble Cr waste. In the case of polymerization, where the solid catalyst remains as a small contaminant of the polymer material, it is necessary to use catalysts with very high activity in order to generate product with a very low metal content, so that chromium leaching does not pose a health risk.

As my work is a study of surface organochromium chemistry, this chapter will focus on the chromium-catalyzed polymerization of ethylene. Principal differences between Phillips-type catalysts and organochromium-based catalysts, as well as the proposed mechanisms, will be discussed.

1.2 Metal-catalyzed Ethylene Polymerization

Polyethylene is the most widely used plastic in the world. About 40 million tons were produced in 1996,[4] of which there are three commercially important varieties: high-density polyethylene (HDPE), low-density polyethylene

(LDPE) and linear low-density polyethylene (LLDPE). LDPE is prepared at high pressures and temperatures with free radical initiators, while HDPE is produced using Ziegler-Natta or supported chromium catalysts. Recently, LLDPE has been manufactured by the metal-catalyzed copolymerization of ethylene with α-olefins.[5]

Three processes are used commercially to make HDPE: solution, slurry and gas phase.[6] All are called "low pressure" processes (< 50 atm) to distinguish them from the free radical or "high-pressure" process (> 85 atm) which makes highly branched LDPE. In the solution process, the polymerization is performed at 125-170°C in a hydrocarbon solvent which dissolves the polymer as it forms. The reaction usually slows as the solution becomes viscous because it becomes difficult to stir ethylene into the liquid phase. In contrast, the slurry process uses a poor solvent and low temperature (60-100°C) to prevent dissolving or even swelling of the polymer. The solvent acts solely as a diluent which serves to transfer heat and keep the catalyst in contact with ethylene and other reactants. Finally, the gas phase process is much like the slurry method in that polymer particles are formed at similar temperatures. A bed of catalyst/polymer is fluidized by circulating ethylene which also serves as coolant.

Whatever the merits of each process in continuous commercial operations, the slurry process is most convenient for batch polymerization studies in the laboratory. The diluent permits precise control of the temperature and serves to dissolve ethylene and other reactants that must contact the catalyst during polymerization.

1.2.1 Ziegler-Natta Catalysts

In the 1950s, Karl Ziegler in Germany discovered that certain combinations of transition metal compounds and organometallic compounds polymerize

ethylene at low temperatures and pressures to give polyethylene that has an essentially linear structure.[7] This material is now referred to as high-density polyethylene (HDPE). Following close on the heels of Ziegler's discovery was the recognition, in 1960 by Giulio Natta in Italy, that catalysts of the type described by Ziegler were capable of polymerizing α-olefins to yield stereoregular polymers.[8] The catalysts developed by Ziegler and Natta became known as Ziegler-Natta catalysts. Their joint discovery of these polymerization processes was recognized by the 1963 Nobel prize in chemistry.

The number of compounds and combinations of compounds that fit into the category of Ziegler-Natta catalysts[9-11] are far too numerous to describe here. A Ziegler-Natta catalyst is a combination of a transition metal compound of an element from Groups IV to VIII and an organometallic compound of a metal from Groups I to III of the Periodic Table. By convention, the transition metal compound is referred to as the catalyst and the organometallic compound as the cocatalyst, although the cocatalyst may be required in much greater quantity than the catalyst itself.

Most commonly, the catalyst component consists of halides or oxyhalides of titanium, vanadium, chromium, molybdenum or zirconium. Compounds of iron and cobalt have also been found to be effective. Some ligands other than halide or oxyhalide that have been investigated include alkoxy, acetonyl, cyclopentadienyl and phenyl. Cocatalysts are usually hydrides, alkyls or aryls, of metals such as aluminum, lithium, zinc, tin, cadmium, beryllium and magnesium. By far the most important and most thoroughly studied Ziegler-Natta systems are combinations of titanium trihalides and tetrahalides with trialkylaluminum compounds.[12]

The catalysts are prepared by mixing the components in a dry, inert solvent in the absence of oxygen, usually at a low temperature. They are characterized by

high reactivity towards many nonpolar monomers and are usually capable of producing polymers with a high degree of stereoregularity. Catalyst activity changes with time, and it is not uncommon for maximum activity to be reached after an aging period of one or two hours. The nature of insoluble Ziegler-Natta catalysts is not well understood. For $TiCl_x$-AlR_3 (x = 3 or 4; R = alkyl) systems, ligand exchange reactions initially take place. Organotitanium(IV) compounds are believed to undergo reduction via homoleptic bond cleavage. Because of the heterogeneous nature of the catalyst, it is certain that reduction of Ti(IV) is not complete. On the other hand, soluble catalysts appear to form well-defined complexes. For example, the soluble complex formed by triethylaluminum and bis(cyclopentadienyl)titanium dichloride has been shown by elemental and X-ray analysis to have the following structure:[12]

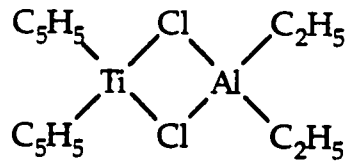

A wide variety of non-polar monomers are polymerizable by Ziegler-Natta catalysts. Catalyst activity decreases with increasing steric hindrance about the double bond. The observed order of reactivity for 1-alkenes is:[12]

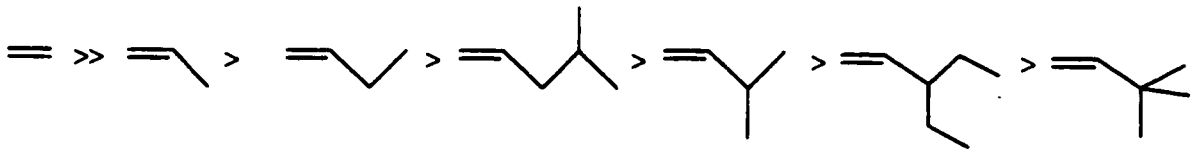

Random copolymers of ethylene and α-olefins are obtained with Ziegler-Natta catalysts, ethylene being much more reactive than the higher alkenes. The reactivity ratios vary with the nature and physical state of the

catalyst. With heterogeneous catalysts, a wide range of compositions is generally obtained while more homogeneous polymer compositions are obtained with soluble catalysts.

The control of stereochemistry is one of the most fascinating aspects of Ziegler-Natta polymerization, like the isotacticity for polypropylene is for 95%.

1.2.2 Supported Chromium Catalysts

About one-third of all high-density polyethylene is currently manufactured with chromium catalysts, in which the metal is chemically bound to a high-surface area support such as silica. The principal chromium catalysts are the Phillips-type catalyst based on inorganic chromium, and the Union Carbide catalyst, based on organometallic chromium.

1.2.2.1 Phillips-type Catalysts

Cr/SiO_2 catalysts have been intensively studied for polymerization since 1951, when J. P. Hogan and R. L. Banks at Phillips Petroleum Co. discovered that these systems catalyze the polymerization of olefins.[13] The Phillips catalyst is currently responsible for one-third of the global production of high-density polyethylene.

The Phillips catalyst is prepared by impregnation of silica with an inorganic chromium compound, for example, CrO_3, $CrO_2(OR)_2$, or various Cr(III) salts such as chromium(III) acetate. The silica surface is treated with approximately 1 wt.% Cr.[14] This operation is followed by calcination in oxygen at high temperature (500°C) in order to activate the catalyst. CrO_3 begins to decompose above 200°C, releasing O_2 and generating α-Cr_2O_3.[15] Cr(VI) surface compounds stabilized against thermal degradation by attachment to the silica surface coexist with Cr_2O_3 and are supposed to be the precursors of the

polymerization active sites.[13,16] The nature of the Cr(VI) surface compounds has been suggested to be chromate- or dichromate-like, eqs 1.1 and 1.2.[13]

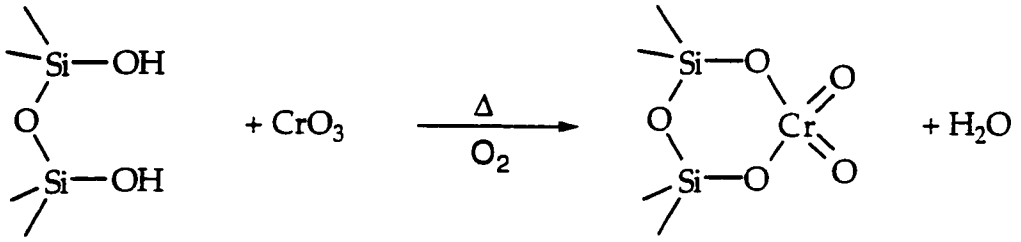

(1.1)

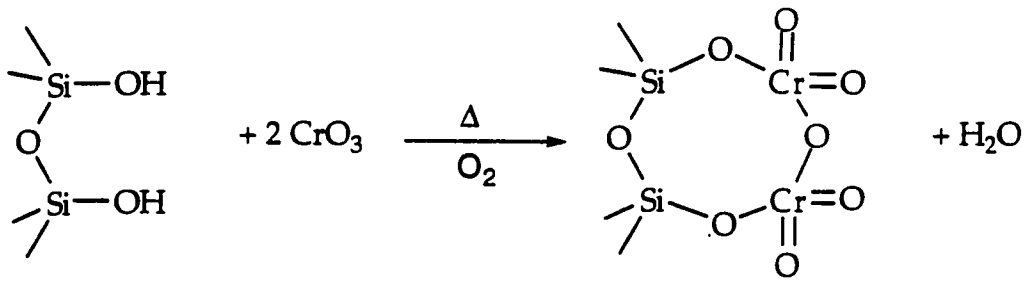

(1.2)

The identification of surface structures has proven difficult and controversial. By measuring the weight change upon impregnation of CrO_3, Hogan[13] concluded that about two hydroxyls were consumed for each chromium attached, and therefore the initial structure must be chromate-like. However, he did not rule out later rearrangement to dichromate during activation at high temperatures. Zecchina *et al.*,[16] working at 600°C, as well as Krauss[17] at 500°C, came to the opposite conclusion. Finding that only one hydroxyl was lost for each chromium, they concluded that dichromate was the major species present.[18] McDaniel[18] later offered a contrary interpretation of the same data. In yet another approach, Zecchina's group examined the geometry of both proposed species.[16] They concluded that the chromate structure fills the silica surface nicely, whereas dichromate would introduce strain and is therefore less likely.

Recently, Rebensdorf and Larsson[19] proposed that polymerization can take place only when the chromium ions are paired as dichromate. This

reasoning was advanced to explain why nonsupported chromium(VI) compounds failed to exhibit any activity. However, McDaniel[20] demonstrated by the reaction of CrO_2Cl_2 with silica that the direct formation of dichromate species is not possible in the absence of oxygen and at low temperature (200°C) where Cr(VI) is stable, and therefore concluded that the paired chromium structure is not present on the silica surface during the preparation of the Phillips catalyst.

Upon contact with ethylene at 100°C, the surface chromium(VI) is reduced, ultimately forming the catalytically active site and liberating formaldehyde as the oxidation product[21], eq 1.3.

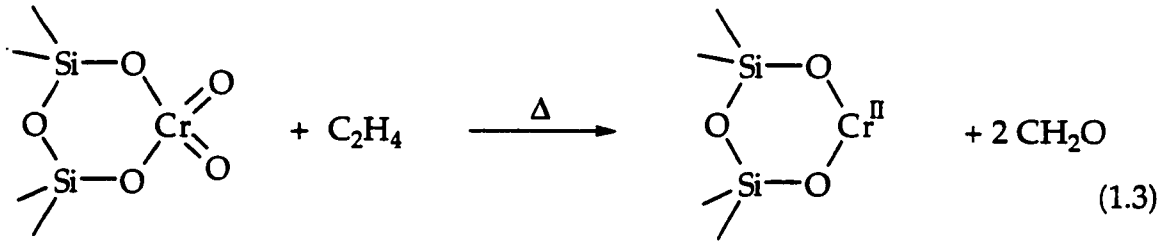

(1.3)

The catalyst is not active immediately after introduction of ethylene into the reactor at 100°C, but undergoes a dormant period or induction time.[14] This is thought to correspond to the slow reduction of Cr(VI) to the active valence[13,22] by ethylene or to the displacement by ethylene of the oxidation products such as formaldehyde.[21] When the catalyst is prereduced at 300°C with carbon monoxide, ethylene polymerization is initiated immediately.[6]

Since the discovery of the Phillips catalyst, oxidation states from Cr(II) to Cr(V) have been proposed as the valence state of the active site.[6] The difficulty in identifying the active species stems from the simultaneous presence of several valence states of chromium and changes in valence state as a result of contact with reactant, solvent and diluent. A further complication arises from the

low concentration of active sites in the presence of much larger quantities of inert chromium.[6]

1.2.2.2 Organochromium Catalysts

A number of organochromium compounds have been synthesized and tested for olefin polymerization activity. It has been demonstrated that chromocene, Cp_2Cr (Cp = cyclopentadienyl), by itself is unreactive for ethylene polymerization. However, treatment of highly dehydroxylated silica with chromocene generates a catalyst which is very active.[23] This catalyst was discovered in the early 70's by G. Karapinka and developed by F. Karol and coworkers at Union Carbide.[24]

The Union Carbide catalyst polymerizes ethylene at low pressure and low temperatures. For slurry polymerizations at 90°C, the activity of the catalyst is proportional to ethylene pressure over the range 80-500 psi. Above 400 psi, the catalyst is so active that temperature control is difficult. The chromocene catalyst does not require any preactivation treatment to induce ethylene polymerization activity.[24]

The reaction of the organometallic complex with hydroxyl groups on the silica surface results in loss of a cyclopentadienyl ligand and formation of surface-bound CpCr(II) fragments,[24] eq 1.4.

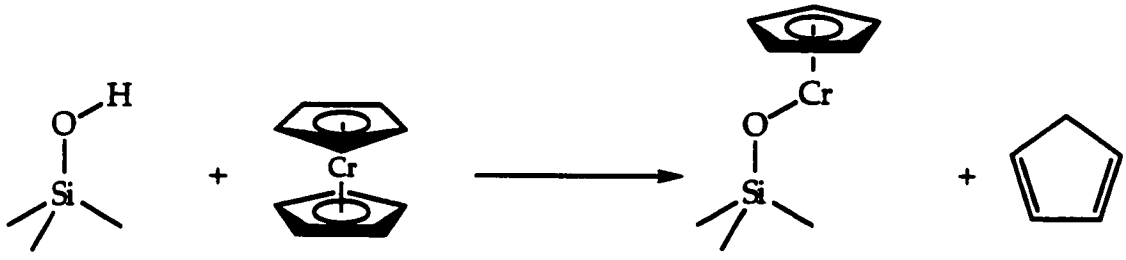

(1.4)

The remaining cyclopentadienyl ligands do not initiate polymer chain growth; rather, they remain coordinated to chromium during catalysis.[24,25]

The valence of the deposited chromium species was measured by polarography[23] after hydrolysis. These experiments indicated that 96% of the recovered chromium was in the divalent state. However, careful studies of these catalysts concluded that the catalytically active sites represent a very small fraction (<1%) of the surface-bound chromium.[26] Thus, whatever analytical or spectroscopic information is available probably pertains to inactive chromium species.

1.2.3 Catalyst Comparisons

The kind of high density polyethylene produced depends on the nature of the catalyst. A comparison of the activity, polymer molecular weight and hydrogen response of the Phillips catalyst, Union Carbide catalyst and a Ziegler-Natta catalyst is shown in Table 1.1.

The Union Carbide catalyst and the Phillips catalyst have in common high activity in the absence of cocatalyst.[24] Ziegler-Natta catalysts have even higher activities but require a cocatalyst.[12]

The polymers obtained from all of these catalysts are highly linear. Their molecular weights are relatively low for the Phillips catalyst, and extremely high for the Union Carbide catalyst[27] and Ziegler-Natta catalysts.[12] The molecular weight distribution is broader for the Phillips catalyst than is generally obtained from Ziegler-Natta catalysts, for which molecular weight distributions are less than 3.[6] This is thought to be a consequence of the existence of a variety of active sites on the Phillips catalyst. For the Union Carbide catalyst, the molecular weight distribution is much narrower, and close to that produced by Ziegler-Natta catalysts.[28]

Table 1.1 Comparison of three catalysts for ethylene polymerization

	Phillips catalyst[14] CrO_3/SiO_2	Union Carbide catalyst[27] Cp_2Cr/SiO_2	Ziegler-Natta catalyst[29] $TiCl_3/(C_2H_5)_2AlCl$
Typical activity g PE/ g cat/ hr/ atm C_2H_4	5000	2500	6000
Cocatalyst	no	no	yes
H_2 response	+	++++	+
Average molecular weight	300 000	4 000 000	2 000 000
Molecular weight distribution	18	5	3
Copolymerization of α-olefins	-	----	++

The chromocene catalyst under slurry conditions has the unique feature of very high chain-transfer response to hydrogen. This property allows fine control over the molecular weight of the resulting polymer.[24] The sensitivity of the catalyst to hydrogen transfer also leads to a highly saturated polymer, whereas the Ziegler-Natta and chromium trioxide on silica catalysts form polymers with significant terminal unsaturation.[13,30]

The Phillips catalyst has a high selectivity for ethylene and other α-olefins. It can also copolymerize ethylene with other comonomers. The chromocene catalyst exhibits high selectivity for ethylene over propylene, and no copolymerization is observed.

1.3 Proposed Mechanism of Initiation of Ethylene Polymerization by Supported Chromium Catalysts

The mechanism of polymerization of ethylene by supported chromium catalysts has been extensively studied. The overall reaction pathway is described in three separate stages: initiation, propagation and chain termination.[6] The initiation step encompasses the coordination of the very first monomer to the active site and the formation of one or more Cr-C σ-bonds. Subsequent monomers insert during propagation to form a growing alkyl chain bound to chromium. Termination involves the elimination of the polymer chain from the chromium center.

The initiation step for ethylene polymerization by reduced Cr/SiO_2 catalysts is poorly understood. In particular, the mechanism of incorporation of the first ethylene remains controversial. It has been studied mainly by infrared spectroscopy.[31-38] Hogan[13] suggested that polymerization is initiated by monomer insertion into an (unobservable) Cr-H bond. Some groups have suggested that surface silanols provide the source of hydrogen atoms.[33,39] Protonation of supported chromous ions would generate the needed Cr-H bond into which the first ethylene can insert, Scheme 1.1.[39] Alternatively, it has been suggested that ethylene adsorption occurs directly on the surface silanol, followed by coordination to an adjacent chromium ion concurrent with migration of the silanol proton to the metal center, Scheme 1.2.[33] However, mechanisms involving silanols are considered by some to be unlikely, since excellent catalysts can be obtained using highly dehydroxylated supports.[6]

Metallacycle or carbene mechanisms avoid the necessity of a source of additional hydrogen atoms.[32] For example, two ethylene molecules coordinated to the same chromium center can cyclize to form a metallacyclopentane species,

Scheme 1.1 Protonation of silica-supported chromous ions to initiate ethylene polymerization[39]

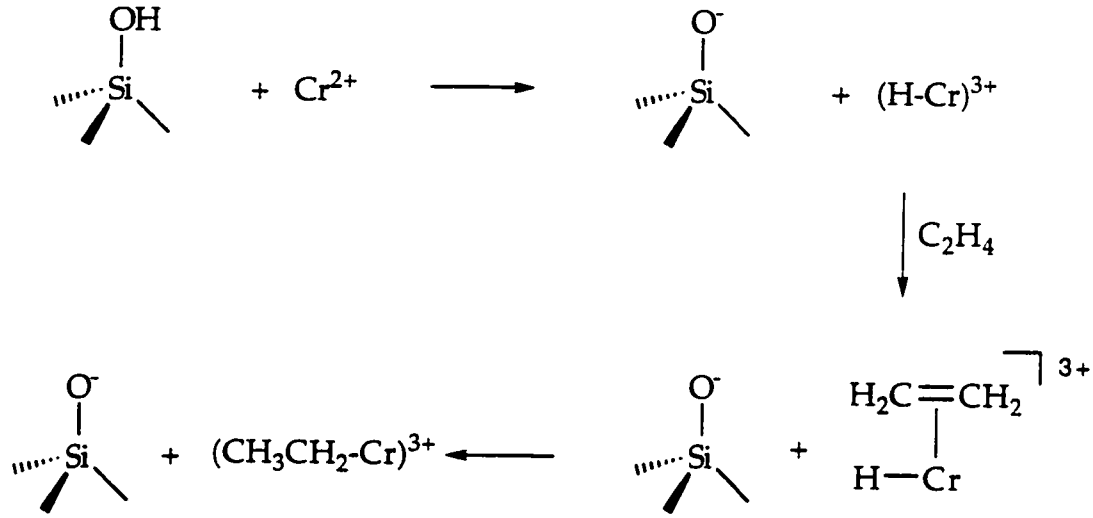

Scheme 1.2 Ethylene-induced migration of silanol protons to chromium[33]

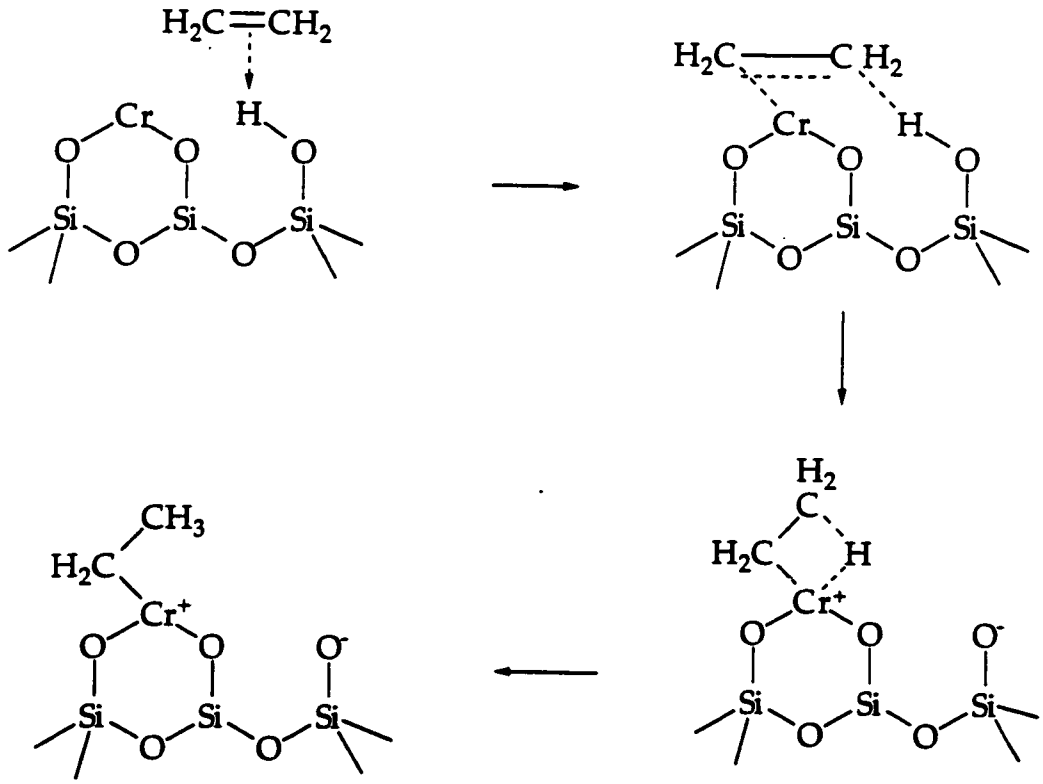

Scheme 1.3, fate a.[32] Repeated ethylene insertions into the metallacycle have been suggested as propagation steps which create a polymer chain with no endgroups.[32]

The metallacyclopentane can undergo β-H elimination to generate a homoallylic species, Scheme 1.3, fate a'.[6] Chain growth may then proceed by the Cossee mechanism, with insertion at either the chromium-alkyl bond or the Cr-H bond. Another possibility is formation of a (vinyl)Cr hydride through the dissociative adsorption of ethylene, Scheme 1.3, fate b.[38]

Scheme 1.3 Metallacyclopentane/metal carbene mechanisms for initiation of polymerization[41]

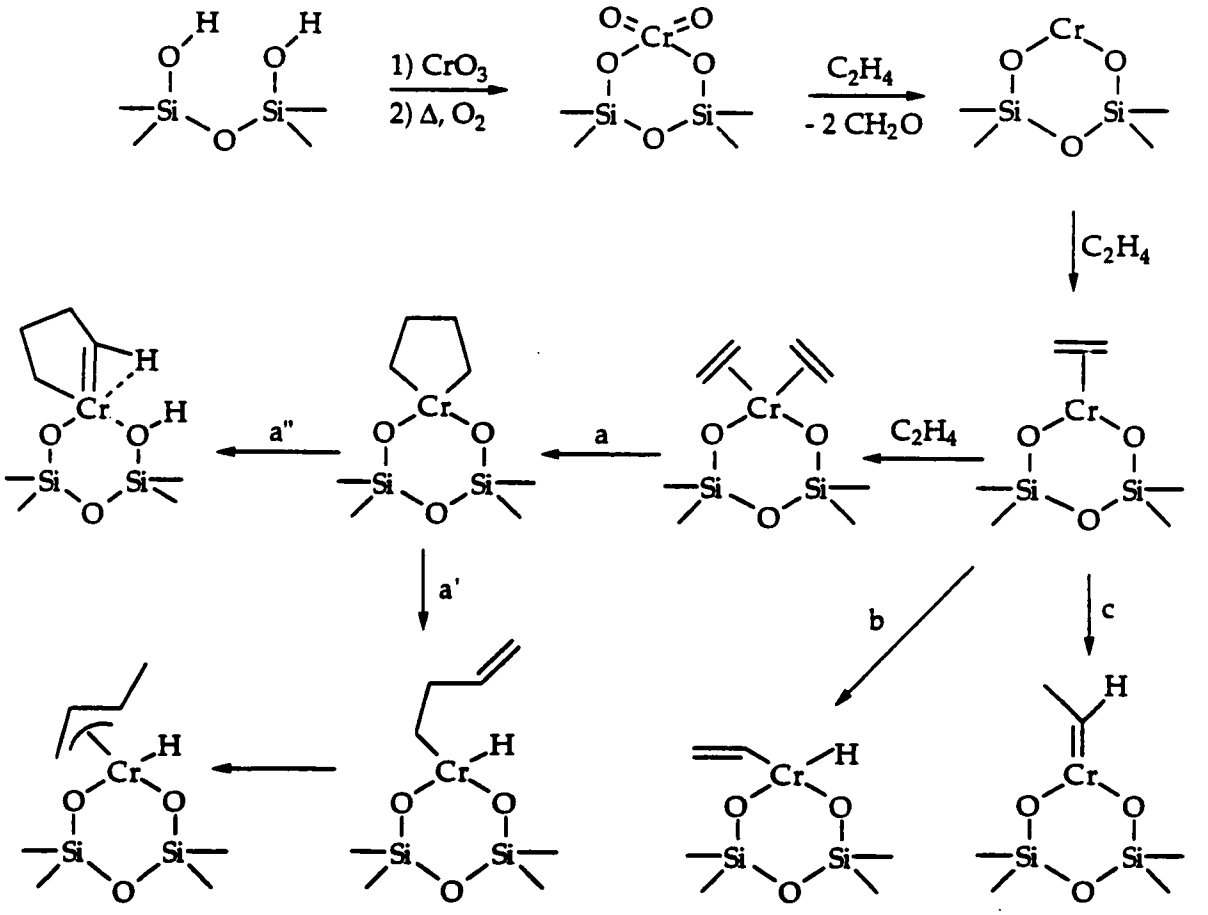

Alternately, the metallacyclopentane species could undergo α-hydrogen elimination onto an oxygen atom linking the chromium to the support to generate a metallacyclocarbene, fate a".[32] More recently, it has been suggested that adsorption of ethylene onto a chromium site may occur to form a terminal carbene via rearrangement of the π-complex, Scheme 1.3, fate c.[34] Carbenes are thought to polymerize ethylene via a Green-Rooney mechanism.[34]

Yet another suggestion for the initiation step is the generation of alkylidene species via dissociative chemisorption of ethylene onto adjacent chromium sites, Scheme 1.4.[38]

Scheme 1.4 Metal carbene/metallacycle mechanism on adjacent active sites[38]

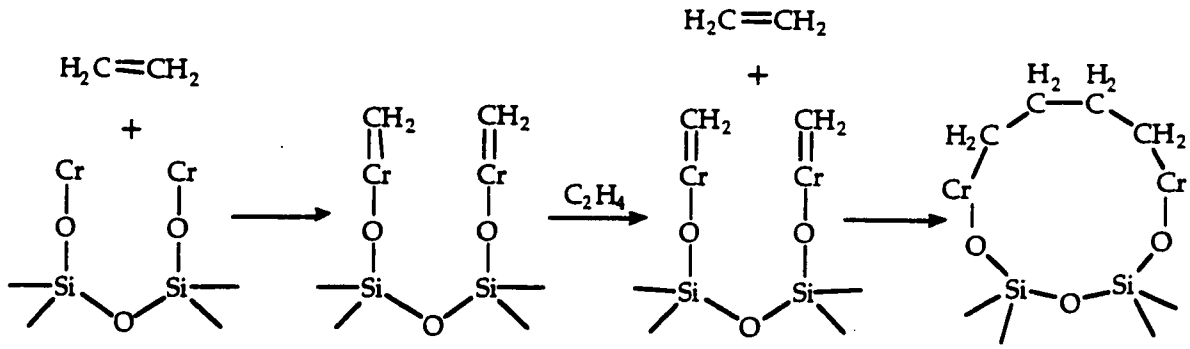

The subsequent reaction with ethylene was suggested to form a bridge between the two chromium sites.

Despite many investigations and much effort, little is known with certainty about the mechanism of polymerization by supported chromium catalysts. After more than three decades of intense scrutiny, there are still many conflicting ideas regarding the structure, valence and mechanism of formation of the active site. Even the oxidation state of the active chromium is still debated.[6] The same questions arise about the mechanism of initiation, the structure and the valence

of the active site in the Union Carbide catalyst. It is not at all obvious how silica-supported chromocene might initiate the polymerization of ethylene, because it lacks an alkyl or hydride ligand to undergo the first migratory insertion of olefin.

1.4 Homogeneous Model Systems for Ethylene Polymerization Catalysts

A major obstacle to better mechanistic understanding is the scarcity of well-defined model systems for chromium-based heterogeneous catalysts.[3] The creation of a single-site catalyst would be an important contribution to the field. In this light, some researchers have undertaken to prepare soluble models of supported chromium catalysts which polymerize ethylene.

Karol et al.[40] prepared the first molecular compounds which were thought to be models of the Union Carbide catalyst. They reported that the reactions of chromocene with alcohols and silanols yield exclusively dimeric monocyclopentadienyl chromium alkoxides, eq 1.5.

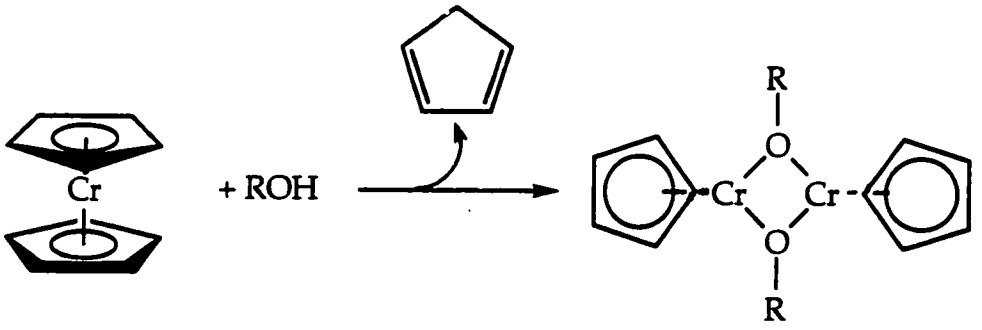

(1.5)

These dimeric complexes do not show any catalytic activity for ethylene polymerization under the typical conditions used for the Union Carbide catalyst. However, the addition of alkylsilanes such as $CH_3(CH_2)_4SiH_3$ to these chromium compounds lead to active catalysts. The polymerization behavior of these activated materials resembles that of the supported chromocene catalyst.

In order to investigate features of ethylene polymerization by the Union Carbide catalyst, Theopold and co-workers have explored the reactivity of cyclopentadienyl chromium alkyls in the +II and +III oxidation states.[41] Their first success was the discovery of $[C_5Me_5Cr(THF)_2Me]BPh_4$ (THF = tetrahydrofuran),[42,43] which polymerizes ethylene at 20°C and 1 atm, eq 1.6. Such compounds were claimed to be close models of the active site for the heterogeneous catalyst. Other chromium(III) alkyls, such as $[\eta_5\text{-}Me_4C_5SiMe_2\text{-}\eta_1\text{-}N^tBu]CrCH_2SiMe_3$[44] are also able to polymerize ethylene.

$$C_2H_4 \xrightarrow[20°C,\ 1\ atm]{cat} \text{polyethylene} \qquad (1.6)$$

cat =

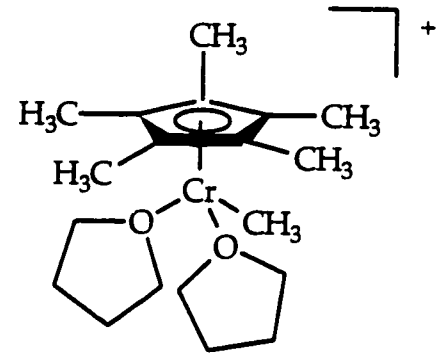

In contrast, monocyclopentadienyl chromium(II) alkyls are poor polymerization catalysts.[45] Theopold concluded that Cr(III) is a more likely oxidation state for the active site than Cr(II).

Carrick *et al.*[21] attempted to model the Phillips catalyst in homogeneous solution. A cyclohexane solution of bis(triphenylsilyl)chromate catalyzed the polymerization of ethylene at T > 130°C and pressures from 350 - 15 000 atm, eq 1.7, in the absence of cocatalyst. Addition of an aluminum alkyl caused reduction of chromium and onset of ethylene polymerization at room temperature and atmospheric pressure.

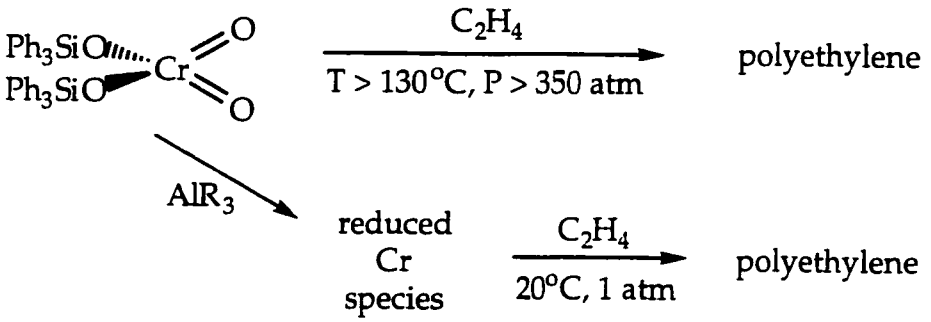

(1.7)

Feher *et al.*[46] prepared a chromium ester of a silasesquioxane. This is probably the best available structural model of the oxidized Phillips catalyst. Addition of two equivalents of $AlMe_3$ to benzene solutions of this compound produced dark orange solutions which polymerized ethylene under mild conditions (20°C, 1 atm), eq 1.8. However no further information about the oxidation state or chemical nature of the active catalyst in this system was reported.

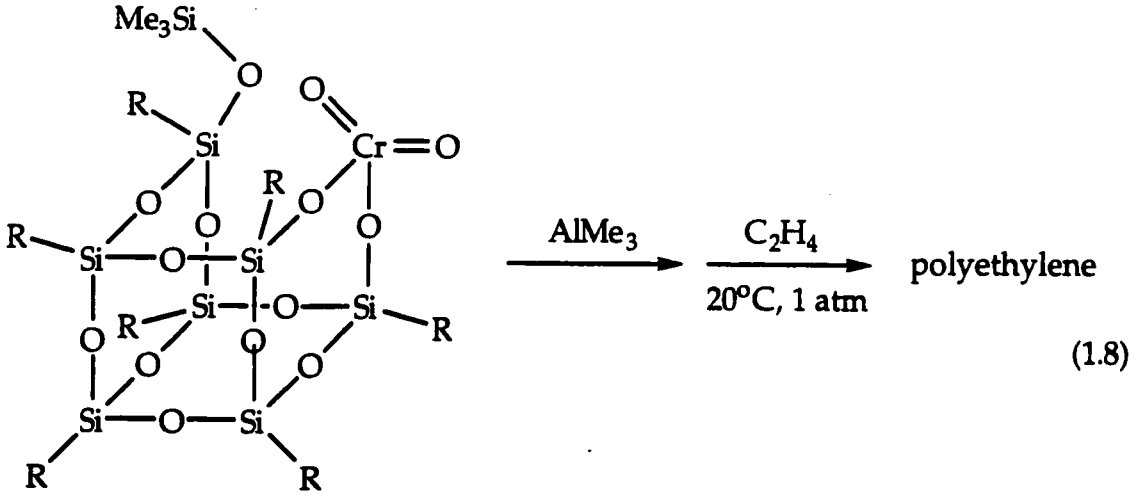

(1.8)

Until recently, it was considered firmly established that the active site of the Phillips catalyst must contain chromium in a highly reduced state; while the exact oxidation state of the metal remained unproven, it was widely believed to be +II. Krauss and Stach[47] showed that silica-supported chromium can be quantitatively

reduced with carbon monoxide to Cr(II), and the resulting material is indistinguishable in its polymerization behavior from the Phillips catalyst. It was surprising, then, when Gibson and Coles[48] reported a highly active homogeneous catalyst derived from a bis(imido)chromium(VI) precursor, eq 1.9. While the active species in this system has not yet been structurally characterized, the spectroscopic evidence consistent with a cationic bis(imido)chromium(VI) alkyl.

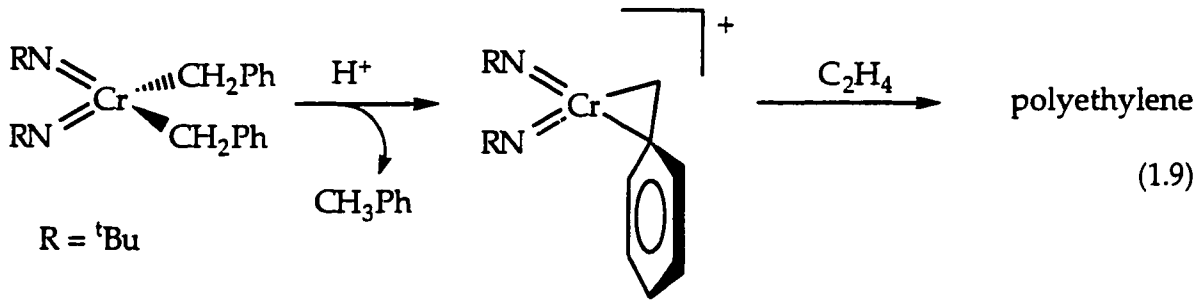

(1.9)

One of the pitfalls in modeling heterogeneous chemistry with soluble model complexes is caused by the assumption that the oxide support is inert. Since there is a strong Cr-silica interaction in these systems, this assumption is probably not well-founded. Another approach to creating well-defined models is to use the surface of silica itself as part of the ligand complement of the metal. In the rest of this chapter, the feasibility of this approch will be established.

1.5 Surface Chemistry of Silica

Amorphous silicas are used in many technologies such as mineral processing, ceramics and adsorbents.[49] Silica is also an oxide widely used in catalysis. Its surface is composed of relatively unreactive siloxanes, ≡SiOSi≡, and a variety of hydroxyl sites. The number and kind of surface hydroxyl groups determines the physicochemical properties of these materials. Lewis acid/base

sites are absent unless the silica is activated at very high temperatures,[50] and Bronsted acidity is low.[51]

Silica is by far the most studied oxide. Most spectroscopic studies have been carried out on pyrogenic silicas, which are amorphous, high surface area and high purity materials. Therefore we chose to use a fumed silica from Degussa, trade-name Aerosil™. This silica is prepared at high temperature by flame hydrolysis of silicon tetrachloride (see chapter 2). It is non-porous, and is readily pressed into optically transparent self-supporting discs for transmission IR studies. The number of silanol groups on a fully hydrated silica surface has been found to be about 4.9/nm^2 regardless of the type of silica used.

Thermal treatment of silica under vacuum leads to the elimination of physisorbed water, then condensation of hydroxyl groups with concomitant formation of siloxane bridges,[52] eq 1.10.

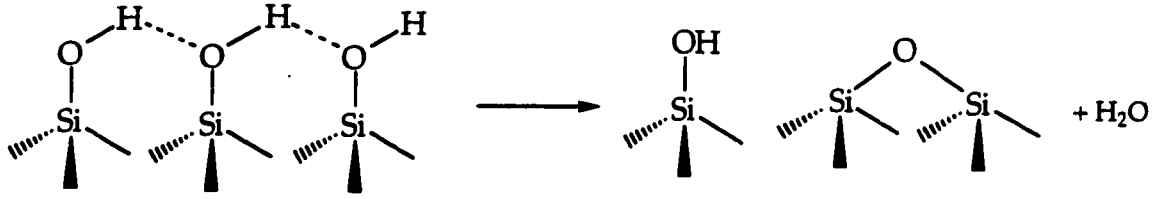

(1.10)

Two IR spectral changes accompany this reaction: the peak due to isolated silanols increases in intensity and becomes more symmetrical, while the peak due to the hydrogen-bonded pairs of hydroxyl groups decreases, Figure 1.2. The increase in intensity of the IR vibration due to isolated silanols during the initial stages of partial dehydroxylation results from the condensation of pairs of silanols in the hydrogen-bonded network.

After activation of the silica at 450°C under dynamic vacuum, the silanol density drops to 1.2-1.5/nm^2.[53] However if the silica is dehydroxylated at 200°C, the density of the hydroxyls groups is 2.6/nm^2.[53] This partial dehydroxylation leads to

three types of hydroxyl groups: geminal, vicinal and isolated, Figure 1.1. Vicinal and geminal hydroxyl groups cannot undergo internal condensation.

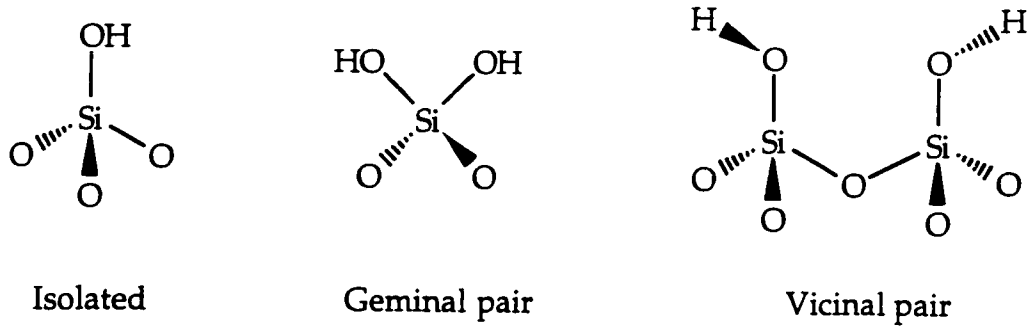

Isolated Geminal pair Vicinal pair

Figure 1.1 Types of hydroxyl groups on the silica surface

Since dehydration and rehydration processes reflect basic underlying features of the organization of hydroxyl sites on the silica surface, the study of such phenomena plays an central role in the description of surface structure.

Various crystal faces of quartz, β-cristobalite and β-tridymite have been suggested as models for the amorphous silica surface,[54-57] which has been described as a heterogeneous assortment of small crystalline domains, resembling these different crystal faces.

In 1958, DeBoer and Vleeskins[54] suggested a model for the silica surface based on the (111) face of β-cristobalite or similar faces of β-tridymite, as represented in Figure 1.3. The hydroxyl groups on this surface are separated by about 5 Å and are arranged in a hexagonal array, which corresponds to a silanol density of silanols of 4.55/100 Å^2. This value is close to the experimental value of 4.6 found in dehydration/rehydration studies of various silica gels by the same authors.[54]

The mechanism for dehydration and rehydration of the silica surface was also discussed by Hockey.[55] He postulated that the hydroxyl groups on untreated silicas arise from the presence of defects in the lattice structure. These defects

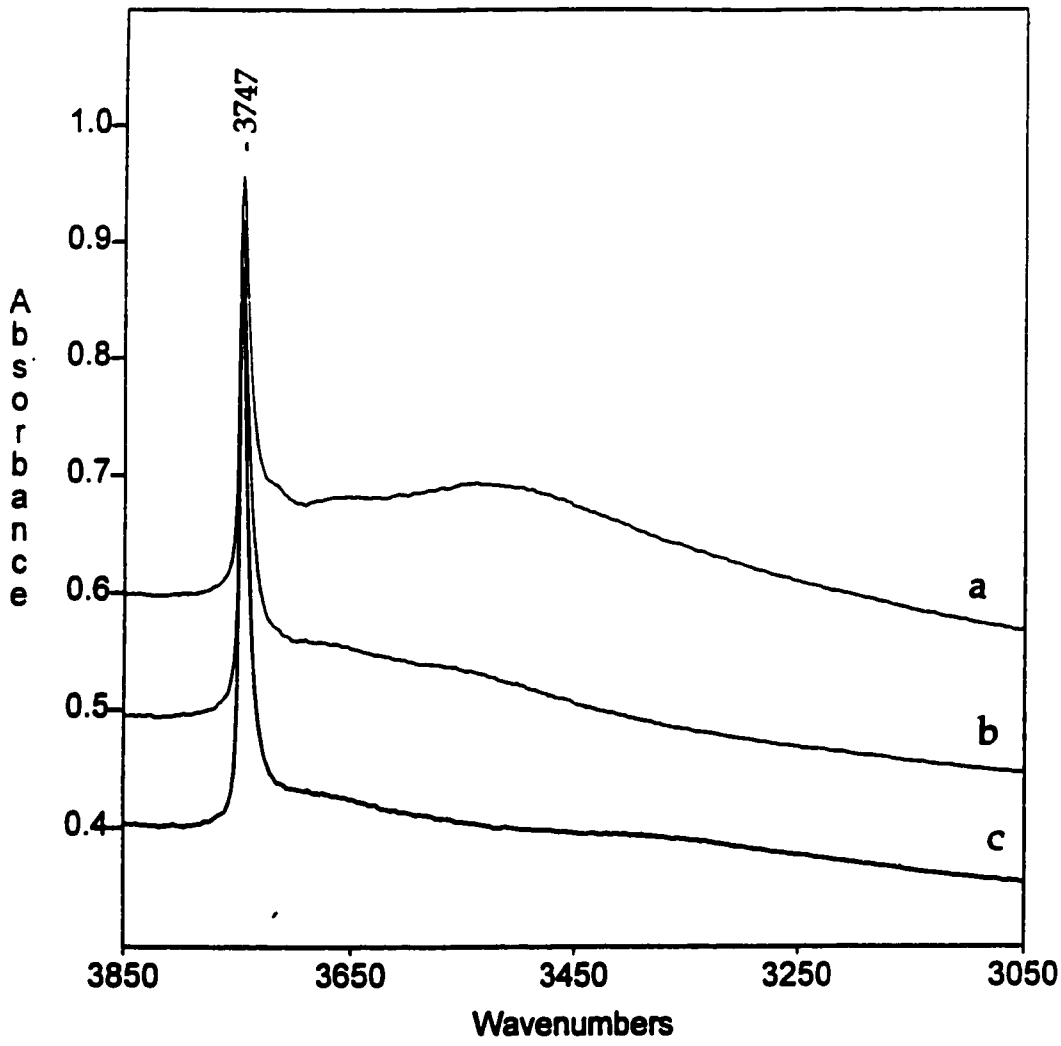

Figure 1.2 Infrared spectra of self-supporting disks of silica showing the effect of temperature on the hydroxyl group distribution. (a) Silica-25, (b) silica-200 and (c) silica-500, where the appended number indicates the temperature of activation in °C.

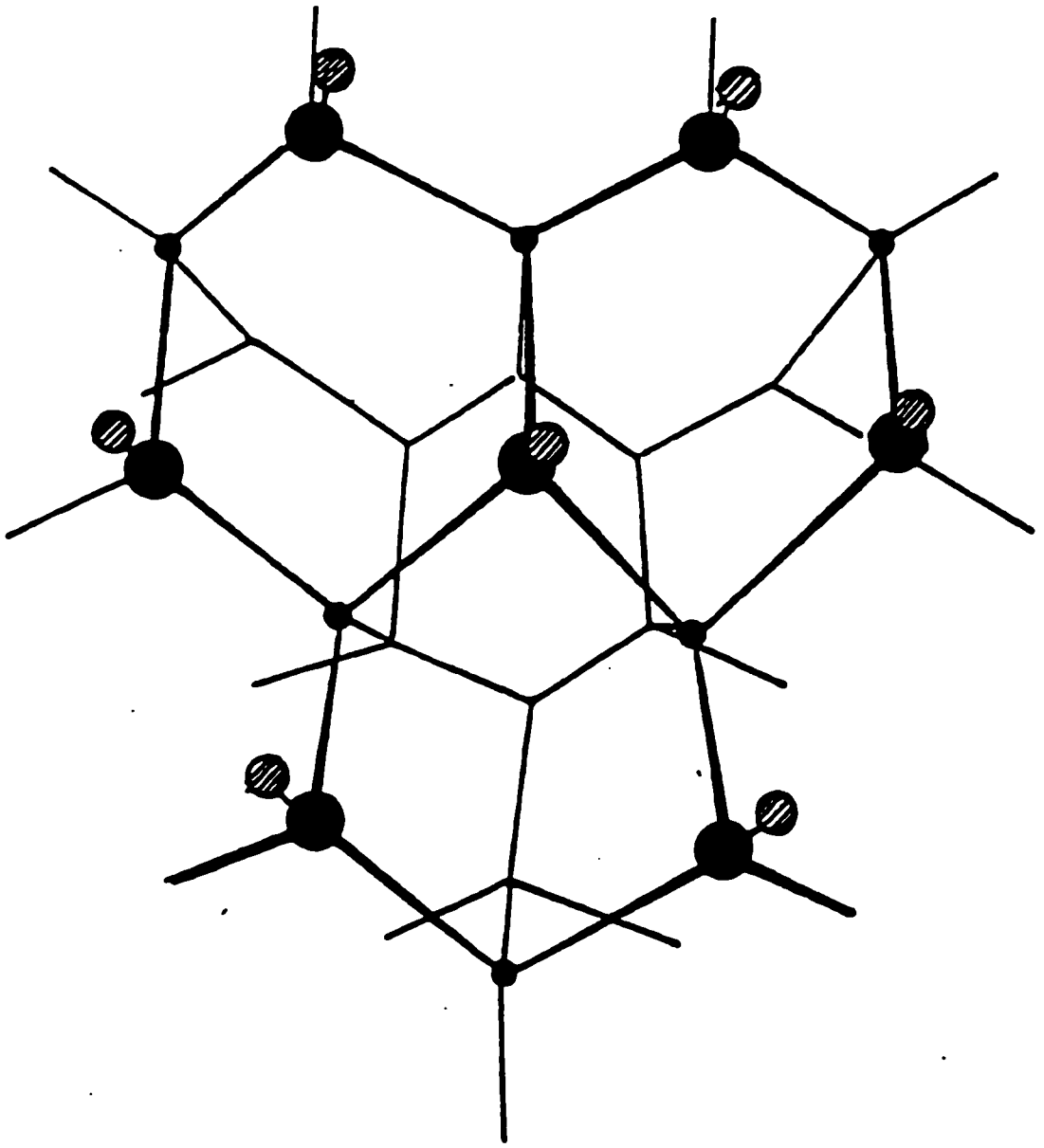

Figure 1.3 Model of the (111) face of β-cristobalite proposed by DeBoer and Vleeskins showing the arrangement of surface hydroxyls. Large black circles indicate surface silicon atoms, small hatched circles indicate hydroxyl groups.[54]

occur on the surface, giving rise to geminal and isolated hydroxyl groups. Because of their relatively close proximity, hydroxyls on such defect surfaces may condense at moderate temperatures (about 450°C), resulting in the β-cristobalite structure.

The DeBoer-Vleeskins model, in conjunction with the lattice-defect mechanism of Hockey, has a number of difficulties. Studies indicate that some surface hydroxyls are present as pairs even after being heated above 450°C. This is inconsistent with the geometry of the (111) face of β-cristobalite. Reducing the hydroxyl density below 4.55/100 $Å^2$ is impossible, according to the model, due to the constraints imposed by the underlying lattice. Nevertheless, silica surfaces are capable of supporting a hydroxyl group density of less than 1.0/100 $Å^2$, with little decrease in overall surface area.

In 1968, Peri and Hensley[56] proposed a surface model that eliminates some of the inadequacies of the DeBoer-Vleeskins model and predicts the existence of paired hydroxyl groups at all levels of dehydration of the silica surface. They proposed that the amorphous silica surface is similar to the (100) face of β-cristobalite. Each surface silicon atom supports a geminal pair of hydroxyl groups, located in rows, Figure 1.4a. According to the Peri-Hensley model, the process of dehydration first involves the random condensation of hydroxyl groups in the same row, Figure 1.4b. The density of the hydroxyl groups on the silica surface after dehydration is then 4.56/100 $Å^2$.

According to the Peri-Hensley model, only paired hydroxyl groups remain on the surface after dehydration. Isolated hydroxyl groups are not predicted by the model. In Figure 1.4b, geminal pairs (sites 1) and vicinal pairs (sites 2) are illustrated. Further dehydration of the surface involves the condensation of vicinal pairs, generating sites where two SiO_4 tetrahedra are connected by an edge. Peri and Hensley calculated the maximum hydroxyl concentration on the surface

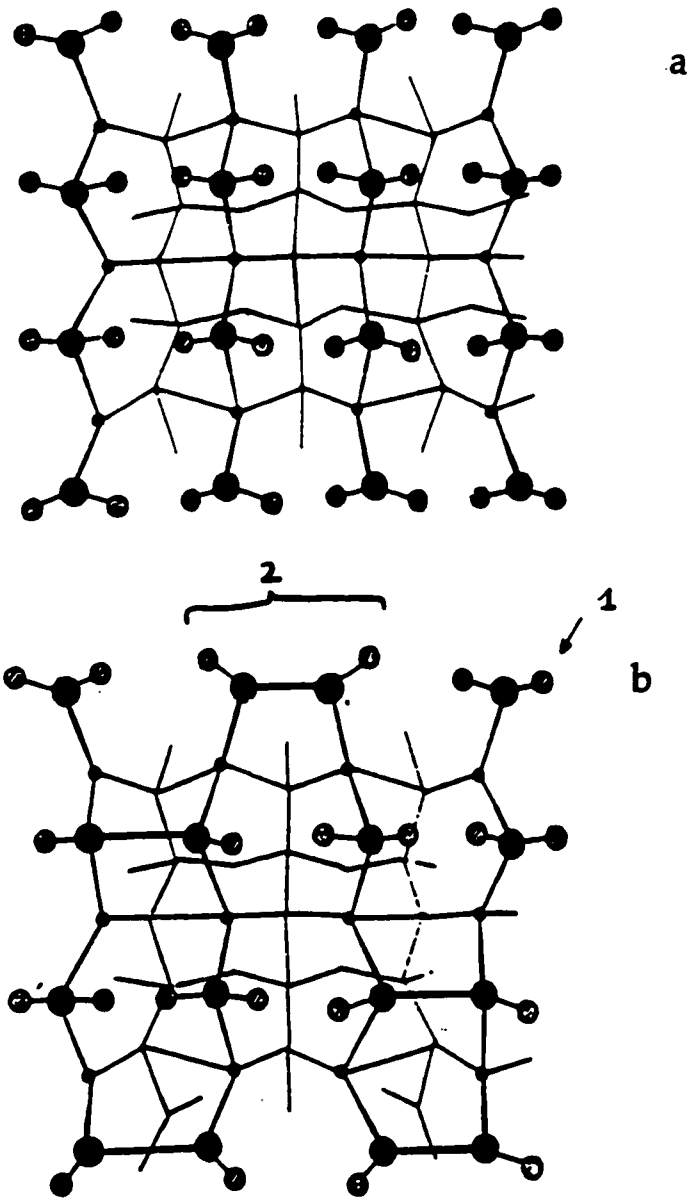

Figure 1.4 Surface geometry of the (100) face of β-cristobalite, (a) completely hydrated; (b) following partial dehydration. Large circles indicate surface silicon atoms, small circles indicate hydroxyl groups.[56]

at high temperature to be 1.2 /100 Å^2, leaving only geminal hydroxyl groups. The condensation of the hydroxyl groups within geminal pairs to form Si=O sites is not likely based on known silicon chemistry.

Another model was postulated by Peri and Hensley in which the silica surface resembles the (111) face of β-cristobalite, but also contains randomly-distributed isolated silanols. The formation of isolated and vicinal hydroxyls, and condensation of adjacent hydroxyls, are plausible. In this model, full dehydration leads to 1.5 hydroxyl groups /100 Å^2.

In 1980, Maciel and Sindorf proposed a mixed-surface model. This model consists of hypothetical sections of (100) surface adjoining sections of (111) surface, as illustrated in Figure 1.5. The condensation of adjacent hydroxyls of geminal sites gives rise to vicinal pairs. The CP-MAS NMR spectrum of unheated silica gel is consistent with a heterogeneous silica surface consisting of separate regions resembling the (100) and (111) faces of β-critobalite, and provided the first proof that geminal hydroxyls exist in unactivated silica gels. The authors reported that the population of geminal hydroxyl groups is 15%.[58]

1.6 Surface Organometallic Chemistry

Knowledge of the mechanisms of many homogeneous catalytic reactions has grown rapidly in recent decades.[59] This phenomenon is due largely to rapid advances in molecular chemistry, especially organometallic chemistry, which has allowed the direct observation of a variety of elementary steps. In contrast, knowledge about mechanisms of reactions catalyzed by solids remains more limited; even the nature of the catalyst-reactant interaction is usually uncertain.

Surface organometallic chemistry (SOMC)[59,60] deals with the reactivity of organometallic and coordination compounds with surfaces. One of the strategies of this chemistry is to immobilize organometallic complexes on solid surfaces

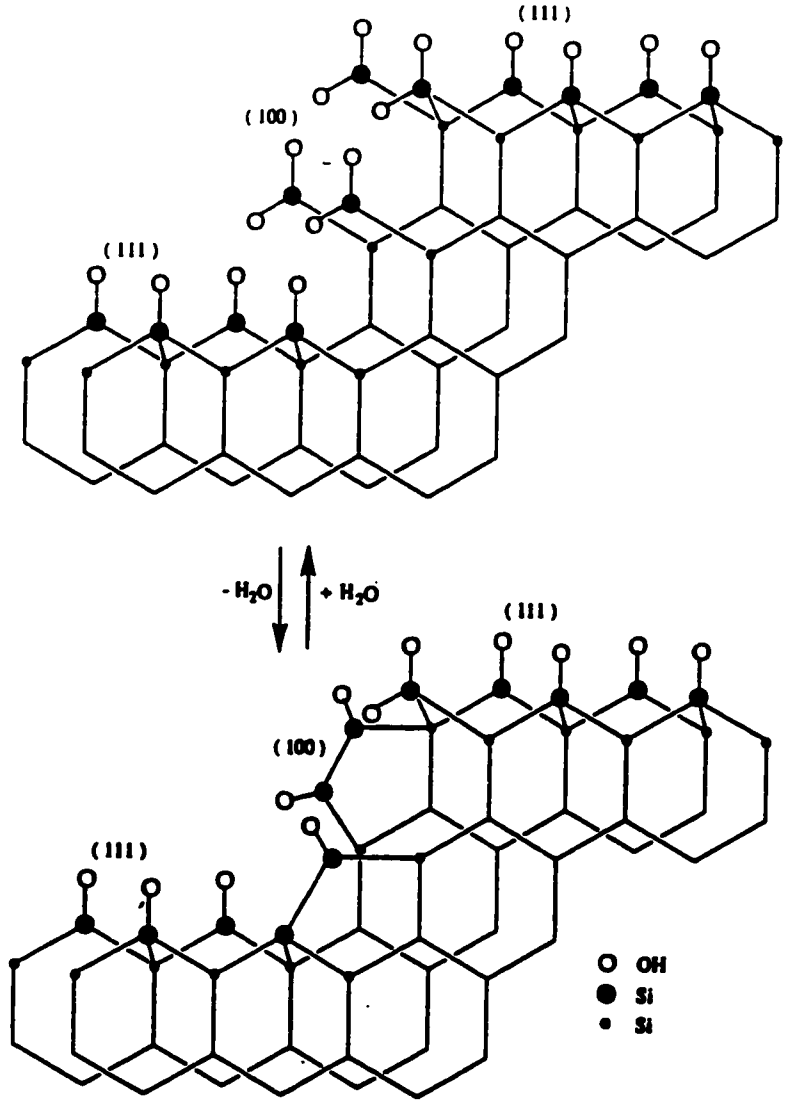

Figure 1.5 Mixed-surface model proposed by Maciel and Sindorf showing the reversible dehydration of the silica surface. (a) Original (fully hydrated) surface, and (b) partially dehydrated surface.

such as those of inorganic oxides, zeolites or metals, in order to prepare relatively well-defined surface species as models for heterogeneous catalysts.[59] SOMC aims to define the reactivity of the first atomic layer of a surface with organometallic molecules and to control it so as to obtain no more than a monolayer of the new material. This approach governs the choice of the metal atom, its oxidation state, ancillary ligands and the reaction conditions.

The surfaces of many inorganic oxides can be treated like a multidentate ligand in molecular chemistry. The reactions which occur on the surface may be described in the same way as reactions occurring in solution. Although supported organometallic complexes macroscopically resemble heterogeneous catalysts, their relatively uniform structure, reactivity and distribution make them microscopically homogeneous in nature.

The systematic study of the reactivity of organometallic compounds with surfaces may eventually have an impact on surface catalysis rivaling that of organometallic chemistry on homogeneous catalysis.

1.7 References

1) Muzart, J. *Chem. Rev.* **1992**, *92*, 113-140.

2) Theopold, K. H. *Eur. J. Inorg. Chem.* **1998**, 15-24.

3) Theopold, K. H. *CHEMTECH* **1997**, 26-32.

4) Reisch, M. S. *Chem. Eng. News* **May 26, 1997**, 14.

5) Karol, F. J. *CHEMTECH* **1983**, *13*, 222.

6) McDaniel, M. P. *Adv. Catal.* **1985**, *33*, 47-98.

7) Ziegler, K.; Holzkamp, E.; Breil, H.; Martin, H. *Angew. Chem.* **1955**, *67*, 541.

8) Natta, G. *J. Polym. Sci.* **1960**, *48*, 219.

9) Boor Jr, J. *Ziegler-Natta Catalysts and Polymerizations*; Academic Press: New York, 1979.

10) Reich, L.; Schindler, A. *Polymerization by Organometallic Compounds*; Wiley-Interscience: New York, 1966.

11) Ketley, A. D. *The Stereochemistry of Macromolecules*; Dekker: New York, 1967.

12) Stevens, P. M. *Polymer Chemistry: An Introduction*; Oxford University Press: New york, 1990.

13) Hogan, J. P. *J. Polym. Sci.: A-1* **1970**, *8*, 2637-2652.

14) McDaniel, M. P.; Welch, M. B. *J. Catal.* **1983**, *82*, 98-109.

15) Pullukat, T. J.; Hoff, R. E.; Shida, M. *J. Appl. Polym. Sci.* **1981**, *26*, 2927.

16) Zecchina, A.; Garrone, E.; Ghiotti, G.; Morterra, C.; Borello, E. *J. Phys. Chem.* **1975**, *79*, 966.

17) Krauss, H. L.; Hums, E. *Z. Naturforsch* **1979**, *34B*, 1628.

18) McDaniel, M. P. *J. Catal.* **1981**, *67*, 71.

19) Rebensdorf, B.; Larsson, R. *J. Mol. Catal.* **1981**, *11*, 247.

20) McDaniel, M. P. *J. Catal.* **1982**, *76*, 17-28.

21) Baker, L. M.; Carrick, W. L. *J. Org. Chem.* **1970**, *35*, 774.

22) Clark, A. *Catal. Rev.* **1970**, *3*, 145-173.

23) Carrick, W. L.; Chasar, A. G.; Smith, J. J. *J Am. Chem. Soc.* **1960**, *82*, 5319.

24) Karol, F. J.; Karapinka, G. L.; Wu, C.; Dow, A. W.; Johnson, R. N.; Carrick, W. L. *J. Polym. Sci.: A-1* **1972**, *10*, 2621-2637.

25) Karol, F. J.; Johnson, R. N. *J. Polym. Chem., Polym. Sci. Ed.* **1975**, *13*, 1607-1617.

26) Fu, S. L.; Rosynek, M. P.; Lunsford, J. H. *Langmuir* **1991**, *7*, 1179-1187.

27) Freeman, W. J.; Wilson, D. R.; Ernst, R. D.; Smith, P. D.; Klendworth, D. D.; McDaniel, M. P. *J. Polym. Sci: A, Polym. Chem.* **1987**, *25*, 2063.

28) McDaniel, M. P. *J. Polym. Sci., Polym. Chem. Ed.* **1983**, *21*, 1217.

29) Grieveson, B. M. *Makromol. Chem.* **1965**, *84*, 93.

30) Groenewege, M. P.; Schuyer, J.; Smidt, J.; Tuijnman, C. A. In *Crystalline Olefin Polymers*; Doak, R. A. V. and Doak, K. W., Eds.; Interscience: New York, 1965; pp. 771-772.

31) Ghiotti, G.; Garrone, E.; Coluccia, S.; Morterra, C.; Zecchina, A. *J. Chem. Soc., Chem. Commun.* **1979**, 1032.

32) Ghiotti, G.; Garrone, E.; Zecchina, A. *J. Mol. Catal.* **1988**, *46*, 61-77.

33) Jozwiak, W. K.; Dalla Lana, I. G.; Fiederow, R. *J. Catal.* **1990**, *121*, 183.

34) Kantcheva, M.; Lana, I. G. D.; Szymura, J. A. *J. Catal.* **1995**, *154*, 329-334.

35) Nishimura, M.; Thomas, J. M. *Catal. Lett.* **1993**, *19*, 33.

36) Vikulov, K.; Spoto, G.; Coluccia, S.; Zecchina, A. *Catal. Lett.* **1992**, *16*, 117.

37) Zecchina, A.; Spoto, G.; Ghiotti, G.; Garrone, E. *J. Mol. Catal.* **1994**, *86*, 423.

38) Zielinski, P.; Dalla Lana, I. G. *J. Catal.* **1992**, *137*, 368.

39) Groeneveld, C.; Wittgen, P. P. M. M.; Swimmen, H. P. M.; Wernsen, A.; Schuit, G. C. A. *J. Catal.* **1983**, *83*, 346-361.

40) Karol, F. J.; Wu, C.; Reichle, W. T.; Maraschin, N. J. *J. Catal.* **1979**, *60*, 68.

41) Richeson, D. S.; Hsu, S.-W.; Fredd, N. H.; Van Duyne, G.; Theopold, K. H. *J. Am. Chem. Soc.* **1986**, *108*, 1491.

42) Thomas, B. J.; Theopold, K. H. *J. Am. Chem. Soc.* **1988**, *110*, 5902.

43) Thomas, B. J.; Noh, S. K.; Schulte, G. K.; Sendlinger, S. C.; Theopold, K. H. *J. Am. Chem. Soc.* **1991**, *113*, 893-902.

44) Liang, Y.; Yap, G. P. A.; Rheingold, A. L.; Theopold, K. H. *Organometallics* **1996**, *15*, 5284-5286.

45) Heintz, R. A.; Ostrander, R. L.; Rheingold, A. L.; Theopold, K. H. *J. Am. Chem. Soc.* **1994**, *116*, 11387-11396.

46) Feher, F. J.; Blanski, R. L. *J. Chem. Soc. Chem. Commun.* **1990**, 1614-1616.

47) Krauss, H. L.; Stach, H. *Z. Anorg. Allg. Chem.* **1969**, *366*, 280.

48) Coles, M. P.; Dalby, C. I.; Gibson, V. C.; Clegg, W.; Elsegood, M. R. J. *J. Chem. Soc., Chem. Commun.* **1995**, 1709-1711.

49) Leonardelli, S.; Facchini, L.; Fretigny, C.; Tougne, P.; Legrand, A. P. *J. Am. Chem. Soc.* **1992**, *114*, 6412-6418.

50) Morrow, B. A.; Cody, I. A. *J. Phys. Chem.* **1976**, *80*, 1976.

51) Child, M. J.; Heywood, M. J.; Yong, G. H.; Rochester, C. H. *J. Chem. Soc. Faraday Trans. I* **1982**, *78*, 2005.

52) McDonald, R. S. *J. Phys. Chem.* **1958**, *62*, 1168.

53) Morrow, B. A. In *Stud. Surf. Sci. Catal.*, 1990; Vol. 57A, pp. 161-224.

54) DeBoer, J. H.; Vleeskins, J. M. *Proc. K. Ned. Akad. Wet.* **1958**, *B61*, 85-93.

55) Hockey, J. A. *Chem. Ind. (London)* **1965**, 57-63.

56) Peri, J. B.; Hensley, A. L., Jr. *J. Phys. Chem.* **1968**, *72*, 2926-2933.

57) Boehm, H. P. *Adv. Catal.* **1966**, *16*, 179-274.

58) Sindorf, D. W.; Maciel, G. E. *J. Am. Chem. Soc.* **1983**, *105*, 1487-1493.

59) Basset, J. M.; Gates, B. C.; Candy, J.-P.; Choplin, A.; Leconte, M.; Quignard, F.; Santini, C. *Surface Organometallic Chemistry: Molecular Approaches to Surface Catalysis*; Kluwer: Dordrecht, 1988.

60) Basset, J. M.; Choplin, J. *J. Mol. Catal.* **1985**, *21*, 95.

Chapter 2

Experimental Techniques

2.1 Reagents

2.1.1 Solid Support for Surface Metal Complexes

A nonporous pyrogenic silica (Degussa Aerosil™-200) was used as the oxide support in all experiments. This silica is produced by flame hydrolysis of $SiCl_4$,[1] eqs 2.1 and 2.2, and has a surface area of 200 m^2/g.

$$SiCl_4 + O_2 \rightarrow SiO_2 + 2\,Cl_2 \quad (2.1)$$

$$2\,H_2O + 2\,Cl_2 \rightarrow 4\,HCl + O_2 \quad (2.2)$$

This method produces high purity, amorphous SiO_2.

2.1.2 Gases

CD_2CD_2 (98% D), D_2 (99% D) and DCl (98% D) (Cambridge Isotopes), NO, CH_2CH_2, propene and HCl (Matheson Gas Products), CO, O_2, H_2 (Air Products) were either purchased in glass bulbs or transferred into glass bulbs prior to use. A known pressure of the desired gas was transferred into the reactors through a high vacuum line equipped with a Baratron capacitance manometer. Gases such as CD_2CD_2, CH_2CH_2, H_2, D_2, NO and CO were first passed through a trap containing a mixture of BTS Deoxo Catalyst (Caledon Laboratories Ltd.) and 3 Å molecular sieves (Aldrich) to remove any oxygen and water present. The trap was previously activated under a flow of H_2 at 200°C for 4 hours, followed by heating at 150°C under dynamic vacuum for 2 hours in order to remove H_2O. O_2 was passed through a trap containing only 3 Å molecular sieves to remove traces of water. HCl and DCl were used as received. DCl was stored in a reactor with a high

vacuum Teflon stopcock (Young Glass), and was transferred into the experimental reactors via predeuterated glass lines greased with perfluorinated Krytox. (To deuterate glass lines, 10 Torr DCl were charged into the vacuum system for 10 min, followed by dynamic vacuum. This operation was repeated once or twice. This procedure is necessary because DCl reacts with both glass and hydrocarbon-based greases, where it undergoes H/D exchange. This makes quantitative experiments inexact.)

2.1.3 Commercial Liquids, Solid Reagents and Solvents

Liquids used as reagents were purchased in the highest purity commercially available. Acetone, norbornene, 1-hexene, cyclohexene, cyclopentene, ^{t}BuOH, allylic alcohol, benzylic alcohol and neopentyl alcohol (Aldrich) were dried by stirring over CaH_2 (Aldrich) at room temperature, followed by fractional distillation under N_2, and were stored under N_2 in glass reactors equipped with high vacuum stopcocks and containing 3 Å molecular sieves. ^{t}Bu-d_9-OD (99% D, Aldrich) was stored under N_2 in a glass reactor over molecular sieves. Styrene (Aldrich) was distilled under reduced pressure from CaH_2 and stored in a glass reactor over molecular sieves. D_2O (98% D, Cambridge Isotopes) was used as received. Before use, each liquid reagent was subjected to several freeze-pump-thaw cycles in order to remove dissolved gases, then was introduced into the experimental reactor vessel via the gas phase through a high vacuum manifold. $(CH_3)_3CCOCl$ (98%, Aldrich) was distilled under reduced pressure immediately prior to use. Br_2 (99.99%, Aldrich) was used as received. $(CH_3)_3SiCH_2MgCl$ (1 M in diethylether, Aldrich), and neopentyl bromide (98%, Aldrich) were used as received.

The solids PPh_3, $LiAlD_4$, $LiNEt_2$, $CrCl_3$·3THF and anhydrous $CrCl_3$ (Aldrich) were used as received. Mg (Aldrich) was oven-dried at 150°C for 24 hours before

use. $(CH_3)_3SiOH$ vapor was prepared immediately before use in a Schlenk tube containing powdered $(CH_3)_3SiONa$ (Aldrich). 1.3 Torr HCl was added and the Schlenk tube was shaken.

The solvents used for the different chromium(IV) complex syntheses, such as diethylether, THF, pentane, benzene and dimethylformamide, were distilled immediately prior to use over sodium/benzophenone or sodium-potassium alloy/benzophenone.

2.1.4 Molecular Chromium Complexes

All manipulations involving air sensitive organometallic compounds were carried out on a Schlenk vacuum line with a base pressure of 20 mTorr, under an inert atmosphere of N_2.

2.1.4.1 Tetraalkylchromium(IV) Complexes

The molecular complexes $Cr(CH_2C(CH_3)_3)_4$, **1a**, $Cr(CD_2C(CH_3)_3)_4$, **1-α-D_4**, and $Cr(CH_2Si(CH_3)_3)_4$, **1b**, were synthesized from $CrCl_3$·3THF and their corresponding Grignard reagents: $(CH_3)_3CCH_2MgBr$ for **1a**, $(CH_3)_3CCD_2MgBr$ for **1-α-D_4**, and $(CH_3)_3SiCH_2MgCl$ for **1b**, eq 2.3.[2,3]

$$2\ CrCl_3{\cdot}3THF + 6\ RMgX \rightarrow CrR_4 + CrR_2 + 6\ MgXCl + 6\ THF \qquad (2.3)$$

1a	$R = CH_2C(CH_3)_3$, X = Br
1-α-D_4	$R = CD_2C(CH_3)_3$, X = Br
1b	$R = CH_2Si(CH_3)_3$, X = Cl

All CrR_4 complexes in this work are paramagnetic and do not give useful NMR spectra.

2.1.4.1.1 $Cr(CH_2C(CH_3)_3)_4$

* *Synthesis of* $(CH_3)_3CCH_2MgBr$. A 500 mL 3-necked flask, equipped with a 20 mL dropping funnel, a condenser, and with two entrance ports for N_2 (one on top of the condenser), was charged with Mg (1.9 g, 79.4 mmol) and purged with three cycles of vacuum/N_2. Under N_2, 40 mL of diethylether were added, and the mixture was stirred at room temperature. Neopentyl bromide (10 g, 66.2 mmol) was added dropwise via the dropping funnel to the colorless solution. The initiation of the Grignard reaction was judged by the appearance of a light green-gray color, which became darker as the addition of NpBr proceeded. The dark green solution was refluxed for 16 hours, when maximum consumption of the magnesium was attained. The Grignard reagent NpMgBr in ether (51 mL), thus obtained, was transferred via cannula into a Schlenk tube, and stored under N_2 at -18°C.

The concentration of NpMgBr in diethylether was determined as follows. To a 50 mL Schlenk tube under N_2, 1 mL of NpMgBr in ether was introduced, then treated with an excess of HCl (15 mL, 0.1 M). The mixture was back-titrated with a solution of NaOH (3.4 mL, 0.1 M) to give a concentration of NpMgBr of 1.16 M in diethylether. Given the total volume of the Grignard solution, the yield of NpMgBr was calculated to be 89%.

* *Synthesis of* $Cr(CH_2C(CH_3)_3)_4$. $CrCl_3$·3THF (2.1 g, 5.6 mmol) was introduced to a 200 mL Schlenk tube, then purged with three cycles of vacuum/N_2. 25 mL of diethylether were added and the mixture was stirred at room temperature. To the suspension, 21 mL of $(CH_3)_3CCH_2MgBr$ (24.7 mmol, 1.16 M in ether) were added dropwise by syringe over 15 min. During this time, the color of the solution changed from purple to black. The deep brown-black mixture was stirred for 1 hour at room temperature, after which time the solution

color was maroon. The solution was then hydrolysed with 50 mL aqueous saturated ammonium chloride (previously degassed for 30 min by bubbling N_2 through the solution). After phase separation, the maroon ether layer was transferred through a cannula into a 100 mL Schlenk tube containing dry $MgSO_4$, then decanted into another Schlenk tube where the solvent was removed under vacuum. The maroon residue was purified by sublimation under high vacuum (10^{-4} Torr). $CrNp_4$ was obtained in 39% yield based on 50% max. The tetraneopentylchromium(IV) complex is volatile, very air-sensitive and intensely colored, and was stored in the freezer under N_2.

The purity of the $CrNp_4$ was checked by a chloride test. A small amount of $CrNp_4$ was sublimed into a 10 mL Schlenk tube, then dissolved under N_2 in 5 mL of hexane. 1 mL of aqueous silver nitrate (0.1 M) was added to the $CrNp_4$ solution and the mixture was stirred at room temperature for 1 hour. No silver chloride precipitate was observed.

UV-visible spectra were obtained under an inert N_2 atmosphere. A solution of $CrNp_4$ in hexane was introduced by syringe into a 1 cm quartz cuvette tightly closed with a rubber septum and previously purged for 30 min with N_2. The UV-visible spectrum of $CrNp_4$ consists of a peak at 474 nm and a minimum at 418 nm, similar to that reported in the literature.[3]

For EPR spectroscopy, a Schlenk-type reactor equipped with high vacuum stopcock was prepared. A quartz tube (5 mm OD/4 mm ID, 20 cm in length) was welded at right angles via a graded seal to the reactor. A solution of $CrNp_4$ in hexane (prepared in the same manner as described above) was introduced. The liquid solution was subjected to three freeze-pump-thaw cycles. The quartz tube containing ca. 1 mL of $CrNp_4$ in hexane was submerged in a liquid N_2 trap, and sealed off with a flame leaving the sample under vacuum. The EPR spectrum of $CrNp_4$ in hexane is a broad line at room temperature, but becomes a

poorly resolved doublet centered at g = 1.986 at 180 K and a well-defined doublet characteristic of a d^2 system, centered at g = 1.986 at 147 K, (see Figures 3.4b and c, respectively). Literature EPR spectra of $CrNp_4$ show the same behavior.[3]

2.1.4.1.2 $Cr(CH_2Si(CH_3)_3)_4$

The synthesis of $Cr(CH_2Si(CH_3)_3)_4$ was performed in the same manner as described above for the synthesis of $CrNp_4$. To a purple solution of $CrCl_3$·3THF (4.2 g, 11.2 mmol) suspended in diethylether was added dropwise by syringe over 15 min, 51.6 mL of $(CH_3)_3SiCH_2MgCl$ (51.6 mmol, 1 M in ether). Over the next 15 min the solution changed color from pink to dark purple. The dark solution was allowed to stir at room temperature for approximately 1 hour at which time 50 mL of saturated aqueous ammonium chloride solution (degassed with N_2 for 30 min) were added. The deep purple organic phase was separated, then dried over $MgSO_4$. The solvent was then removed by evaporation under vacuum. The solid purple $Cr(CH_2Si(CH_3)_3)_4$ was purified by sublimation under high vacuum, and isolated in 42% yield. $Cr(CH_2Si(CH_3)_3)_4$ is air sensitive, therefore it was stored under N_2 in the freezer.

No silver chloride precipitate was observed when a solution of $Cr(CH_2Si(CH_3)_3)_4$ in pentane was added to a silver nitrate solution.

The UV-visible spectrum of $Cr(CH_2Si(CH_3)_3)_4$ in pentane shows a peak at 530 nm and a minimum at 436 nm, very close to the literature spectrum.[2]

2.1.4.1.3 $Cr(CD_2C(CH_3)_3)_4$

* *Synthesis of* $(CH_3)_3CCD_2OH$. Neopentyl alcohol deuterated in the α-position was prepared by reduction of pivaloyl chloride with $LiAlD_4$,[4] eq 2.4.

$$(CH_3)_3CCOCl \xrightarrow[2.\ H_2O]{1.\ LiAlD_4} (CH_3)_3CCD_2OH \qquad (2.4)$$

A 500 mL three-necked flask, equipped with a 20 mL dropping funnel, a condenser, and with an entrance port for N_2, was purged with three cycles of vacuum/N_2. Under N_2, $LiAlD_4$ (2.0 g, 47.6 mmol) was introduced, then 150 mL of diethyl ether were added. To the white suspension of $LiAlD_4$ in ether was added dropwise from the dropping funnel pivaloyl chloride $(CH_3)_3CCOCl$ (10.5 g, 87.4 mmol) over 2 hours at -78°C (cooled with an acetone/liquid N_2 bath). The solution was stirred for 1 hour at room temperature, then cooled again to -78°C. The reaction mixture was hydrolyzed with 100 mL of distilled water added dropwise, followed by 5 mL 10 M NaOH in order to dissolve the white precipitate. The diethyl ether layer was separated from the mixture and dried over $MgSO_4$. The solvent was removed by rotary evaporator to afford the product as a white crystalline solid (7.5 g, 83.5 mmol, 95 % yield). ^1H and ^{13}C NMR spectra (frequency 300 MHz and 75 MHz, respectively) were recorded on a Bruker AMX-300 spectrometer. ^1H NMR ($CDCl_3$, 25°C): δ 2.8 (s, 1H, OH), 0.9 (s, 9H, CMe_3). ^{13}C NMR ($CDCl_3$, 25°C): δ 72 (quintet, $\underline{C}D_2CMe_3$), 32 (s, $CD_2\underline{C}Me_3$), 26 (s, $CD_2C\underline{Me}_3$).

* *Synthesis of* $(CH_3)_3CCD_2Br$. Neopentyl-d_2-bromide was prepared from neopentyl-d_2-alcohol in the presence of Ph_3PBr_2,[5] eq 2.5.

$$(CH_3)_3CCH_2OH + PPh_3 + Br_2 \rightarrow (CH_3)_3CCH_2Br + O{=}PPh_3 + HBr \qquad (2.5)$$

Under N_2, in a 250 mL two-necked flask equipped with a condenser, PPh_3 (17.4 g, 67 mmol), dissolved in dimethylformamide (25 mL) was introduced. Then Np-d_2-OH (5.0 g, 55.6 mmol) was added to the colorless mixture. Through a 5 mL dropping funnel, bromine (3.6 mL, 67 mmol) was added dropwise to the colorless solution over 2 hours at room temperature. The addition of Br_2 was deemed complete when the yellow-orange color persisted. After being

refluxed for 20 hours, the orange mixture had turned yellow and a large amount of solid had formed. The yellow solution was distilled under N_2 at atmospheric pressure, and the colorless solution which was collected was washed with 3 x 25 mL water and 3 x 25 mL pentane. The organic layer was first dried over $MgSO_4$. The neopentyl-d_2-bromide was then dried by stirring over P_2O_5, followed by trap-to-trap distillation, in order to remove all the water. This operation was repeated several times. 7.3 g (48.1 mmol, 86% yield) of neopentyl-d_2-bromide was obtained. ^{1}H NMR ($CDCl_3$, 25°C): δ 0.9 (s, 3H, CMe_3). ^{13}C NMR($CDCl_3$, 25°C): δ 47.5 (quintet, $\underline{C}D_2CMe_3$), 32.4 (s, $CD_2\underline{C}Me_3$), 26.9 (s, $CD_2C\underline{Me}_3$).

* *Synthesis of $(CH_3)_3CCD_2MgBr$.* Even after repeated attempts to dry and purify the labeled neopentyl bromide, the Grignard reaction proved difficult to initiate. Therefore it was initiated with unlabeled neopentyl bromide.

50 mL of diethylether were added to a 3-necked flask containing Mg (1.6 g, 66.7 mmol). Unlabeled NpBr (0.4 mL, 0.5 g, 0.64 mmol) was added dropwise from a dropping funnel to the colorless solution. When the green-gray color was observed after 5 min, the labeled Np-d_2-Br (6.2 mL, 7.44 g, 48 mmol) was then added dropwise. The subsequent steps were performed in the same way as described above for the synthesis of NpMgBr.

The concentration of Np-d_2-MgBr in diethylether was determined as before, to give a concentration of 0.45 M in diethylether. 50 mL of Np-d_2-MgBr in ether were obtained, therefore the yield of Np-d_2-MgBr was calculated to be 47%.

The percent isotope enrichment of the Np-d_2-MgBr was determined by GC-MS. 5 mL of the Grignard solution synthesized above was hydrolyzed by H_2O. The labeled and unlabeled neopentanes were collected and analyzed by measuring the relative intensities of the *tert*-butyl fragment peaks at m/e = 57 and 59 (see below). The theoretical isotope enrichment of the Np-d_2-MgBr was calculated to be ca. 94% α-D_2 and 6% α-H_2, based on the volumes of labeled and

unlabeled NpBr used in its synthesis. Experimentally, it was found to be 93% α-D_2 and 7% α-H_2.

* *Synthesis of* $Cr(CD_2C(CH_3)_3)_4$. $Cr(CD_2C(CH_3)_3)_4$ was prepared as described for $Cr(CH_2C(CH_3)_3)_4$, only the quantities of all reagents were reduced. $Cr(CD_2C(CH_3)_3)_4$ was synthesized from $CrCl_3$·3THF (1.0 g, 2.7 mmol) and 25 mL of the isotopically-labeled Grignard reagent (11.3 mmol, 0.45 M in Et_2O) in 15 mL of diethylether. The mixture was hydrolyzed with 15 mL saturated aqueous ammonium chloride. $Cr(CD_2C(CH_3)_3)_4$ was stored under N_2.

The isotope enrichment of $Cr(CD_2C(CH_3)_3)_4$ was determined by GC-MS. Into a Schlenk tube equipped with a high vacuum stopcock, a small amount of $Cr(CD_2C(CH_3)_3)_4$ was sublimed and subsequently reacted with 3 Torr HCl vapor. The gas phase was recovered and neutralized by condensation into a reactor containing powdered NaOH. The neopentane present was then analyzed. The predicted isotope content was 93% $C(CH_3)_3(CD_2H)$ and 7% $C(CH_3)_4$, based on the analysis of the labeled Grignard reagent. The observed isotope content was 90% $C(CH_3)_3(CD_2H)$ and 10% $C(CH_3)_4$, as judged by GC-MS.

The chloride test was performed on $Cr(CD_2C(CH_3))_4$ in hexane, as described previously. No silver chloride precipitate was observed.

2.1.4.2 Tetrakis(diethylamido)chromium(IV)

Tetrakis(diethylamido)chromium(IV), $Cr(N(CH_2CH_3)_2)_4$, was synthesized from anhydrous $CrCl_3$ and $LiN(CH_2CH_3)_2$, eqs 2.6 - 2.7.[6] Spontaneous disproportionation of $Cr(N(CH_2CH_3)_2)_3$ during sublimation under high vacuum generates volatile $Cr(N(CH_2CH_3)_2)_4$.

$$CrCl_3 + 3\,LiN(CH_2CH_3)_2 \rightarrow Cr(N(CH_2CH_3)_2)_3 + 3\,LiCl \qquad (2.6)$$

$$2\,Cr(N(CH_2CH_3)_2)_3 \rightarrow Cr(N(CH_2CH_3)_2)_2 + Cr(N(CH_2CH_3)_2)_4 \qquad (2.7)$$

Into a Schlenk-type reactor purged with three cycles of vacuum/N_2, $LiN(CH_2CH_3)_2$ (4.5 g, 56.8 mmol) was introduced through a transfer tube. 80 mL THF were added, and the solution became clear brown. The mixture was stirred for 5 min at room temperature, then cooled to -78°C. Anhydrous $CrCl_3$ (3.0 g, 18.9 mmol) was then added in portions from a Gouch tube, which resulted in an immediate color change from clear brown to deep green. The mixture was then allowed to attain room temperature, and was stirred for 12 hours. The solvent was removed by evaporation under vacuum, and the residue extracted with 3 x 50 mL pentane. The green mixture was transferred by cannula into a Schlenk tube, then evaporated to dryness under vacuum (10^{-3} Torr). The residue was sublimed under high vacuum (10^{-4} Torr) at room temperature to give a green oil.

The purity of $Cr(N(CH_2CH_3)_2)_4$ was checked by the chloride test, which gave no silver chloride precipitate.

A UV-visible spectrum was obtained under N_2, as described previously. The UV-visible spectrum of a solution of $Cr(N(CH_2CH_3)_2)_4$ in pentane showed a peak at 734 nm and a minimum at 516 nm, values close to those reported in the literature.[6]

2.1.4.3 Tetra-t-butoxochromium(IV)

Tetra-t-butoxochromium(IV), $Cr(OC(CH_3)_3)_4$, was prepared by the metathetical reaction of $Cr(N(CH_2CH_3)_2)_4$ with ^tBuOH, eq 2.8.[7]

$$Cr(N(CH_2CH_3)_2)_4 + 4\,(CH_3)_3COH \rightarrow Cr(OC(CH_3)_3)_4 + 4\,HN(CH_2CH_3)_2 \qquad (2.8)$$

Under N_2, in a Schlenk tube containing $Cr(N(CH_2CH_3)_2)_4$ (2.1 g, 6.3 mmol), 5 mL benzene were added. ^tBuOH (5.4 g, 72.9 mmol, 7 mL) was added dropwise with a syringe to the green solution. Over the next 30 min, the color of

the solution changed from green to purple and then became deep blue, and was stirred at 40°C for 2 hours. The solvent and excess ^tBuOH were removed by evaporation under vacuum. $Cr(O^tBu)_4$, a deep blue solid, was purified by high vacuum sublimation at room temperature. $Cr(O^tBu)_4$ was stored under N_2.

2.2 Preparation of Supported Chromium Complexes

2.2.1 Pretreatment of Silica

A standard pretreatment procedure was adopted in order to ensure reproducibility of the experiments. For all reactions, silica-500 (the appended number indicating the temperature, in °C, at which the silica was treated) was calcined at 500°C in presence of 300 Torr dry ultrapure O_2 for 2 hours in order to remove adsorbed hydrocarbons. The silica was then partially dehydroxylated at 500°C for 2 hours under dynamic vacuum ($<10^{-4}$ Torr). To obtain silica dehydroxylated at 200°C, the silica-500 was rehydrated with two cycles of H_2O vapor at 450°C for 3 hours and then partially dehydroxylated under dynamic vacuum at 200°C for 2 hours. The silica-200 was also prepared by simply heating silica at 200°C for 2 hours under dynamic vacuum. These thermal treatments do not change the surface area of the silica, but they do standardize the number of surface hydroxyl groups.[8]

Deuterated silica was prepared by two different methods: exchange with D_2O, or DCl. The first method using D_2O is more time-consuming. The silica is treated with four cycles of D_2O vapor at 450°C for 4 hours followed by dynamic vacuum at 490°C for 15 hours. For the preparation of deuterated silica-500, the pellet was then dehydroxylated at 500°C under dynamic vacuum for an additional 2 hours. However, the preparation of deuterated silica-200 requires an additional cycle of D_2O vapor. The temperature was lowered to 150°C and the silica was rehydrated for 16 hours, followed by evacuation of the water. The silica was then

dehydroxylated at 200°C for 2 hours under dynamic vacuum. This method gave >90% deuteration of the surface hydroxyl groups. The extent of deuteration was judged by the relative decrease in intensity of the ν(SiO-H) vibration at 3747 cm^{-1} and by the appearance of the ν(SiO-D) vibration at 2762 cm^{-1}. In the second method, the silica was first dehydroxylated then exposed to three to four cycles of exposure to 50 Torr DCl for 10 min, followed by dynamic vacuum at room temperature. This method also gave >90% deuteration of surface hydroxyl groups. Silica is not chlorinated by DCl at room temperature.[9]

2.2.2 Breakseal Techniques

A breakseal reactor, Figure 2.1, was assembled and leak-tested on a high vacuum line. The chromium(IV) compounds and some liquid reagents were transferred from their storage vessels by sublimation into a breakseal submerged in liquid N_2, via a glass "U"-tube connector. While the product was still frozen in liquid N_2, the breakseal was sealed off from the rest of the reactor at the restriction with a torch, leaving the reagent sealed inside the breakseal under static vacuum.

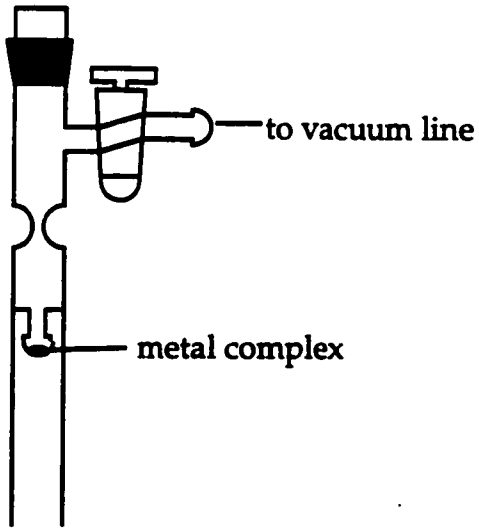

Figure 2.1 Schematic of a breakseal reactor

A hammer, usually made from a piece of iron sealed inside a glass tube, was

placed in the open end side of the breakseal, and held in place with a magnet, as shown in Figure 2.2. A restriction was created in the glass to facilitate sealing off the breakseal after reaction. The open end of the breakseal was then attached to the desired reactor, Figures 2.2 and 2.3.

2.2.3 Grafting of Organometallic Complexes

After thermal treatment of the silica, the breakseal containing the molecular precursor was broken using the hammer. The thermal treatment part of the reactor, containing the silica, was placed in liquid N_2. The organometallic complex was sublimed *in vacuo* at room temperature from the breakseal to the cold trap for 1 to 24 hours depending on its volatility. The reactor was then removed from the cold trap, and left to stand for several hours at room temperature until the reaction was complete. Unreacted material was then desorbed from the silica surface by immersing the breakseal sidearm for several hours in a liquid N_2 trap. The sidearm was removed by sealing it off with a torch at the restriction. Cr-modified silica was thus isolated inside the reactor vessel for further manipulations, which were performed *in situ* without exposing the samples to solvents or inert gas atmosphere at any time during the experiment.

2.3 Characterization of Silica-Supported Chromium Complexes

2.3.1 Infrared Spectroscopy

All IR experiments were performed in a high vacuum *in situ* IR cell, Figure 2.2, equipped with either KCl, CaF_2 or ZnSe windows. KCl is hygroscopic and is not appropriate for experiments where H_2O/D_2O is used. CaF_2 is insoluble in water but also opaque below 1000 cm^{-1}. ZnSe is not sensitive to water and is transparent to 400 cm^{-1}, but is fragile. Transmission infrared spectra were recorded on a Mattson Research Series FT-IR spectrometer equipped with a DTGS detector and purged

with CO_2-free dry air. Background and sample spectra were recorded by co-adding 32 scans at a resolution of 2 cm^{-1}. Gas phase IR spectra were recorded at a resolution of 0.75 cm^{-1}.

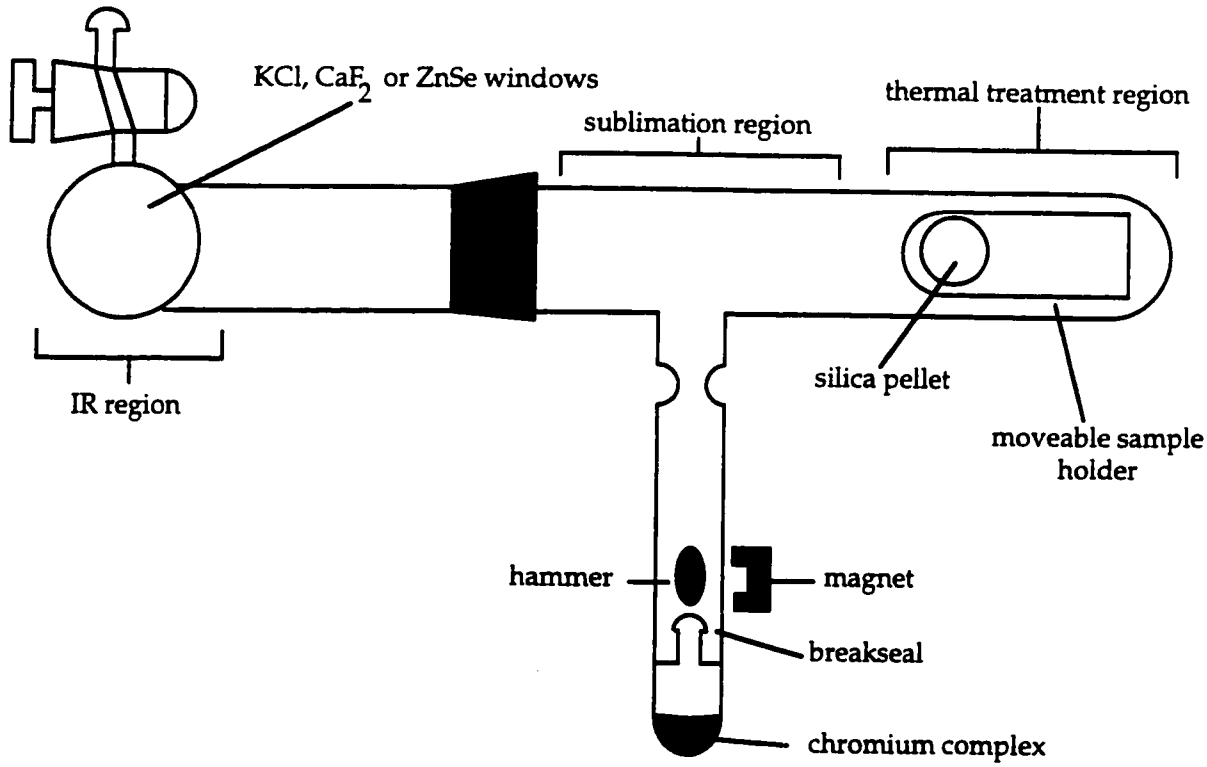

Figure 2.2 Schematic of an *in situ* IR cell

For IR surface experiments, the silica was pressed (125 kg/cm^2) into a self-supporting disk with a diameter of 1.6 cm containing approximately 15 mg of silica per cm^2. The silica pellet was then placed in a sample holder inside the IR cell. For all other experiments, the silica was compacted by pressing it into thick disks which were then finely ground in a mortar.

The pyrex sample holder containing the silica disk is first situated in the IR cell in the thermal treatment zone in order to calcine and/or partially dehydroxylate the silica. After cooling the sample holder to room temperature, the

silica disk slides to the IR window zone in order to record a baseline spectrum of the silica. The IR cell is aligned in the IR spectrometer, so that the beam traverses the solid sample. The spectrum of the windows is recorded by removing the sample holder from the IR window zone.

Next, the breakseal attached to the IR reactor is broken using the magnetic hammer. The sample holder is moved to the thermal treatment zone and submerged in a liquid N_2 trap. The chromium(IV) complex is sublimed under vacuum onto the inner pyrex walls and the sample holder in the sublimation-thermal region of the IR cell. Then the cold trap is removed to allow the chromium(IV) complex to react with the silica. The sample holder is then placed face down immediately above the breakseal, which is once again submerged in a liquid N_2 trap to cause unreacted material to be desorbed back into the breakseal. The breakseal is then removed at the restriction with a torch.

2.3.2 EPR Spectroscopy

All experiments other than IR were performed in high vacuum Schlenk tubes using breakseals to admit the organometallic compounds. The supported chromium complexes for EPR experiments were prepared in Schlenk-type reactors equipped with high vacuum stopcocks. One or two cylindrical quartz tubes (8 m m O.D., 15 cm length) were attached to quartz-pyrex graded seals and then were welded at right angles to the main body of the reactor, Figure 2.3. Compacted silica (as described above) was used for Schlenk experiments. The pretreatment and modification of the silica surface were performed in the same manner as described previously. Once all manipulations were complete, approximately 50 mg samples were transferred *in vacuo* into the quartz tube. The sample was then sealed off under vacuum with a flame 20 cm above the silica.

EPR spectra were measured at variable temperature from 78 K to 300 K. The

spectra were recorded on a Bruker ER 200 spectrometer operating at 9.450 GHz, with a sweep time of 500 sec.

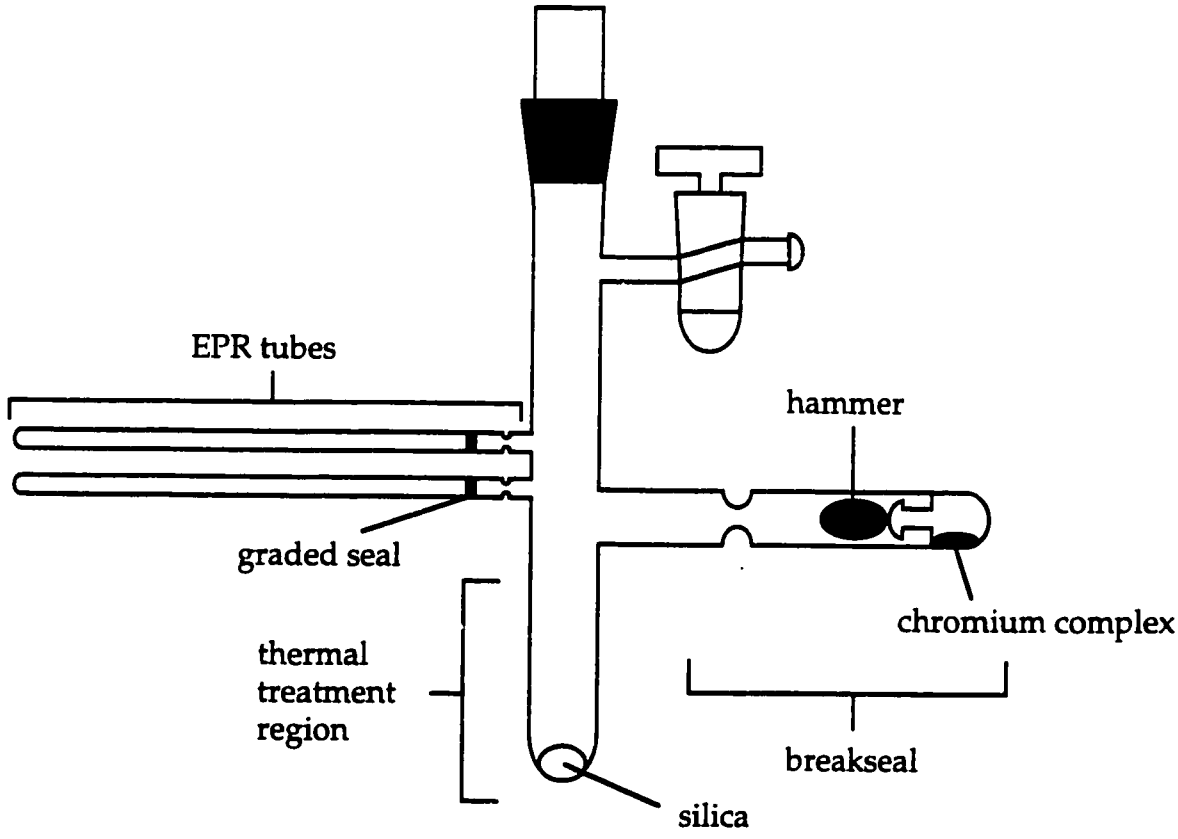

Figure 2.3 Schematic of an EPR reactor

2.3.3 Solid State NMR Spectroscopy

Samples for solid state NMR spectroscopy were prepared in the same manner as for EPR samples, with the exception that the samples were transferred *in vacuo* into 5 mm pyrex NMR tubes welded onto the main tube at right angles, then sealed off at 30 mm lengths with a torch to give tubes containing approximately 35 mg of sample, which were placed in a 35 mm zirconia rotor. ^{2}H Magic Angle Spinning (MAS) NMR and static solid-state NMR were recorded at a frequency of 30.7 MHz on a Bruker ASX-200 spectrometer. The spectra were

collected using a 3.4 μs 90° pulse and a relaxation delay of 1 s. The samples were spun at 3000 - 4000 Hz.

2.3.4 Diffuse Reflectance UV-visible Spectroscopy

50 mg samples (prepared as described above for EPR experiments) were transferred into 2x5 mm rectangular quartz tubing, also welded onto the Schlenk tube. The samples were sealed off *in vacuo* with a torch above a graded seal. Diffuse reflectance UV-visible spectra were recorded on a Varian Cary 1E spectrometer equipped with an integrating sphere diffuse reflectance attachment, and referenced to Spectralon.

2.3.5 Elemental Analysis

The amount of chemisorbed metal was determined by quantitative extraction at the end of each experiment. The chromium was extracted by stirring 20-40 mg of the modified silica with 5 mL 5 M NaOH to give solutions containing ca. 0.4 mg Cr/mL. Then 1 mL 30% H_2O_2 was added to oxidize the metal to Cr(VI). The yellow solution was boiled for 5 hr, then diluted with water to 50 mL. Spectra were recorded in quartz cuvettes with 1 cm path length and referenced to a $NaOH/H_2O_2$ solution containing approximately the same amount of silica as the chromium samples. The UV-visible spectra were recorded on a HP 8451A diode array spectrometer. The absorbance at λ_{max} = 374 nm was converted to chromium concentration by comparison to a calibration curve prepared with Na_2CrO_4, Figure 2.4.[10] The accuracy of this method was verified by ICP. A comparison of the chromium loading was performed on a sample using both techniques. By ICP, 0.21% Cr was found, compared to 0.20% Cr by the UV-visible method.

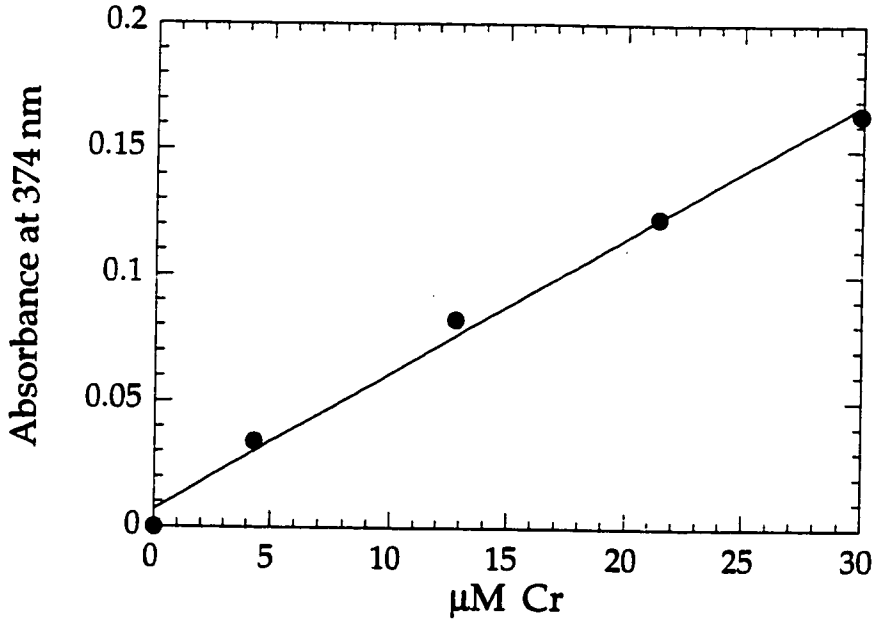

Abs = ε l * [Cr]		
	Value	Error
ε	5700	190
Chisq	0.00022155	NA
R	0.99364	NA

Figure 2.4 Calibration curve for chromium analysis

2.3.6 Magnetic Susceptibility

A special reactor was designed for magnetic susceptibility measurements performed by Scott Tripp at Quantum Design in San Diego, California. The main part of reactor was made of 7 mm OD/5 mm ID quartz tubing 75 cm in length. At the closed end of the quartz tube, a quartz rod (10 cm long and 7 mm OD) was attached. The open end of the quartz tube was attached to a pyrex tube through a graded seal. Two sidearms were attached: a breakseal containing the chromium complex and a tube to contain the silica (where the grafting reaction takes place). The reactor was equipped with a high vacuum stopcock. A quartz rod (25 cm long, 5 mm OD) sealed to a quartz tube filled with iron filings (in order to hold the rod in place with a magnet) was placed inside the pyrex tube above the quartz tubing, Figure 2.5. The pretreatment of the silica and the synthesis of the surface complex were performed as described above. Once the reaction was complete, approximately 70 mg of the silica-supported chromium complex was transferred *in vacuo* to the bottom of the quartz tube. The movable rod inside the reactor was lowered down to compress the modified silica. The sample was then sealed off with a torch 10 cm above the silica leaving the sample sandwiched between two solid pieces of quartz.

Susceptibility was measured as a function of temperature (4 - 300 K) on a Quantum Design SQUID magnetometer. The instrument operates at 5 Tesla, using a 3 cm Reciprocating Sample Option scan at 1 Hz with iterative regression, 10 cycles per measurement and 5 measurements per average. The reference was the same quantity of unmodified silica.

Magnetic susceptibility measurements were also performed by Dr. Laurie Thompson at Memorial University, Newfoundland. For these experiments, a different holder was required. The samples were prepared in the same manner as for the EPR samples, however, instead of being transferred into quartz EPR tubes,

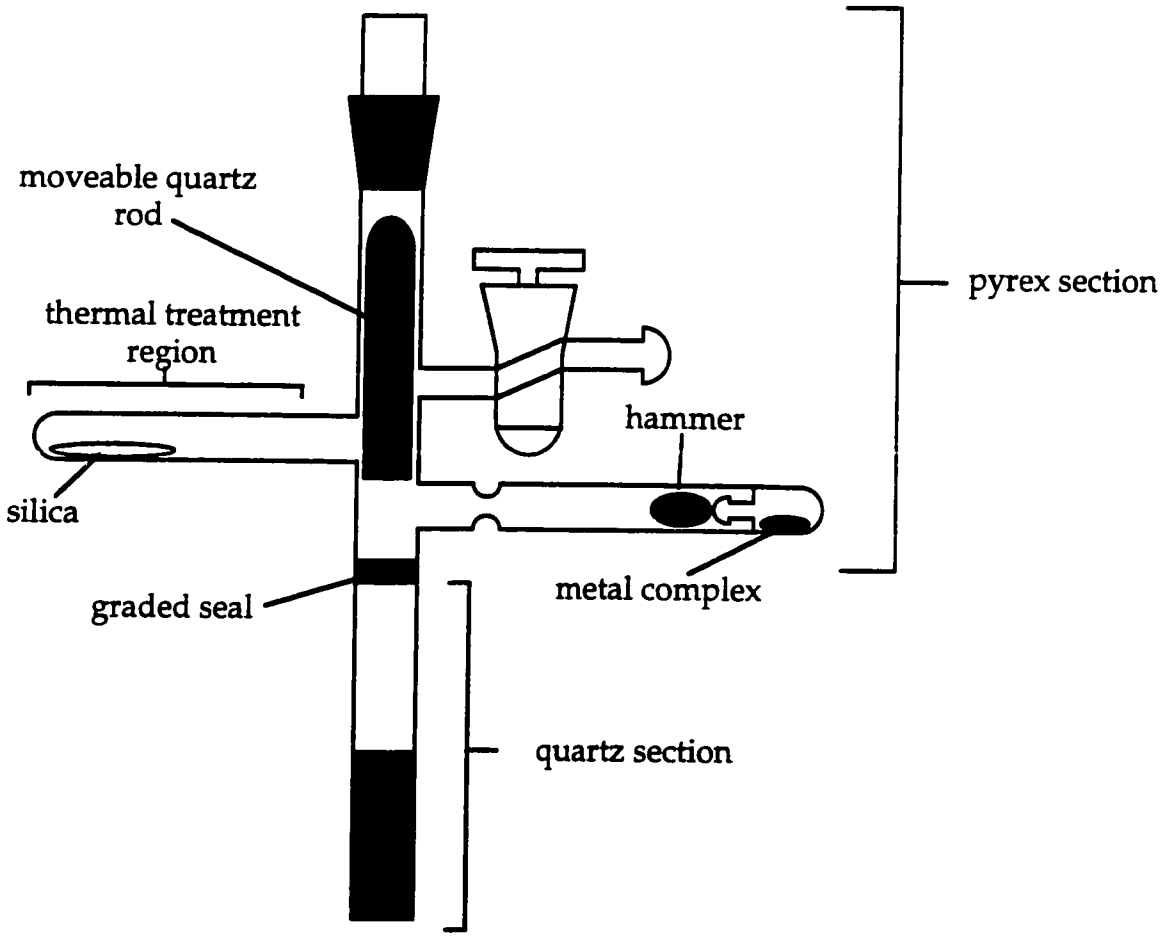

Figure 2.5 Schematic of the magnetic susceptibility reactor

15-20 mg samples were transferred into 5 mm OD/5 mm ID quartz tubing approximately 8 cm in length. The samples occupied 0.5 - 1 cm of height in the bottom of the quartz tube. Samples were sealed off *in vacuo* with a flame 5 cm above the silica.

Magnetic susceptibility was measured as a function of temperature on a Quantum Design MPMS5S SQUID magnetometer. The samples were examined in the temperature range 2 - 300 K, with a 3000 G field. The samples in quartz tubes were mounted inside a straw supported on an inverted quartz tube (5 mm OD/5 mm ID, 8 cm in length) and held in place by a compressed paper insert to prevent sample movement. The sample in the tube assembly was centered at 3 K and

3000 G. A reference of unmodified silica was prepared in exactly the same way.

Calculation of the magnetic moment of supported complexes. The molar susceptibility, χ_M, has units cm^3/mol and is defined as

$$\chi_M = \chi^* (mwt) \tag{2.10}$$

where mwt is the molecular weight, and χ is the gram susceptibility. The molar susceptibility χ_M is related to the molar magnetization (or the molar magnetic moment), M, in cm^3/G mol, or emu, where H is the field strengh in G, eq 2.11.

$$\chi_M = M/H \tag{2.11}$$

For an ideal paramagnet, the molar susceptibility after diamagnetic correction, χ_M^{corr}, is a function of the temperature, eq 2.12, where C is the Curie constant in cm^3 G K/mol.

$$\chi_M^{corr} = C/T \tag{2.12}$$

Values for χ_M are obtained from magnetization as a function of temperature and a plot of $1/\chi_M^{corr}$ is made as a function of T. The slope C^{-1} is the inverse of the Curie constant, and the line intersects the origin. Some plots of $1/\chi_M$ versus 1/T do not intercept the origin; the equation which describes their behaviour is the Curie-Weiss expression, eq 2.13.

$$\chi_M^{corr} = C/(T+\theta) \tag{2.13}$$

The constant θ is the x-intercept. Its value is related to the nature of the long-range

magnetic interactions present in the sample.

According to classical statistical mechanics, the Curie constant can be expressed as in eq 2.14:

$$C = N\mu^2/(3k) \tag{2.14}$$

where N is Avogadro's number, k is the Boltzmann constant, and μ is the magnetic moment per molecule (in B.M.). Therefore

$$\mu = 2.827(C)^{1/2} \tag{2.15}$$

To calculate the magnetic moment per chromium atom, C must be obtained from the experimental measurement of sample magnetization.[11] The relationship between the molar magnetization and the Curie constant is

$$\chi_M^{corr} = M/H = C/(T+\theta) \tag{2.16}$$

from which we obtain the expression for the experimental magnetization I, eq 2.17.

$$I = M * n = C * H^* m_{Cr}/(T+\theta) * mwt \tag{2.17}$$

where n is the number of moles of the paramagnetic compound present, m_{Cr} is the mass of Cr in the sample and mwt is 51.9 g/mol.

The value of the Curie constant is extracted from the non-linear curve fit of the plot of magnetic moment versus temperature, (e.g., Figure 3.6). C′ is the parameter from the non-linear curve fit to eq 2.17. The parameter C′ is expressed by the relation in eq 2.18.

$$C' = C * H * m_{Cr}/mwt \qquad (2.18)$$

Once C is calculated from C', the effective magnetic moment per metal atom is then obtained from eq 2.15. It is compared to the spin-only magnetic moment, expressed by eq 2.19:

$$\mu_{s.o.} = (n(n+2))^{1/2} \qquad (2.19)$$

where n is the number of unpaired electrons per metal atom. This formula assumes that the orbital moment does not contribute significantly to the magnetic moment.

2.4 Analysis of Volatile Reaction Products

Gases were analyzed qualitatively and quantitatively by IR, GC and GC-MS. Absolute pressure measurements were made using a Baratron capacitance manometer.

2.4.1 Qualitative Analysis

Volatile reaction products were analyzed qualitatively by *in situ* IR, or transferred cryogenically for GC and GC-MS analyses. If HCl or DCl were also present, the gases were first condensed with liquid N_2 into a separate bulb containing powdered NaOH, which quantitatively removes the acid prior to analysis of the hydrocarbon.

Volatile gaseous products were analyzed on a Hewlett-Packard 5710A gas chromatograph with a Porasil packed column and an FID detector. Light hydrocarbons (C_1-C_3) were injected isothermally at 22°C, whereas heavy

hydrocarbons were injected at 85 - 150°C depending on the boiling point of the volatile product being analyzed. The identities of all gases were confirmed with the retention times of standards under the same conditions.

Volatile gases evolved from isotope labeling reactions were analyzed by GC-MS. Mass spectra were recorded on two apparatus: an HP 5890 Series II gas chromatograph with a Kratos Concept 2H mass selective detector and a J&W DB-1 column (30 m long, 0.2 mm i.d, 0.33 μm film) and a HP 5890 Series gas chromatograph and a J&W DB-1 column (30 m long, 0.2 mm i.d, 0.33 μm film) .

2.4.2. Isotopomer Analysis

The distribution of neopentane isotopomers can be determined from their fragment ion intensities. The cracking pattern of neopentane is well known. The parent ion is usually too weak to be observed in EI mode, so the highest molecular weight ion is due to the *tert*-butyl fragment. The mass spectrum of unlabeled neopentane generates a *tert*-butyl fragment at m/e = 57.

Statistically, a neopentane-d_n isotopomer (n = 1-3) generates 3 equiv. of *tert*-butyl-d_n fragments at m/e = (57 + n), and 1 equiv. of *tert*-butyl-d_0 at m/e = 57, provided all D atoms are attached to the same carbon atom, Scheme 2.1.

Scheme 2.1 Neopentane-d_n isotopomer fragmentation

$$C(CH_3)_3(CD_nH_{3-n})^+ \xrightarrow{-CH_3} 3/4\, C(CH_3)_2(CD_nH_{3-n})^+$$

$$\xrightarrow{-CD_nH_{3-n}} 1/4\, C(CH_3)_3^+$$

The deuterium content of labeled neopentanes was calculated by measuring the relative intensities (I_{57}, I_{58}, I_{59} and I_{60}) of the *tert*-butyl fragment peaks at

m/e = 57, 58, 59 and 60, respectively, and solving a set of linear equations.[12,13] The total amounts of neopentane-d_1, -d_2, and -d_3 written as I'_{58}, I'_{59} and I'_{60}, respectively, are calculated from the relative intensities I_{58}, I_{59} and I_{60}, eqs 2.20, 2.21 and 2.22, since neopentane-d_n also contributes one time out of four to the intensity of the peak at m/e = 57.

$$I'_{58} = I_{58} + 1/3\,(I_{58}) = 4/3\,I_{58} \tag{2.20}$$

$$I'_{59} = I_{59} + 1/3\,(I_{59}) = 4/3\,I_{59} \tag{2.21}$$

$$I'_{60} = I_{60} + 1/3\,(I_{60}) = 4/3\,I_{60} \tag{2.22}$$

The total amount of neopentane-d_0 (I'_{57}) is calculated by measuring the relative intensity (I_{57}) of the peak m/e = 57, then subtracting the amounts of neopentane-d_1, -d_2, and -d_3 (corresponding to one-third of the measured intensities of m/e = 58, 59 and 60), eq 2.23. The remaining intensity at m/e = 57 is due to neopentane-d_0.

$$I'_{57} = I_{57} - 1/3\,(I_{58} + I_{59} + I_{60}) \tag{2.23}$$

The molar fractions of neopentane-d_n can be written as the amount of neopentane-d_n divided by the total amount of neopentane, as exemplified by eq 2.24.

$$n_{57} = I'_{57} / (I'_{57} + I'_{58} + I'_{59} + I'_{60}) \tag{2.24}$$

For reactions in which tetramethylsilane was the product, the peak intensities at m/e = 72 and 73 of the trimethylsilylmethyl fragment ion and of the deuterium-labeled trimethylsilylmethyl isotopomer were measured instead.

For heavier reaction products, such as dibromoneopentane, the modified silica was washed with $CHCl_3$. The solution containing the non-volatile product

was injected into the GC-MS after extraction of the metal using a syringe equipped with a Spartan-3 syringe filter (having a pore size of 5 μm).

2.4.3 Quantitative Analysis

The high vacuum system consists of a main vacuum manifold and a gas manifold, each equipped with Baratron capacitance manometers (either 10 or 1000 Torr scale depending on the pressure range required). The line is attached to a mercury diffusion pump, capable of maintaining a base pressure of $<10^{-4}$ Torr, backed by a rotary pump. The main vacuum manifold contains three entrance ports where reaction vessels can be attached.

2.4.3.1 Volumetric Analyses

In experiments where one gas was the sole volatile product, absolute pressure measurements were made using a Baratron capacitance manometer. The gas was collected in a known volume reactor and the pressure was read directly on the 1000 Torr Baratron capacitance manometer. Knowing the pressure of the gas, the volume of the gas reactor and the temperature, the number of moles of gas was calculated using the ideal gas law.

2.4.3.2 IR Spectroscopy

The gases liberated by reactions of organochromium complexes with silica and in subsequent reactions were analysed by IR spectroscopy. The IR spectrum of the gas was compared to the IR spectrum of a pure sample and quantified by integration of the intensity in the ν(C-H) or δ(C-H) region of the gas phase IR absorbance spectrum. Infrared calibration curves were prepared using gas standards with pressures in the range 1-10 Torr. Each calibration curve was constructed by measuring the gas phase IR absorbance as a function of pressure.

Calibration curves for neopentane, tetramethylsilane, $HNEt_2$ and ^tBuOH were made, Figures 2.6 a-d, respectively. In experiments where HCl or DCl were present, the gas phase was first condensed with liquid N_2 into a separate IR cell equipped with CaF_2 windows and containing powdered NaOH, which quantitatively removes the acid prior to analysis of the hydrocarbon.

2.5 Kinetic Studies

Kinetic studies were undertaken of the thermolysis of the silica-supported chromium species and of olefin polymerization. In the first case, evolution of volatile products upon thermolysis of silica-supported chromium species was studied kinetically. Approx. 100 mg of compacted silica was placed in the bottom of an *in situ* IR cell. Thermal pretreatment of the silica and preparation of the silica-supported chromium species were carried out as previously described. The IR cell was aligned in the IR spectrometer, so that the beam sampled the gas phase above the solid sample. A preheated tube furnace equipped with a thermocouple (± 1 K) was placed around the bottom of the IR cell where the modified silica was located.

For studies of olefin polymerization kinetics, a specially-designed Schlenk-type reactor equipped with a high vacuum stopcock and 6 breakseals sealed on at right angles to the main body of the reactor was prepared. Two breakseals containing the organochromium complex were welded next to the bottom of the reactor, Figure 2.7. 400 to 600 mg of compacted silica were placed in the bottom of the reactor and modified with the organochromium complex as described above. 70 to 80 mg of the modified silica were transferred *in vacuo* into each breakseal and sealed off with a flame. A hammer was placed in the open end of the breakseal containing the modified silica, which was then attached to a IR cell. A known pressure of olefin was introduced into the IR cell which was placed inside the IR spectrometer, so that the IR beam sampled the gas phase. Once aligned, the IR cell

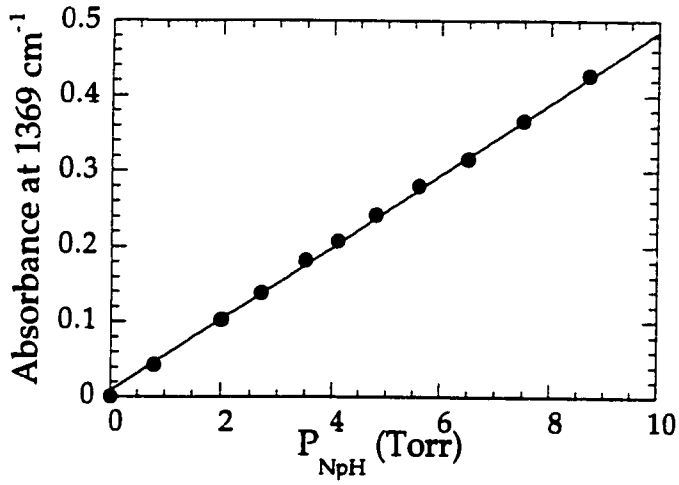

a

$Abs_{1369} = a*P_{NpH} + b$		
	Value	Error
a	0.0083309	0.0031351
b	0.047709	0.0005634
Chisq	0.00034106	NA
R	0.9993	NA

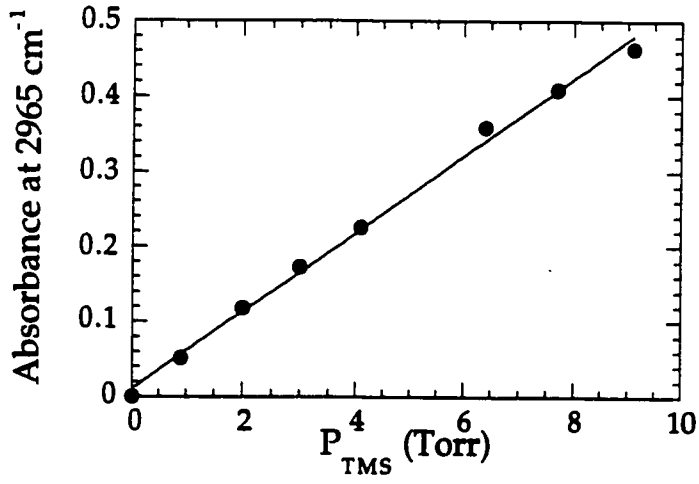

b

$Abs_{2965} = a*P_{TMS} + b$		
	Value	Error
a	0.010454	0.006921
b	0.051702	0.0013391
Chisq	0.00081668	NA
R	0.99799	NA

Figure 2.6 Calibration curves for (a) neopentane; (b) tetramethylsilane

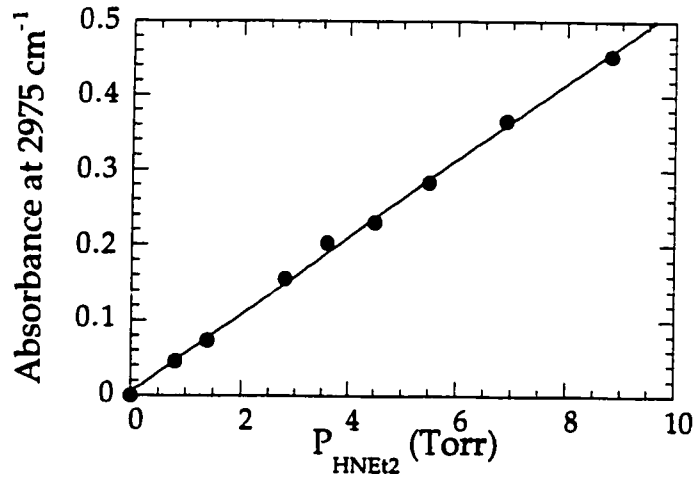

c

$Abs_{2975} = a*P_{HNEt2} + b$		
	Value	Error
a	0.0050241	0.0040581
b	0.051499	0.00086312
Chisq	0.00035581	NA
R	0.99902	NA

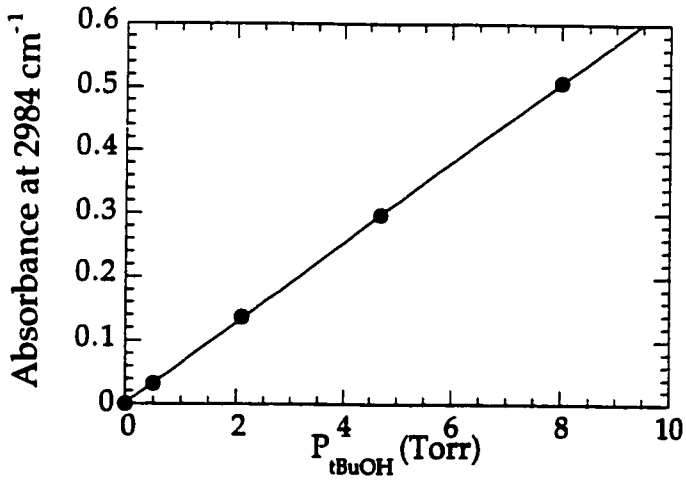

d

$Abs_{2984} = a*P_{t\text{-}BuOH} + b$		
	Value	Error
a	0.0012509	0.00092605
b	0.063311	0.0001295
Chisq	1.052e-05	NA
R	0.99999	NA

Figure 2.6 Calibration curves for (c) $HNEt_2$; (d) ^tBuOH

was not moved for the duration of the experiment. In order to maintain the temperature constant during the reaction, the breakseal was placed either in a water bath (21°C) or a preheated ceramic tube furnace equipped with a thermocouple. The breakseal was carefully broken using the hammer to initiate the reaction.

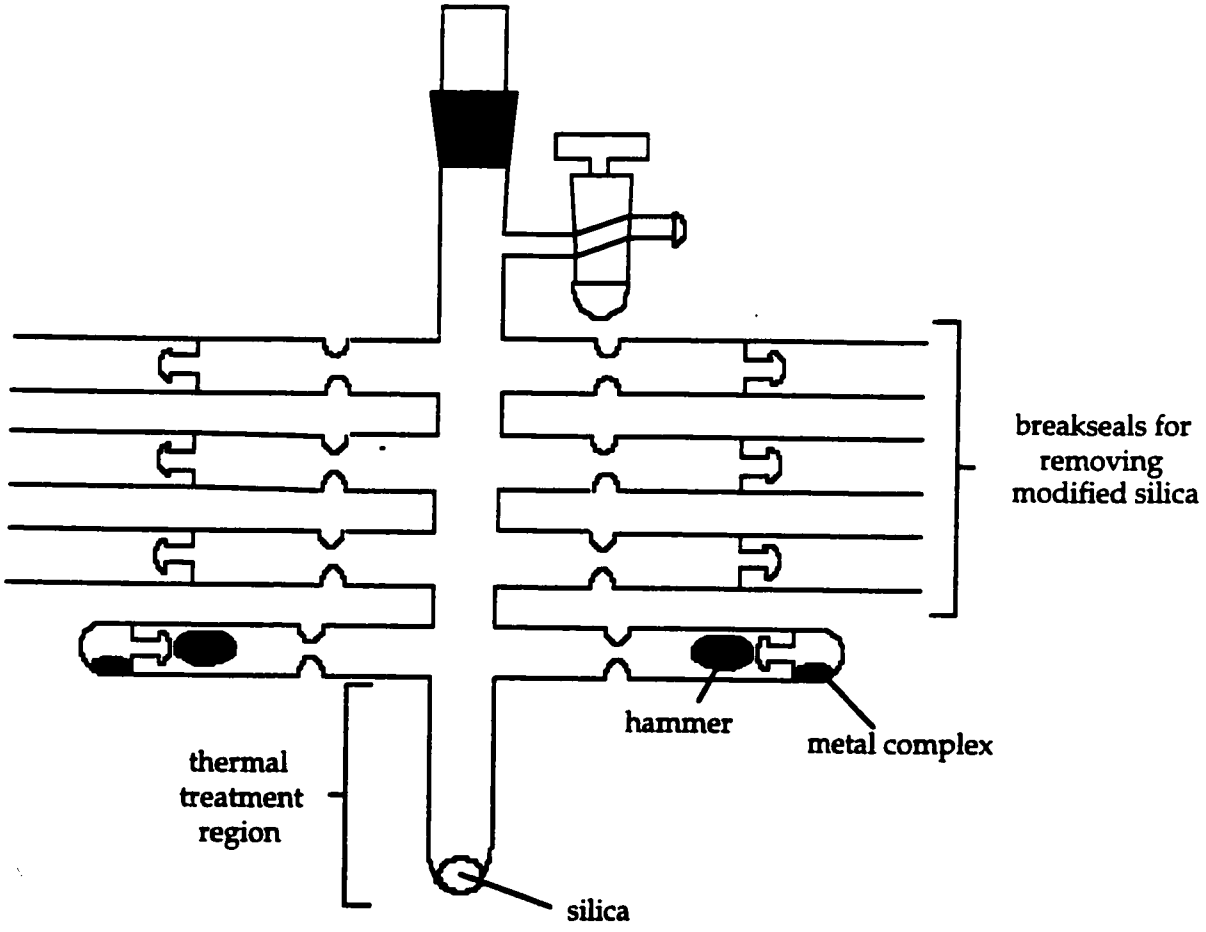

Figure 2.7 Schematic of a reactor for preparing large quantities of Cr/silica used in kinetics studies

In both types of experiments, the gas phase IR absorbance spectrum was recorded at regular time intervals, without moving the IR cell, until the reaction was complete. The relative amount of product in the gas phase was evaluated by performing an integration of the ν(CH) spectral region, 3200 - 2800 cm^{-1}, to give the absorbance values (A_t) shown in the Figures. Non-linear least-squares fits were performed with three variable parameters (A_0, A_∞ and k), to the first-order integrated rate equation $A_t = A_0 + (A_\infty - A_0)(e^{-kt})$, using the program Kaleidagraph (Abelbeck Software). Activation parameters were derived from a straight line fit to a plot of ln(k/T) versus 1/T. According to the Eyring equation, eq. 2.25, a plot of ln(k/T) versus 1/T yields a straight line with slope $-\Delta H^{\ddagger}/R$ and intercept $[\ln(R/Nh) + (\Delta S^{\ddagger}/R)]$.

$$\ln(k/T) = \ln(R/Nh) + \Delta S^{\ddagger}/R - \Delta H^{\ddagger}/RT \qquad (2.25)$$

The errors in the activation parameters were calculated from the following error propagation formulas, eqs. 2.26 and 2.27, which were derived from the Eyring equation.[14]

$$(\sigma\Delta H^{\ddagger})^2 = R^2 T_{max}^2 T_{min}^2/\Delta T^2\{(\sigma T/T)^2[(1 + T_{min}\Delta L/\Delta T)^2 + (1 + T_{max}\Delta L/\Delta T)^2] + 2(\sigma k/k)^2\} \qquad (2.26)$$

$$(\sigma\Delta S^{\ddagger})^2 = R^2/\Delta T^2\{(\sigma T/T)^2[T_{max}^2(1 + T_{min}\Delta L/\Delta T)^2 + T_{min}^2(1 + T_{max}\Delta L/\Delta T)^2] + (\sigma k/k)^2(T_{max}^2 + T_{min}^2) \qquad (2.27)$$

where $\Delta T = (T_{max} - T_{min})$ and $\Delta L = [\ln(k_{max}/T_{max}) - \ln(k_{min}/T_{min})]$.

2.6 Ethylene Polymerization Studies

The special reactor described for kinetics studies of olefin polymerization was also used for the preparation of catalyst samples for activity testing at Nova Chemicals (Calgary) and Union Carbide (West Virginia). Instead of breakseals, pyrex ampules were welded onto the main body of the reactor and were sealed with 150 to 200 mg of modified silica.

2.6.1 Nova Chemicals Catalyst Testing Protocol

All experiments were conducted in a bench scale reactor (BSR). The BSR is a 2L semi-batch, stirred steel reactor with ethylene feed on demand, catalyst supplied at the beginning, no discharge during the reaction and has its own purification systems for ethylene, nitrogen and hydrogen. In a 160 g reactor bed, the catalyst (sealed in the ampule) was added with or without scavenger (which is 250 mg total mass of silica support and 4 wt% triethylaluminium). Ethylene was supplied on demand at 200 psi total reactor pressure for 60 min with stirring at a speed of 1800 rpm. Hydrogen was metered in by maintaining the pressure constant inside the reactor. The polymerization reaction was terminated by venting the reactor.

2.6.2 Union Carbide Catalyst Testing Protocol

All polymerization runs were carried out in a 1 L stirred autoclave. Typically about 50 to 100 mg of catalyst was charged under nitrogen, then 50 to 75 μL Et_3Al (1 M in hexane) scavenger were added and 500 mL hexane as diluent. The reactor pressure was held at 400 psi ethylene for 30 to 120 min. In some experiments, 60 psi H_2 was added during the run and was metered in by monitoring the increase in pressure in the reactor. 43 mL of hexene was introduced into the reactor for certain experiments on comonomer incorporation. At the end of each run, the hexane was flashed off, leaving dry polyethylene.

2.7 Polymer Characterization

2.7.1 Molecular Weight and Polydispersity

Polymers chains are made up of sequences of chemical repeating units and branches that may be arranged regularly or irregularly on the backbone.[15,16] The repeating unit can be very simple in chemical structure, e.g., CH_2 for polyethylene, or very complicated. The number of connected repeating units, n, can range from 2 to 100,000. The process of condensation polymerization can be written in the following form:

$$n\,M \rightarrow (\text{-M-M-M-M-}) \tag{2.27}$$

where M is the monomer. The polymerization reaction is statistical in nature and does not generate a single molecule of a specific length n. Rather, many condensation reactions occur simultaneously, generating many molecules of various lengths, so that the polymers are generally polydisperse. This means that in a given sample the individual molecules are not all the same size and there is a range of molecular weights. Therefore it is the average value of the molecular weight which is determined.

The simplest average value is the number relative molecular weight, denoted M_n. Each polymer fraction is considered to consist of a specific number N_i of molecules of each molecular weight M_i. The total number of molecules in the polymer sample therefore is specified by $\sum_{i=1}^{\infty} N_i$. The relative weight of N_i molecules of molecular weight M_i, is N_iM_i, therefore the number average molecular weight M_n can be written as eq 2.28.

$$M_n = \frac{\sum_{i=1}^{\infty} N_i M_i}{\sum_{i=1}^{\infty} N_i} \tag{2.28}$$

In contrast to the number average molecular weight (which is the summation of the mole fraction of each species present multiplied by its molecular weight), the weight average molecular weight, denoted M_w, is the average weight of the polymer as defined in eq 2.29.

$$M_w = \frac{\sum_{i=1}^{\infty} N_i M_i^2}{\sum_{i=1}^{\infty} N_i M_i} \qquad (2.29)$$

The weight average molecular weight M_w is always greater than the number average molecular weight M_n. The ratio M_n/M_w is an indicator of the breadth of the molecular weight range in a polymer sample. This ratio is called the polydispersity index, or PDI.

Molecular weight and molecular weight distributions of polyethylene were characterized by high-temperature size exclusion chromatography (SEC) at 140°C on a Waters Model 150C+ instrument, using a series of columns: 1-polymer labs PL Gel Guard (7.5 * 50 mm), 1-polymer labs PL Gel 50A (7.5 * 300 mm) and 3-Shodex AT-806MS (8 * 250 mm). 1,2,4-trichlorobenzene stabilized with BHT was used as the mobile phase. 0.1% (wt/vol) of polyethylene was solubilized in trichlorobenzene at ca. 165 - 170°C for 60 minutes with gentle stirring for the last 5 min. 300 µL polyethylene solution was injected into the GPC. NBS 1496 polyethylene (0.1 % (wt/vol)) with M_n 15700 and M_w 190000 and HS 7028 polyethylene with M_n 27529 and M_w 135578 were used as calibration and control standards, respectively.

2.7.2 NMR Spectroscopy

For NMR experiments, solutions of 0.25% polyethylene[17] or polypropylene in 1,2,4-trichlorobenzene were prepared at 125°C. C_6D_6 was added as an internal

frequency lock. Polystyrene was dissolved in $CDCl_3$. ^1H and ^{13}C $\{^1H\}$ NMR spectra (frequency 500 MHz and 125 MHz, respectively) were recorded on a Bruker AMX-500 spectrometer. ^1H NMR spectra were collected using a 3.0 μs 45° pulse and an interpulse decay of 4.7 s, ^{13}C NMR spectra were collected using 5 μsec 45° pulse and an interpulse delay of 1.5 s.

The calculations of monomer incorporation and branching frequencies were performed on a ^{13}C NMR spectrum of a polyethylene sample recorded at Union Carbide. The polyethylene backbone and side chain chemical shift assignments in ppm were referenced to internal tetramethylsilane standard at 0 ppm as a function of branch length, Table 2.1. (Note that γ-carbon chemical shifts, which occur near 30.4 ppm, are not given because they are often obscured by the major 30 ppm resonance for the "n" equivalent, recurring methylene carbons.) The assignments for each carbon are as reported by Randall.[18]

A nomenclature system initiated by Randall[19] was established as follows: methylene carbons located along the backbone of an ethylene-1-olefin copolymer chain are identified by a Greek letters, indicating the location of the nearest methine carbons in either direction. Methine and side branch carbons for short-chain branches are identified as the center unit of either triad, pentad, etc. It is also necessary to identify the location of each carbon in the various type of branches. Carbons in side-chain are identified by an Arabic numeral "i" which designates the position in the branch starting with the methyl carbon as "1", Figure 2.8.

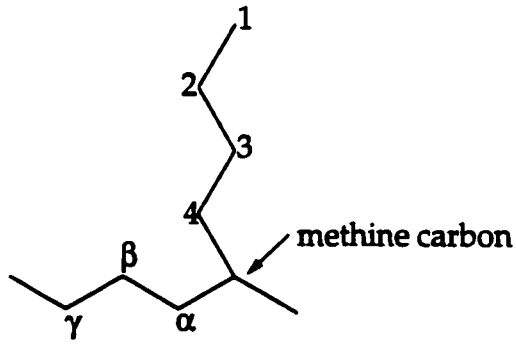

Figure 2.8 Carbon Labelling in ethylene-1-olefin copolymers

Table 2.1 Polyethylene backbone and side-chain chemical shifts in ppm from TMS, as a function of branch length

	backbone resonances			branch resonances					
Branch length	Methine	α-carbon	β-carbon	1	2	3	4	5	6
1	33.3	37.6	27.5	20.0					
2	39.7	34.1	27.3	11.2	26.7				
3	37.8	34.4	27.3	14.6	20.3	36.8			
4	38.2	34.6	27.3	14.1	23.4	-	34.2		
5	38.2	34.6	27.3	14.1	22.8	32.8	26.9	34.6	
6	38.2	34.6	27.3	14.1	22.8	32.8	30.4	27.3	34.6

^{13}C NMR studies of ethylene-based polymers led to the conclusion that branches six carbons in length cannot be distinguished from those that are longer than six carbons. Therefore the designation "branches, six and longer" describes all linear branches six and more carbons in length.[20]

Accurate spectral integration over well-resolved regions gives the comonomer mole fraction. This procedure permits quantitative determination of sequence distributions in the polymer. The ^{13}C NMR spectrum is divided into spectral regions, which are described in Table 2.2 according to the range in ppm which contributes to the designated sequences. Each region is designated by a letter A, B, C, etc.[20] (In practice, the "region G" is omitted from the calculations because of a long methyl spin-lattice relaxation time T_1.[20])

Table 2.2 Various spectral regions in the ^{13}C NMR spectrum of ethylene-1-olefin copolymer.

regions	chemical shift ppm	sequence assignements
A	41.0 to 21.0	all backbone resonances and some branch resonances
B	11.5 to 10.9	the methyl resonance from a butene included in the chain (an ethyl branch) at 11.2 ppm
C	14.9 to 14.3	the methyl resonance from a pentene included in the chain (a propyl branch) at 14.6 ppm
D	20.5 to 19.7	the methyl resonance from a propylene included in the chain (a methyl branch) at 20.0 ppm and a penultimate carbon from a pentane included in the chain (a propyl branch) at 20.3 ppm
E	23.7 to 23.1	the penultimate carbon from a hexene incorporated in a chain (a butyl branch) at 23.4 ppm
F	23.1 to 22.5	the penultimate carbon from a heptane or longer olefin incorporated in the chain (a pentyl or longer branch) at 22.8 ppm
G	14.3 to 13.9	the methyl resonance from hexene or longer olefins incorporated in the chain (butyl or longer branches) at 14.1 ppm

2.7.3 Thermal Analysis

Differential Scanning Calorimetry (DSC) experiments were performed with a Thermoanalysis Instrument Automated DSC. A 5 to 10 mg polyethylene sample was weighed and placed in an aluminum DSC pan. Cyclic heat-cool-heat experiments were performed on each sample. The PE sample was heated from 0°C to 200°C at 10°C/min under nitrogen. The sample was held isothermal at 200°C for

one minute, then cooled at 10°C/min. The sample was held isothermal at 0°C for one minute then heated at 10°C/min to 200°C.

2.8 References

1) Heaney, P. J.; Prewitt, C. T.; Gibbs, G. V. *Silica: Physical Behavior, Geochemistry and Materials Applications;* Mineralogical Society of America: Washington, D. C., 1994.

2) Mowat, W.; Shortland, A.; Yagupsky, G.; Hill, N. J.; Yagupsky, M.; Wilkinson, G. *J. Chem. Soc., Dalton Trans.* **1972**, 533-542.

3) Mowat, W.; Shortland, A. J.; Hill, N. J.; Wilkinson, G. *J. Chem. Soc., Dalton Trans.* **1973**, 770-778.

4) Wijnberg, J. B. P. A.; Wierig, P. G.; Steinberg, H. *Synthesis* **1981**, 901-903.

5) Wiley, G. A.; Hershkowitz, R. L.; Rein, B. M.; Chung, B. C. *J. Am. Chem. Soc.* **1964**, *86*, 964-965.

6) Basi, J. S.; Bradley, D. C.; Chisholm, M. H. *J. Chem. Soc. (A)* **1971**, 1433-1436.

7) Alyea, E. C.; Basi, J. S.; Bradley, D. C.; Chisholm, M. H. *J. Chem. Soc. (A)* **1971**, 772-776.

8) Morrow, B. A. In *Stud. Surf. Sci. Catal.*; 1990; Vol. 57A, pp. 161-224.

9) Haukka, S.; Lakomaa, E.-L.; Root, A. *J. Phys. Chem.* **1993**, *97*, 5085-5094.

10) Haukka, S.; Saastamoinen, A. *Analyst* **1992**, *117*, 1381-1384.

11) Wold, A.; Dwight, K. *Solid State Chemistry;* Chapman Hall: London, 1993.

12) Cheon, J.; Rogers, D. M.; Girolami, G. S. *J. Am. Chem. Soc.* **1997**, *119*, 6804-6813.

13) Schrock, R. R.; Fellmann, J. D. *J. Am. Chem. Soc.* **1978**, *100*, 3359-3370.

14) Morse, P. M.; Spencer, M. D.; Wilson, S. R.; Girolami, G. S. *Organomet.* **1994**, *13*, 1646-1655.

15) Stevens, P. M. *Polymer Chemistry: An Introduction;* Oxford University Press: New York, 1990.

16) Koenig, J. L. *Spectroscopy of Polymers;* Wiley: Washington, DC, 1992.

17) Smith, P. D.; McDaniel, M. P. *J. Polym. Sci.: A: Polym. Chem.* **1990**, *28*, 3587-3601.

18) Randall, J. C. *Polymer Characterization by ESR and NMR*; ACS Symposium Series 142: Washington, D. C., 1980.

19) Randall, J. C. *J. Polym. Sci., Polym. Phys. Ed.* **1973**, *11*, 275.

20) Randall, J. C. *Rev. Macromol. Chem. Phys.* **1989**; *C29*, 201-317.

Reactions of Tetraalkylchromium(IV) Complexes with Silica Surfaces

3.1 Introduction

In 1973, Ballard at ICI obtained the first surface organometallic complex of zirconium by reaction of tetrakis(π-allyl)zirconium with partially dehydroxylated silica.[1] This reaction was then extended to other organometallic systems MR_4 (M = Zr, Ti, Hf, and R = norbornyl, naphthyl, benzyl, neopentyl) and other inorganic oxides such as alumina and titania.[2-5] Homoleptic metal alkyls undergo cleavage of one or more metal-carbon bond to give species bound to the surface. The surface reaction is accompanied by the evolution of alkane or alkene. However, the overall stoichiometry of the surface reaction seems to depend upon the nature and the degree of hydroxylation of the oxide.[1,3-7] Thus the composition of the surface organometallic complex suggested for these materials is not precise; mixtures of surface species are thought to be present on the surface in most systems.[3-5,7]

In the early 1990s, the reaction of $ZrNp_4$ (Np is neopentyl) with silica was reported to give the first well-defined trisalkylzirconium(IV)-silica complex.[8] Further studies in this field have investigated transition metal alkyls of Group IV, MR_4 (M = Hf,[9] Ti[10,11] and R = Np) and Group V where the oxidation state is (V), as in $Ta(=CHCMe_3)Np_3$[12] or (IV), as in $V(CH_2SiMe_3)_4$.[13] These organometallic complexes react readily with surface hydroxyl groups of inorganic oxides such as silica and alumina.

We intended to prepare analogous oxide-supported organochromium complexes, using as reactants the volatile homoleptic molecular precursors CrR_4, where R is a ligand such as neopentyl or trimethylsilylmethyl. The molecular

precursors are readily synthesized and stable at room temperature. The homoleptic nature of the precursor limits the number of possible surface reactions.

A previous attempt to graft CrR_4 on the surface of silica failed.[14] A brief report of the interaction of CrR_4 with silica concluded that only physisorption occurs, based on the similarity in color of the treated silica to the molecular precursors.[15]

Before undertaking this study, the reactivity of CrR_4 complexes towards the surface hydroxyl groups of silica was therefore expected to be low, since they are known to be completely unreactive towards alcohols and even water.[16] However, the surface silanols of Aerosil are slightly acidic (pKa ~ 4)[17] and CrR_4 is known to undergo protonolysis by acids.[18]

In this chapter, we report the preparation, characterization and reactivity of well defined silica-supported chromium(IV) species.

3.2 Synthesis of Surface Organometallic Complexes

The temperature at which the silica surface is treated determines the silanol content on the surface, and these values are well-documented and reproducible. Upon heating under dynamic vacuum (10^{-4} Torr), adsorbed water is removed, followed by condensation of neighboring hydroxyls to give a partially dehydroxylated silica surface. When the silica is heated to 200°C, the hydroxyl density decreases from an initial value of 4.9/nm^2 to 2.6 OH/nm^2, while at 500°C only 1.2 OH/nm^2 remain.[17] Silicas subjected to these thermal treatments will be referred to as silica-200 and silica-500, respectively.

The reaction of the molecular complexes $Cr(CH_2C(CH_3)_3)_4$, **1a**, and $Cr(CH_2Si(CH_3)_3)_4$, **1b**, with a silica surface partially dehydroxylated at 200°C or 500°C was performed in the total absence of solvent. Sublimation of each complex onto a silica sample at room temperature resulted in a change of the initially colorless

silica disk to orange (**1a**) or pink (**1b**). The supported surface organometallic complexes are therefore intensely colored but slightly different in hue compared to their molecular precursors **1a** and **1b** which are maroon and purple, respectively. The color of the silica disk is preserved even after prolonged desorption of unreacted (physisorbed) CrR_4 to a liquid N_2 trap, which indicates that irreversible chemisorption does indeed occur at at room temperature, contrary to a literature report.[15]

3.3 Characterization of Surface Organometallic Complexes

3.3.1 Infrared Spectroscopic Characterization

The spectrum of a self-supporting disk of silica-200 has a sharp band at 3747 cm^{-1}, attributed to non-hydrogen-bonded surface hydroxyl groups, with a broad low frequency shoulder assigned to hydroxyl groups perturbed by hydrogen-bonding, Figure 3.1a. The broad bands at 1977, 1868 and 1647 cm^{-1} are overtones and combinations of the intense Si-O-Si fundamental modes originating in the bulk of the silica, and which render the silica virtually opaque below 1200 cm^{-1}, although there are two "windows" of partial transparency from 100 to 850 cm^{-1} and from 750 to 600 cm^{-1}. The overtone bands are unchanged by any reactions which occur at the surface and which therefore do not alter the bulk structure of silica.

When CrR_4 (**1a** or **1b**) is sublimed at room temperature in an *in situ* IR cell onto a self-supporting disk of either silica-500 or silica-200, new bands characteristic of alkyl groups appear. Those in the region 3000-2800 cm^{-1} are assigned to C-H stretching vibrations, in the region 1500-1300 cm^{-1} to methyl and methylene deformations, Figures 3.1 and 3.2. Bands assigned to methyl rocking modes coupled to Si-C stretching in the case of **1b** are found in the region 750-680 cm^{-1}.

IR frequencies characteristic of silica-supported chromium complexes are compiled in Table 3.1. No significant differences were observed between the IR

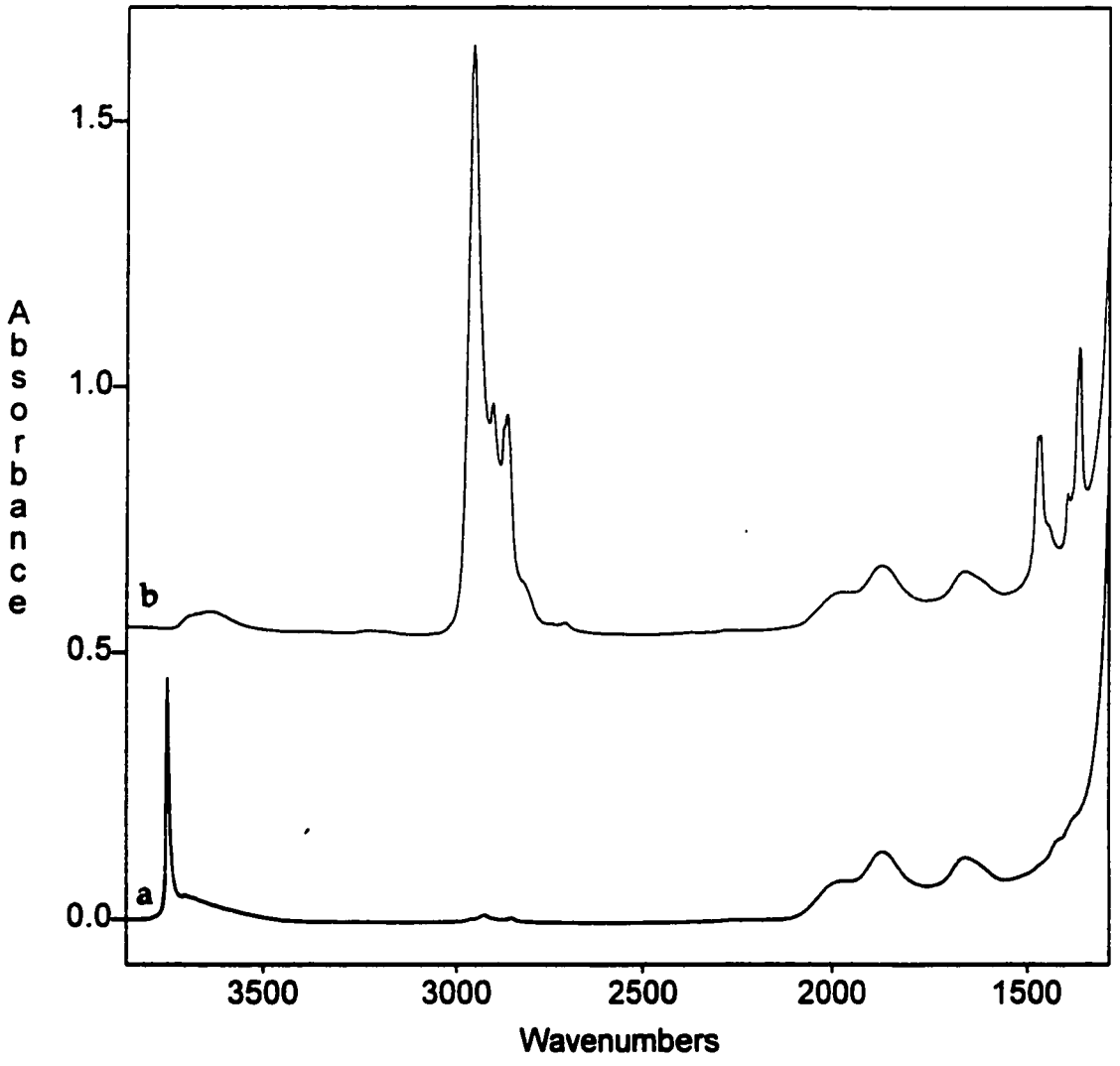

Figure 3.1 Transmission infrared spectra of (a) a self-supporting disk of silica, partially dehydroxylated at 200°C; (b) after reaction with $Cr(CH_2C(CH_3)_3)_4$

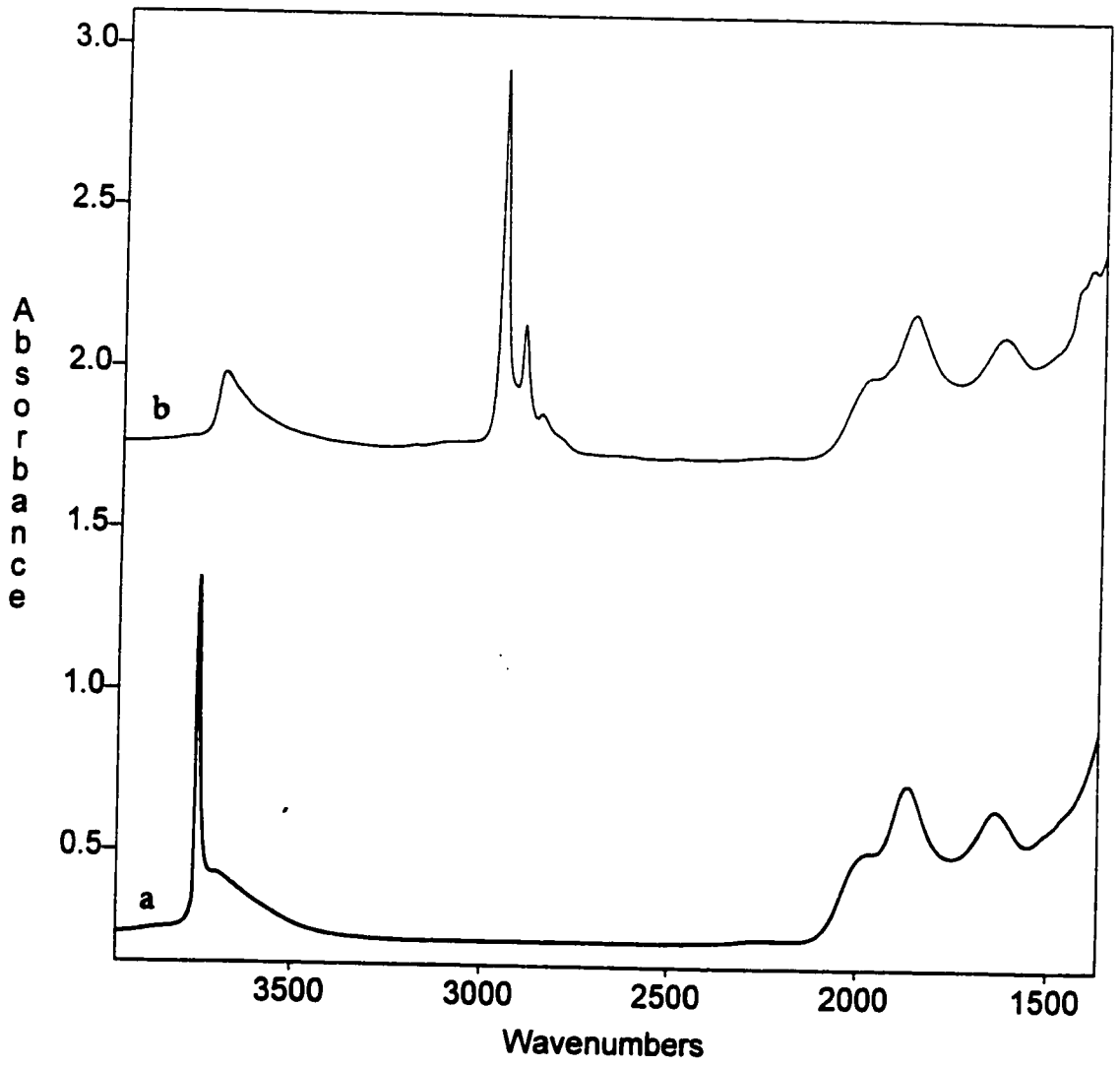

Figure 3.2 Transmission infrared spectra of (a) a self-supporting disk of silica, partially dehydroxylated at 200°C; (b) after reaction with $Cr(CH_2Si(CH_3)_3)_4$

Table 3.1 Infrared frequencies (cm^{-1}) of silica modified by $Cr((CH_2C(CH_3)_3)_4$ and $Cr((CH_2Si(CH_3)_3)_4$

$(\equiv SiO)_nCr(CH_2C(CH_3)_3)_{4-n}$	$(\equiv SiO)_nCr(CH_2Si(CH_3)_3)_{4-n}$	Assignment[19]
2955	2956	$\nu_{as}(CH_3)$
2905	2899	$\nu_{as}(CH_2)$
2868	2848	$\nu_s(CH_3)$
2824	2808	$\nu_s(CH_2)$
1471,1466	1435,1406	$\delta_{as}(CH_3)$
1394		$\delta_{as}(CH_2)$
1368,1360	1311	$\delta_s(CH_3)$
748	747, 734	$\rho(CH_3)$, ν(Si-C)
	693	ρ(Si-C)

spectra of silica-200 and silica-500 modified by the same organometallic complex.

The silica band at 3747 cm^{-1}, assigned to ν(SiO-H), disappears completely during grafting, and is not regenerated when unreacted CrR_4 is desorbed. A very broad band at ca. 3690 cm^{-1} in the O-H stretching region remains after reaction with CrR_4. It is assigned to OH groups which are inaccessible, possibly located in the bulk of the silica structure.[17] These observations suggest that the mode of chemisorption of CrR_4 on silica is reaction with surface hydroxyl groups.

In the gas phase, a hydrocarbon product was detected during grafting. It was identified as the protonated ligand RH, by comparison of the gas phase IR spectra to the spectra of the pure compounds neopentane and tetramethylsilane.

3.3.2 Electronic Spectroscopy

Diffuse absorbance UV-visible spectra of the modified silicas contain bands that are slightly blue-shifted compared to those of their molecular precursors. The spectrum of **1a** supported on silica has a peak at 456 nm, whereas **1a** in hexane has a peak at 474 nm and a well-defined minimum at 418 nm.[18] The minimum at *ca.* 400 nm in the spectrum of **1a** on silica is very shallow, as shown in Figure 3.3a.

Similarly, the peak in the spectrum of **1b** on silica occurs at 513 nm, while **1b** itself has a peak at 538 nm.[16] The spectrum of **1b** on silica also contains a band at ca. 384 nm, and two shoulders at 482 and 586 nm, Figure 3.3b, which are not present in the spectrum of molecular **1b**.

Since the differences in the UV-visible spectra between the molecular and grafted complexes are not dramatic, color is not a sensitive indicator of the occurrence (or lack thereof) of chemisorption. The blue-shift of λ_{max} is, however, consistent with the replacement of one or more alkyl ligands by oxygen-donor ligands derived from the silica surface. For comparison, the UV-visible spectrum of $Cr(O^tBu)_4$ has λ_{max} at 400 nm.

3.3.3 Nuclearity and Oxidation State of Grafted Complexes

A variety of physical methods are used for the determination of oxidation states of organometallic complexes. The appropriate method depends on the nature of the metal and the stability of the corresponding complex. EPR[16,18,20-23] and magnetic susceptibility measurements[18] have already been applied to the characterization of molecular CrR_4 complexes.

EPR spectroscopy is used to characterize the electronic properties of paramagnetic organometallic complexes and provide insight into their structure and bonding. The degree of covalence of metal-ligand bonding in paramagnetic complexes can be evaluated from g values, which reflect the amount of unpaired

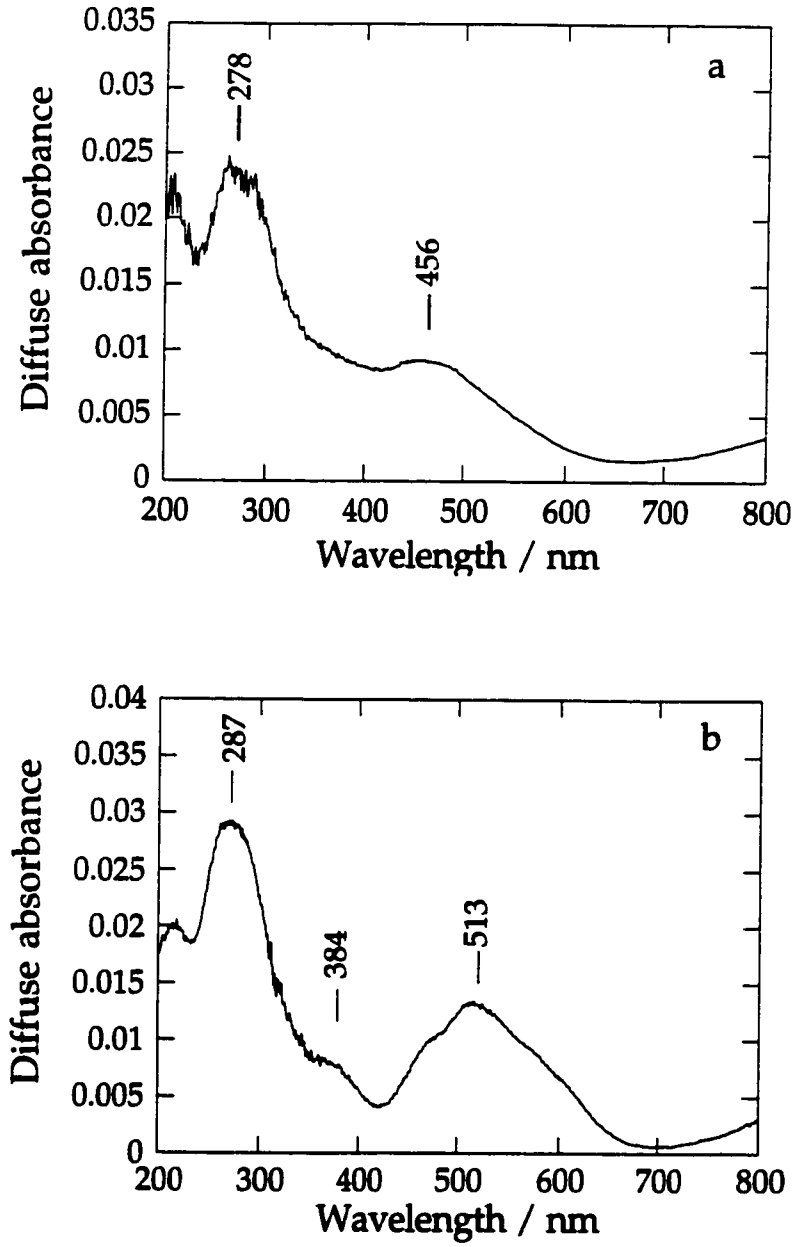

Figure 3.3 Diffuse reflectance UV-visible spectra of silica-500 modified with (a) $Cr(CH_2C(CH_3)_3)_4$, **1a**, and (b) $Cr(CH_2Si(CH_3)_3)_4$, **1b**

spin density on the metal, and the magnitude of the metal and the ligand nuclear hyperfine coupling constants, which indicate the metal and ligand orbital contributions to the ground state through spin-orbit coupling. Electron paramagnetic resonance has been used to demonstrate the oxidation state of CrR_4, since some d^2 chromium(IV) systems exhibit well-defined EPR spectra. In general, at room temperature the spectrum of CrR_4 consists of a single, narrow, intense line at mid-field (H_o near 3270 gauss).[22] On cooling to -196°C, the EPR spectrum resolves into a doublet. The EPR spectra of d^2 ions can be interpreted in terms of the spin hamiltonian, where the transitions between spin levels lead to a triplet of doublets centered on the field corresponding to the g-value of the triplet. The zero-field splitting is very small for CrR_4 and the ligand field is nearly tetrahedral, leading to a large separation between the e and t_2 levels. A significantly broadened mid-field line was observed in some cases, indicating that large R groups distort the tetrahedral symmetry of the ligand field.

In the solid state, CrR_4 (R = Np) exhibits a magnetic moment of ca. 2.89 B.M., measured at room temperature on the Gouy-Rankine balance. This value indicates that the d electrons are not spin paired and corresponds to a high spin d^2 Cr(IV) system.

3.3.3.1 Electron Paramagnetic Resonance

The EPR spectrum of the product of reaction of $Cr(CH_2C(CH_3)_3)_4$ with silica-200 is a broad line at 298 K. On cooling to 88 K, a slight inflection point was observed at g = 1.984, Figure 3.4. A similar spectrum was obtained for **1a** grafted on silica-500. The spectrum is similar in appearance to that of molecular precursor $Cr(CH_2C(CH_3)_3)_4$ in hexane, which is a broad line at room temperature but narrows upon cooling to 180 K to give a poorly resolved doublet centered at g = 1.986, Figure 3.5a. Upon further cooling to 147 K, $C(CH_2C(CH_3)_3)_4$ exhibits the

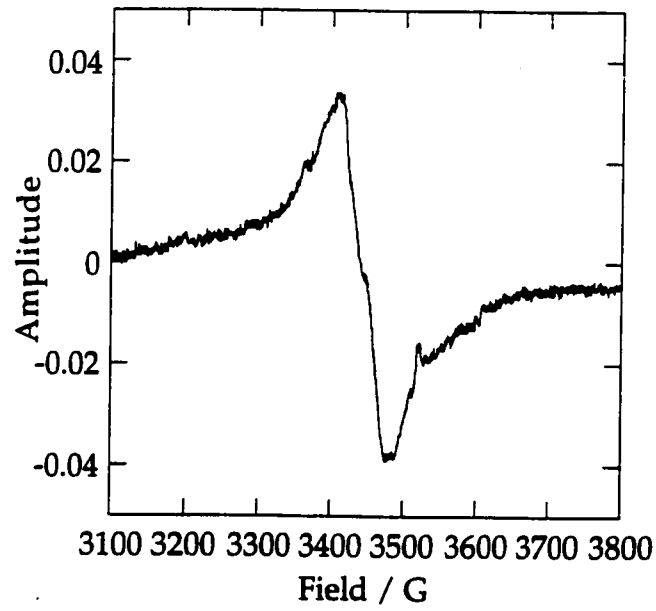

Figure 3.4 EPR spectrum of silica-200 modified by $Cr(CH_2C(CH_3)_3)_4$ on silica-200, at 88K

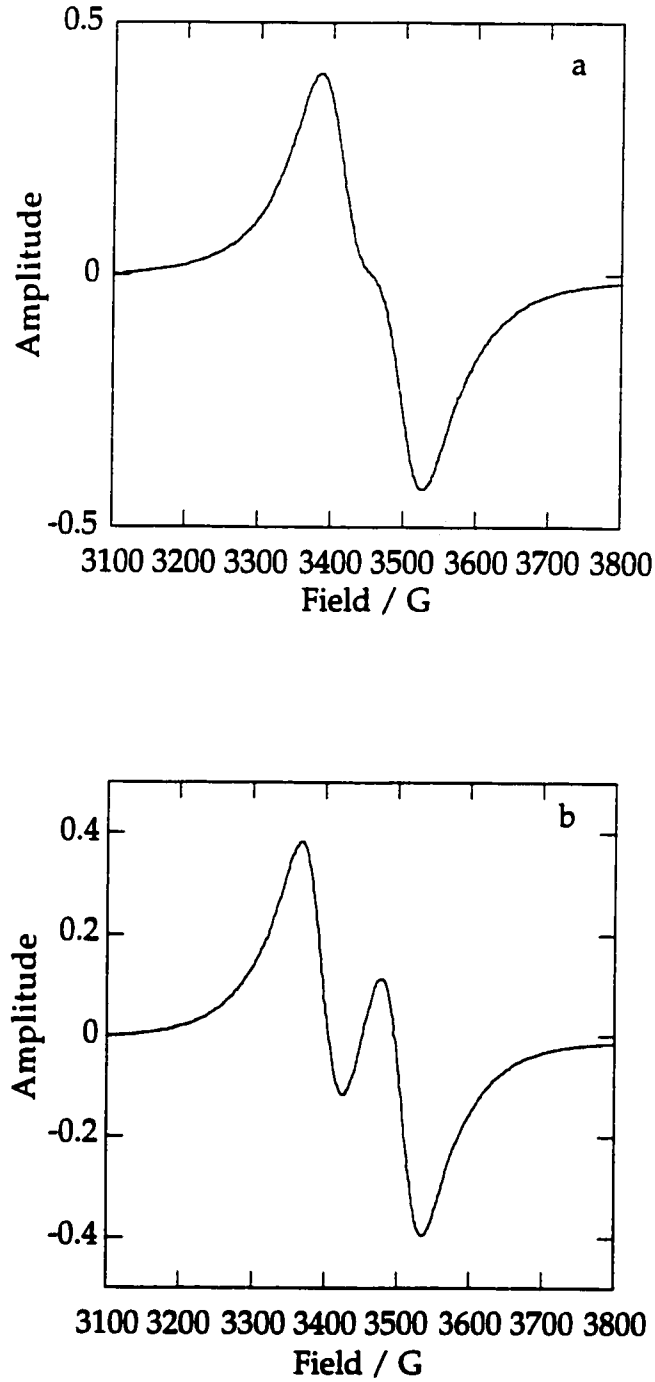

Figure 3.5 EPR spectra of $Cr(CH_2C(CH_3)_3)_4$, **1a**, (a) at 180 K in hexane (b) at 147 K in hexane.

characteristic doublet spectrum of a d^2 system, centered at g = 1.986,[18] Figure 3.5b.

The EPR spectra of $Cr(CH_2SiMe_3)_4$, **1b**, on silica-200 and -500 show essentially the same behavior as the neopentyl analogue. The g value of 1.982 compares well to molecular **1b**, which has g = 1.984 and D = 0.063 cm^{-1}.[18]

From these observations, we conclude that EPR spectra are consistent with the presence of chromium(IV) on silica surface. Nevertheless, other oxidation states of chromium may not detected by the EPR technique. In order to determine quantitatively the average oxidation state of grafted complexes, magnetic susceptibility studies were undertaken.

3.3.3.2 Magnetic Susceptibility

The modified silicas are magnetically dilute materials, since they contain typically 1% Cr dispersed in a diamagnetic silica matrix. The magnitudes of the room temperature moments are extremely small. However, at low temperature (<100 K), the solids show typical Curie-Weiss behavior, Figure 3.6. From the fitted curve, the value of μ_{eff} for $CrNp_4$/silica-500 is 2.68 B.M., compared to 2.7 B.M. for molecular precursor **1a** and 2.9 B.M. for **1b**,[18] and close to the spin-only value expected for a d^2 system, 2.83 B.M. There is evidence for very weak antiferromagnetic coupling from the Néel temperature, θ = 7 K. We conclude that the grafted species are essentially magnetically isolated, mononuclear d^2 systems.

3.4 Stoichiometry of the Reaction of CrR_4 with Silica

3.4.1 On Silica-500

The reaction between CrR_4 and silica-500 results in the evolution of alkane RH (R = $CH_2C(CH_3)_3$ or $CH_2Si(CH_3)_3$) as the only volatile product, confirmed by gas phase IR and GC analysis. The amount of alkane was quantified by absolute pressure measurement with a capacitance manometer and

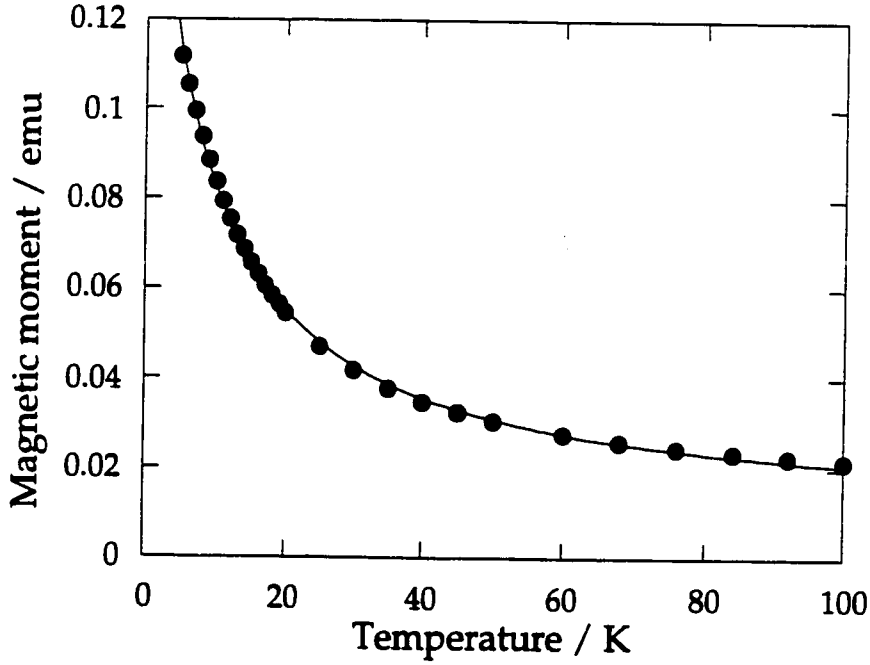

I = C'/T + θ		
	Value	Error
C'	1.2351	0.0302
θ	6.7805	0.2778

Figure 3.6 Temperature-dependence of the magnetic moment of 21 mg $CrNp_4$/silica-500 with 1.02 wt.% Cr loading.

by quantitative gas phase IR spectroscopy, using the integrated intensity of the ν(CH) region.

For example, when a 9.8 mg self-supporting disk of silica-500 was exposed to excess **1a**, 3.6 μmol of neopentane was formed. After desorption of unreacted **1a**, chemisorbed Cr was extracted from the silica. The sample contained 1.9% Cr by mass, or 3.6 μmol Cr. From the known surface area (200 m^2/g) and hydroxyl content of silica-500 before the reaction (1.2 OH/nm^2), we calculate that the initial quantity of hydroxyl groups present on the 9.8 mg disk was 4.0 μmol.

The experiment described above was repeated for a variety of silica sample sizes (10 - 100 mg) and Cr loadings ranging from 0.2 - 2.0 wt%. Based on the average of 5 experiments, 0.92 ± 0.05 mol RH are liberated per mol of grafted Cr on silica-500. This result suggests that the following stoichiometric reaction occurs:

$$\equiv SiOH + CrR_4 \rightarrow \equiv SiOCrR_3 + RH \qquad (3.1)$$

1a **2a** $R = CH_2C(CH_3)_3$

1b **2b** $R = CH_2Si(CH_3)_3$

where ≡SiOH represents a hydroxyl group on the silica surface. The results for various Cr loadings are summarized in Table 3.2. The stoichiometry of eq 3.1 is observed regardless of Cr loading in the range 0.13 - 0.89 Cr/OH. The highest Cr loading achieved was slightly less than 1 Cr/OH, even with a large excess of CrR_4.

The products **2a** and **2b** retain three alkyl groups per Cr, and these are susceptible to protonolysis. Treatment with 10 Torr $HCl_{(g)}$ causes the colors of both **2a** and **2b** to change to green, and liberates 2.90 ± 0.01 RH/Cr, eq 3.2, Table 3.2.

$$\equiv SiOCrR_3 + \text{xs } HCl \rightarrow \text{"}\equiv SiOCrCl_3\text{"} + 3\,RH \qquad (3.2)$$

2a,b

Table 3.2 Quantitative product analysis for the reaction of CrR_4 with silica-500

CrR_4[a]	products of grafting				products of protonolysis	
	mmol Cr[b]	Cr/OH[c]	mmol RH[b]	RH/Cr	mmol RH[b]	RH/Cr
1b	0.050	0.13	0.048	0.95		
1a	0.205	0.50	0.173	0.84	0.595	2.89
1a	0.210	0.53	0.201	0.96		
1a	0.247	0.62	0.216	0.87	0.719	2.91
1a	0.363	0.89	0.359	0.98		
average				0.92 ± 0.05		2.90 ± 0.01

[a] R is $CH_2C(CH_3)_3$, **1a**, or $CH_2Si(CH_3)_3$, **1b**.

[b] All quantities are reported normalized per g of silica.

[c] Ratio of the amount of chemisorbed Cr to the initial amount of surface hydroxyl groups; there are 0.40 mmol OH/g silica-500.

The product $\equiv SiOCrCl_3$ was not characterized further, however, Cr analysis after protonolysis confirmed that the metal remains chemisorbed rather than being liberated from the surface as volatile $CrCl_4$.[16]

The average stoichiometries of the surface reactions on silica-500 are consistent with those reported for the grafting of homoleptic tetraalkyl complexes of Ti, Zr and Hf.[1-3,8] The reaction of CrR_4 with silica-500 therefore gives a surface complex whose *average* formula is $\equiv SiOCrR_3$, **2**. In order to obtain the average ratio R/Cr = 3, species such as $(\equiv SiO)_2CrR_2$ can only be present if (a) unreacted CrR_4 is also present, or (b) a reaction of CrR_4 with silica which does not liberate RH also occurs. The first possibility is excluded by the stability of the material to prolonged desorption; physisorbed volatile CrR_4 is completely removed under these

conditions. The second possibility can be accommodated by the reaction of CrR_4 with siloxane bridges, eq 3.3.

$$\equiv SiOSi\equiv + CrR_4 \rightarrow \equiv SiOCrR_3 + \equiv SiR \qquad (3.3)$$

Similar reactions have been observed on highly dehydroxylated silica with $Ni(\eta^3\text{-}C_3H_5)_2$,[24] $AlMe_3$[25] and $Zr(CH_2C(CH_3)_3)_4$.[26] However, the occurrence of reaction 3.3 is inconsistent with the disappearance of 93% of the ν(C-H) intensity upon treatment with HCl, since ≡SiR species are unreactive under these conditions. Therefore we conclude that the average formula of **2** accurately represents the major species, a tris(alkyl)chromium(IV) fragment, on the silica-500 surface.

3.4.2 On Silica-200

On silica-200, a grafting reaction similar to eq 3.1 occurs, with liberation of RH as the only volatile product. However, in this case, based on an average of 28 experiments, (1.87 ± 0.03) equivalents of RH are evolved per chemisorbed Cr, consistent with the stoichiometry shown in eq 3.4.

$$\underset{\textbf{1a,b}}{2\equiv SiOH + CrR_4} \rightarrow \underset{\textbf{3a,b}}{(\equiv SiO)_2CrR_2} + 2\,RH \qquad (3.4)$$

Once again, this stoichiometry is independent of Cr loading. Although silica-200 has a hydroxyl content approximate twice that of silica-500, the maximum loading of Cr on silica-200 is not higher, being ca. 0.4 mmol Cr/g silica, which corresponds to slightly less than the maximum value of 0.5 Cr/OH predicted by eq 3.4. The products **3a** and **3b** retain an average of only two alkyl ligands per Cr, confirmed by

protonolysis with 10 Torr $HCl_{(g)}$ to give (1.9 ± 0.1) RH/Cr, eq 3.5.

$$(\equiv SiO)_2CrR_2 + \text{xs HCl} \rightarrow \text{"}(\equiv SiO)_2CrCl_2\text{"} + 2\ RH \qquad (3.5)$$

3a,b

The results are summarized in Tables 3.3 and 3.4 for **3a** and **3b**, respectively.

On silica-200, the average formula is therefore $(\equiv SiO)_2CrR_2$, **3**. It seems reasonable to suppose that **3** is formed step-wise by initial reaction of **1** to form **2**, followed by reaction of **2** with an adjacent ≡SiOH, due to the greater proximity of the latter on silica-200 compared to silica-500. Using cristobalite as a model for amorphous silica, the closest approach between the oxygen atoms of surface hydroxyl groups in the same row is ca. 2.5 Å,[27] creating a reasonable bidentate binding geometry for the silica "ligand". The proposed reaction mechanism consists of eq 3.1 followed by eq 3.6.

$$\equiv SiOCrR_3 + \equiv SiOH \rightarrow (\equiv SiO)_2CrR_2 + RH \qquad (3.6)$$

Therefore, we should expect to obtain a mixture of $\equiv SiOCrR_3$ and $(\equiv SiO)_2CrR_2$ on silica-200, in a ratio which depends on the relative rates of reactions (3.6) and (3.1). However, in order to justify the observed product ratio RH/Cr = 2, the amount of residual $\equiv SiOCrR_3$ present must be balanced by an equal amount of a monoalkyl species $(\equiv SiO)_3CrR$. The latter is considered unlikely, since the required third hydroxyl group is located in an adjacent row, over 5 Å away.[28] On silica-200, we therefore conclude that the major species is $(\equiv SiO)_2CrR_2$ with an exact ratio RH/Cr = 2.

The grafting of ZrR_4 on silica-200 to give $(\equiv SiO)_2ZrR_2$ has been reported.[1,3] However, it has also been suggested that such Group IV surface

Table 3.3 Quantitative product analysis for the reaction of $Cr(CH_2C(CH_3)_3)_4$ with silica-200

products of grafting					products of protonolysis	
wt.% Cr	mmol Cr[a]	Cr/OH[b]	mmol RH[a]	RH/Cr	mmol RH[a]	RH/Cr
0.87	0.168	0.20	0.310	1.85		
1.22	0.236	0.27	0.441	1.87	0.437	1.85
1.25	0.241	0.28	0.463	1.92		
1.27	0.245	0.29	0.466	1.90		
1.28	0.247	0.39	0.487	1.97		
1.30	0.250	0.29	0.465	1.86		
1.37	0.264	0.30	0.488	1.85	0.499	1.89
1.39	0.268	0.31	0.506	1.89		
1.45	0.279	0.32	0.530	1.90		
1.89	0.364	0.42	0.695	1.91		
1.90	0.366	0.42	0.688	1.88		
1.92	0.369	0.43	0.697	1.89		
1.92	0.370	0.43	0.699	1.89	0.707	1.91
1.92	0.371	0.43	0.714	1.92		
1.93	0.372	0.43	0.703	1.89	0.696	1.87
1.94	0.373	0.43	0.711	1.90		
1.94	0.374	0.43	0.720	1.93		
average				1.90 ± 0.03		1.88 ± 0.02

[a] All quantities are reported normalized per g of silica.

[b] Ratio of the amount of chemisorbed Cr to the initial amount of surface hydroxyl groups, 0.86 mmol OH/g silica-200.

Table 3.4 Quantitative product analysis for the reaction of $Cr(CH_2Si(CH_3)_3)_4$ with silica-200

products of grafting					products of protonolysis	
wt.% Cr	mmol Cr[a]	Cr/OH[b]	mmol RH[a]	RH/Cr	mmol RH[a]	RH/Cr
0.21	0.041	0.05	0.080	1.94		
1.04	0.195	0.23	0.366	1.85		
1.13	0.217	0.25	0.412	1.90	0.410	1.89
1.22	0.235	0.27	0.449	1.91		
1.28	0.246	0.29	0.465	1.89		
1.56	0.301	0.35	0.548	1.82		
1.82	0.353	0.41	0.667	1.89		
1.87	0.360	0.43	0.680	1.89		
1.92	0.369	0.43	0.708	1.92	0.701	1.90
1.92	0.370	0.43	0.714	1.93		
1.92	0.372	0.43	0.714	1.93		
average				1.89 ± 0.03		1.90 ± 0.01

[a] All quantities are reported normalized per g of silica.

[b] Ratio of the amount of chemisorbed Cr to the initial amount of surface hydroxyl groups, 0.86 mmol OH/g silica-200.

organometallic complexes are mixtures of mono-, bis- and tris(alkyl)metal fragments.[6,11] In this study, we confirm that the precise as well as the average value of n is indeed 2. In retrospect, it seems reasonable that the "intramolecular" reaction (3.6) should be preferred over "intermolecular" reaction (3.1), since the second substitution at Cr takes place while the organometallic fragment is grafted in position next to a surface hydroxyl group. The second hydroxyl group will be sterically inaccessible due to the presence of the surface organometallic fragment, and therefore unlikely to be available for reaction with physisorbed CrR_4.

3.5 Molecular Modeling

A rudimentary computer modeling study of the surface organometallic fragments was undertaken in order to estimate the surface area occupied by the grafted species. Because of the difficulties in modeling the extended silica surface, we limited our model to a system in which the silica surface is simulated by $(HO)_3SiO$ (for silica-500) or $[(HO)_2SiO]_2O$ (for silica-200), connected by oxygen bridges to the chromium center. The structures were fully optimized on a Silicon Graphics computer using the Spartan 4.0 software package, as shown in Figures 3.7 and 3.8 for silica-500 and silica-200, respectively. The Cr-C bond lengths are 2.07 Å, the Cr-C-C angles range from 109 to 113° and the C-Cr-C angles are 109-110°.[29]

The surface area occupied by the tris(neopentyl) complex $(\equiv SiO)Cr(CH_2CMe_3)_3$ was estimated to be 90 Å^2, Figure 3.9b. The total area occupied by these fragments at our highest loading; 0.36 mmol Cr/g silica-500, is therefore 200 m^2, which represents a full monolayer on Aerosil-200 (surface area 200 m^2/g).

The bis(neopentyl) complex $(\equiv SiO)_2Cr(CH_2CMe_3)_2$ occupies an estimated surface area of 60 Å^2, Figure 3.10b. On silica-200, the maximum loading (0.37 mmol

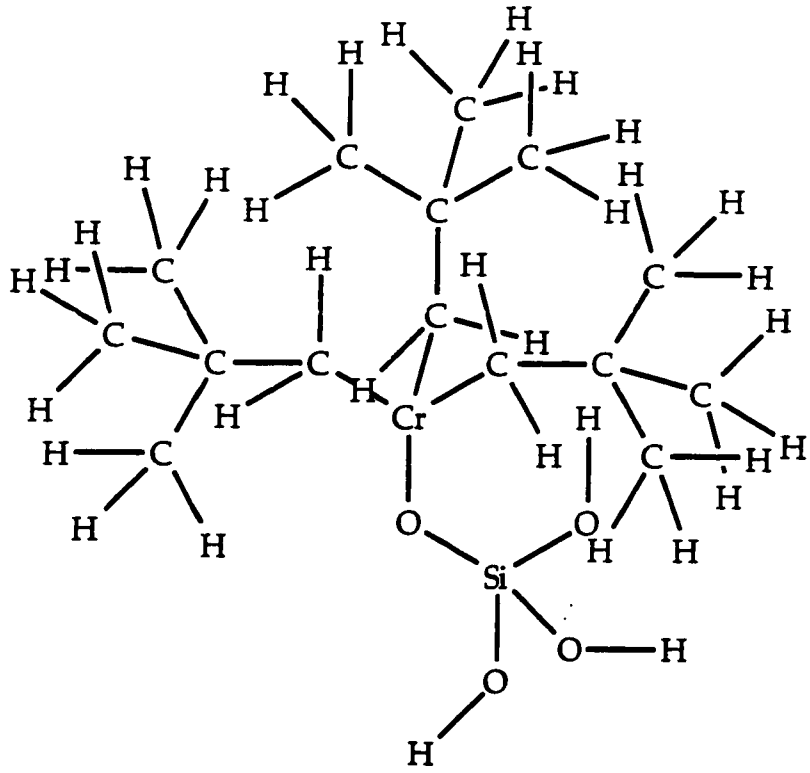

Figure 3.7 Model of $(HO)_3SiOCr(CH_2CMe_3)_3$

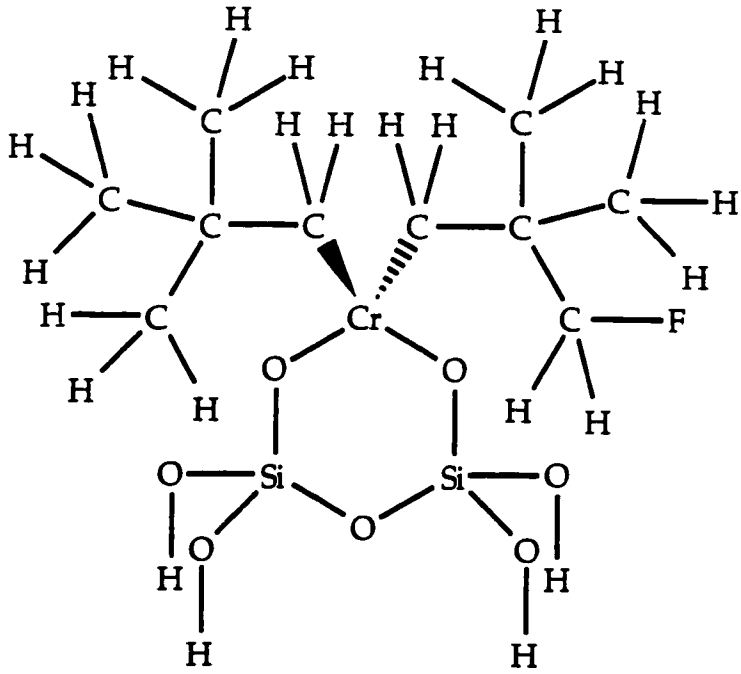

Figure 3.8 Model of $(\mu\text{-O})[(HO)_2SiO]_2Cr(CH_2C(CH_3)_3)_2$

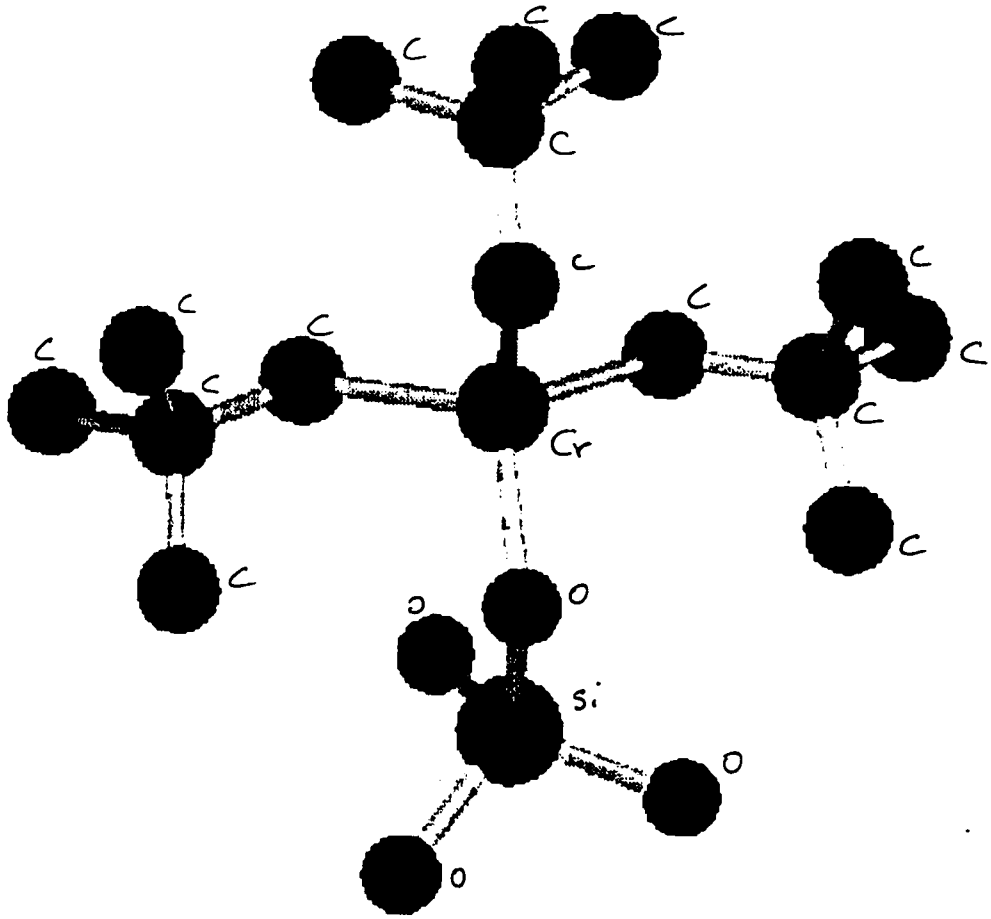

Figure 3.9 Molecular modeling of $(HO)_3SiOCr(CH_2CMe_3)_3$ (a) side view ball-stick representation.

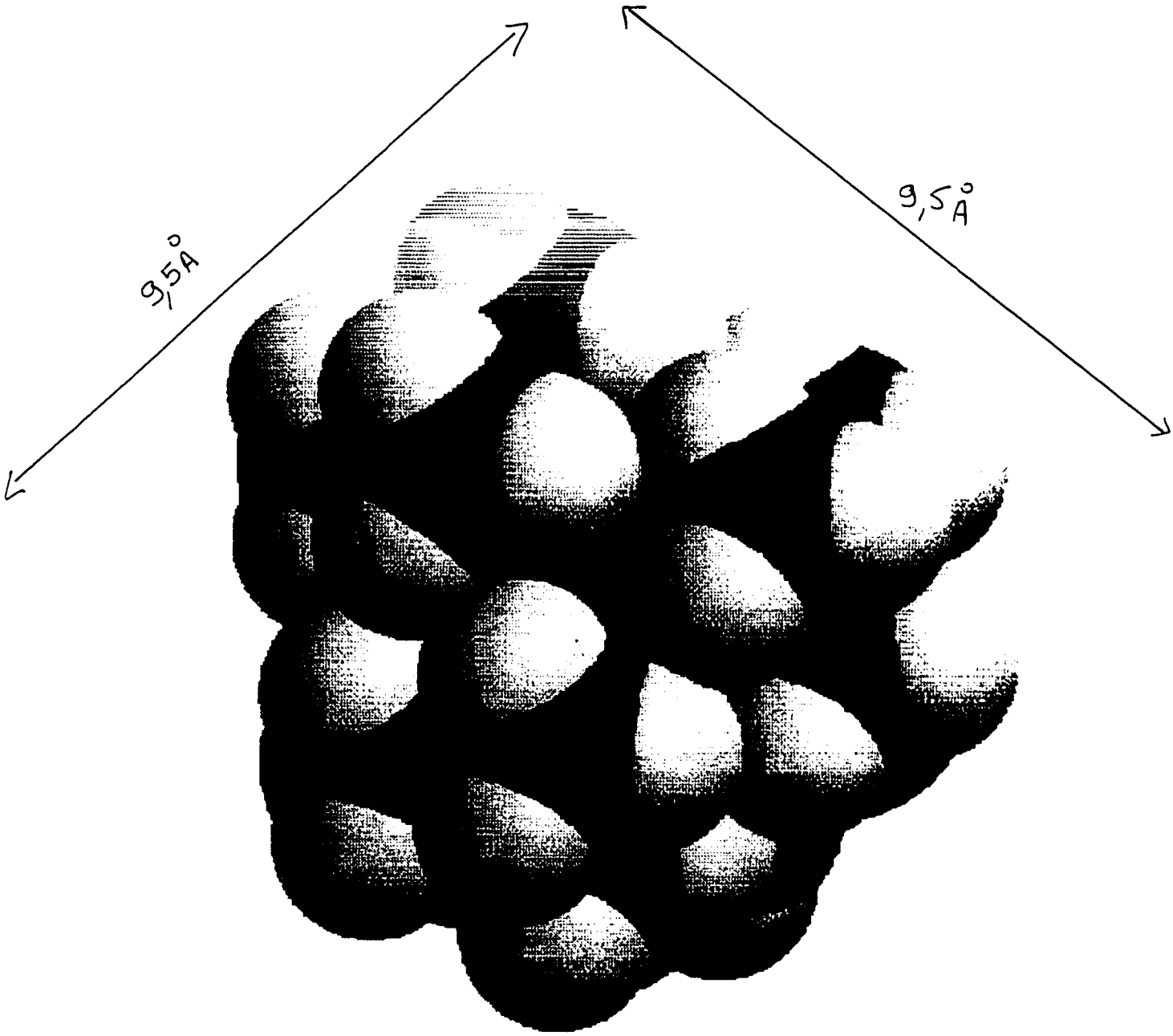

Figure 3.9 (continued) Molecular modeling of $(HO)_3SiOCr(CH_2CMe_3)_3$ (b) top view, space-filling representation.

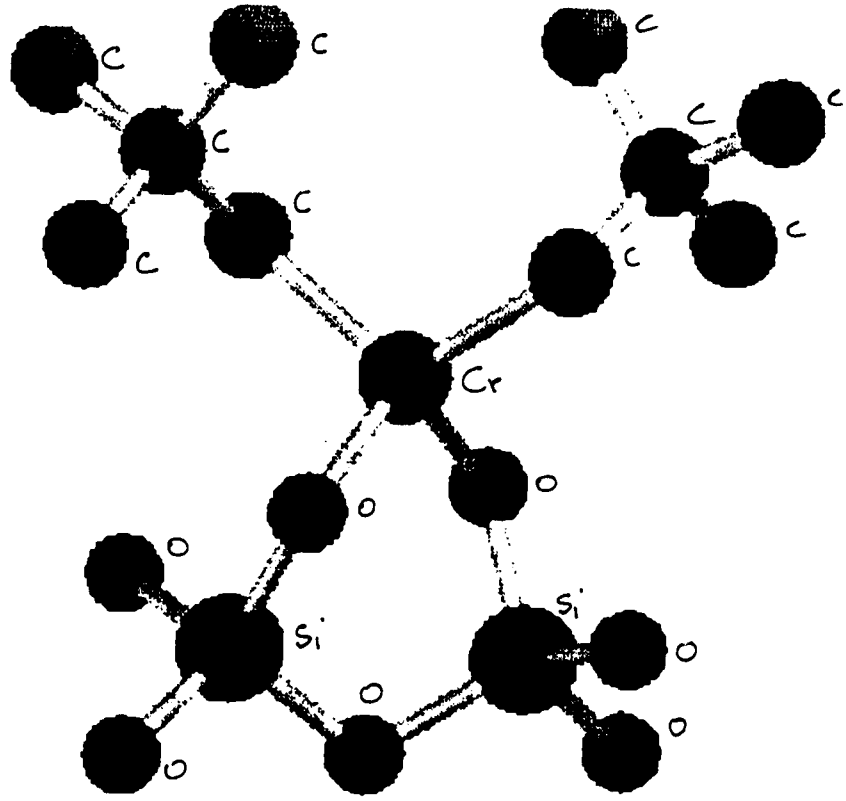

Figure 3.10 Molecular modeling of (μ-O)[$(HO)_2SiO]_2Cr(CH_2C(CH_3)_3)_2$ (a) side view ball-stick representation.

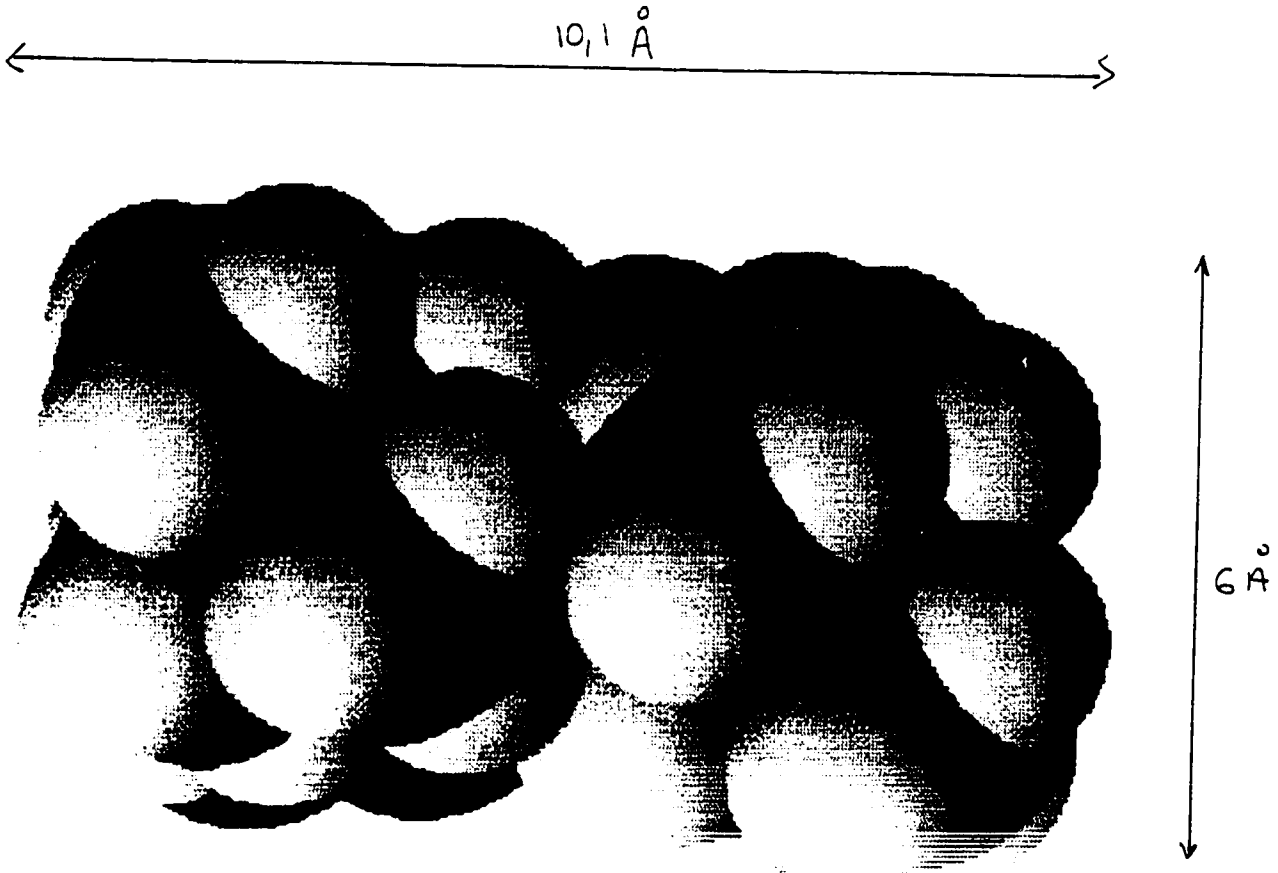

Figure 3.10 (continued) Molecular modeling of $(\mu\text{-O})[(HO)_2SiO]_2Cr(CH_2C(CH_3)_3)_2$ (b) top view, space-filling representation.

Cr/ g silica-200) corresponds to a coverage of 130 m^2/g, achieved when slightly less than all the surface hydroxyls have been consumed. We believe that only 90% of the hydroxyls on silica surface-200 are available to react with the tetraalkylchromium(IV). Further reaction with siloxane sites, as in eq 3.3, does not occur in the remaining available space on the silica surface.

3.6 Mechanism of Grafting

Our study of the stoichiometry of the reactions of CrR_4 with silica gave average values for the number of ligand substitutions on surface species, and the maximum loading values in Tables 3.2, 3.3 and 3.4 suggest that CrR_4 is chemisorbed onto silica exclusively by reaction with the surface hydroxyl groups. We undertook to probe the mechanism of these reactions by chemisorption on deuterated silica. Deuterium was incorporated into the hydroxyl groups of silica by repeated exposure to D_2O or DCl, until ca. 90% exchange was achieved (estimated by the loss of intensity of the ν(SiO-H) peak at 3747 cm^{-1} in the IR spectrum). Upon addition of DCl or D_2O, the silanol groups of the silica surface, initially characterized in the IR by bands at 3747 and 3650 cm^{-1}, decreased in intensity while two new bands at 2762 and 2650 cm^{-1} appeared, indicating the formation of deuterated silanol groups on the surface.

Reaction of $Cr(CH_2EMe_3)_4$, E = C, Si, with deuterated silica liberated 1 (silica-500) or 2 (silica-200) equivalents of alkane (neopentane or tetramethylsilane), as before. For silica-500, both unlabeled and monodeuteroalkane were detected, in the ratio 19:81 (± 2, average of 5 experiments), Table 3.5. For silica-200, alkane-d_0 and -d_1 were detected in the ratio 17:83 (± 2, average of 7 experiments), Table 3.6. The ratio of isotopomers shows no dependence on Cr loading.

Blank experiments verified that deuterated silica does not catalyze H/D

Table 3.5 Isotopomer distribution in volatile products from grafting of CrR_4 on deuterated silica-500

CrR_4[a]	% SiOD[b]	% RD	% RH	mmol Cr[c]	mmol RH[c]	RH/Cr
1a	90	81	19	0.355	0.316	0.89
1a	89	80	20	0.364	0.328	0.90
1a	90	82	18	0.360	0.320	0.89
1b	91	82	18	0.351	0.332	0.92
1b	88	80	20	0.360	0.328	0.91
average		81 ± 2	19 ± 2			0.90 ± 0.02

[a] R is $CH_2C(CH_3)_3$, **1a**, or $CH_2Si(CH_3)_3$, **1b**.

[b] Extent of deuteration estimated by decrease in ν(SiO-H) intensity in the IR.

[c] All quantities are reported normalized per g of silica.

exchange in neopentane, nor does $(\equiv SiO)_2Cr(CH_2CMe_3)_2$.

A simple electrophilic attack of surface deuterons on the metal-carbon bond will account for the major product alkane-d_1 on either silica-500 or silica-200. Alternately, oxidative addition of SiO-D followed by reductive elimination of R-D would give the same products. The appearance of ca. 20% non-deuterated alkane can be accounted for by incomplete silica deuteration, as shown by IR.

The mechanism proposed in Scheme 3.1 for the reaction of physisorbed $Cr(CH_2EMe_3)_4$, E = C, Si with deuterated silica-500 leads to the liberation of one equiv. of monodeuteroalkane and the formation of a grafted trisalkylchromium(IV) fragment, without a (presumably) high energy Cr(VI) hydride intermediate.

The recovery of a second equiv. of alkane during the reaction of $Cr(CH_2EMe_3)_4$ with silica-200 leads us to propose the reaction of a nearby ≡SiO-D with

Table 3.6 Isotopomer distribution in volatile products from grafting of CrR_4 on deuterated silica-200

CrR_4[a]	% SiOD[b]	% RD	% RH	mmol Cr[c]	mmol RH[c]	RH/Cr
1a	60	52	48	0.341	0.651	1.91
1a	89	82	18	0.343	0.638	1.86
1a	90	84	16	0.352	0.669	1.90
1a	89	82	18	0.359	0.679	1.89
1a	90	83	17	0.361	0.678	1.88
1b	88	81	19	0.345	0.655	1.90
1b	89	82	18	0.362	0.677	1.87
1b[d]	61	54	46	0.350	0.662	1.89
average		83 ± 2	17 ± 2			1.89 ± 0.03

[a] R is $CH_2C(CH_3)_3$, **1a**, or $CH_2Si(CH_3)_3$, **1b**.

[b] Extent of deuteration estimated by decrease in ν(SiO-H) intensity by IR.

[c] All quantities are reported normalized per g of silica.

[d] This run not included in averages.

Scheme 3.1 Mechanism for reaction of $Cr(CH_2EMe_3)_4$ on deuterated silica-500

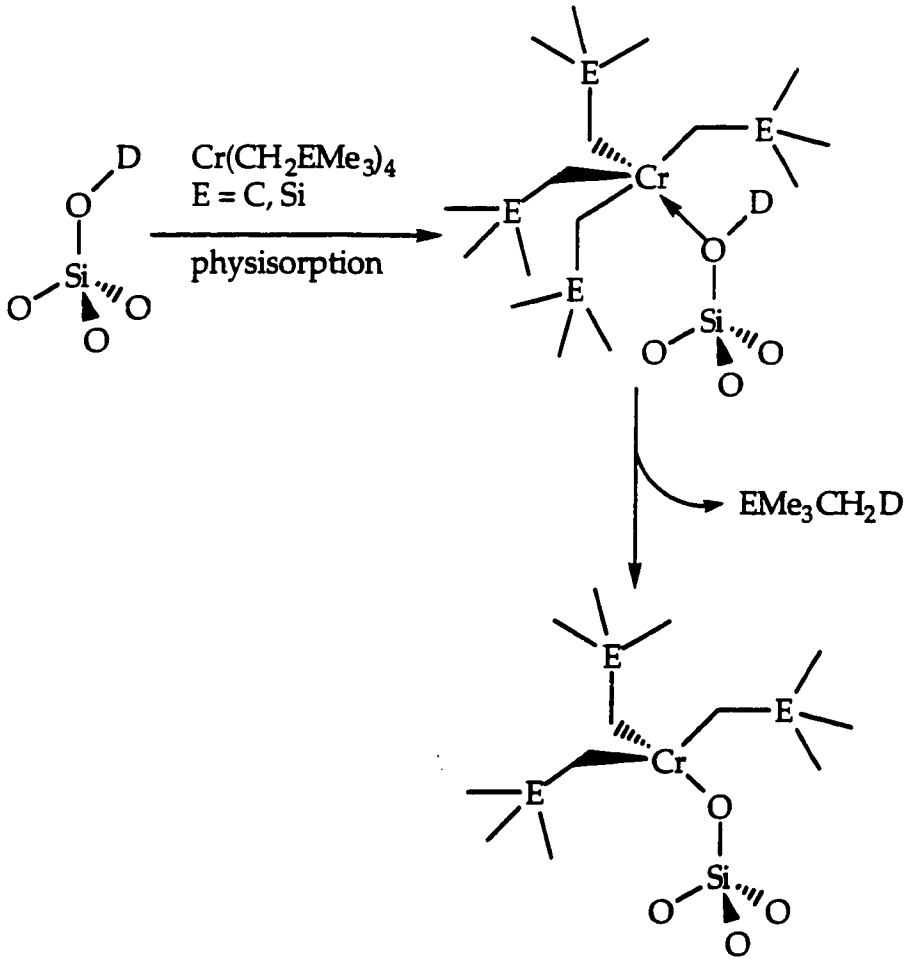

$(\equiv SiO)Cr(CH_2EMe_3)_3$. Elimination of a second equivalent of monodeuteroalkane leads to the formation of $(\equiv SiO)_2Cr(CH_2EMe_3)_2$. In order to explain the quantitative formation of $(\equiv SiO)_2Cr(CH_2EMe_3)_2$ on silica-200, we could propose that the surface hydroxyl groups on partially dehydroxylated amorphous silica-200 are not randomly distributed, but that they occur in well-ordered pairs.[30] Alternately, the surface may restructure to move the second hydroxyl group into position for reaction, Scheme 3.2.

Scheme 3.2 Mechanism for reaction of $Cr(CH_2EMe_3)_4$ with deuterated silica-200

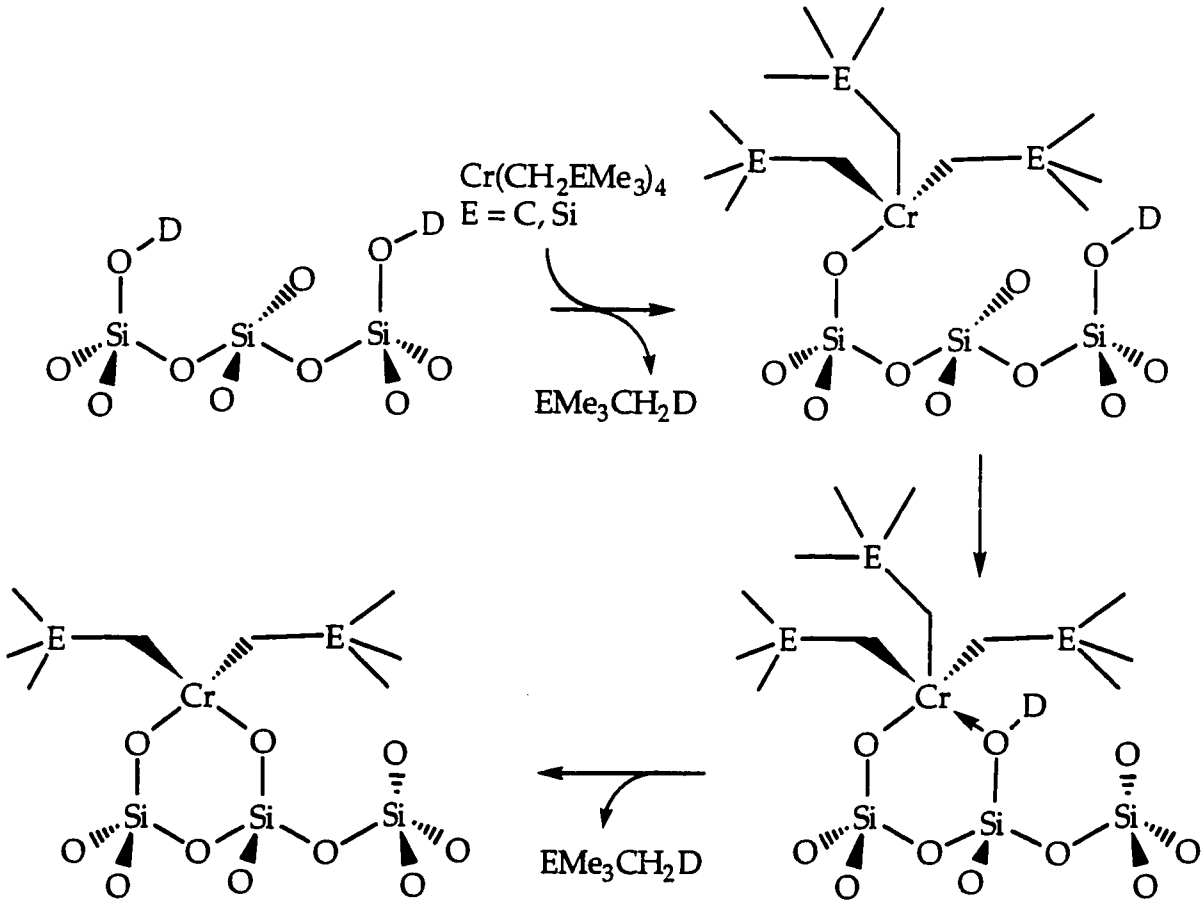

3.7 Reactivity Survey of Supported Alkylchromium(IV) Fragments

Although the molecular complexes $Cr(CH_2EMe_3)_4$ are stable in vacuum at room temperature and display remarkable chemical inertness, they do react rapidly with oxygen and nitric oxide. In both reactions, no well-defined products were isolated. Water and alcohols do not react, nor do ethylene or carbon monoxide. Homoleptic alkyl chromium(IV) compounds are very sensitive to light.[16,18]

A brief exploration of the reactivity of surface organometallic analogues of these compounds was undertaken to compare with known molecular chemistry.

3.7.1 Reaction with Water

The grafted species $(\equiv SiO)Cr(CH_2EMe_3)_3$, **2**, and $(\equiv SiO)_2Cr(CH_2EMe_3)_2$, **3**, where E is C or Si, are unreactive towards water, like their molecular analogues CrR_4.[16,18] Introduction of 50 Torr water vapor into the reactor at room temperature caused no change in either the colors or the infrared spectra of the solids, and no volatile gases were liberated.

3.7.2 Reaction with O_2

The supported species **2** and **3** are extremely sensitive to O_2. Upon addition of 10 Torr dry O_2, they immediately lose their characteristic colors and become yellow. The intensities of the bands in the ν(C-H) region of the IR spectrum decrease and new bands appear in the region 1680-1570 cm^{-1}. The latter are characteristic of hydrocarbon oxidation products containing carbonyl groups. Also, CO and CO_2 were detected in the gas phase by IR. This deep oxidation was observed in all attempts to vary the temperature and pressure of O_2; consequently, we were not able to identify the initial product in the reactions of the surface species with O_2.

3.7.3 Reactions with CO and Ethylene

The complexes $(\equiv SiO)Cr(CH_2EMe_3)_3$, **2**, and $(\equiv SiO)_2Cr(CH_2EMe_3)_2$, **3**, also proved to be unreactive towards CO (20 Torr) and ethylene (10 Torr). No evidence for insertion was observed by IR spectroscopy at room temperature.

3.7.4 Reaction with NO

Spectral changes were recorded after addition of 15 Torr of NO. Although no modification occurred in the ν(C-H) region, two new bands were observed at 1854 and 1716 cm^{-1}, which persisted under dynamic vacuum. Pairs of bands in this

region have been attributed to the symmetric and antisymmetric N-O stretching modes of bis(nitrosyl)chromium species supported on silica.[31]

3.8 Conclusion

The reactions of molecular precursors CrR_4 (**1a**, R is neopentyl, **1b**, R is trimethylsilylmethyl) with the surfaces of partially dehydroxylated silicas lead to the formation of discrete mononuclear surface organometallic fragments. Each reaction gives a single chemisorbed product, whose nature depends on the density of the surface hydroxyl groups.

The well-defined silica-supported paramagnetic alkylchromium(IV) complexes have been characterized by IR and magnetic susceptibility. Their average chemical formulae are consistent with tris(alkyl) and bis(alkyl) complexes which are predominant on silica-500 and silica-200, respectively. On silica subjected to prior dehydroxylation at 500°C, one Cr is grafted per hydroxyl group and one equiv. of alkane is evolved, giving $\equiv SiOCrR_3$, **2**. On silica dehydroxylated at 200°C, each Cr is grafted onto two hydroxyl groups and two equivalents of alkane are evolved, giving $(\equiv SiO)_2CrR_2$, **3**.

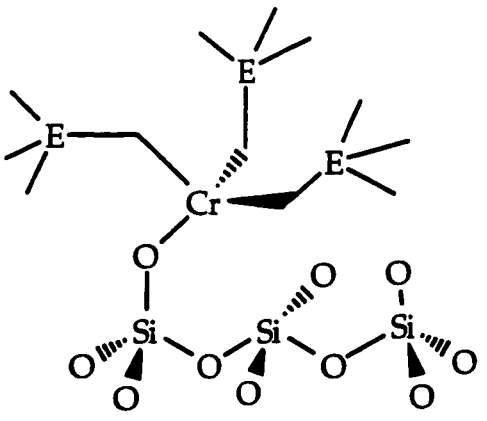

2 (silica-500)

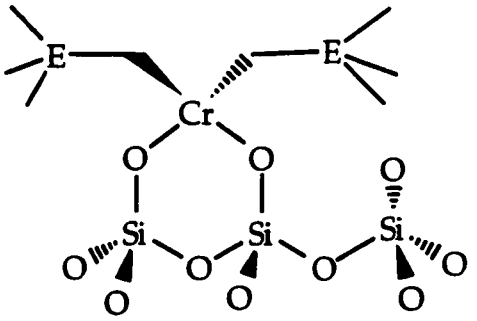

3 (silica-200)

E = C or Si

When CrR_4 reacts with deuterated hydroxyl groups, monodeuteroalkanes are liberated. A chemisorption mechanism is proposed in which grafting occurs by direct cleavage of the metal-carbon bond by the surface protons/deuterons. Chemisorbed Cr species retain the oxidation state and nuclearity of their parent molecular precursors, as shown by UV-vis, EPR spectroscopy and magnetic susceptibility measurements. The silica-supported complexes **2** and **3** show little reactivity. They are unreactive towards water, CO and ethylene,[15] but highly sensitive to O_2.

Cr(IV) alkyls and hydrides have been proposed as active centres for polymerization in industrial Cr/silica catalysts.[32] However, it seems likely that less coordinatively saturated species are responsible for the activity. This hypothesis will be discussed in detail in the following chapter.

3.9 References

1) Ballard, D. G. H. *Adv. Catal.* **1973**, *23*, 263-325.

2) Efimov, O. A.; Min'kov, A. I.; Zakharov, V. A.; Yermakov, Y. I. *Kinet. Katal.* **1976**, *17*, 995.

3) Schwartz, J.; Ward, M. D. *J. Mol. Catal.* **1980**, *8*, 465.

4) Zakharov, V. A.; Dudchenko, V. K.; Paukshtis, E. A.; Karachiev, L. G.; Yermakov, Y. I. *J. Mol. Catal.* **1977**, *2*, 421.

5) Vasnetsov, S. A.; Nosov, A. V.; Mastikhin, V. M.; Zakharov, V. A. *J. Mol. Catal.* **1989**, *53*, 37.

6) Candlin, J. P.; Thomas, H. *Adv. Chem. Ser.* **1974**, *132*, 212-239.

7) Zakharov, V. A.; Dudchenko, V. K.; Minkov, O. A.; Yefimov, O. A.; Chomyakova, L. G.; Babenko, V. I.; Yermakov, Y. I. *Kinet. Katal.* **1976**, *17*, 738.

8) Quignard, F.; Lecuyer, C.; Bougault, C.; Lefebvre, F.; Choplin, A.; Olivier, D.; Basset, J.-M. *Inorg. Chem.* **1992**, *31*, 928.

9) D'Ornelas, L.; Reyes, S.; Quignard, F.; Choplin, A.; Basset, J.-M. *Chem. Lett.* **1993**, 1931.

10) Rosier, C.; Niccolai, G. P.; Basset, J. M. *J. Am. Chem. Soc.* **1997**, *119*, 12408-12409.

11) Holmes, S. A.; Quignard, F.; Choplin, A.; Teissier, R.; Kervennal, J. *J. Catal.* **1998**, *176*, 173-181.

12) Dufaud, V.; Niccolai, G. P.; Thivolle-Cazat, J.; Basset, J. M. *J. Am. Chem. Soc.* **1995**, *117*, 4288-4294.

13) Amor Nait Ajjou, J.; Rice, G.; Scott, S. L. *J. Am. Chem. Soc.* **1998**, *120*, 13436-13443.

14) McDaniel, M. P. *Adv. Catal.* **1985**, *33*, 47-98.

15) Smith, P. D.; McDaniel, M. P. *J. Polym. Sci.: A: Polym. Chem.* **1990**, *28*, 3587-3601.

16) Mowat, W.; Shortland, A.; Yagupsky, G.; Hill, N. J.; Yagupsky, M.; Wilkinson, G. *J. Chem. Soc., Dalton Trans.* **1972**, 533-542.

17) Morrow, B. A. In *Stud. Surf. Sci. Catal.*, 1990; Vol. 57A, pp. 161-224.

18) Mowat, W.; Shortland, A. J.; Hill, N. J.; Wilkinson, G. *J. Chem. Soc., Dalton Trans.* **1973**, 770-778.

19) Colthrup, N. B.; Daly, L. H.; Wilberley, S. E. *Introduction to Infrared and Raman Spectroscopy*; Academic Press: New York, 1964.

20) Kruse, W. *J. Organomet. Chem.* **1972**, *42*, C39-C42.

21) Stavropoulos, P.; Savage, P. D.; Tooze, R. P.; Wilkinson, G.; Hussain, B.; Motevalli, M.; Hursthouse, M. B. *J. Chem. Soc., Dalton Trans.* **1987**, 557-562.

22) Ward, G. A.; Kruse, W.; Bower, B. K.; Chien, J. C. W. *J. Organomet. Chem.* **1972**, *42*, C43-C46.

23) Cardin, C. J.; Cardin, D. J.; Roy, A. *J. Chem. Soc., Chem. Commun.* **1978**, 899-900.

24) Yermakov, Y. I.; Kuznetsov, B. N.; Karakchiev, L. G.; Derbeneva, S. S. *Kinet. Catal.* **1973**, *14*, 611-616.

25) Yates, D. J. C.; Dembinski, G. W.; Kroll, W. R.; Elliott, J. J. *J. Phys. Chem.* **1969**, *73*, 911-921.

26) Scott, S. L.; Basset, J. M. , unpublished results.

27) Peri, J. B.; Hensley, A. L., Jr. *J. Phys. Chem.* **1968**, *72*, 2926-2933.

28) Inumaru, K.; Okuhara, T.; Misono, M. *J. Phys. Chem.* **1991**, *95*, 4826-4832.

29) Gramlich, V.; Pfefferkorn, K. *J. Organomet. Chem.* **1973**, *61*, 247-248.

30) Morrow, B. A.; McFarlan, A. J. *J. Non-Cryst. Solids* **1990**, *120*, 61-71.

31) Beck, D. D.; Lunsford, J. H. *J. Catal.* **1981**, *68*, 121-131.

32) Candlin, J. P. In *Catalysis and Chemical Processes*; Pearce, R. and Patterson, W. R., Eds.; Blackie & Son: London, 1981; pp. 242-245.

Chapter 4

Silica-Supported Chromium(IV) Alkylidene Complexes

4.1 Introduction

R. R. Schrock's discovery in 1974 of spontaneous α-hydrogen abstraction in pentakis(neopentyl)tantalum(V), $Ta(CH_2C(CH_3)_3)_5$, was a landmark event in organometallic chemistry. The product neopentylidene complex, $(CH_3)_3CCH_2)_3Ta{=}CHC(CH_3)_3$,[1] was the first alkylidene to be characterized, and its discovery set off an explosive development of the chemistry of alkylidene compounds, in particular, the isolation of a large number of high-oxidation-state organometallic complexes of niobium and tantalum. Originally these compounds were limited to those containing neopentylidene ligands. Other ligand systems such as $(CH_3)_3SiCH_2$, $PhCH_2$ and CH_3 were later observed to form alkylidenes.[2-4] Further exploration of this field led to the investigation of transition metal alkyls of Group VI, (M = Mo, W, and R = $(CH_3)_3CCH_2$, $(CH_3)_3SiCH_2$, $PhCH_2$, Me),[5-7]and Group IV, (M = Ti, Zr, Hf and R = $(CH_3)_3CCH_2$, Me).[4,8-11] However, some presumed alkylidene complexes of these metals were not isolated because of their instability.

The isolation of alkylidene derivatives spurred the investigation of mechanisms in new fields of chemistry such as catalytic olefin metathesis and thin film synthesis by vapor deposition. In addition, alkylidenes can be employed in stoichiometric reactions as Wittig-type reagents to produce olefins from ketones.[2] Alkylidene complexes of first-row transition metals are rarely stable enough to be isolated, although evidence for their participation in C-H activation[12,13] and chemical vapor deposition of metal carbide films[13] has rekindled interest in their synthesis. In a model reaction, the photo-induced transformation of coordinated ethylene to ethylidene was recently described on a W(IV) calix[4]arene complex.[14]

Kinetics studies of alkylidene formation are uncommon and usually predicated on analyses of product ratios. In molecular chemistry, the kinetics of the alkyl→alkylidene transformation are often difficult to observe because one of the two forms is not stable.[3,4,13,15,16] However, a study of the thermolysis of $Ta(CH_2Ph)_5$ showed that it was transformed 3 times faster than $Ta(CD_2Ph)_5$.[3] The kinetic isotope effect k_H/k_D is compelling evidence that an α-C-H(D) bond is cleaved in the rate-determining step. Thermal decomposition of $(\eta^5\text{-}C_5Me_5)_2Ti(CH_3)_2$ in solution follows first-order kinetics, producing a non-isolable titanium alkylidene product. Deuterium-labeling studies showed the reaction to be intramolecular α-H abstraction, with a primary kinetic isotope effect of 2.9 at 98°C.[9]

The success of thermolysis of alkyl complexes to form alkylidene derivatives depends both on steric effects and on the nature of the metal itself. It seems that sterics play a crucial role. Schrock and Fellmann postulated two thermolysis pathways for the conversion of transition-metal alkyl complexes into their alkylidene derivatives, Scheme 4.1.[17] In the first mechanism, the α-H abstraction is intramolecular (eq 4.1), and gives rise to a terminal alkylidene, while in the second it is intermolecular (eq 4.2), and generates a bridging alkylidene. When the alkyl group is small, for example R=Me, intermolecular α-hydrogen abstraction is the first thermolytic reaction, and is also the rate-determining step.[18,19] When the alkyl group becomes bulkier, the intermolecular mechanism becomes less favorable for steric reasons, while the intramolecular mechanism becomes more favorable due to relief of steric interactions.[18]

High-valent alkylidene complexes are now relatively common for the heavier group VI metals Mo and W. Chromium carbene chemistry, on the other hand, tends to be dominated by low-valent derivatives, for which there are now many examples since their discovery by Fischer in 1964.[20] Carbene complexes of

Scheme 4.1 Intramolecular and intermolecular mechanisms for α-hydrogen abstraction in transition-metal alkyl complexes

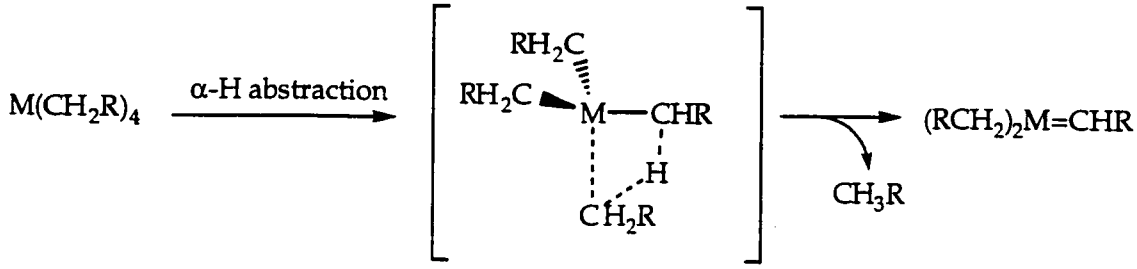

(4.1)

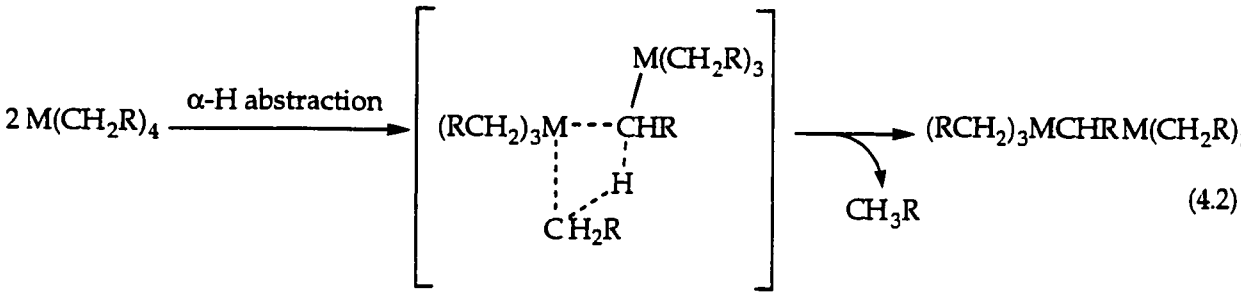

(4.2)

chromium in higher oxidation states (alkylidenes) are quite rare;[12,21-23] there are to our knowledge only two high-valent Cr alkylidenes reported in the literature. Gibson and co-workers reported the first stable chromium(VI) alkylidene complex obtained upon thermolysis of the bis(alkyl)bis(imido) complex, $[Cr(NC_6H_3Pr^i_2\text{-}2,6)(CH_2CMe_3)_2]$.[12] Gambarotta *et. al.* reported the first synthesis of a Cr(III) alkylidene complex, (TMEDA)Cr(=CHPh)(CH_2Ph), where TMEDA = [N,N,N′,N′,-tetramethylethylenediamine], prepared by transmetallation of $CrCl_2$(TMEDA) with $PhCH_2Li$.[21] Filippou reported the first isolated Cr(II) aminocarbene complex resulting from protonation of a chromium phenylcarbyne complex. This complex could be considered a Cr(IV) alkylidene.[22] Finally, Armentrout *et. al.* generated gas phase singly-charged chromium ions, which formed gaseous chromium methylidene ions, "$CrCH_2^+$", in their reactions with ethylene, cyclopropane and methane.[23]

In the previous chapter, we confirmed that the reactions of organometallic complexes $Cr(CH_2E(CH_3)_3)_4$, where E = C, Si, with an amorphous silica surface can occur with two different reaction stoichiometries. On silica partially dehydroxylated at 500 or 200°C, the reactions of homoleptic chromium tetraalkyls give supported tris and bis(alkyl)chromium(IV) complexes, as shown in eq 4.3.

$$n \equiv SiOH + Cr(CH_2E(CH_3)_3)_4 \rightarrow (\equiv SiO)_nCr(CH_2E(CH_3)_3)_{4-n} + (4-n)\, E(CH_3)_4 \qquad (4.3)$$

$n = 1$ (SiO_2-500)

$n = 2$ (SiO_2-200)

Since polymerizations catalyzed by oxide-supported Cr are usually conducted at elevated temperatures (typically 80-120°C),[24-26] we investigated the behavior of the grafted species $(\equiv SiO)Cr(CH_2E(CH_3)_3)_3$ and $(\equiv SiO)_2Cr(CH_2E(CH_3)_3)_2$, as a function of temperature.

4.2 Thermolysis of the Grafted Complexes

Silica-supported tris(alkyl) and bis(alkyl) complexes of chromium(IV) were heated *in vacuo* in order to study their thermal stability. We note that the molecular complexes CrR_4 are reported to be thermally stable in hexane at 80°C (R = Np) and 95°C ($R = CH_2SiCH_3$) for several days.[27]

The tris(neopentyl)chromium(IV) fragment on silica is stable upon heating at 80°C *in vacuo* for 2 hours, as judged by the intensity of the ν(C-H) region in the IR spectrum, which decreased by less than 10% during this time. In contrast, the bis(neopentyl) complex **3a** undergoes a dramatic thermal transformation in the same time period, with significant loss of ν(C-H) intensity. Therefore, we set out to study in more detail the thermal reaction of the supported bis(alkyl)chromium(IV) complexes, in order to explain the loss of alkyl groups during thermolysis.

4.2.1 IR Spectroscopic Evidence

The surface complexes $(\equiv SiO)_2Cr(CH_2C(CH_3)_3)_2$, **3a**, or $(\equiv SiO)_2Cr(CH_2Si(CH_3)_3)_2$, **3b**, were heated, typically at 69°C and 150°C, respectively, in vacuum (ca. 10^{-4} Torr) for 4 hours. The absorbance in the ν(C-H) region of the IR spectrum of a self-supporting silica disk decreased by (51.3 ± 1.9)% (**3a**, average of 55 independent experiments), and (50.2 ± 3.1)% (**3b**, average of 31 independent experiments) of their original intensity, as judged by *in situ* integration of the ν(C-H) region, Tables 4.1 and 4.2. The extent of alkyl group loss is independent of the Cr loading.

Concurrent with the halving of the intensity of the alkyl vibrations on the silica pellet, Figure 4.1, alkane (**3a**, neopentane; **3b**, tetramethylsilane) was evolved and was the only volatile gas product detected by IR and GC.[28] Heating for an additional 10 hours at the thermolysis temperature failed to effect any other spectral change or further release of gas. However if the temperature was raised above 80°C (**3a**) or 190°C (**3b**), subsequent loss of alkyl groups was observed, Figure 4.2.

The IR spectra in Figure 4.1 show that the quantity of surface hydroxyl groups does not decrease during thermolysis of $(\equiv SiO)_2Cr(CH_2C(CH_3)_3)_2$. Experiments with close to 2 wt.% Cr do not contain sufficient unreacted hydroxyl groups to undergo a quantitative protonolysis reaction with $(\equiv SiO)_2Cr(CH_2C(CH_3)_3)_2$ or $(\equiv SiO)_2Cr(CH_2Si(CH_3)_3)_2$. Therefore, the residual ≡SiOH cannot be the proton source which liberates a neopentyl or trimethylsilylmethyl ligand as neopentane and tetramethylsilane. Since the thermolysis reaction occurs in vacuum in the absence of solvent, the only other proton sources available are the grafted species $(\equiv SiO)_2Cr(CH_2C(CH_3)_3)_2$ or $(\equiv SiO)_2Cr(CH_2Si(CH_3)_3)_2$, themselves.

Table 4.1 Quantitative IR analyses of *in vacuo* thermolysis of $(\equiv SiO)_2Cr(CH_2C(CH_3)_3)_2$

Wt.% Cr on silica	T (°C)	% loss of surface ν(CH)[a]	Wt.% Cr on silica	T (°C)	% loss of surface ν(CH)[a]	Wt.% Cr on silica	T (°C)	% loss of surface ν(CH)[a]
0.65	69	50.2	1.83	110	49.8	1.94	69	51.6
0.76	69	55.1	1.85	69	49.7	1.94	69	51.4
0.87	69	51.7	1.87	69	51.2	1.94	69	51.4
1.05	69	50.1	1.89	69	51.9	1.94	69	53.2
1.22	90	47.2	1.89	69	50.7	1.94	69	52.9
1.25	69	52.9	1.90	69	49.8	1.94	69	49.8
1.27	69	52.9	1.90	69	48.4	1.94	69	51.2
1.30	69	49.9	1.90	69	48.5	1.94	69	49.7
1.39	82	48.9	1.91	69	48.0	1.95	69	49.6
1.42	69	49.8	1.91	69	47.9	1.95	69	50.1
1.45	69	52.2	1.92	69	48.3	1.95	69	49.8
1.54	69	51.9	1.92	69	49.6	1.95	69	50.2
1.58	71	51.4	1.92	69	50.9	1.95	69	47.3
1.61	69	52.1	1.92	69	49.5	1.95	69	52.6
1.65	69	51.7	1.93	69	51.3	1.95	69	49.6
1.72	69	50.1	1.93	69	51.1	1.95	69	49.9
1.74	62	47.2	1.93	69	49.8	1.95	69	50.3
1.76	75	52.6	1.93	69	52.1	average of all experiments:		
1.79	69	51.8	1.94	69	49.7	(51.3 ± 1.9)%		

[a] Based on *in situ* integration of the IR spectrum of the silica pellet in the ν(CH) region, 3200 - 2800 cm^{-1}, which is proportional to the number of alkyl ligands on the surface.

Table 4.2 Quantitative IR analyses of *in vacuo* thermolysis of $(\equiv SiO)_2Cr(CH_2Si(CH_3)_3)_2$

wt. % Cr on silica	T (°C)	% loss of surface ν(CH)[a]	wt. % Cr on silica	T (°C)	% loss of surface ν(CH)[a]
0.45	150	51.2	1.79	150	48.6
0.75	150	50.5	1.82	150	49.6
0.79	150	51.7	1.87	150	49.2
0.82	100	49.6	1.88	150	53.2
0.86	130	48.5	1.89	150	50.9
0.92	150	51.9	1.89	150	49.4
0.94	150	51.0	1.90	150	51.2
0.97	150	48.9	1.90	150	49.9
1.04	150	47.9	1.90	150	50.3
1.13	150	49.9	1.91	150	51.0
1.22	190	53.0	1.91	150	51.8
1.28	150	51.9	1.91	150	48.6
1.45	150	49.8	1.92	150	53.1
1.56	150	49.7	1.92	150	52.9
1.69	150	51.1	1.93	150	52.4
1.76	150	48.9			
average of all experiments: (50.2 ± 3.1)%					

[a] Based on *in situ* integration of the IR spectrum of the silica pellet in the ν(CH) region, 3200 - 2800 cm^{-1}, which is proportional to the number of alkyl ligands on the surface.

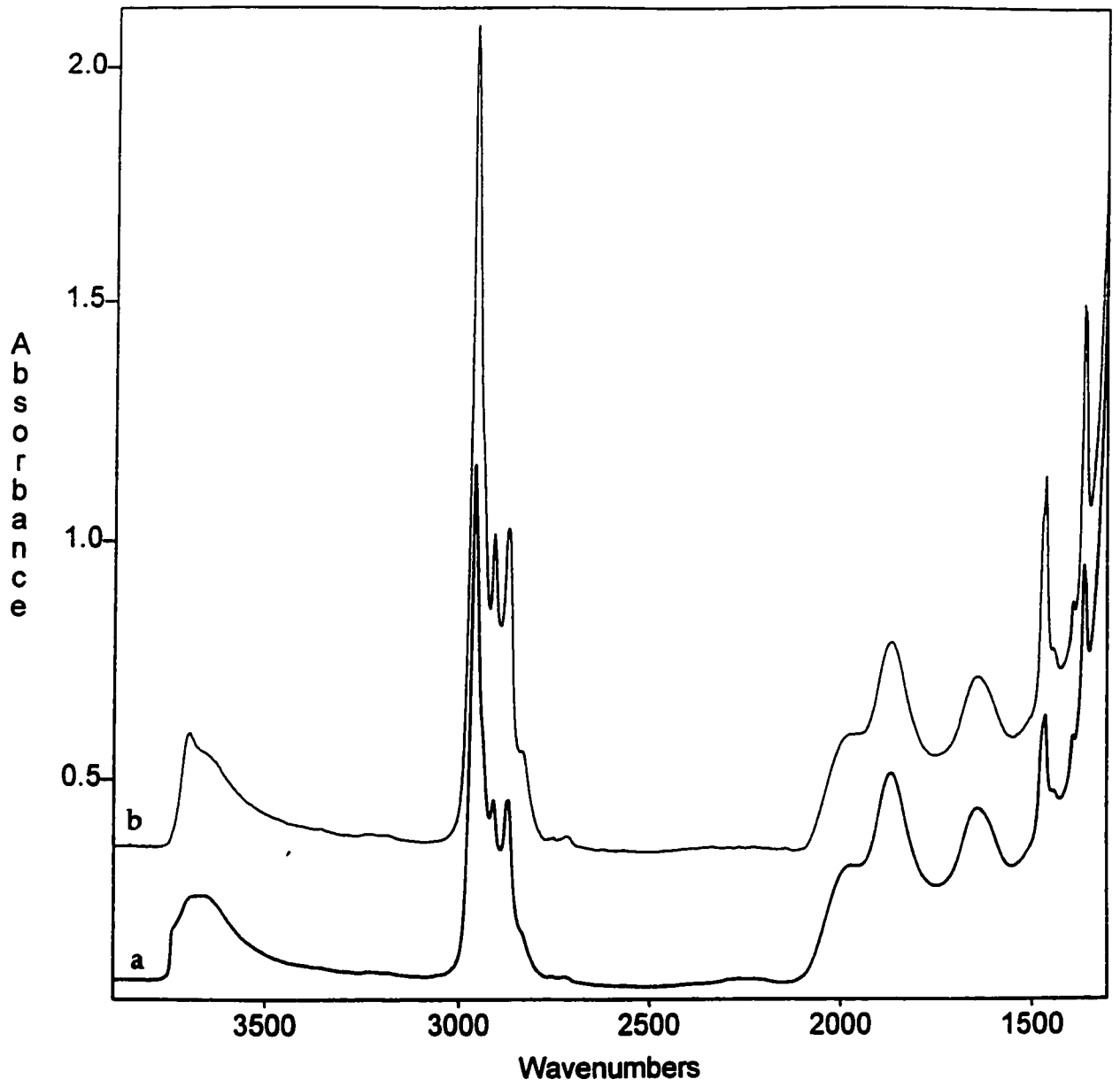

Figure 4.1 Transmission infrared spectra of (a) $(\equiv SiO)_2Cr(CH_2C(CH_3)_3)_2$, 1.94 wt.% Cr, at room temperature, and (b) after heating in vacuum at 69°C for 4 hours, at which time the integrated ν(C-H) intensity in the region 3000-2800 cm^{-1} had decreased by 51%.

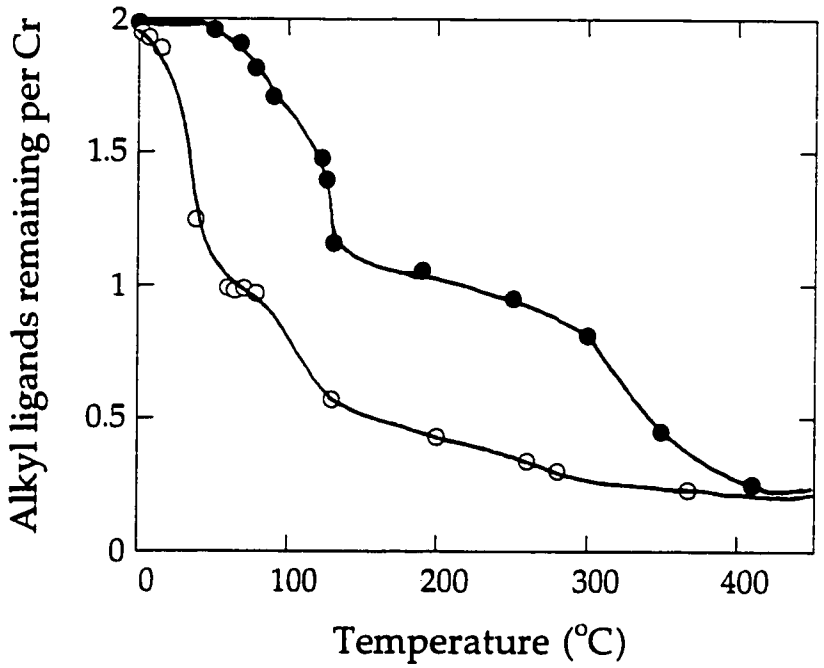

Figure 4.2 Thermal evolution of $(\equiv SiO)_2Cr(CH_2C(CH_3)_3)_2$ (open circles) and $(\equiv SiO)_2Cr(CH_2Si(CH_3)_3)_2$ (filled circles) in vacuum. The modified silicas were heated at each temperature for 30 min before recording their IR spectrum.

4.2.2 Post-thermolysis Magnetic Susceptibility

The oxidation state of $Cr(CH_2C(CH_3)_3)_4$ being IV, the surface complex $(\equiv SiO)_2Cr(CH_2C(CH_3)_3)_2$ is paramagnetic, as shown in the previous chapter. It was necessary, however, to verify whether the oxidation state remains IV upon thermolysis of $(\equiv SiO)_2Cr(CH_2C(CH_3)_3)_2$.

The temperature-dependent magnetic susceptibility of the modified silica after thermal treatment exhibits simple Curie-Weiss behavior above 8 K, Figure 4.3. The effective magnetic moment is 2.77 B.M. per Cr atom, and is consistent with retention of mononuclear non-interacting d^2 Cr(IV) surface organometallic complexes even after thermolysis. Thus, the oxidation state of Cr does not change during the reaction, nor do the grafted chromium complexes aggregate upon heating.

4.3 Composition of Supported Cr Complexes Formed upon Thermolysis

In vacuo thermolysis of $(\equiv SiO)_2Cr(CH_2C(CH_3)_3)_2$, **3a**, at 69°C liberates (0.89±0.03) neopentyl ligands per Cr (average of 55 experiments) as neopentane, Table 4.3 and eq 4.4.

$$(\equiv SiO)_2Cr(CH_2C(CH_3)_3)_2 \xrightarrow{69°C} (\equiv SiO)_2Cr(C_5H_{10}) + C(CH_3)_4 \qquad (4.4)$$

3a **4a**

Since simultaneous with the evolution of neopentane, the intensity of the IR bands on the silica pellet in the C-H region decreased by half, we suggested that the new surface complexes **4** must be either chromium(IV) alkylidene complexes or metallacycles, Scheme 4.2.

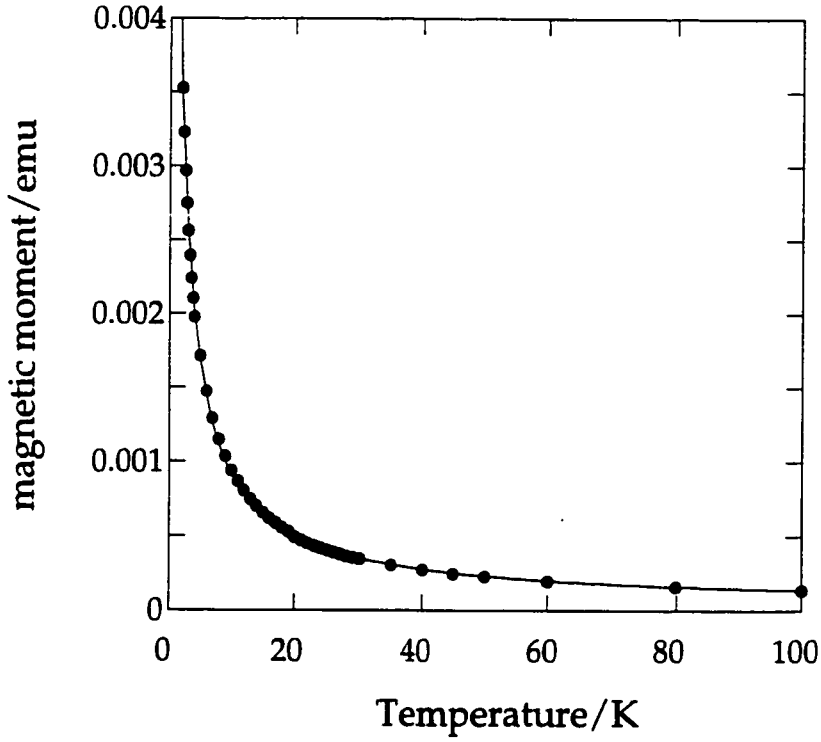

I = C' / (T + θ)		
	Value	Error
C'	0.0094324	0.0000089
θ	0.7304	0.0295

Figure 4.3 Temperature-dependent magnetic susceptibility after thermolysis of $(\equiv SiO)_2Cr(CH_2C(CH_3)_3)_2$. The solid line is the curve fit to the Curie-Weiss law.

Table 4.3 Quantitative analysis of volatile products in the thermolysis of $(\equiv SiO)_2Cr(CH_2C(CH_3)_3)_2$ and subsequent protonolysis

products of thermolysis				products of protonolysis by HCl or **DCl**		
% Cr	mmol Cr[a]	mmol NpH[a]	NpH/Cr	mmol NpH[a]	NpH/Cr	% Np-d_2[b]
0.65	0.125	0.114	0.91			
0.76	0.146	0.126	0.86			
0.87	0.168	0.146	0.87	0.195	**0.87**	72
1.05	0.202	0.184	0.91	0.181	0.90	
1.22	0.236	0.217	0.92			
1.25	0.241	0.207	0.86			
1.27	0.245	0.213	0.87			
1.30	0.250	0.213	0.85			
1.39	0.268	0.236	0.88	0.239	0.89	
1.42	0.274	0.252	0.92			
1.45	0.279	0.243	0.87	0.246	**0.88**	71
1.54	0.297	0.270	0.91			
1.58	0.304	0.280	0.92			
1.61	0.310	0.279	0.90			
1.65	0.317	0.273	0.86			
1.72	0.331	0.291	0.88	0.305	**0.92**	69
1.74	0.335	0.285	0.85			
1.76	0.339	0.295	0.87			
1.79	0.344	0.303	0.88			

Table 4.3, continued.

% Cr	mmol Cr[a]	mmol NpH[a]	NpH/Cr	mmol NpH[a]	NpH/Cr	Np-d_2[b]
1.83	0.353	0.325	0.92			
1.85	0.356	0.331	0.93			
1.87	0.360	0.328	0.91	0.324	**0.90**	71
1.89	0.364	0.324	0.89			
1.89	0.364	0.317	0.87			
1.90	0.367	0.327	0.89			
1.90	0.367	0.316	0.86			
1.90	0.367	0.338	0.92			
1.91	0.368	0.342	0.93			
1.91	0.368	0.346	0.94			
1.92	0.370	0.329	0.89	0.337	0.91	
1.92	0.370	0.355	0.96			
1.92	0.370	0.344	0.93			
1.92	0.370	0.329	0.89			
1.93	0.372	0.335	0.90			
1.93	0.372	0.339	0.91			
1.93	0.372	0.327	0.88			
1.93	0.372	0.335	0.90			
1.94	0.374	0.325	0.87			
1.94	0.374	0.333	0.89			
1.94	0.374	0.355	0.95			

Table 4.3, continued.

% Cr	mmol Cr[a]	mmol NpH[a]	NpH/Cr	mmol NpH[a]	NpH/Cr	Np-d_2[b]
1.94	0.374	0.344	0.92			
1.94	0.374	0.337	0.90			
1.94	0.374	0.337	0.90			
1.94	0.374	0.340	0.91			
1.94	0.374	0.333	0.89			
1.94	0.374	0.329	0.88			
1.95	0.376	0.346	0.92			
1.95	0.376	0.350	0.93			
1.95	0.376	0.327	0.87			
1.95	0.376	0.357	0.95			
1.95	0.376	0.327	0.87			
1.95	0.376	0.331	0.88			
1.95	0.376	0.327	0.87			
1.95	0.376	0.338	0.90			
1.95	0.376	0.331	0.88			
			average 0.89 ± 0.03		average 0.90 ± 0.03	average (71 ± 1)%

[a] All quantities are reported normalized per g of silica.

[b] Extent of deuteration estimated by the tert-butyl fragment ion intensities at m/z = 57 or 59 by GC-MS.

Scheme 4.2 Possible structures for $(\equiv SiO)_2Cr(C_4EH_{10})$, where E = C or Si

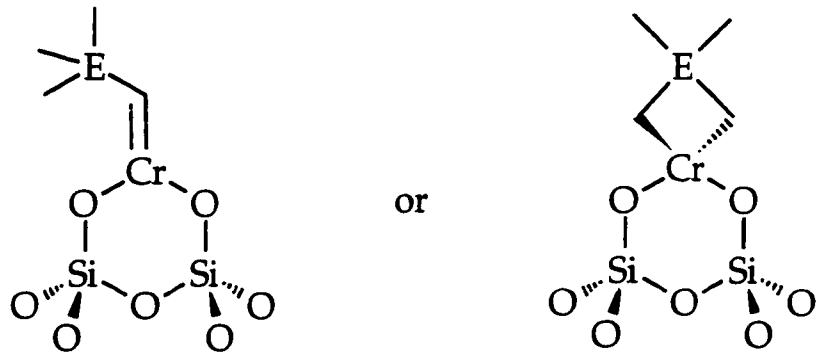

The reaction of **4a** with anhydrous HCl(g) (50 Torr, room temperature, 1 hour) liberated (0.90 ± 0.01) neopentane/Cr as the exclusive volatile product. Treatment of the same surface species with DCl(g) under similar conditions caused the evolution of (0.89 ± 0.02) neopentane/Cr as predominantly (71%) neopentane-d_2, as the isotopomer $(CH_3)_3C(CD_2H)$, eq 4.5. The isotopic composition of the neopentane was determined by GC/MS, using the intensities of the tert-butyl fragments to calculate isotopomer ratios.

$$(\equiv SiO)_2Cr(C_5H_{10}) + 2\ HCl/DCl \rightarrow "(\equiv SiO)_2CrCl_2" + C(CH_3)_4/(CH_3)_3C(CD_2H) \qquad (4.5)$$

4a

Incomplete deuteration of neopentane in reactions with DCl is probably due to HCl contamination, since H/D exchange occurs readily on glass surfaces.

We note that thermolytic γ-H elimination followed by reaction with DCl would give neopentane-d_2 but as a different isotopomer: $C(CH_3)_2(CH_2D)_2$. Since we observed only $C(CH_3)_3(CD_2H)$, the possibility of a metallacycle complex can be excluded. We assign the formula $(\equiv SiO)_2Cr{=}CHC(CH_3)_3$ to **4a**.

Thermolysis of $(\equiv SiO)_2Cr(CH_2Si(CH_3)_3)_2$, **3b**, typically at 150°C, produced one

equivalent of $Si(CH_3)_4$ as the only gaseous product, Table 4.4, and a new surface complex $(\equiv SiO)_2Cr(C_4SiH_{10})$, **4b**, with (50 ± 3)% of the ν(CH) intensity on the modified silica remaining. The product **4b** is assumed to be an alkylidene, eq 4.6, by analogy with the formula of **4a**.

$$\underset{\textbf{3b}}{(\equiv SiO)_2Cr(CH_2Si(CH_3)_3)_2} \xrightarrow{150°C} \underset{\textbf{4b}}{(\equiv SiO)_2Cr{=}CHSi(CH_3)_3} + Si(CH_3)_4 \qquad (4.6)$$

Thermolyses of $(\equiv SiO)_2Cr(CH_2E(CH_3)_3)_2$ were also undertaken following grafting of CrR_4 on deuterated silica. The $E(CH_3)_4$ liberated was 100% undeuterated in each case.

Reported alkylidene ν(=C-H) frequencies vary from 2900-2400 cm^{-1}, where the low frequencies are observed for highly distorted (T-shaped) alkylidenes.[29] No low frequency IR band was observed in the spectra of **4a** or **4b**. We assume that it overlaps with other ν(C-H) modes in the region 2900-2800 cm^{-1}. The Cr=C vibration (ca. 1100 cm^{-1}) is obscured by the intense absorption of silica in this region.

The alkylidene complexes $(\equiv SiO)_2Cr{=}CHE(CH_3)_3$, where E = C or Si, have no precedent in the molecular chemistry of Cr(IV), although thermolysis of bis(alkyl) complexes is a well-documented route to metal alkylidenes. The thermal decomposition of $Cr(CH_2C(CH_3)_3)_4$ was reported to liberate neopentane, although no intermediates were isolated.[30,31] However, thermolysis of $Ti(CH_2C(CH_3)_3)_4$ to give transient $Ti(CH_2C(CH_3)_3)_2(=CHC(CH_3)_3)$ was recently inferred from kinetic isotope effects.[13] On the silica surface, the grafting of a supported Ta(V) neopentylidene complex was suggested to involve α-H elimination.[32] We propose that the unusual and unsaturated complexes $(\equiv SiO)_2Cr{=}CHEMe_3$ are stabilized on

Table 4.4 Quantitative analysis of volatile products in the thermolysis of $(\equiv SiO)_2Cr(CH_2Si(CH_3)_3)_2$ and subsequent protonolysis

products of thermolysis				products of protonolysis by HCl	
% Cr	mmol Cr[a]	mmol TMS[a]	TMS/Cr	mmol TMS[a]	TMS/Cr
0.45	0.087	0.078	0.90		
0.75	0.145	0.129	0.89		
0.79	0.152	0.140	0.92		
0.82	0.158	0.149	0.94		
0.86	0.166	0.146	0.88		
0.92	0.177	0.159	0.90		
0.94	0.181	0.156	0.86		
0.97	0.187	0.163	0.87	0.165	0.89
1.04	0.195	0.174	0.89		
1.13	0.217	0.195	0.90		
1.22	0.235	0.214	0.91		
1.28	0.246	0.231	0.94		
1.45	0.279	0.240	0.86	0.254	0.91
1.56	0.301	0.292	0.97		
1.69	0.326	0.303	0.93		
1.76	0.339	0.305	0.90		
1.79	0.345	0.300	0.87		
1.82	0.353	0.339	0.96		
1.87	0.360	0.310	0.86	0.317	0.88

Table 4.4, continued.

% Cr	mmol Cr[a]	mmol TMS[a]	TMS/Cr	mmol TMS[a]	TMS/Cr
1.88	0.362	0.315	0.87		
1.89	0.364	0.331	0.91		
1.89	0.364	0.349	0.96		
1.90	0.366	0.344	0.94	0.322	0.88
1.90	0.366	0.340	0.93		
1.90	0.366	0.318	0.87		
1.91	0.369	0.325	0.88		
1.91	0.369	0.339	0.92		
1.91	0.369	0.329	0.89	0.328	0.89
1.92	0.370	0.333	0.90		
1.92	0.370	0.352	0.95	0.337	0.91
1.93	0.372	0.350	0.94		
			average 0.91 ± 0.04		average 0.89 ± 0.02

[a] All quantities are reported normalized per g of silica.

the silica surface by their immobility, which prevents bimolecular dimerization and/or disproportionation reactions.

The α-H elimination reaction in d^2 bis(alkyl)metal complexes is generally favorable when the metal is known to form stable d^0 alkylidene complexes.[11] One example of a stable Cr(VI) neopentylidene has now been reported.[12] The driving force for alkylidene formation from bis(alkyl)metal complexes is both enthalphic as

well as entropic,[33] and the enthalpic term contains contributions from both steric and electronic effects. Two electron-withdrawing siloxy ligands increase the electrophilicity of the metal, favoring the alkylidene over the bis(alkyl) form.[11] At the same time, the second siloxy "ligand" forces the metal closer to the silica surface compared with the mono-substituted analogue $(\equiv SiO)CrR_3$. The latter is free to adopt a larger Si-O-Cr angle to relieve steric strain. The consequent increased crowding at the metal center in $(\equiv SiO)_2CrR_2$ may cause the $Cr\text{-}C_\alpha\text{-}C_\beta$ angle to open up, enhancing the rate of α-H elimination. The greater thermal stability of $(\equiv SiO)_2Cr(CH_2Si(CH_3)_3)_2$ compared to $(\equiv SiO)_2Cr(CH_2C(CH_3)_3)_2$ is consistent with lower steric crowding in $(\equiv SiO)_2Cr(CH_2Si(CH_3)_3)_2$ due to the larger size of Si, which causes the methyl groups to be further from the metal. This effect has previously been noted for $Ta(CH_2E(CH_3)_3)_5$ (E is C or Si).[15] It is likely that electronic effects also contribute to the stability trends, since metal-carbon bonds tend to be stronger in trimethylsilylmethyl complexes compared to their neopentyl analogues.[34,35]

4.4 α-Deuterium-Labeling Experiments

The mechanism of neopentane formation was further investigated by synthesis of $(\equiv SiO)_2Cr(CD_2C(CH_3)_3)_2$, with neopentyl ligands labeled by deuterium in the α positions. The reaction of $Cr(CD_2C(CH_3)_3)_4$ (90% $\alpha\text{-}D_2$) with partially dehydroxylated silica-200 gave $(\equiv SiO)_2Cr(CD_2C(CH_3)_3)_2$, **3-αD$_4$**, and was accompanied by the liberation of (1.89 ± 0.02) equivalents of neopentane, consisting of neopentane-d_2 (89%) and neopentane-d_0 (11%), eq 4.7.

$$2\,\equiv SiOH/D + Cr(CD_2C(CH_3)_3)_4 \rightarrow \underset{\textbf{3-}\alpha\textbf{D}_4}{(\equiv SiO)_2Cr(CD_2C(CH_3)_3)_2} + 2\,C(CH_3)_3(CHD_2)/C(CH_3)_3(CD_3) \qquad (4.7)$$

The theoretical yield of neopentane-d_2 upon grafting of **1-α-D_8** is 90%. When the silica hydroxyl groups were labeled with deuterium (>85% ≡SiO<u>D</u>) prior to reaction with $Cr(CD_2C(CH_3)_3)_4$ (90% α-D_2), the hydrocarbon released during grafting contained three deuterium atoms, 79% $C(CH_3)_3(CD_3)$, eq 4.7.

The infrared spectrum of **3-αD_4**, Figure 4.4, contains two low intensity peaks at 2163 and 2103 cm^{-1}, assigned to $\nu_{as}(CD_2)$ and $\nu_s(CD_2)$, respectively. Upon thermolysis of $(\equiv SiO)_2Cr(CD_2C(CH_3)_3)_2$ at 69°C, both peaks decreased in intensity until they disappeared into the baseline noise. The failure to detect a new band in the IR spectrum which could be assigned to ν(=C-D) may be due to the low oscillator strengths and hence weak intensities of C-D vibrations. The results of the deuterium-labeling experiments are summarized in Table 4.5.

Thermolysis of $(\equiv SiO)_2Cr(CD_2C(CH_3)_3)_2$ *in vacuo* produced neopentane which was identified by GC-MS as (71 ± 1)% $C(CH_3)_3(CD_3)$, consistent with α-D abstraction, eq 4.8. The results are summarized in Table 4.6.

$$\underset{\textbf{3-}\alpha\textbf{D}_4}{(\equiv SiO)_2Cr(CD_2C(CH_3)_3)_2} \xrightarrow{69°C} \underset{\textbf{4-}\alpha\textbf{D}}{(\equiv SiO)_2Cr{=}CDC(CH_3)_3} + C(CH_3)_3(CD_3) \qquad (4.8)$$

Whereas thermolysis of unlabeled $(\equiv SiO)_2Cr(CH_2C(CH_3)_3)_2$ was half-complete in 2.5 hours at 69°C, thermolysis of $(\equiv SiO)_2Cr(CD_2C(CH_3)_3)_2$ was only half-complete in 7.5 hours at the same temperature. This difference in reactivity is not consistent with metallacycle formation by γ-H elimination, nor with Cr-C bond homolysis, but does support our assignment of the mechanism as α-H elimination.

Three silica-supported chromium complexes can be formed from 90% α-D-labeled **1a**, as shown in Scheme 4.3. Upon thermolysis, assuming that

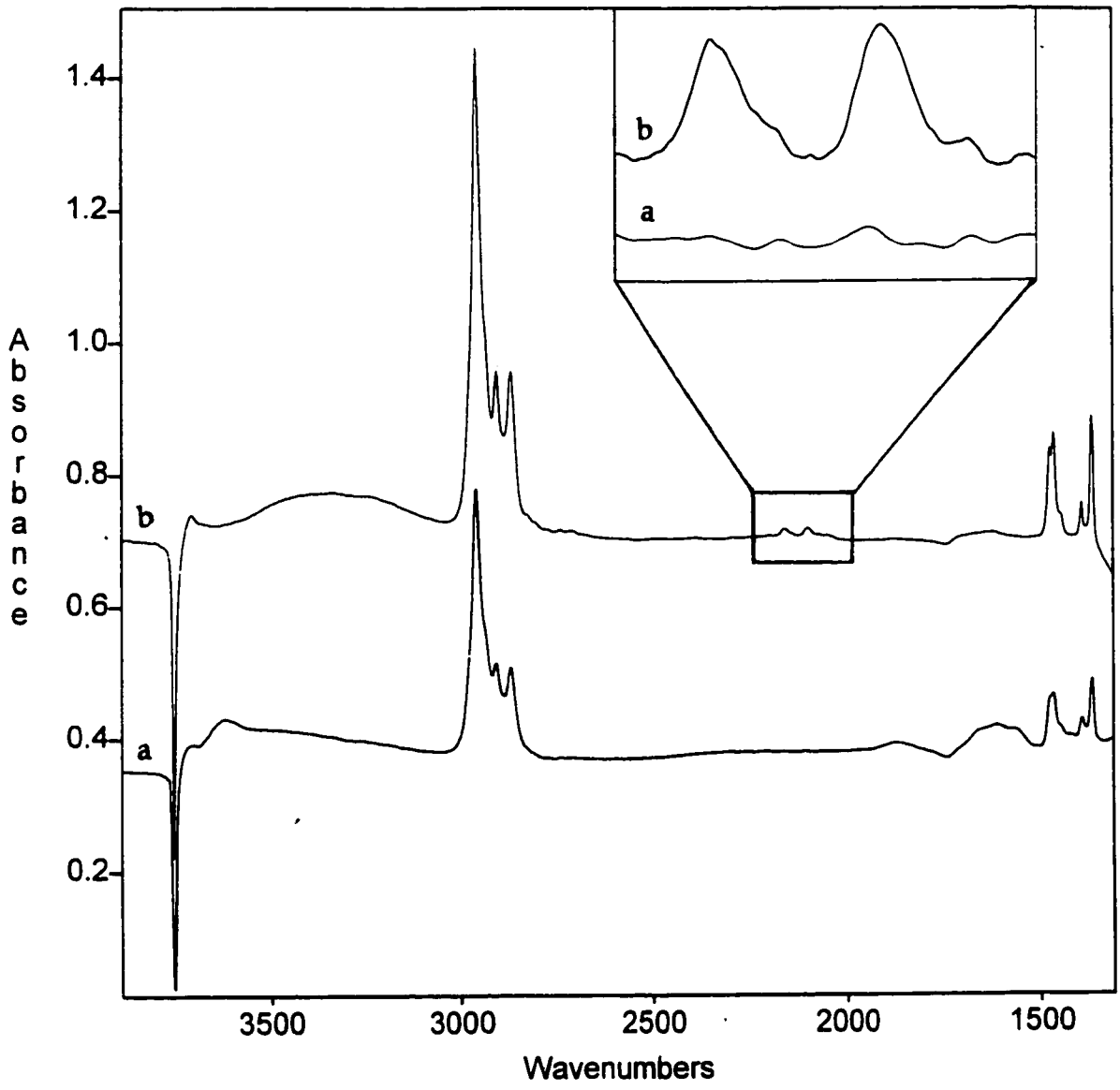

Figure 4.4 Transmission infrared spectra of (a) $(\equiv SiO)_2Cr(CD_2C(CH_3)_3)_2$ at room temperature, and (b) after heating in vacuum at 69°C for 10 hours.

Table 4.5 Quantitative and isotope analysis of the reaction of $Cr(CD_2C(CH_3)_3)_4$ with silica-200

wt. % Cr	mmol Cr [a]	Cr/OH[b]	mmol neopentane[a]	neopentane/ Cr	% Np-d_2[c]	% Np-d_3[d]
1.32	0.254	0.295	0.480	1.89	90	
1.56	0.300	0.349	0.558	1.86		78
1.76	0.339	0.394	0.637	1.88	89	
1.82	0.351	0.408	0.670	1.91		81
1.87	0.360	0.419	0.680	1.89	88	
				avg. 1.89 ± 0.02	avg. 89 ± 1	avg. 79 ± 1

[a] All quantities are reported normalized per g of silica.

[b] Ratio of the amount of chemisorbed Cr to the initial amount of surface hydroxyl groups; 0.86 mmol OH/g silica-200.

[c] Reaction of $Cr(CD_2C(CH_3)_3)_4$ on unlabeled silica-200; extent of neopentane deuteration estimated by the tert-butyl fragment ion intensities at m/z = 57 and 59.

[d] Reaction of $Cr(CD_2C(CH_3)_3)_4$ on D-labeled silica-200; extent of neopentane deuteration estimated by the tert-butyl fragment ion intensities at m/z = 57 and 60.

Table 4.6 Quantitative and isotope analysis of the thermolysis of $(\equiv SiO)_2Cr(CD_2C(CH_3)_3)_2$

		product of thermolysis					
wt. % Cr	mmol Cr [a]	mmol neopentane[a]	neopentane/Cr	% Np-d_3[b]	% Np-d_2[d]	% Np-d_1[c]	% Np-d_0
1.32	0.254	0.226	0.90	72	17	11	0
1.56	0.300	0.261	0.87	71	16	12	0
1.76	0.339	0.292	0.86	72	17	11	0
1.82	0.351	0.326	0.93	71	18	11	0
1.87	0.360	0.320	0.89	70	17	13	0
			avg. 0.89 ± 0.03	avg. 71 ± 1	avg. 17 ± 1	avg. 12 ± 1	0

[a] All quantities are reported normalized per g of silica.

[b] Extent of deuteration estimated by the tert-butyl fragment ion intensities at m/z = 57 and 60

[c] Extent of deuteration estimated by the tert-butyl fragment ion intensities at m/z = 57 and 58.

[d] Extent of deuteration estimated by the tert-butyl fragment ion intensities at m/z = 57 and 59.

α-H abstraction is kinetically preferred over α-D abstraction whenever possible, the predicted isotopomer yields are 81% Np-d_3, 18% Np-d_2, and 1% Np-d_0.

Scheme 4.3 Predicted isotopomer distribution from thermolysis of 90% α-D_2-labeled $CrNp_4$

$$0.81\ (\equiv SiO)_2Cr(CD_2C(CH_3)_3)_2 \xrightarrow{\Delta} 0.81\ [Np\text{-}d_3 + (\equiv SiO)_2Cr{=}CDC(CH_3)_3]$$

$$0.18\ (\equiv SiO)_2Cr[(CD_2C(CH_3)_3)(CH_2C(CH_3)_3)] \xrightarrow{\Delta} 0.18\ [Np\text{-}d_2 + (\equiv SiO)_2Cr{=}CHC(CH_3)_3]$$

$$0.01\ (\equiv SiO)_2Cr(CH_2C(CH_3)_3)_2 \xrightarrow{\Delta} 0.01\ [Np\text{-}d_0 + (\equiv SiO)_2Cr{=}CHC(CH_3)_3]$$

Finally, the subsequent reaction of $(\equiv SiO)_2Cr{=}CDC(CH_3)_3$ with anhydrous HCl or DCl(g) (20 Torr, room temperature, 1 hour) caused the evolution of 0.89 ± 0.03 equivalents of neopentane. In the case of reaction with HCl, the product was 73% $C(CH_3)_3(CH_2D)$ (the rest being unlabeled neopentane), whereas with DCl the product was (78 ± 2)% (average of 4 independent experiments) of the isotopomer $C(CH_3)_3(CD_3)$, eq 4.9.

$$(\equiv SiO)_2Cr{=}CDC(CH_3)_3 + HCl/DCl \rightarrow \text{“}(\equiv SiO)_2CrCl_2\text{”} + C(CH_3)_3(CH_2D)/C(CH_3)_3(CD_3) \quad (4.9)$$

4-αD

The expected yield, in the latter experiment, is 81% Np-d_3 based on the 81% contribution of $(\equiv SiO)_2Cr(CD_2C(CH_3)_3)_2$ in Scheme 4.3. The fact that no neopentane-d_4 was observed supports our contention that γ-H elimination is not significant. The results of these thermolysis experiments are summarized in Table 4.7.

Deuterium-labeling experiments therefore confirm that the thermolysis process is an α-H elimination which yields a supported alkylidene complex, $(\equiv SiO)_2Cr=C(H/D)C(CH_3)_3$. Substantial kinetic isotope effects for α-H/D elimination have been previously reported for α-H eliminations from transition metal neopentyl complexes,[11] including, most recently, the thermolysis of tetraneopentyltitanium.[13]

Although similar labeling studies were not feasible for $(\equiv SiO)_2Cr(CH_2Si(CH_3)_3)_2$ (due to the unavailability of the selectively-labeled Me_3SiCD_2 ligand), its behavior is so similar to that of $(\equiv SiO)_2Cr(CH_2C(CH_3)_3)_2$ in all other respects (vide infra) that we are confident in proposing an analogous alkylidene formulation for $(\equiv SiO)_2Cr=CHSi(CH_3)_3$.

4.5 Kinetics Studies of Thermolysis Reactions

Several mechanisms are possible for the formation of the alkylidene complexes: intramolecular α-H abstraction by chromium or by the adjacent neopentyl ligand, intermolecular α-H abstraction or Cr-C homolysis followed by H abstraction by the neopentyl radical.[3] In order to investigate the mechanism of formation of the alkylidene complexes, we undertook a study of the kinetics of thermolysis reactions of $(\equiv SiO)_2Cr(CH_2C(CH_3)_3)_2$, $(\equiv SiO)_2Cr(CH_2Si(CH_3)_3)_2$ and $(\equiv SiO)_2Cr(CD_2C(CH_3)_3)_2$, shown in equations 4.4, 4.6 and 4.8.

A powdered sample of $(\equiv SiO)_2Cr(CH_2C(CH_3)_3)_2$ was heated *in vacuo* at 69°C in an *in situ* IR cell and the spectrum of the gas phase above the sample was

Table 4.7 Quantitative and isotope analysis of subsequent protonolysis of thermolyzed $(\equiv SiO)_2Cr(CD_2C(CH_3)_3)_2$

		products of protonolysis	
		by HCl	by DCl
mmol neopentane[a]	neopentane/Cr	% Np-d_1[b]	% Np-d_3[c]
0.231	0.91		75
0.267	0.89		77
0.298	0.88	73	
0.323	0.92		80
0.313	0.87		78
	avg. 0.89 ± 0.03	73	avg. 78 ± 2

[a] All quantities are reported normalized per g of silica.

[b] Extent of deuteration estimated by the tert-butyl fragment ion intensities at m/z = 57 and 58.

[c] Extent of deuteration estimated by the tert-butyl fragment ion intensities at m/z = 57 and 60.

recorded at regular time intervals. By integration of the ν(CH) region of the gas phase IR spectrum (*i.e.*, the appearance of the product neopentane), we were able to monitor the progress of the surface reaction, since neopentane is the only volatile product of the reaction and it is not adsorbed on the silica surface. The kinetics of one such reaction are shown in Figure 4.5a. A single exponential three parameter (first-order) curve fit yielded k(69°C) = (0.0046 ± 0.0002) min^{-1}. A second experiment using an independently prepared sample of $(\equiv SiO)_2Cr(CH_2C(CH_3)_3)_2$ gave k(69°C) = (0.0046 ± 0.004) min^{-1}, demonstrating the reproducibility of the rate constant. The data is displayed as a semilog plot in Figure 4.5b, showing its linearity over four half-lives.

The rate constant for thermolysis of $(\equiv SiO)_2Cr(CD_2C(CH_3)_3)_2$, **3-αD4**, was obtained in a similar fashion. Thermolysis of **3-αD4** is also first-order but significantly slower than thermolysis of $(\equiv SiO)_2Cr(CH_2C(CH_3)_3)_2$, Figure 4.5a, consistent with a substantial primary kinetic isotope effect. The rate constant at 69°C is (0.00165 ± 0.0004) min^{-1} (average of two independent experiments), Table 4.8, giving k_H/k_D = 2.8 at 69°C. The magnitude of the kinetic isotope effect for thermolysis of $(\equiv SiO)_2Cr(CH_2/CD_2)C(CH_3)_3)_2$ at 69°C is similar in magnitude to those reported for α-H elimination reactions of molecular complexes in solution. Kinetic isotope effects of about 3 were reported for α-H eliminations from TaR_5 (R = Me, CH_2Ph, $CH_2{}^tBu$)[3,17] in reactions later confirmed to be intramolecular and first-order.[4,15] Since thermolyses of $(\equiv SiO)_2Cr(CH_2C(CH_3)_3)_2$, $(\equiv SiO)_2Cr(CH_2Si(CH_3)_3)_2$ and $(\equiv SiO)_2Cr(CD_2C(CH_3)_3)_2$ are all first-order, this rules out intermolecular reactions; as well, the magnetic moments of the products $(\equiv SiO)_2Cr{=}C(H/D)C(CH_3)_3$ support mononuclear formulations for the alkylidenes, therefore the mobility of surface organometallic complexes required for intermolecular reactions is unlikely. Tertiary systems CrR_xCl_{3-x} readily decompose by metal-carbon bond homolysis,[36] but Cr complexes with primary alkyl ligands do not undergo homolysis.[37] The

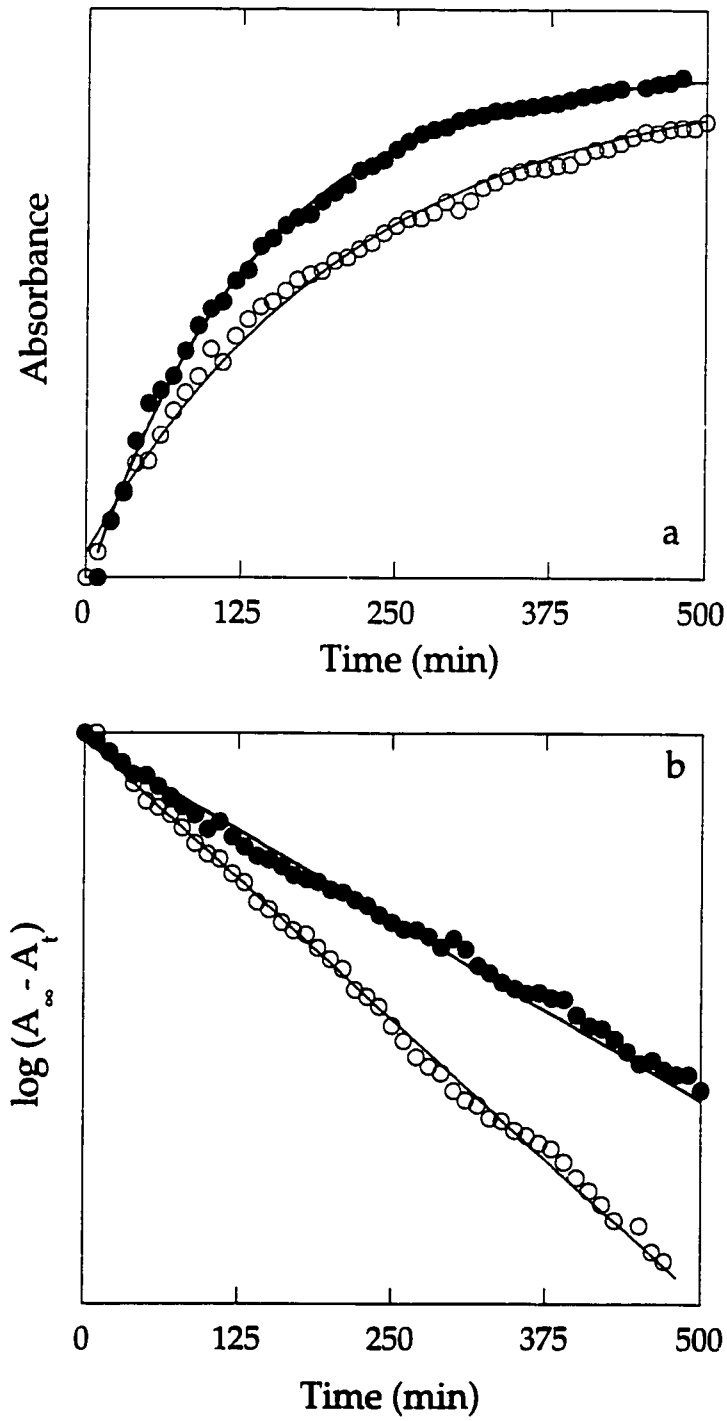

Figure 4.5 Time-resolved evolution of $C(CH_3)_4$ from $(\equiv SiO)_2Cr(CH_2C(CH_3)_3)_2$ (filled circles), and $(\equiv SiO)_2Cr(CD_2C(CH_3)_3)_2$ (open circles) at 69°C: (a) absorbance of *in situ* gas phase IR spectra, ν(CH) region, as a function of time; (b) semilog plots of data from (a). The solid lines are (a) non-linear least square and (b) linear fits to the first-order integrated kinetic rate equation.

Table 4.8 First-order rate constants for alkane elimination

Surface complex	Temperature / °C	k / min^{-1} [a]
$(\equiv SiO)_2Cr(CH_2C(CH_3)_3)_2$	62	0.0023 ± 0.0004
	69	0.0046 ± 0.0002
	69	0.0046 ± 0.0004
	71	0.0054 ± 0.0003
	75	0.0073 ± 0.0002
	82	0.0083 ± 0.0002
	90	0.0099 ± 0.0002
	110	0.0123 ± 0.0040
$(\equiv SiO)_2Cr(CD_2C(CH_3)_3)_2$	69	0.0015 ± 0.0004
	69	0.0018 ± 0.0004
	110	0.0096 ± 0.0001
$(\equiv SiO)_2Cr(CH_2Si(CH_3)_3)_2$	60	0.0011[b]
	100	0.0073 ± 0.0002
	130	0.015 ± 0.002
	150	0.020 ± 0.001
	190	0.029 ± 0.003

[a] Errors are from non-linear least squares fit to a single exponential rate law, using data from at least four half-lives.

[b] Estimated from the first two half-lives.

absence of radical coupling products and the sizable primary kinetic isotope effect support a mechanistic assignment of intramolecular α-H elimination.[37]

Kinetics experiments with $(\equiv SiO)_2Cr(CH_2C(CH_3)_3)_2$ were performed at various temperatures between 62 and 110°C, Figure 4.6a. At each temperature, one equivalent of neopentane was the exclusive gaseous product of thermolysis. Each kinetic curve was fit with a single exponential function; the rate constants are tabulated in Table 4.8. From these results, the Eyring plot in Figure 4.6b was constructed. We note that the plot is not linear. In light of this behavior, the primary kinetic isotope effect (measured above 69°C) was redetermined at a higher temperature.

The thermolysis of $(\equiv SiO)_2Cr(CD_2C(CH_3)_3)_2$ at 110°C gave one equivalent of $C(CH_3)_4$ as 70% $C(CH_3)_3(CD_3)$ with $k = (0.0096 \pm 0.0001)\ min^{-1}$, yielding $k_H/k_D = 1.2$ at 110°C. Reaction of $(\equiv SiO)_2Cr{=}CDC(CH_3)_3$ formed at 110°C with HCl(g) liberated 73% $C(CH_3)_3(CH_2D)$, as expected. Therefore the alkylidene is still generated at the higher thermolysis temperature, albeit with a lower kinetic isotope effect.

The evolution of $SiMe_4$ from $(\equiv SiO)_2Cr(CH_2Si(CH_3)_3)_2$ was monitored in the same way as for $(\equiv SiO)_2Cr(CH_2C(CH_3)_3)_2$ and was also first-order. The kinetics of thermolysis of $(\equiv SiO)_2Cr(CH_2Si(CH_3)_3)_2$ was also studied at several temperatures from 60 - 190°C, Figure 4.7a. The rate constants, Table 4.8, were used to construct an Eyring plot, which is also non-linear, Figure 4.7b.

For both surface complexes, the slope of the Eyring plot gradually decreases as the temperature increases, implying that $\Delta H^{\ddagger}_{obs}$ is not constant. This kind of behavior is typical of a multistep mechanism, eq 4.10, where B is a steady-state intermediate.[38]

$$A \underset{k_{-1}}{\overset{k_1}{\rightleftharpoons}} B \xrightarrow{k_2} C \qquad (4.10)$$

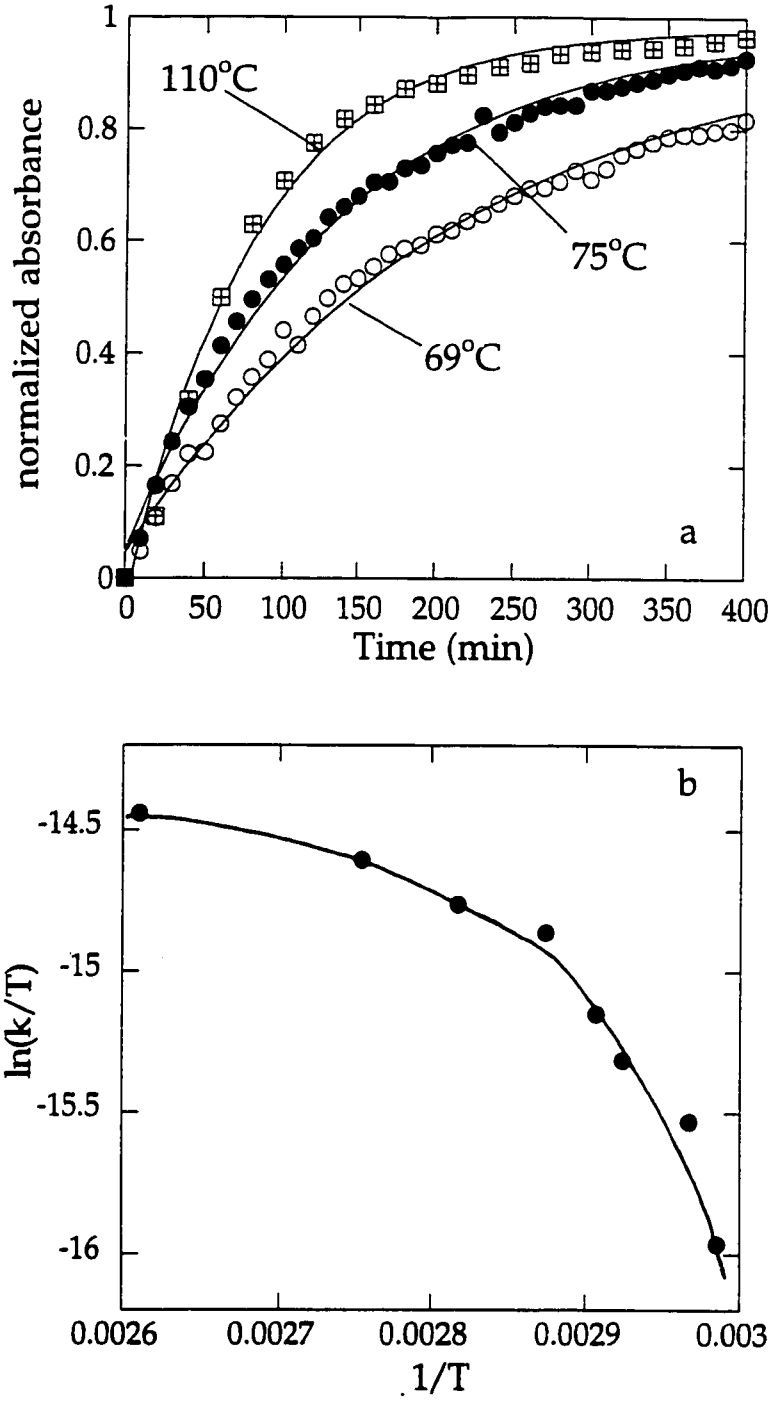

Figure 4.6 (a) Time-resolved evolution of $C(CH_3)_4$ from $(\equiv SiO)_2Cr(CH_2C(CH_3)_3)_2$ at various temperatures. Absorbances have been normalized in order to show all data on the same scale. Solid curves are three-parameter single exponential fits to the first-order integrated kinetic rate equation. (b) Eyring plot of the temperature-dependence of rate constants for the thermolysis of $(\equiv SiO)_2Cr(CH_2C(CH_3)_3)_2$. Data are given in Table 4.8.

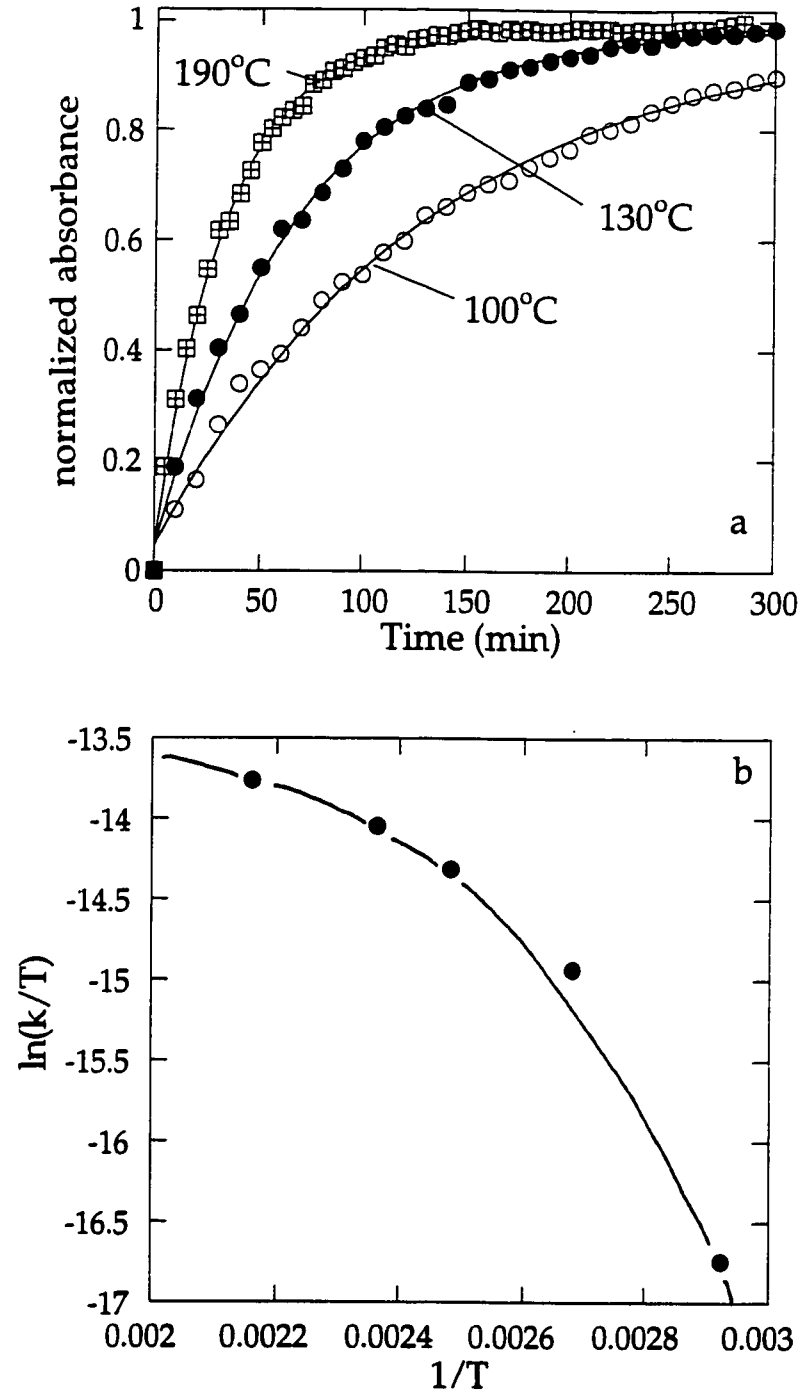

Figure 4.7 (a) Time-resolved evolution of $Si(CH_3)_4$ from $(\equiv SiO)_2Cr(CH_2Si(CH_3)_3)_2$ at various temperatures. Absorbances have been normalized in order to show all data on the same scale. Solid curves are three-parameter single exponential fits to the first-order integrated kinetic rate equation. (b) Eyring plot of the temperature-dependence of rate constants for the thermolysis of $(\equiv SiO)_2Cr(CH_2Si(CH_3)_3)_2$. Data are given in Table 4.8.

In this case, the Eyring plot ln(k/T) versus (1/T) in the range where k_{-1} and k_2 are comparable will be non-linear and curved downward. This curvature indicates that the apparent activation enthalpy decreases with increasing temperature.

We therefore suggest a mechanism for α-H elimination consisting of two consecutive reactions, where the apparent activation enthalpy contains contributions from both steps.[18] Each step must be intramolecular but have a different kinetic isotope effect. A mechanism which is consistent with all these observations and available to Cr(IV) is reversible intramolecular α-H elimination to form a (neopentyl)(neopentylidene)Cr(VI) hydride, followed by reductive elimination of neopentane, Scheme 4.4.

Scheme 4.4 Mechanism of thermolysis of silica-supported bis(neopentyl)chromium(IV) involving α-hydrogen abstraction

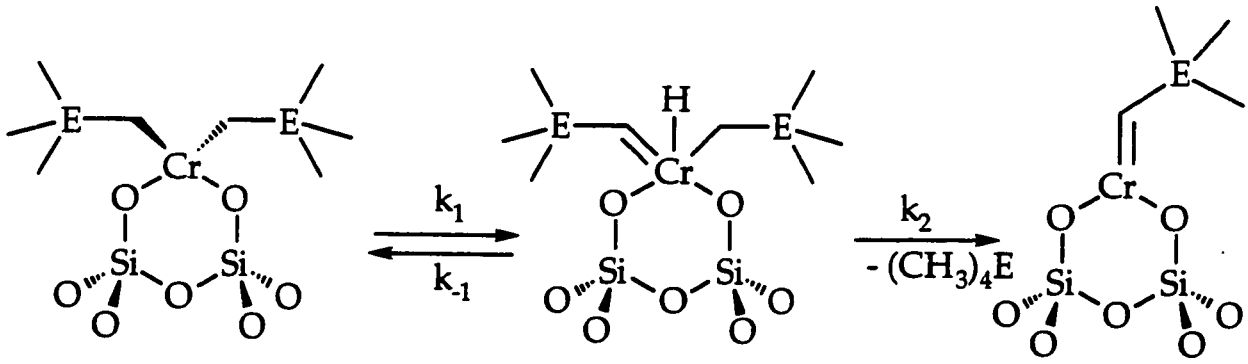

The Eyring plot for thermolysis of $(\equiv SiO)_2Cr(CH_2Si(CH_3)_3)_2$ is also concave downwards, suggestive of a similar two-step metal hydride pathway. We associate formation of the hydride complex with the higher kinetic isotope effect and a moderate activation barrier. Reductive elimination of alkane is associated with the lower kinetic isotope effect and a lower activation barrier. Kinetic isotope effects for reductive elimination of alkane are usually small or even inverse.[38]

4.6 Uniformity of Supported Organochromium Complexes

The identical kinetic behavior of each surface organometallic fragment during thermolysis implies that *all* the surface structures are bis(alkyl), since they undergo elimination of alkane quantitatively and with a single first-order rate constant. Rates of reactions on surfaces are extremely sensitive to small changes in bonding of surface species,[39] therefore the reproducible single exponential behavior of these thermolysis reactions is not consistent with the presence of widely different coordination environments at the surface metal atoms. We thus confirm that the formulation of the surface complexes $(\equiv SiO)_2Cr(CH_2E(CH_3)_3)_2$ proposed in the previous chapter is exact on a microscopic as well as a macroscopic level. Indeed, the coordination geometry of the surface complexes, which is determined by the separation between each member of a pair of reacting surface hydroxyls, must be very similar in all cases.

There are several possible ways that such uniformity in local surface environments might arise. First, we may consider that the surface hydroxyl groups on partially dehydroxylated amorphous silica are not randomly distributed, but that they occur in well-ordered pairs. Such an ordering was proposed for silicas treated below 450°C; above this temperature the pair structure was thought to be lost.[40] IR spectroscopy[41] and NMR techniques[42] have long been applied to the problem of characterization of surface hydroxyls on a variety of silicas. The proportion of geminal pairs is constant[43] or may even increase[44,45] with the dehydroxylation temperature, according to ^{29}Si NMR studies. However, vicinal and isolated hydroxyls are indistinguishable by solid-state NMR, and all three kinds of non-hydrogen-bonded hydroxyls are indistinguishable by vibrational spectroscopy (geminal and vicinal pairs are not capable of internal hydrogen-bonding).[46,47] The IR spectrum of silica-200 shows two kinds of surface hydroxyls: a sharp peak at 3747 cm^{-1} corresponding to isolated/vicinal/geminal hydroxyls, and a

broad band to lower wavenumbers corresponding to hydrogen-bonded hydroxyls.[48] We believe that it is unlikely that an unmodified amorphous silica possesses the unique kind of paired hydroxyl surface structure that would be required to produce the uniform surface organometallic complexes we have made.

A second possible way to attain uniformity in surface structure is by reorganization of the surface during or after grafting.[49] This could be achieved either by migration of surface hydroxyl groups or migration of singly-bound surface organometallic fragments $\equiv SiOCrR_3$. We previously showed that a 200 m^2/g silica surface is fully covered by tris(neopentyl)chromium(IV) fragments when the metal content reaches ca. 0.37 mmol Cr/g.[28] On silica-200, this loading is achieved when slightly less than half of the surface hydroxyls have been consumed. Since full surface coverage leaves little room for mobility of surface organometallic fragments, we believe it is more likely that unreacted surface hydroxyl groups migrate until they locate the optimal position for reaction with an already-grafted tris(alkyl)metal fragment. This mechanism generates the most stable surface environment which is suggested to occur when the metal occupies a position in a 6-membered siloxane ring. A third possibility, which may operate as well, is that grafting occurs on a variety of hydroxyl pairs, but that the surface is flexible enough to allow the resulting surface organometallic complexes to achieve the optimum transition state geometry for α-H elimination via molecular vibrations.

Finally, α-H elimination is probably surface-assisted, via coordination of an additional surface oxygen "ligand". Base-assisted alkane elimination has precedent in the formation of a benzylidene complex from $[Cp^*Nb(NR)(CH_2Ph)_2(PMe_3)]$.[50] The alkylidenes $(\equiv SiO)_2Cr{=}CHE(CH_3)_3$ may maintain tetracoordination by interaction with surface siloxane oxygens, Scheme 4.5.

Scheme 4.5 Stabilization of the chromium(IV) alkylidene surface species through reversible coordination of a surface siloxane oxygen.

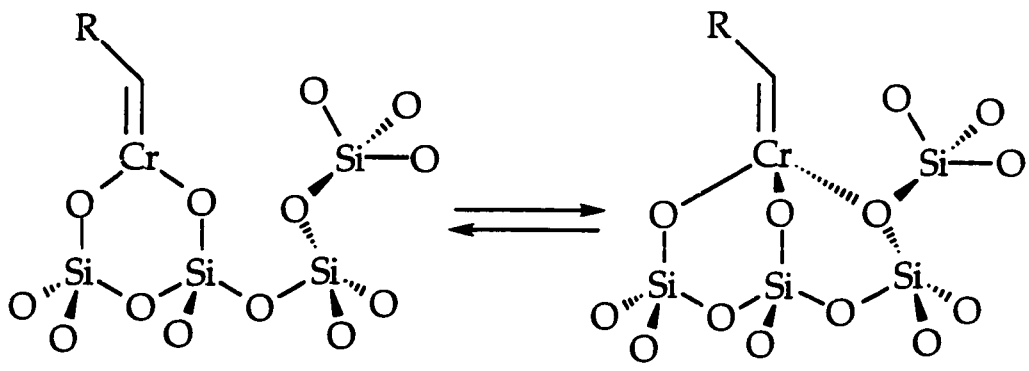

This coordination is readily reversible, and an incoming ligand could displace the siloxane oxygen. The ability of the silica surface to stabilize coordinatively unsaturated species and then regenerate them to allow substrate binding has been suggested as the reason why a supported olefin hydrogenation catalyst, $Os_3(CO)_{10}(\mu\text{-}H)(\mu\text{-}OSi\equiv)$ has better catalytic properties than molecular $Os_3(CO)_{10}(\mu\text{-}H)(\mu\text{-}OPh)$.[51]

4.7 Reactivity of Chromium(IV) Alkylidenes

Spectroscopic evidence for the alkylidene nature of the paramagnetic surface complex $(\equiv SiO)_2Cr{=}CHC(CH_3)_3$ proved difficult to obtain. Its IR spectrum does not contain a low frequency ν(CH) mode, although these vibrations are sometimes masked by other C-H modes.[29] We therefore probed the chemistry of $(\equiv SiO)_2Cr{=}CHC(CH_3)_3$ with some characteristic test reactions for high-valent metal alkylidenes. Since there are so few literature reports of high-valent Cr alkylidene complexes, their reactivity is of great interest.

4.7.1 Reaction with Water

Upon addition of water vapor to $(\equiv SiO)_2Cr=CHC(CH_3)_3$, a reaction took place resulting in liberation of neopentane into the gas phase. The orange silica pellet changed color to yellow, in contrast to the behavior of both **3a** and $CrNp_4$ which are unreactive towards water. The infrared spectrum of the modified silica showed a decrease in intensity of the ν(C-H) bands. Vibrations attributable to "Cr=O" were not detected.

4.7.2 Reaction with Bromine

The reaction of excess $Br_2(g)$ with $(\equiv SiO)_2Cr=CHC(CH_3)_3$ gave 1,1-dibromo-2,2-dimethylpropane, eq 4.11, within minutes at room temperature.

$$(\equiv SiO)_2Cr=CHC(CH_3)_3 + 2\,Br_2 \rightarrow C(CH_3)_3(CHBr_2) + "(\equiv SiO)_2CrBr_2" \qquad (4.11)$$

The organic product is the result of electrophilic attack on the metal-carbon double bond.[52] It was identified by its mass spectrum, with major peaks at m/e = 217, 215, 213 ($C_4H_7Br_2$), 135, 133 (C_4H_6Br) and 53 (C_4H_6). The absence of mass peaks at m/e = 151, 137 and 69 allow us to exclude the other possible isomer, 1,3-dibromo-2,2-dimethylpropane.

Reaction 4.11 is completely consistent with the characterization of $(\equiv SiO)_2Cr=CHC(CH_3)_3$ as a terminal alkylidene complex.

4.7.3 Reaction with Acetone

The room temperature reaction of $(\equiv SiO)_2Cr=CHC(CH_3)_3$ with acetone vapor immediately gave a trace of the expected olefin 2,4,4-trimethyl-2-pentene from the pseudo-Wittig reaction,[2] eq 4.12, as well as the condensation product 4-methyl-3-penten-2-one.

$$(\equiv SiO)_2Cr{=}CHC(CH_3)_3 + (CH_3)_2CO \rightarrow (CH_3)_2C{=}CHC(CH_3)_3 \qquad (4.12)$$

The surface product was not identified. This reaction is characteristic of alkylidene complexes.[2]

4.7.4 Reaction with Styrene

$(\equiv SiO)_2Cr(CH_2E(CH_3)_3)_2$ does not react with styrene at room temperature, however, when the surface complexes were exposed to excess styrene vapor at their typical thermolysis temperatures, or when $(\equiv SiO)_2Cr{=}CHC(CH_3)_3$ and $(\equiv SiO)_2Cr{=}CHSi(CH_3)_3$ were exposed to excess styrene at room temperature, neohexene and trimethylvinylsilane were formed, respectively. This reaction is formulated as a metathetical exchange, eq 4.13.

$$(\equiv SiO)_2Cr{=}CHE(CH_3)_3 + PhCH{=}CH_2 \rightarrow (\equiv SiO)_2Cr{=}CHPh + CH_2{=}CHE(CH_3)_3 \qquad (4.13)$$

E is C, Si

The surface benzylidenes react with styrene to produce polystyrene. This reaction will be discussed further in the next chapter.

4.8 Conclusion

Substitution of alkyl ligands on organometallic complexes by siloxy "ligands" derived from the silica surface tends to enhance their thermal stability. For example, $(\equiv SiO)(\equiv SiOH)Rh(\eta^3\text{-allyl})_2$[49] and $(\equiv SiO)Ni(\eta^3\text{-allyl})$[53] are more stable than $Rh(\eta^3\text{-allyl})_3$ and $Ni(\eta^3\text{-allyl})_2$ with respect to reduction to metallic forms. Also, $(\equiv SiO)ZrR_3$[54] and $(\equiv SiO)CrR_3$[28] are thermally more robust than ZrR_4 and CrR_4. This phenomenon can be ascribed at least in part to increased metal-ligand bond

strengths due to the inductive effect of the electron-withdrawing silica "ligand". Similar effects have been remarked in mixed alkyl/halide complexes: for example, $CrRCl_2$ is thermally more stable than CrR_3.[55] Therefore, the facility with which silica-supported bis(alkyl)metal fragments undergo thermolysis was surprising considering that tris(alkyl)chromium(IV) fragments on silica do not show this reactivity.[28] It appears that the second substitution by a siloxy "ligand" on an organometallic fragment does not enhance the stabilizing effect of the first substitution.[36]

Mild thermolysis of silica-supported bis(neopentyl)chromium(IV) causes evolution of neopentane by α-H elimination. The product, stable up to 80°C, was identified as a mononuclear neopentylidenechromium(IV) complex, $(\equiv SiO)_2Cr=CHC(CH_3)_3$, bound to and stabilized by the silica surface. Silica-supported bis(trimethylsilylmethyl)chromium(IV) also undergoes thermolysis, but at 150°C to generate the supported alkylidene complex $(\equiv SiO)_2Cr=CHSi(CH_3)_3$, with concurrent liberation of tetramethylsilane.

The thermal reactions are quantitative suggesting that all surface organometallic complexes possess or can readily access very similar coordination environments. The mechanism of formation of the alkylidene complexes was confirmed by deuterium labeling of neopentyl ligands in the α position.

The temperature dependence of the first-order rate constants for α-H elimination give non-linear Eyring plots which are concave downwards. Therefore a two-step mechanism of reversible (alkyl)(alkylidene)Cr(VI) hydride formation followed by reductive elimination of alkane was proposed.

Treatment of unlabeled $(\equiv SiO)_2Cr=CHC(CH_3)_3$ with dry HCl liberated one equivalent of neopentane, while reaction with DCl gave dideuteroneopentane. Reactions with acetone and Br_2 yielded 2,4,4-trimethyl-2-pentene and 1,1-dibromo-2,2-dimethylpropane, respectively. The surface alkylidene complexes

undergo metathesis with styrene.

In contrast to silica-supported bis(alkyl)Cr(IV) complexes, the Cr(IV) alkylidenes are efficient room temperature olefin polymerization catalysts. The details of the polymerization process initiated by silica-supported chromium alkylidenes will be discussed in the next chapter.

4.9 References

1) Schrock, R. R. *J. Am. Chem. Soc.* **1974**, *96*, 6796.

2) Schrock, R. R. *J. Am. Chem. Soc.* **1976**, *98*, 5399-5400.

3) Schrock, R. R. *J. Organomet. Chem.* **1976**, *122*, 209-225.

4) Malatesta, V.; Ingold, K. U.; Schrock, R. R. *J. Organomet. Chem.* **1978**, *152*, C53-C56.

5) Feldman, J.; Schrock, R. R. In *Prog. Inorg. Chem.*; Lippard, S. J., Ed.; Wiley: New York, 1991; Vol. 39, pp. 1-74.

6) Davidson, P. J.; Lappert, M. F.; Pearce, R. *Chem. Rev.* **1976**, *76*, 219.

7) Schrock, R. R.; Parshall, G. W. *Chem. Rev.* **1976**, *76*, 243.

8) Bulls, A. R.; Schaefer , W. P.; Serfas, M.; Bercaw, J. E. *Organometallics* **1987**, *6*, 1219-1226.

9) McDade, C.; Green, J. C.; Bercaw, J. E. *Organometallics* **1982**, *1*, 1629-1634.

10) Schwartz, J.; Gell, K. I. *J. Organomet. Chem.* **1980**, *184*, C1 - C2.

11) Wood, C. D.; McLain, S. J.; Schrock, R. R. *J. Am. Chem. Soc.* **1979**, *101*, 3210-3222.

12) Coles, M. P.; Gibson, V. C.; Clegg, W.; Elsegood, M. R. J.; Porelli, P. A. *Chem. Commun.* **1996**, 1963-1964.

13) Cheon, J.; Rogers, D. M.; Girolami, G. S. *J. Am. Chem. Soc.* **1997**, *119*, 6804-6813.

14) Giannini, L.; Solari, E.; Floriani, C.; Chiesi-Villa, A.; Rizzoli, C. *J. Am. Chem. Soc.* **1998**, *120*, 823-824.

15) Li, L.; Hung, M.; Xue, Z. *J. Am. Chem. Soc.* **1995**, *117*, 12746-12750.

16) Fryzuk, M. D.; Mao, S. S. H.; Zaworotko, M. J.; MacGillivray, L. R. *J. Am. Chem. Soc.* **1993**, *115*, 5336-5337.

17) Schrock, R. R.; Fellmann, J. D. *J. Am. Chem. Soc.* **1978**, *100*, 3359-3370.

18) Schrock, R. R. *Acc. Chem. Res.* **1979**, *12*, 98.

19) Schrock, R. R. *J. Organomet. Chem.* **1986**, *300*, 249.

20) Fischer, E. O.; Maasboll, A. *Angew. Chem. Int. Ed. Eng.* **1964**, *3*, 580.

21) Hao, S.; Song, J.-I.; Berno, P.; Gambarotta, S. *Organometallics* **1994**, *13*, 1326-1335.

22) Filippou, A. C.; Wössner, D.; Lungwitz, B.; Kociok-Köhn, G. *Angew. Chem., Int. Ed. Engl.* **1996**, *35*, 876-878.

23) Halle, L. F.; Armentrout, P. B.; Beauchamp, J. L. *J. Am. Chem. Soc.* **1981**, *103*, 962-963.

24) Chen, J. D.; Sheldon, R. A. *J. Catal.* **1995**, *153*, 1-8.

25) Chen, J. D.; Lempers, H. B. E.; Sheldon, R. A. *J. Chem. Soc., Farad. Trans.* **1996**, *92*, 1807-1813.

26) McDaniel, M. P. *Adv. Catal.* **1985**, *33*, 47-98.

27) Kruse, W. *J. Organometal. Chem.* **1972**, *42*, C39-C42.

28) Amor Nait Ajjou, J.; Scott, S. L. *Organometallics* **1997**, *16*, 86-92.

29) Nugent, W. A.; Mayer, J. M. *Metal-Ligand Multiple Bonds*; Wiley-Interscience: New York, 1988.

30) Maury, F.; Ossola, F. *Thin Solid Films* **1992**, *207*, 82-89.

31) Maury, F.; Ossola, F.; Schuster, F. *Surf. Coat. Technol.* **1992**, *54/55*, 204-210.

32) Dufaud, V.; Niccolai, G. P.; Thivolle-Cazat, J.; Basset, J.-M. *J. Am. Chem. Soc.* **1995**, *117*, 4288-4294.

33) Luo, L.; Li, L.; Marks, T. J. *J. Am. Chem. Soc.* **1997**, *119*, 8574-8575.

34) Lappert, M. F.; Patil, D. S.; Pedley, J. B. *J. Chem. Soc., Chem. Commun.* **1975**, 830-831.

35) Bruno, J. W.; Marks, T. J.; Morss, L. R. *J. Am. Chem. Soc.* **1983**, *105*, 6824-6832.

36) Sneeden, R. P. A.; Zeiss, H. H. *J. Organomet. Chem.* **1971**, *26*, 101-113.

37) Espenson, J. H. *Acc. Chem. Res.* **1992**, *25*, 222-227.

38) Espenson, J. H. *Chemical Kinetics and Reaction Mechanisms*; McGraw-Hill:

New York, 1981.

39) Somorjai, G. A. *Chemistry in Two Dimensions: Surfaces*; Cornell University Press: Ithaca, 1981.

40) Ballard, D. G. H. *Adv. Catal.* **1973**, *23*, 263-325.

41) Morrow, B. A.; McFarlan, A. J. *J. Phys. Chem.* **1992**, *96*, 1395.

42) Liu, C. C.; Maciel, G. E. *J. Am. Chem. Soc.* **1996**, *118*, 5103-5119.

43) Léonardelli, S.; Facchini, L.; Fretigny, C.; Tougne, P.; Legrand, A. P. *J. Am. Chem. Soc.* **1992**, *114*, 6412-6418.

44) Morrow, B. A.; Gay, I. D. *J. Phys. Chem.* **1988**, *92*, 5569-5571.

45) Kinney, D. R.; Chuang, I.-S.; Maciel, G. E. *J. Am. Chem. Soc.* **1993**, *115*, 6786-6794.

46) Ferrari, A. M.; Ugliengo, P.; Garrone, E. *J. Phys. Chem.* **1993**, *97*, 2671-2676.

47) Michalske, T. A.; Bunker, B. C. *J. Appl. Phys.* **1984**, *56*, 2686-2693.

48) Morrow, B. A.; McFarlan, A. J. *J. Non-Cryst. Solids* **1990**, *120*, 61-71.

49) Somorjai, G. A. *J. Mol. Catal. A: Chem.* **1996**, *107*, 39-53.

50) Cockcroft, J. K.; Gibson, V. C.; Howard, J. A. K.; Poole, A. D.; Siemeling, U.; Wilson, C. *J. Chem. Soc., Chem. Commun.* **1992**, 1668.

51) Choplin, A.; Besson, B.; D'Ornelas, L.; Sanchez-Delgado, R.; Basset, J.-M. *J. Am. Chem. Soc.* **1988**, *110*, 2783-2787.

52) Johnson, M. D. In *The Chemistry of the Metal-Carbon Bond*; Hartley, F. R. and Patai, S., Eds.; Wiley: New York, 1982; Vol. 2, pp. 513-558.

53) Dufour, P.; Houtman, C.; Santini, C. C.; Nédez, C.; Basset, J.-M.; Hsu, L. Y.; Shore, S. G. *J. Am. Chem. Soc.* **1992**, *114*, 4248-4257.

54) Yermakov, Y. I.; Kuznetsov, B. N.; Karakchiev, L. G.; Derbeneva, S. S. *Kinet. Catal.* **1973**, *14*, 611-616.

55) Quignard, F.; Lécuyer, C.; Choplin, A.; Olivier, D.; Basset, J.-M. *J. Mol. Catal.* **1992**, *74*, 353-363.

Chapter 5

Mechanism of Olefin Polymerization Catalyzed by Silica-supported Chromium(IV) Alkylidene Complexes

5.1 Introduction

Four mechanisms have been proposed for the propagation steps in transition-metal-catalyzed olefin polymerization: the Cossee,[1] Green-Rooney,[2] Green-Rooney-Brookhart[3-5] and the hybrid Cossee/Green-Rooney-Brookhart mechanisms.

The Cossee mechanism,[1] Scheme 5.1, requires a vacant coordination site on the metal center in a position adjacent to the growing alkyl chain. A monomer coordinates to the metal at this site, followed by migratory insertion that extends the growing alkyl chain by one monomer unit.

Scheme 5.1 Cossee mechanism

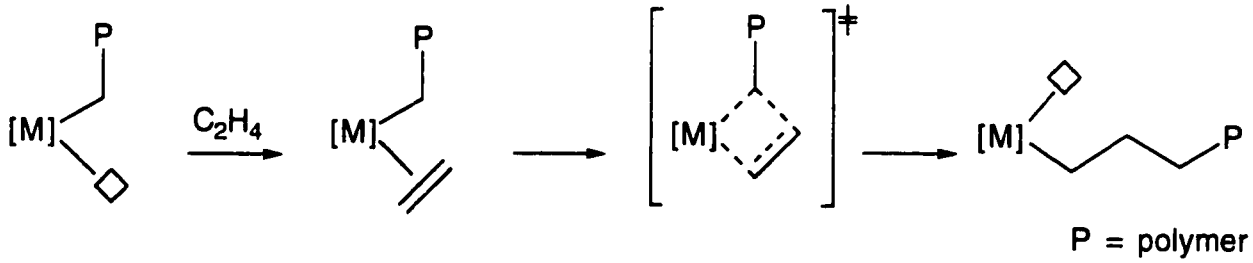

The Green-Rooney mechanism,[2] Scheme 5.2, requires two vacant coordination sites at the metal center. The growing polymer chain first transfers an α-hydrogen to the metal to generate a carbene. An ethylene then coordinates at the remaining vacant site. This is followed by [2+2] cycloaddition across the metal-carbene double bond via a metathesis-type transition state to form a metallacycle. Reductive elimination causes the ring to open, thus producing an

alkyl chain that has been extended by one monomer unit, in conjunction with the regeneration of the two vacant coordination sites at the metal center.

Scheme 5.2 Green-Rooney mechanism

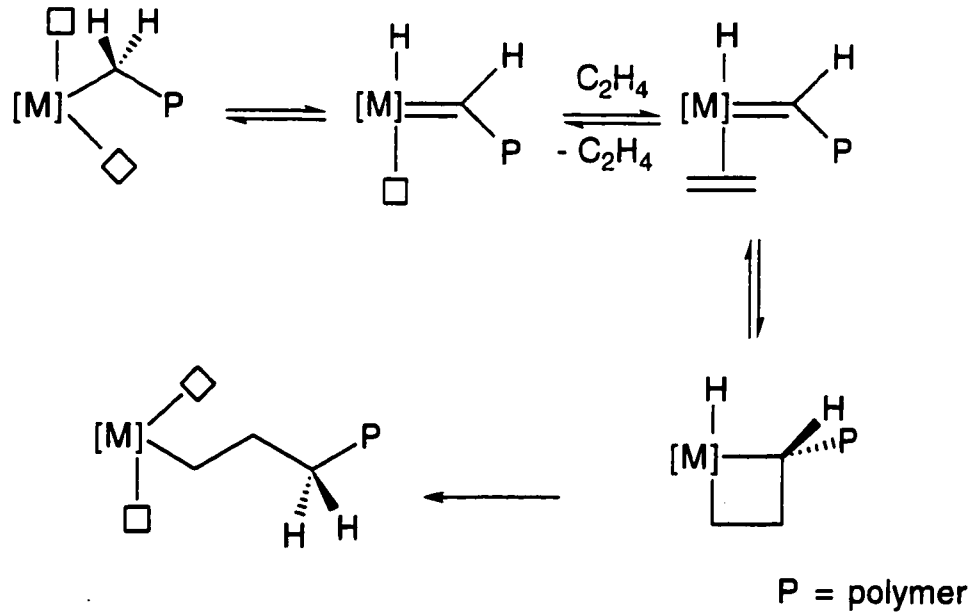

The Green-Rooney-Brookhart mechanism is intermediate to the two previous mechanisms. The hydrogen on the α-carbon of the growing polymer chain is not completely transferred to the metal, but interacts with the metal via a three-center, two electron "agostic interaction",[5,6] Scheme 5.3.

Scheme 5.3 Green-Rooney-Brookhart mechanism

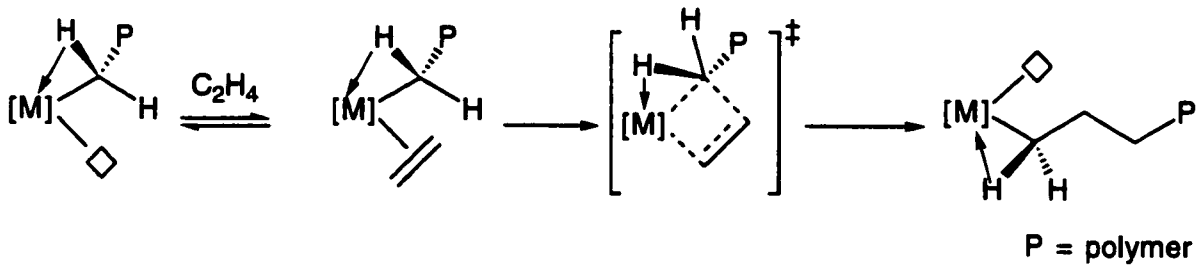

The α-agostic interaction is of particular interest since it has potential to dramatically lower the activation barrier for olefin insertion. It appears that in several catalyst systems insertion of olefins occurs with assistance of an α-H atom of the migratory alkyl group. This interaction is analogous to hyperconjugation, Scheme 5.4, where the electron deficiency at carbon is stabilized by electron donation from a C-H bond on the α-carbon. An α-agostic interaction at a metal center creates a partial positive charge on the α-carbon, which accelerates migratory insertion. Ab initio calculations confirm that insertions are favored by α-agostic interactions.[7] However, not all catalysts show evidence for α-agostic interactions in their ground states.[7]

Scheme 5.4 Analogy between hyperconjugation and α-agostic intaractions[7]

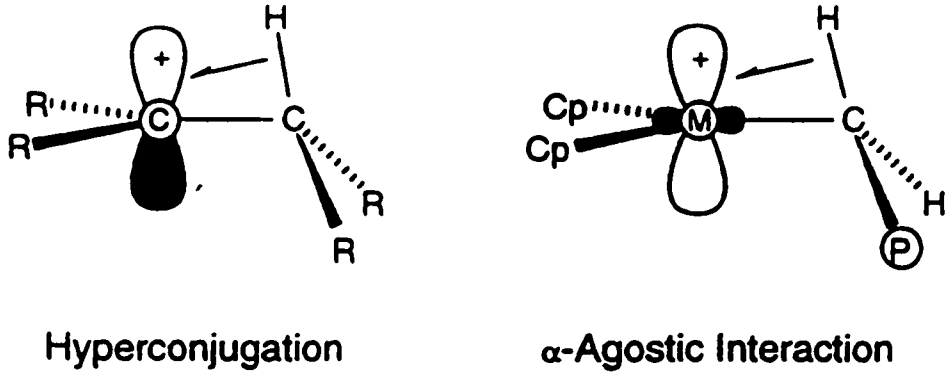

Hyperconjugation α-Agostic Interaction

The fourth polymerization mechanism is a hybrid of the Cossee and Green-Rooney-Brookhart mechanisms, in which the α-agostic interaction occurs only during the transition state.

Termination is understood to occur via β-hydrogen elimination,[1,2,8,9] Scheme 5.5. This mechanism produces polymer chains containing vinyl end groups. Infrared and NMR spectroscopy have shown that polyethylene chains usually contain one vinyl and one methyl end group.[8]

Scheme 5.5 Termination mechanism for ethylene polymerization

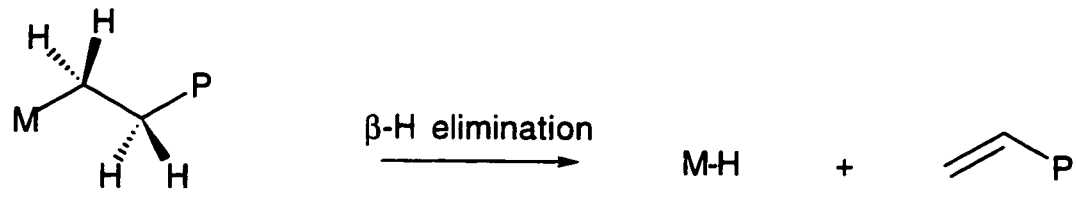

We showed in the previous chapter that bis(alkyl)chromium(IV) surface complexes $(\equiv SiO)_2Cr(CH_2E(CH_3)_3)_2$ undergo thermolysis in vacuum at 70°C or 150°C, respectively, to give new well-defined chemisorbed surface species identified as Cr(IV) alkylidenes, **4a** and **4b**, eq 5.1.[10,11]

$$(\equiv SiO)_2Cr(CH_2E(CH_3)_3)_2 \xrightarrow{\Delta} (\equiv SiO)_2Cr{=}CHE(CH_3)_3 + E(CH_3)_4 \qquad (5.1)$$

3a **4a** (E=C; T = 70°C)

3b **4b** (E=Si; T = 150°C)

In this chapter, we report the reactivity of the supported chromium(IV) alkylidenes towards various olefins, using our results to propose a mechanism for polymerization.

5.2 Reactivity of Silica-supported Chromium(IV) Alkylidenes

5.2.1 Towards Norbornene

When the silica-supported bis(alkyl)chromium(IV) species **3a** or **3b** were exposed to norbornene vapor at room temperature, no reaction was observed. However, when the supported bis(alkyl)chromium(IV) species **3a** or **3b** were exposed to norbornene then heated at their respective thermolysis temperatures, 70°C or 150°C, respectively, or if the thermolyzed species **4a** or **4b** were exposed to

norbornene at room temperature, an increase in intensity was observed in the hydrocarbon regions of the IR spectra of the modified silicas, Figure 5.1. The increase was small, implying that just a small amount of norbornene is fixed on the surface. No volatile products were detected by GC or GC-MS. The inferred metathesis polymerization of norbornene is shown in eq 5.2.

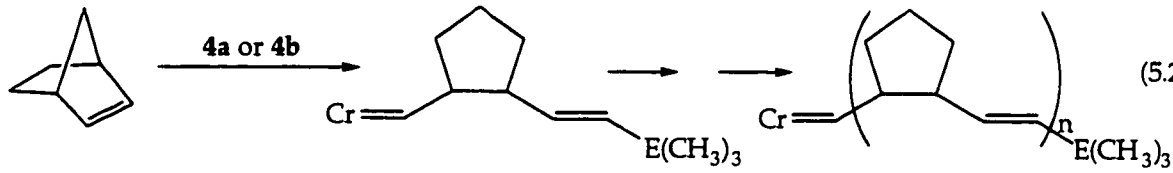

(5.2)

5.2.2 Towards Styrene

At room temperature, there is no reaction between **3** and styrene. However, if **3** is exposed to styrene at its thermolysis temperature, or if either of the alkylidenes **4** are exposed to styrene vapor at room temperature, a reaction takes place. The modified silica remains orange (**4a**) or pink (**4b**), but becomes covered with a white film. Neohexene (from **4a**) and trimethylvinylsilane (from **4b**) were detected by GC-MS following the reaction of the supported alkylidene with styrene. Therefore the initial reaction is formulated as a metathetical exchange, eq 5.3.

$$(\equiv SiO)_2Cr{=}C(H)EMe_3 + PhCH{=}CH_2 \rightarrow (\equiv SiO)_2Cr{=}C(H)Ph + CH_2{=}C(H)EMe_3 \qquad (5.3)$$

E is C, Si

A decrease in the intensity of the ν(C-H) bands of the methyl groups of **4** is consistent with the reaction, Figure 5.2. The surface benzylidene reacts further with styrene, eq 5.4, to produce polystyrene.

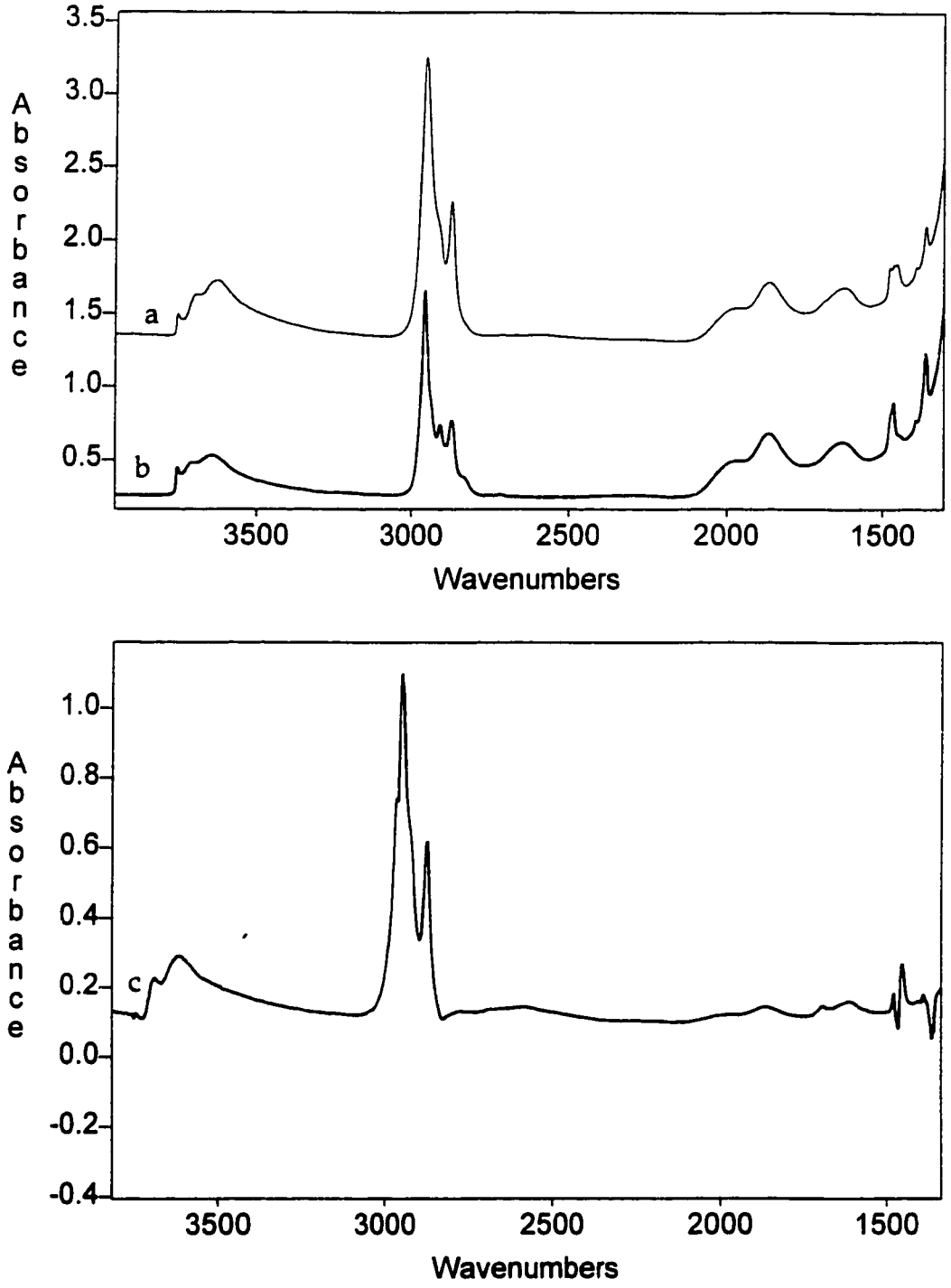

Figure 5.1 Transmission infrared spectra of (a) $(\equiv SiO)_2Cr{=}CHC(CH_3)_3$ at room temperature; (b) after addition of norbornene; (c) difference spectrum, obtained by subtraction of (a) from (b).

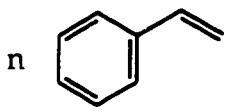

(5.4)

5.2.3 Towards Ethylene

At room temperature, there was no reaction between the supported alkylchromium(IV) species, **3a** or **3b**, and ethylene. However, if **3a** or **3b** were heated in the presence of 60 Torr ethylene at their respective thermolysis temperatures of 70°C and 150°C, or if **4a** or **4b** were exposed to 60 Torr ethylene at room temperature, we observed formation of polyethylene, as well as volatile olefins, eq 5.5.

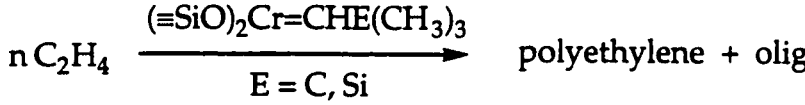

(5.5)

The color of the silica remained orange (**4a**) or pink (**4b**). After a few minutes, a white surface layer was visually detected, and was confirmed by FTIR to be polyethylene, Figure 5.3. The initially fragile silica pellet became rigid, confirming the formation of a hard polymer disk. The results from GC and GC-MS analysis of the gas phase after consumption of all the ethylene revealed no neohexene resulting from metathesis of **4a** with C_2H_4. However, we did detect traces of other olefins containing the neopentylidene ligand. Their origin will be discussed below.

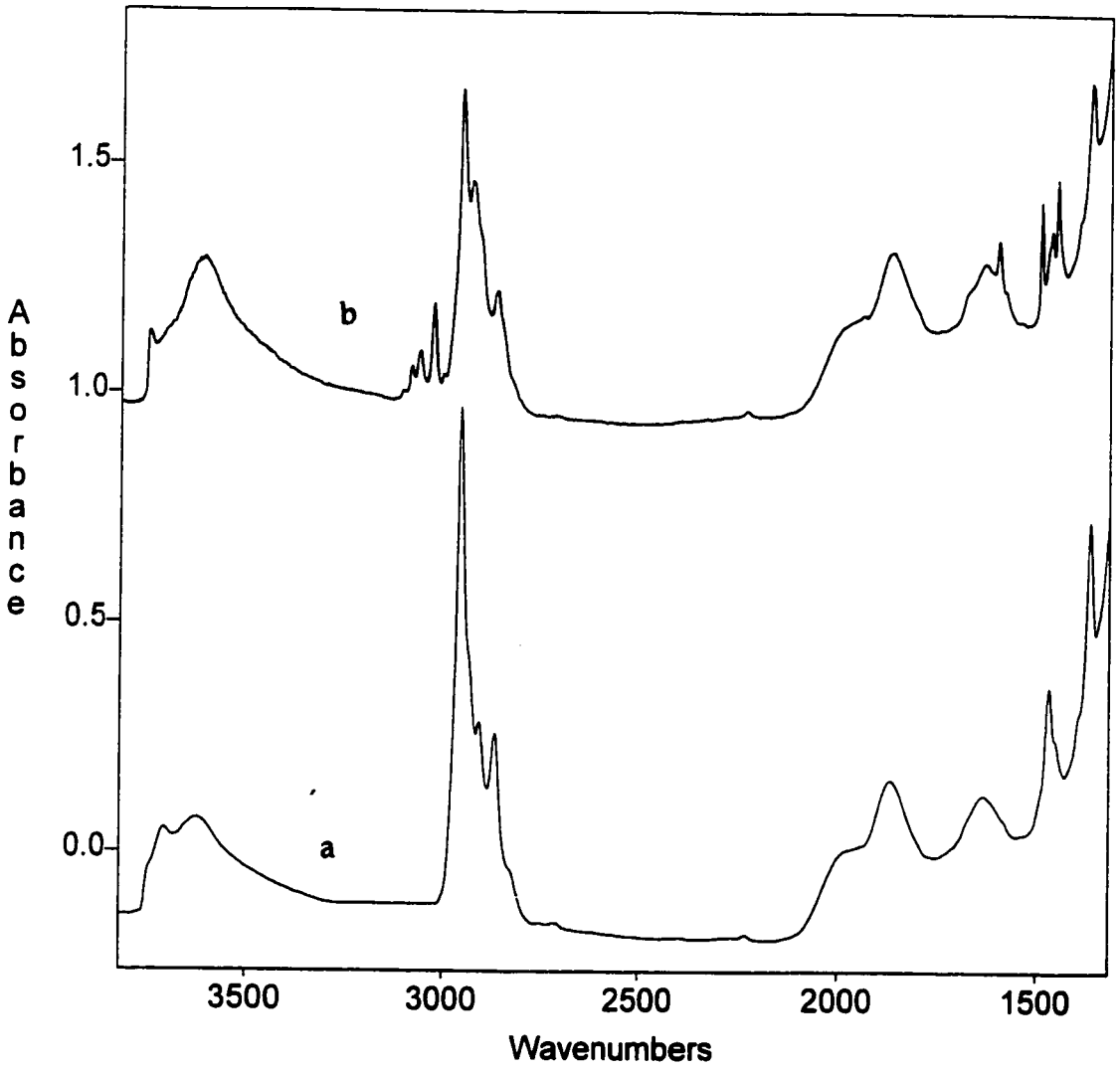

Figure 5.2 Transmission infrared spectra of (a) $(\equiv SiO)_2Cr{=}CHC(CH_3)_3$ and (b) after addition of styrene at room temperature.

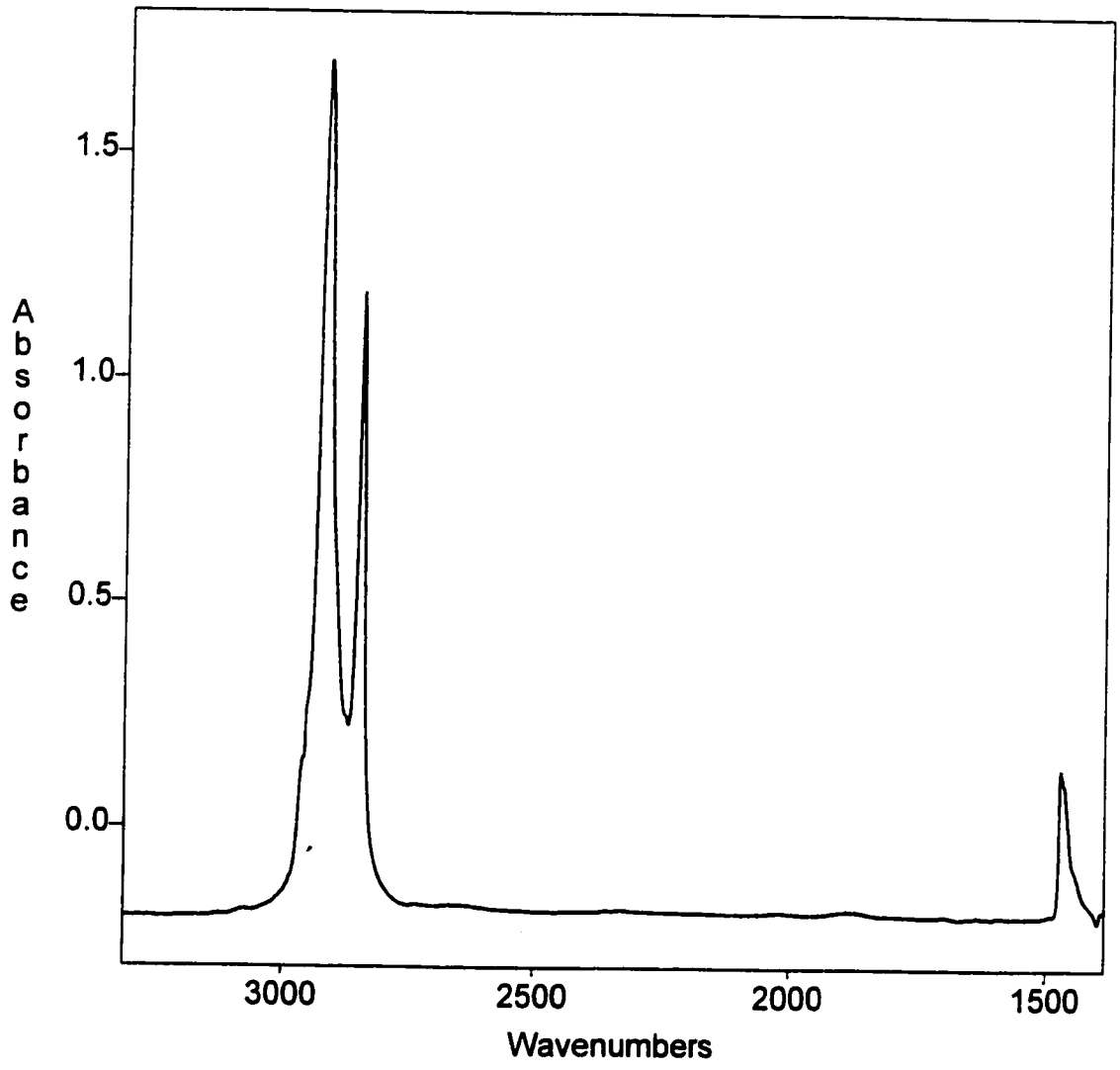

Figure 5.3 Transmission infrared difference spectrum obtained by subtraction of the spectrum of $(\equiv SiO)_2Cr{=}CHC(CH_3)_3$ from the spectrum of $(\equiv SiO)_2Cr{=}CHC(CH_3)_3$ after addition of ethylene at room temperature.

5.2.4 Towards Propylene

When **3a** was exposed to propylene at room temperature, no reaction was observed, but if 80 Torr propylene were added to a pellet of **4a** at room temperature, an immediate reaction took place resulting in the consumption of propylene and the formation of polypropylene. The reaction was initiated immediately, however almost 12 hours were required to completely polymerize the propylene. The silica pellet turned white and rigid upon consumption of all the propylene. "Hard" polymer is characteristic of isotactic polypropylene (see below). The appearance of the polypropylene was monitored by the appearance of characteristic hydrocarbon vibrations in the IR spectrum, Figure 5.4. In the gas phase, a variety of olefins were liberated during polymerization, eq 5.6.

$$n\,C_3H_6 \xrightarrow{(\equiv SiO)_2Cr{=}CHC(CH_3)_3} \text{polypropylene + oligomers} \qquad (5.6)$$

5.2.5 Towards 1-Hexene

When **3a** was exposed to 1-hexene vapor at room temperature, no reaction was observed, however when 1-hexene was added directly to the thermolyzed species **4a**, an immediate reaction took place resulting in the consumption of 1-hexene with simultaneous appearance of IR bands characteristic of poly-1-hexene, Figure 5.5. The color of the modified silica remained pink, however its aspect changed to that of a transparent glassy film, characteristic of a "soft" polymer. By GC and GC-MS, very small amounts of 2-hexene and 3-hexene were detected, indicating that the catalyst also causes isomerization of 1-hexene, eq 5.7.

(5.7)

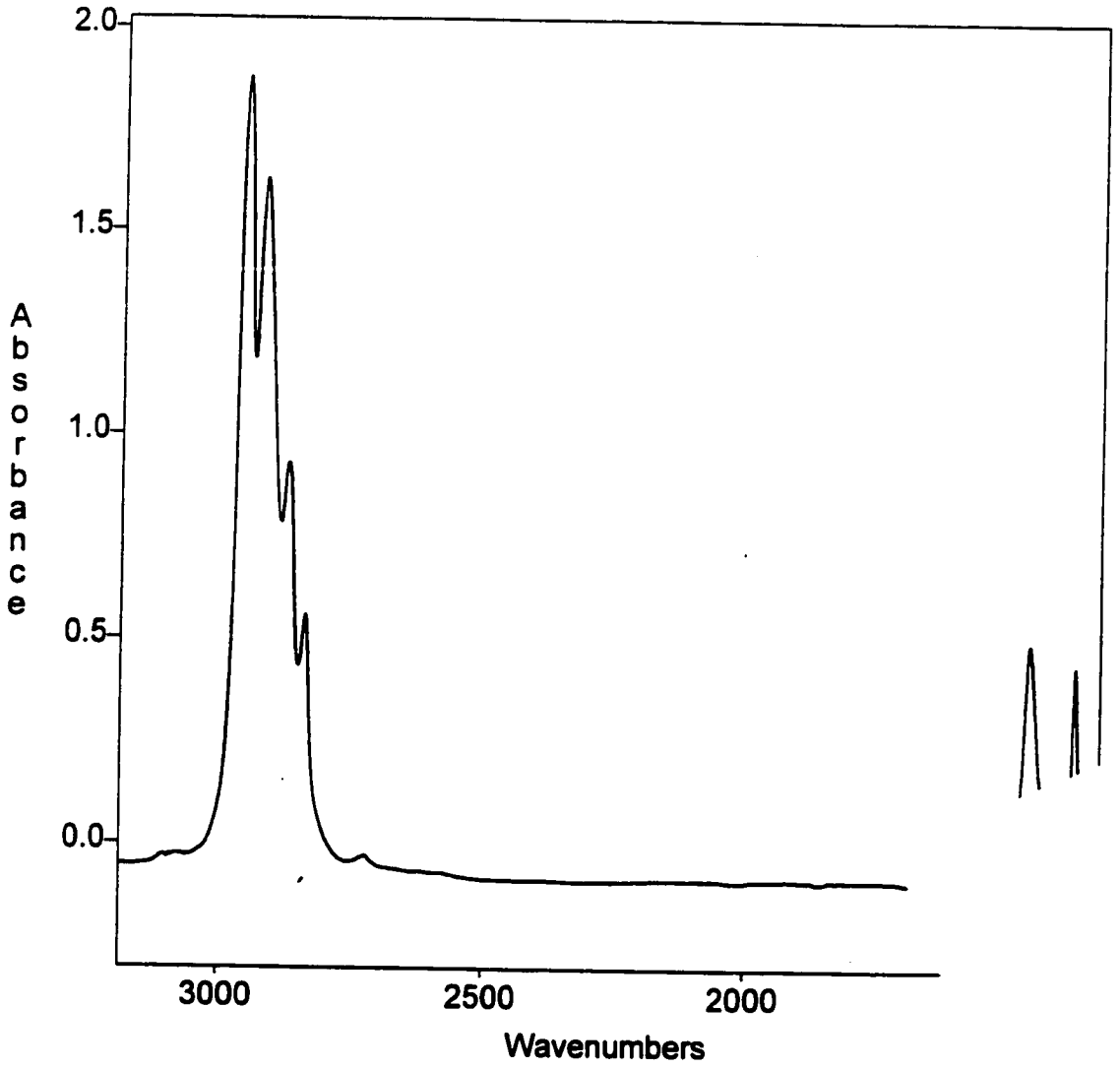

Figure 5.4 Transmission infrared difference spectrum obtained by subtraction of the spectrum of $(\equiv SiO)_2Cr{=}CHC(CH_3)_3$ from the spectrum of $(\equiv SiO)_2Cr{=}CHC(CH_3)_3$ after addition of propylene at room temperature.

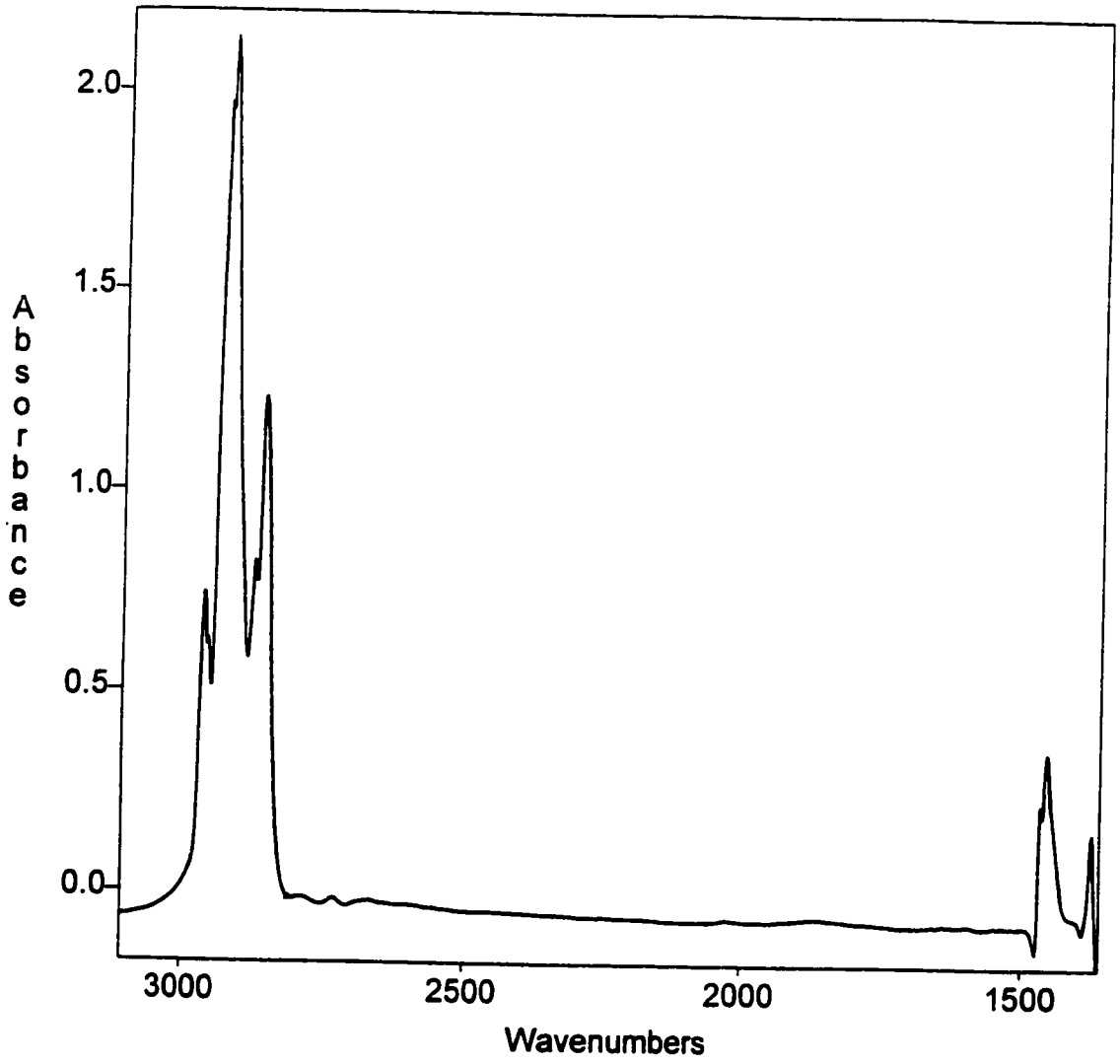

Figure 5.5 Transmission infrared difference spectrum obtained by subtraction of the spectrum of $(\equiv SiO)_2Cr{=}CHC(CH_3)_3$ from the spectrum of $(\equiv SiO)_2Cr{=}CHC(CH_3)_3$ after addition of 1-hexene at room temperature.

5.3 Number of Active Sites

Typical values for the number of active sites on heterogeneous chromium/silica catalysts range from 0.1 to 10% of total chromium, depending on the chromium loading,[12] the ethylene pressure[13] and the method[14,15] used for active site counting. The most widely used methods for the determination of the number of polymerization active sites belong to one of two categories.[14] Inhibition methods involve the addition of a known, substoichiometric amount of a catalyst poison which blocks chain growth. The number of propagation centers is calculated based on the threshold quantity of inhibitor which prevents polymerization completely. This method assumes that inactive sites do not bind the inhibitor. The second method is based on tagging polymer chains either during initiation or chain growth. The incorporation of a radioactive or other label into the growing chain is followed by quenching the polymerization and measuring the number of labels in the polymer. This method assumes that each active site generates a single polymer chain.

The number of propagation centers in chromium oxide catalysts has been determined by the inhibition method using water,[16] carbon tetrachloride[17] and diethylamine[9] as inhibitors. The number of active sites was found to be about 10%, 1%, and 17%, respectively, of the total Cr in the catalyst. Other workers[18] found that only 0.32% of Cr ions were active by inhibiting the polymerization with CO. Using a radio-labeled ^{14}CO tag, and after quenching the polymerization with methanol, Tait *et al.*[13] found that with 1 atm ethylene, only 3.7% of the Cr sites were active, whereas at 11 atm ethylene, the fraction of active chromium was 7.3%. Yermakov and Zakharov[17] determined the number of active centers at relatively low polymerization rates to be about 0.2% of total chromium using labeled methanol as a quenching agent. For comparison, the active site concentration in $TiCl_3$-based Ziegler-Natta catalysts is estimated to be 1%.[19] Marks

et al. [20] estimated that less than 10% of supported organothorium complexes were active in ethylene polymerization using labeled methanol as both tag and quencher.

We investigated what fraction of our supported chromium(IV) alkylidene complexes is active for ethylene polymerization. The number of actives sites in catalyst **4a** was determined by inhibition using O_2. The catalyst was poisoned at room temperature with very small, known amount of O_2, followed by addition of approx. 50 Torr ethylene to initiate polymerization. The experiments were performed at chromium loadings between 0.14 and 0.77 wt.% Cr.

We first established the stoichiometry of the reaction between O_2 and **4a**. 2.7 Torr O_2 was added to a reactor of volume 68 cm^3, containing 89 mg **4a** at 0.45 wt.% Cr loading (*i.e.*, 0.088 mmol Cr/g). After 1 min at room temperature, the reaction was deemed complete (as judged by the stability of the pressure reading on the capacitance manometer). The pressure of O_2 remaining in the reactor was 1.6 Torr. The amount of O_2 which reacted with **4a** was calculated, using the ideal gas law, to be 0.090 mmol per g of silica. Therefore we deduced that one mole of O_2 reacts with one mole of Cr(IV). No polymerization was observed when 45 Torr C_2H_4 were added to **4a** previously poisoned by this amount of O_2, Table 5.1, run 9.

Having established the stoichiometry of the reaction between O_2 and **4a**, the number of active sites in **4a** was determined using various substoichiometric amounts of O_2 as inhibitor. The poisoning of **4a** with O_2 was performed in the same manner as described for the stoichiometric reaction. First, **4a** was exposed to a known pressure of O_2, in the range 0.3 - 1 Torr. No residual pressure or gaseous product was detected when less than a stoichiometric amount of O_2 was added to **4a**. Then a relatively low pressure of ethylene (in the range 40 to 60 Torr) was introduced into the reactor. The occurrence of polymerization was

detected visually by the appearance of white polyethylene on the catalyst surface. The amount of Cr was determined by extraction from a catalyst sample which was not exposed to ethylene. The mass of catalyst, in experiments where polymerization was observed, was determined by subtracting the mass of polymer (calculated from the initial ethylene pressure) from the mass of the solid retrieved from the reactor.

The results are summarized in Table 5.1. The ratio O_2/Cr at which the polymerization is still observed gives the minimum fraction of active sites. Therefore at 50 Torr C_2H_4, the fraction of active sites is between 19 and 25% of total Cr.

After polymerization, the catalyst was exposed to excess $HCl_{(g)}$ and the amount of neopentane liberated was measured by GC-MS. This neopentane is taken to represent surface complexes which have not reacted with ethylene. Compared to the amount of neopentane released by protonolysis of **4a** with HCl (without exposure to C_2H_4, 1 NpH/Cr), the quantity of neopentane found after polymerization of 50 Torr C_2H_4 was 0.67/ Cr. The estimated fraction of active sites by this method is 0.33.

The fraction of active sites was also determined using a pressure of 250 Torr ethylene, Table 5.2. At this pressure, between 27 and 32% of the Cr sites are active.

All our experiments to date indicate that our silica-supported chromium(IV) alkylidenes are well-defined, homogeneous systems, since the bis(alkyl)chromium(IV) complexes undergo elimination of exactly one equivalent of alkane in a clean first-order process. Starting with a well-defined surface species where all the chromium sites have the same primary coordination sphere and the same oxidation state, we had expected that 100% of the Cr sites would be active towards ethylene. However, only ca. 20 and 30% were observed to be active

Table 5.1 Determination of the fraction of active sites in polymerization of ca. 50 Torr C_2H_4 by partial poisoning of $(\equiv SiO)_2Cr{=}CHC(CH_3)_3$ with O_2

run	%Cr	mmol Cr[a]	mmol O_2[a]	O_2/Cr[b]	ethylene pressure (Torr)	polymerization observed
1	0.14	0.028	0.006	0.02	48	yes
2	0.14	0.028	0.002	0.07	45	yes
3	0.45	0.088	0.011	0.125	48	yes
4	0.45	0.088	0.017	0.19	51	yes
5	0.45	0.088	0.023	0.26	55	no
6	0.45	0.088	0.044	0.50	53	no
7	0.45	0.088	0.067	0.76	54	no
8	0.14	0.028	0.024	0.86	44	no
9	0.45	0.088	0.149[c]	1.69	45	no

[a] All quantities are reported normalized per g of silica.

[b] Ratio of the amount of added O_2 to the amount of $(\equiv SiO)_2Cr{=}CHC(CH_3)_3$.

[c] Only 0.099 mmol O_2 were consumed.

Table 5.2 Determination of the fraction of active sites in polymerization of ca. 250 Torr C_2H_4 by partial poisoning of $(\equiv SiO)_2Cr{=}CHC(CH_3)_3$ with O_2

run	%Cr	mmol Cr[a]	mmol O_2[a]	O_2/Cr[b]	ethylene pressure (Torr)	polymerization observed
1	0.77	0.147	0.032	0.22	257	yes
2	0.52	0.098	0.002	0.27	254	yes
3	0.77	0.147	0.047	0.32	256	no
4	0.52	0.098	0.036	0.37	250	no
5	0.52	0.098	0.047	0.48	252	no

[a] All quantities are reported normalized per g of silica.

[b] Ratio of the amount of added O_2 to the amount of $(\equiv SiO)_2Cr{=}CH_2C(CH_3)_3$.

at pressures of 50 and 250 Torr C_2H_4, respectively. Nevertheless, upon increasing the ethylene pressure from 50 to 250 Torr, the fraction of active sites does increase by up to 50%. If we assume that the number of active sites is linearly dependent on the pressure, then under commercial operating conditions (400 psi, or 27 atm ethylene), we extrapolate that close to 100% of the chromium sites could be active. Unfortunately we cannot test this hypothesis, because our reactors are not designed for high pressure.

5.4 Active Oxidation State

The oxidation states of the molecular precursor $Cr(CH_2C(CH_3)_3)_4$,[21] of the surface complex $(\equiv SiO)_2Cr(CH_2C(CH_3)_3)_2$[22] and of the surface alkylidene complex $(\equiv SiO)_2Cr{=}CH_2C(CH_3)_3$[10] have all been shown to be (IV). Due to the possibility of

redox processes during initiation, it seemed important to verify that the oxidation state remains (IV) upon ethylene polymerization. The magnetic susceptibility of the solid after reaction with 50 Torr C_2H_4 exhibits simple Curie-Weiss behavior above 2 K, Figure 5.6. The data was used to calculate an effective magnetic moment of 2.65 B.M. per Cr atom, consistent with retention of mononuclear and non-interacting d^2 Cr(IV) surface organometallic complexes during polymerization. Thus, the average oxidation state of Cr does not change during its reaction with ethylene. Also, subsequent addition of ethylene reinitiates polymerization. We feel confident in concluding that Cr(IV) must be the oxidation state active in ethylene polymerization.

5.5 Kinetics of Ethylene Polymerization

The kinetics of the reaction of $(\equiv SiO)_2Cr{=}CHC(CH_3)_3$, **4a**, with ethylene were investigated. A powdered sample of **4a** was exposed to 78 Torr ethylene in a reactor equipped for *in situ* IR spectroscopy immersed in a 21°C water bath. The IR spectrum of the gas phase was recorded at timed intervals. By integration of the IR intensity in the ν(CH) region (which decreases as ethylene is consumed), we inferred the progress of the polymerization reaction occurring on the surface. A typical data set is shown in Figure 5.7a. The data is fit to a single exponential function, showing the reaction to be pseudo-first-order with $k_{app} = (0.149 \pm 0.008)$ min^{-1} in the presence of 0.76 mg Cr supported on 166 mg SiO_2 (*i.e.*, 0.45 wt.% Cr).

The dependence of the apparent rate constant on the quantity of Cr was evaluated by varying the amount and loading of catalyst. The results are shown in Figure 5.7 and tabulated in Table 5.3. At 21°C, k_{app} is directly proportional to the amount of chromium present, Figure 5.8. This relationship is valid regardless of Cr loading (in the range 0.45 - 0.78 wt.%), implying that the fraction of active sites

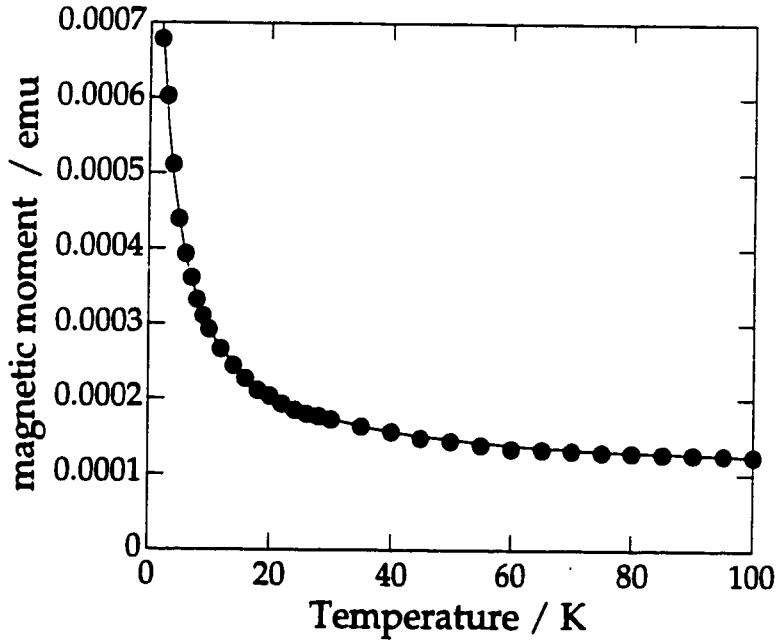

I = C' / (T + θ)		
	Value	Error
C'	0.0023042	0.0000047
θ	1.8497	0.0949

Figure 5.6 Temperature-dependent magnetic susceptibility of 10 mg $(\equiv SiO)_2Cr{=}CHC(CH_3)_3$ (0.5 wt.% Cr) after polymerization of ethylene. The solid line is the curve fit to the Curie-Weiss law.

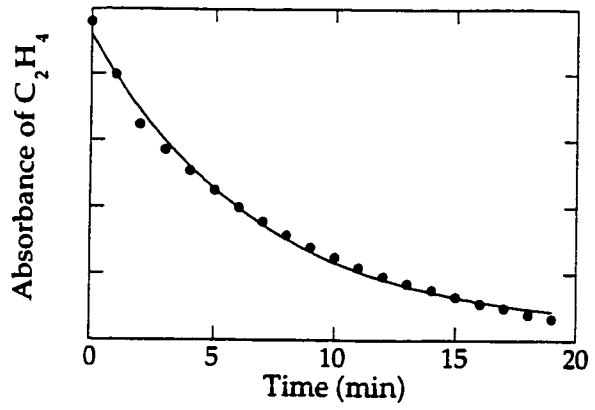

$A = A_\infty + (A_0 - A_\infty)\exp(-k_{app}t)$		
	Value	Error
A_∞	21.630	0.809
A_0	66.132	0.719
k_{app}	0.149	0.008

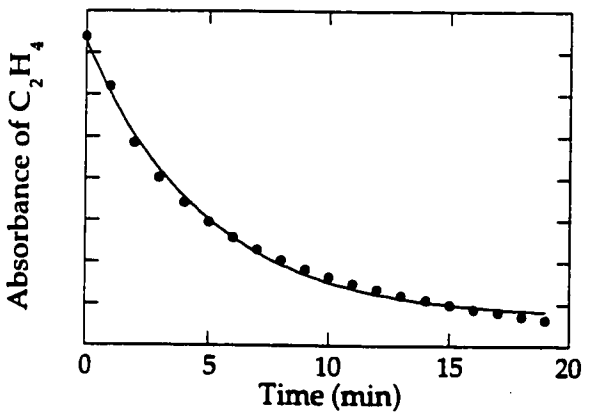

$A = A_\infty + (A_0 - A_\infty)\exp(-k_{app}t)$		
	Value	Error
A_∞	5.311	0.259
A_0	45.497	0.544
k_{app}	0.277	0.008

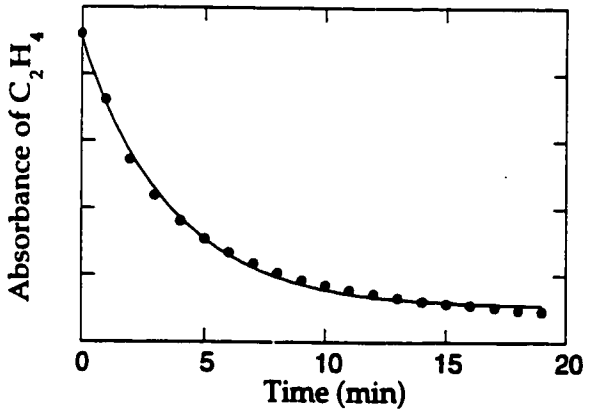

$A = A_\infty + (A_0 - A_\infty)\exp(-k_{app}t)$		
	Value	Error
A_∞	5.311	0.259
A_0	45.497	0.544
k_{app}	0.277	0.008

Figure 5.7 Time-resolved consumption of ethylene during polymerization with $(\equiv SiO)_2Cr{=}CHC(CH_3)_3$, **4a**, at 21°C. (a) 0.45 (b) 0.62 and (c) 0.78 wt.% Cr loading. Solid curves are three-parameter single exponential fits to the first-order integrated kinetic rate equation.

Table 5.3 Apparent first-order rate constants for C_2H_4 polymerization catalyzed by $(SiO)_2Cr=CHCMe_3$

Temperature / °C	wt.% Cr	m_{Cr} / mg	k_{app} / min^{-1} [a]
21	0.99	0.687	0.139 ± 0.006
21	0.45	0.756	0.149 ± 0.008
21[c]	0.45	1.035	0.211 ± 0.006
21	0.62	1.048	0.208 ± 0.008
21	0.78	1.303	0.277 ± 0.008
48	0.35	0.343	0.257 ± 0.003
48	0.62	0.572	0.425 ± 0.002
48	0.78	0.741	0.566 ± 0.002
80	0.35	0.202	0.377 ± 0.002
80	0.62	0.281	0.542 ± 0.003
80	0.78	0.468	0.925 ± 0.004

[a] Errors are from non-linear squares least fit to a single exponential function.

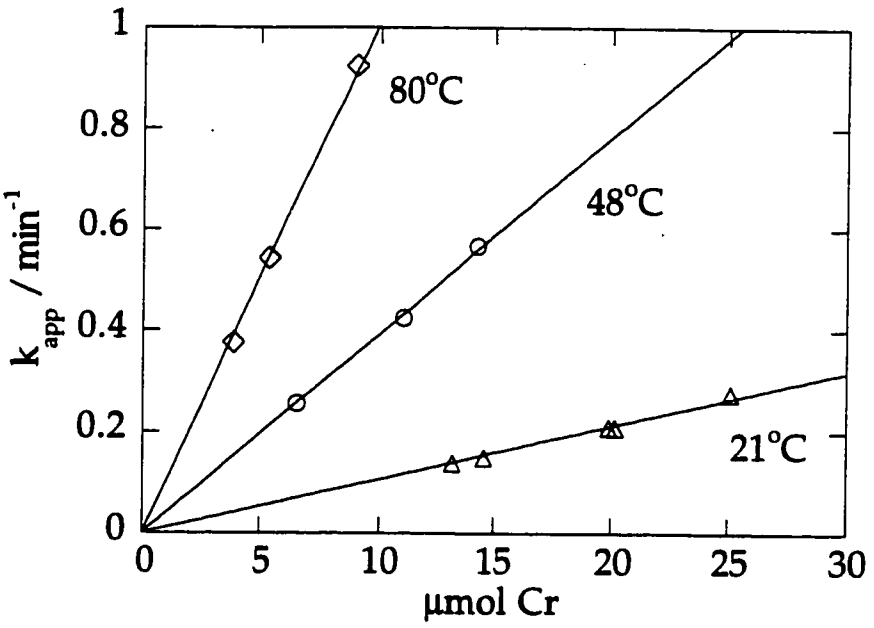

Figure 5.8 Dependence of the observed rate constant k_{app} for ethylene polymerization catalyzed by $(SiO)_2Cr{=}CHCMe_3$ on the quantity of Cr, in the range 0.35 - 0.78 wt.% Cr loading.

is constant in this loading range. Therefore the rate law for polymerization of ethylene at low pressure can be expressed as equation 5.8:

$$-\frac{dP_{C_2H_4}}{dt} = k' m_{Cr} P_{C_2H_4} = k_{app} P_{C_2H_4} \qquad (5.8)$$

where $P_{C_2H_4}$ is the ethylene pressure and m_{Cr} is the mass of Cr present. The second-order rate constant k′ for polymerization of ethylene by $(\equiv SiO)_2Cr{=}CHC(CH_3)_3$ is the slope of the plot of k_{app} as a function of the amount of chromium. At 21°C, k′ = (0.0107 ± 0.0003) min^{-1} $(\mu mol\,Cr)^{-1}$.

It is reasonable to assume that the ethylene-catalyst adduct is a preequilibrium (non-observable) intermediate in the polymerization mechanism, eq 5.9.[23]

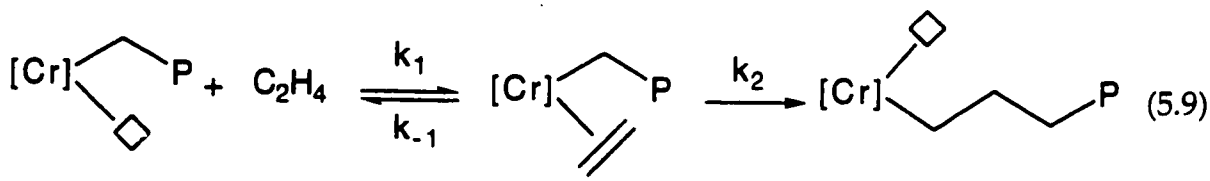

(5.9)

Such a mechanism is expected to show saturation kinetics, according to the Michaelis-Menton equation,[24] eq 5.10.

$$-\frac{dP_{C_2H_4}}{dt} = \frac{\frac{k_1}{k_{-1}} k_2 m_{Cr} P_{C_2H_4}}{1 + \frac{k_1}{k_{-1}} P_{C_2H_4}} \qquad (5.10)$$

If the binding constant for ethylene is small and the ethylene pressure is low, the dominator simplifies to unity, and the rate law is consistent with eq 5.8, where k′ is a composite, eq 5.11.

$$k' = \frac{k_1}{k_{-1}} k_2 \tag{5.11}$$

Note that since the fraction of active sites at low ethylene pressure is ca. 0.2, the real value of k′ is approx. five times higher than that derived from the slope in Figure 5.8. Also, it should be noted that if the active sites vary in their ethylene binding constants and/or rates of ethylene insertion, then our measured value for k′ is a weighted average, eq 5.12:

$$k' = \sum_i n_i k'_i \tag{5.12}$$

where n_i is the mole fraction of site i with rate constant k'_i.

Similar kinetics experiments were performed at temperatures of 48 and 80°C, Figures 5.9 and 5.10, respectively. In all cases, the consumption of ethylene was pseudo-first-order. The apparent rate constants are tabulated in Table 5.3. The observed second-order rate constants were extracted from the dependence of k_{app} on m_{Cr} at each temperature, Figure 5.8. The observed second-order rate constants for ethylene polymerization are summarized in Table 5.4.

The observed rate constants in Table 5.4 were used to construct an Eyring plot, Figure 5.11. The plot is linear. Its slope and intercept yield the observed activation enthalpy and entropy: $\Delta H^{\ddagger}_{obs} = (8 \pm 1)$ kcal/mol and $\Delta S^{\ddagger}_{obs} = (-23 \pm 2)$ cal K^{-1} mol^{-1}.

For the composite rate constant k′, the form of the temperature dependence is given by eq 5.13.[24]

$$k' = \frac{k_1}{k_{-1}} k_2 = \left(\frac{RT}{Nh}\right) \exp\left(\frac{\Delta S_2^{\ddagger}}{R}\right) \exp\left(-\frac{\Delta H_2^{\ddagger}}{RT}\right) \times \exp\left(\frac{\Delta S_1^{\circ}}{T}\right) \exp\left(-\frac{\Delta H_1^{\circ}}{RT}\right) \tag{5.13}$$

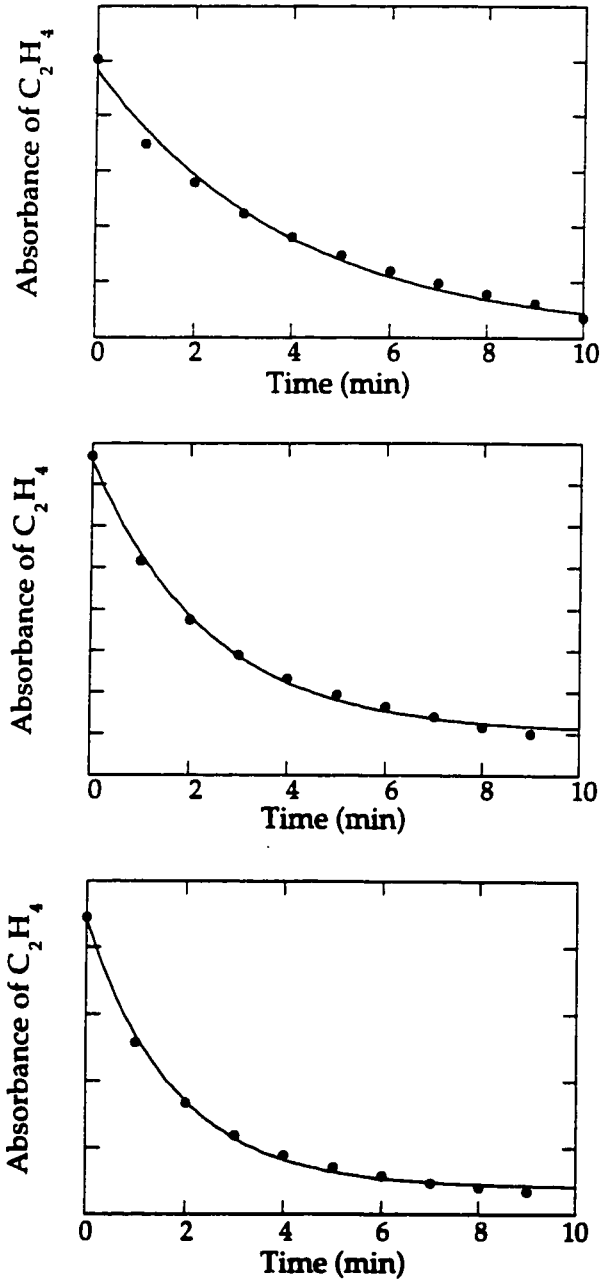

$A = A_\infty + (A_0 - A_\infty)\exp(-k_{app}t)$		
	Value	Error
A_∞	20.789	1.619
A_0	68.230	1.397
k_{app}	0.257	0.003

$A = A_\infty + (A_0 - A_\infty)\exp(-k_{app}t)$		
	Value	Error
A_∞	20.255	1.006
A_0	85.798	1.244
k_{app}	0.425	0.002

$A = A_\infty + (A_0 - A_\infty)\exp(-k_{app}t)$		
	Value	Error
A_∞	14.009	0.404
A_0	54.101	0.682
k_{app}	0.566	0.002

Figure 5.9 Time-resolved consumption of ethylene during polymerization with $(\equiv SiO)_2Cr{=}CHC(CH_3)_3$, **4a**, at 48°C. (a) 0.35 (b) 0.62 and (c) 0.78 wt.% Cr loading. Solid curves are three-parameter single exponential fits to the first-order integrated kinetic rate equation.

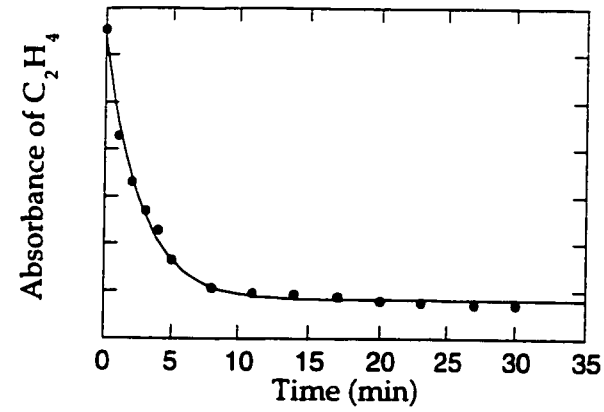

$A = A_{\infty}+(A_0-A_{\infty})\exp(-k_{app}t)$		
	Value	Error
A_{∞}	38.080	0.590
A_0	93.545	1.411
k_{app}	0.377	0.002

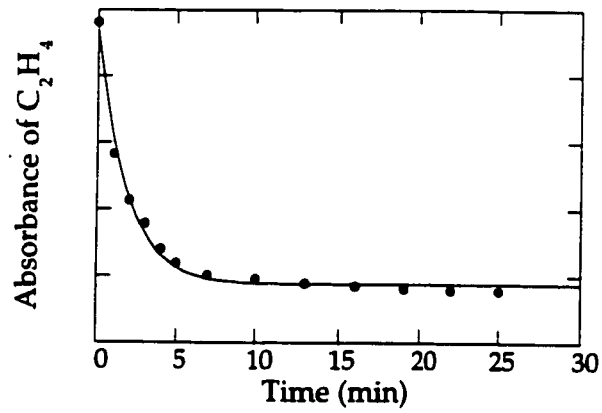

$A = A_{\infty}+(A_0-A_{\infty})\exp(-k_{app}t)$		
	Value	Error
A_{∞}	17.484	0.940
A_0	93.924	2.336
k_{app}	0.542	0.003

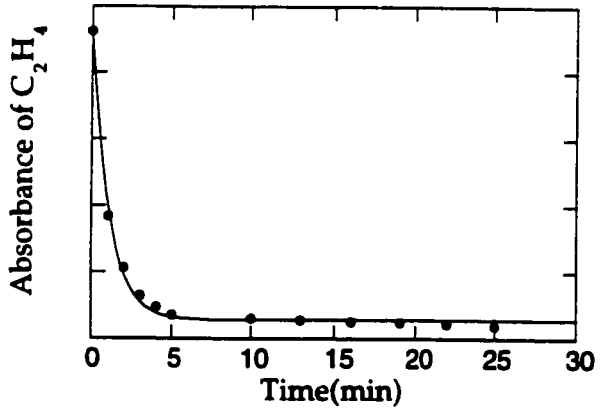

$A = A_{\infty}+(A_0-A_{\infty})\exp(-k_{app}t)$		
	Value	Error
A_{∞}	12.788	0.317
A_0	55.909	0.866
k_{app}	0.925	0.004

Figure 5.10 Time-resolved consumption of ethylene during polymerization with $(\equiv SiO)_2Cr{=}CHC(CH_3)_3$, **4a**, at 80°C. (a) 0.35 (b) 0.62 and (c) 0.78 wt.% Cr loading. Solid curves are three-parameter single exponential fits to the first-order integrated kinetic rate equation.

Table 5.4 Observed second-order rate constants for C_2H_4 polymerization catalyzed by $(SiO)_2Cr=CHCMe_3$ at different temperatures

Temperature / °C	k′ / min^{-1} (μmol Cr)$^{-1}$
21	0.0107 ± 0.0003
48	0.0392 ± 0.0004
80	0.1010 ± 0.0002

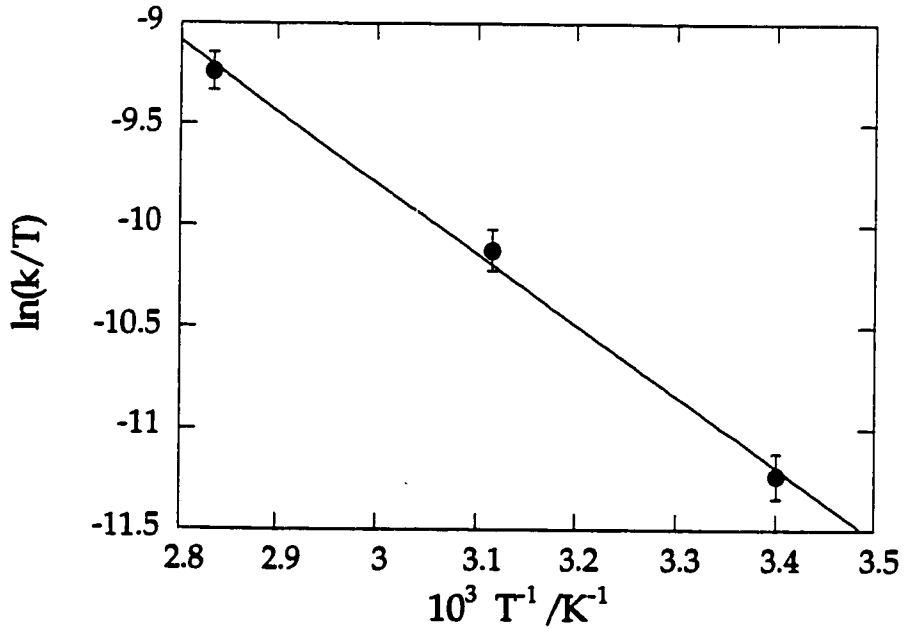

Figure 5.11 Eyring plot of temperature-dependence of rate constants for ethylene polymerization catalyzed by $(SiO)_2Cr=CHCMe_3$.

where R is the gas constant, N is Avogadro's number, h is Planck's constant, $\Delta H_2^{\ddagger}$ and $\Delta S_2^{\ddagger}$ are the activation parameters for migratory insertion and ΔH_1^{o} and ΔS_1^{o} are the enthalpy and entropy of ethylene binding, respectively. Combining terms, we obtain the expression in eq 5.14.[24]

$$\ln\left(\frac{k'}{T}\right) = \ln\left(\frac{R}{Nh}\right) + \left(\frac{\Delta S_1^{\circ} + \Delta S_2^{\ddagger}}{R}\right) - \left(\frac{\Delta H_1^{\circ} + \Delta H_2^{\ddagger}}{RT}\right) \tag{5.14}$$

The Eyring plot $\ln\left(\frac{k'}{T}\right)$ *vs* T^{-1}, should be linear with an apparent activation enthalpy corresponding to the sum of ΔH_1° and $\Delta H_2^{\ddagger}$. Since ΔH_1° is surely negative, the observed activation enthalpy, 8 kcal/mol, is smaller than the value of $\Delta H_2^{\ddagger}$ for the rate-limiting step of migratory insertion.[24] Activation energies for ethylene insertion into metal-σ-alkyl bonds in model Cr(IV) systems have been calculated to range from 6 to 11 kcal/mol.[25] Measured activation enthalpies from 14.7 to 16.0 kcal/mol were reported for olefin insertion into a Nb-H bond.[23]

Previously described kinetics for ethylene polymerization by chromium oxide on silica have also been reported to be first order with respect to ethylene; the measured activation energies ranged from 7.5 kcal/mol[17] to 12.7 kcal/mol.[26] For polymerization by organometallic complexes such as $CrCp_2$[27]and $Cr(allyl)_3$[28] supported on silica, the reported activation energies were 10.1 kcal/mol and 5 kcal/mol, respectively. Values reported for activation energies of ethylene polymerization by $TiCl_3$-based Ziegler-Natta catalysts range from 10 to 14 kcal/mol.[29-31] (An activation enthalpy is larger than an activation energy by ca. 0.6 kcal/mol at room temperature.)[24] Assuming that our experimental 8 kcal/mol enthalpic barrier reflects the requirements of the polymerization propagation steps, the catalyst **4a** appears to react with ethylene by a mechanism comparable to other heterogeneous catalysts. The insertion of ethylene is as facile for Cr(IV) as it

is for Ziegler-Natta systems and for other Cr-based heterogeneous catalysts, including those whose *initial* oxidation states are not IV.

Activation entropies for olefin insertion into a Nb-H bond in solution ranged from -6.7 to -11.2 cal/K·mol.[23] The more negative value of $\Delta S^{\ddagger}_{obs}$, -23 eu, in our system probably reflects a greater loss of entropy upon binding gas-phase ethylene to the catalyst (as compared to dissolved ethylene). In addition, it is possible that an α-agostic interaction, which facilitates alkyl migration, also renders the transition state more rigid, Scheme 5.6.[7]

Scheme 5.6 Transition state for ethylene insertion, showing α-agostic interaction

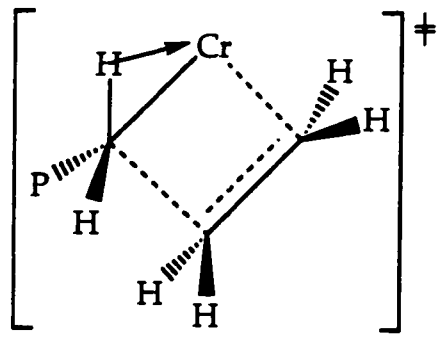

5.6 Kinetics of C_2D_4 Polymerization

Evidence for an α-agostic interaction was sought through kinetics studies of the polymerization of C_2D_4. The apparent rate constants for polymerization of C_2D_4 by **4a** at 21°C, with different Cr loadings (0.52 - 0.99 wt.%), were obtained in a similar fashion to those of C_2H_4, but with integration of the absorbance in the ν(C-D) region. The polymerization of C_2D_4 is pseudo-first-order, Figure 5.12. The rate constants k_{app} are given in Table 5.5. The observed second-order rate constant for polymerization of C_2D_4 at 21°C is (0.0082 ± 0.0002) min^{-1} (μmol Cr)$^{-1}$, from the slope of Figure 5.13. The same Figure shows the data for C_2H_4 at 21°C.

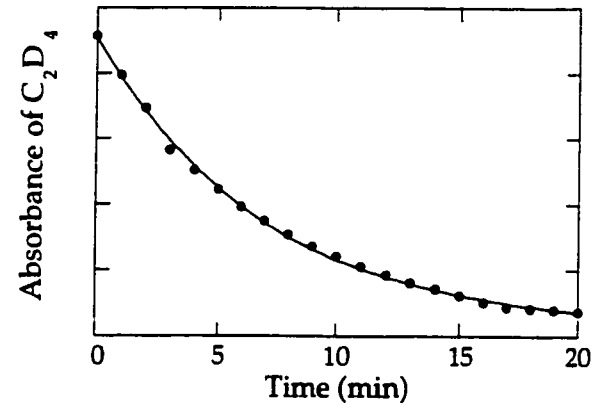

$A = A_\infty + (A_0 - A_\infty)\exp(-k_{app}t)$		
	Value	Error
A_∞	11.258	0.406
A_0	55.355	0.378
k_{app}	0.147	0.004

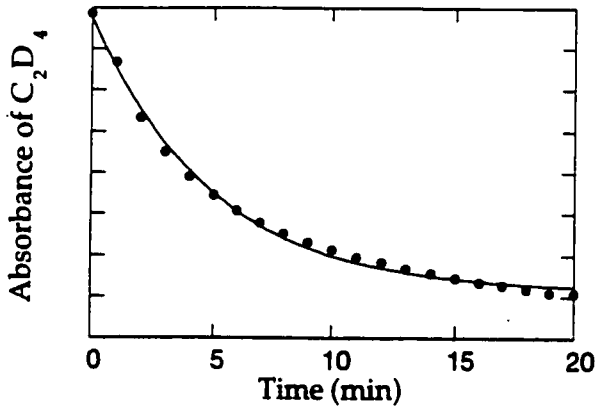

$A = A_\infty + (A_0 - A_\infty)\exp(-k_{app}t)$		
	Value	Error
A_∞	11.269	0.650
A_0	77.494	1.021
k_{app}	0.205	0.008

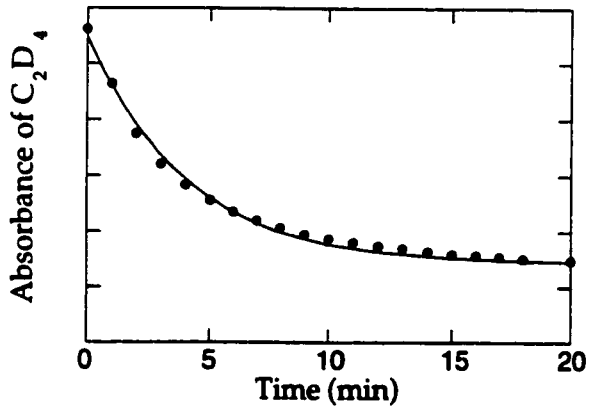

$A = A_\infty + (A_0 - A_\infty)\exp(-k_{app}t)$		
	Value	Error
A_∞	14.303	0.322
A_0	54.944	0.830
k_{app}	0.249	0.010

Figure 5.12 Time-resolved consumption of D-labeled ethylene during polymerization with $(\equiv SiO)_2Cr{=}CHC(CH_3)_3$, **4a**, at 21°C. (a) 0.52 (b) 0.77 and (c) 0.99 wt.% Cr loading. Solid curves are three-parameter single exponential fits to the first-order integrated kinetic rate equation.

Table 5.5 Apparent first-order rate constants for C_2D_4 polymerization catalyzed by $(SiO)_2Cr=CHCMe_3$ at 21°C

wt.% Cr	m_{Cr} / mg	k_{app} / min^{-1} [a]
0.52	0.294	0.146 ± 0.004
0.77	0.420	0.204 ± 0.008
0.99	0.547	0.249 ± 0.010

[a] Errors are from non-linear least squares fit to a single exponential function.

Polymerization of C_2D_4 is slower than C_2H_4 by a factor $k'_H/k'_D = (0.0107/0.0082) = 1.25$.

There are two sources of kinetic isotope effects in migratory insertion reactions. The primary isotope effect arises from deuteration of the growing polymer chain. The α-agostic interaction is stronger for M←H-C_α compared to M←D-C_α.[7] The extent of α-agostic interaction in turn affects the degree of C-C bond formation in the transition state.[7] The theoretical kinetic isotope effect for this kind of interaction has been calculated to be 1.25.[32] A secondary kinetic isotope effect arises from D-substitution on the coordinated olefin. During the migratory insertion reaction, rehybridization of both olefinic carbons from sp^2 to sp^3 must occur. However, deuteration is expected to give rise to an inverse kinetic isotope effect. Values on the order of 0.8 - 0.9 have been suggested for insertion of C_2D_4 into Cp^*_2NbD.[23] An observed kinetic isotope effect of 1.1 was reported by Bercaw[23] for migratory insertion in permethylniobocene(III) olefin hydride complexes $[Cp^*_2Nb(CH_2=CHR)(H)]$ with R = H, Me, Ar. This was interpreted as a composite effect arising from moderation of the primary kinetic isotope effect by the (inverse) rehybridization effect. In our Cr system, the

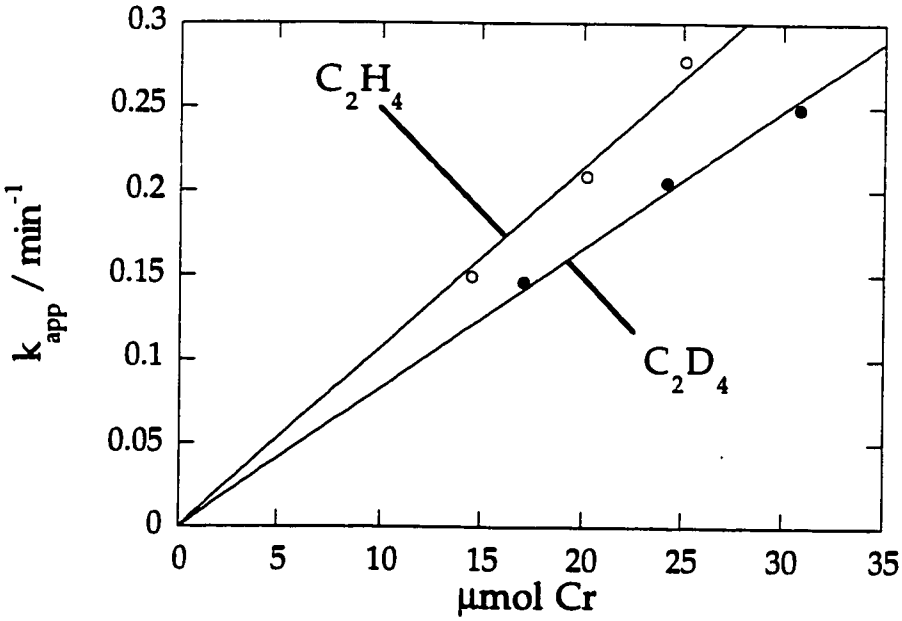

Figure 5.13 Dependence of the observed rate constant k_{app} at 21°C for polymerization of ethylene (open circles), and D-labeled ethylene (filled circles) catalyzed by $(SiO)_2Cr{=}CHCMe_3$ on the quantity of Cr. Cr loadings range from 0.35-0.99 wt.%.

observed kinetic isotope effect of 1.25 is consistent with a significant ground-state α-agostic interaction and an early transition state, in which little rehybridization has occurred.

5.7 Polymerization Induced by $(\equiv SiO)_2Cr(CH_2C(CH_3)_3)_2$

The silica-supported bis(neopentyl)chromium(IV) $(\equiv SiO)_2Cr(CH_2C(CH_3)_3)_2$, **3a**, when was heated to 69°C in the presence of ethylene, shows polymerization after an induction period. The kinetic curve is shown in Figure 5.14. The induction period corresponds to the transformation of **3a** into **4a**, which must occur before polymerization can be initiated. It was not possible to extract rate constants from Figure 5.14, because temperature increased from 20°C to 69°C over the course of the reaction.

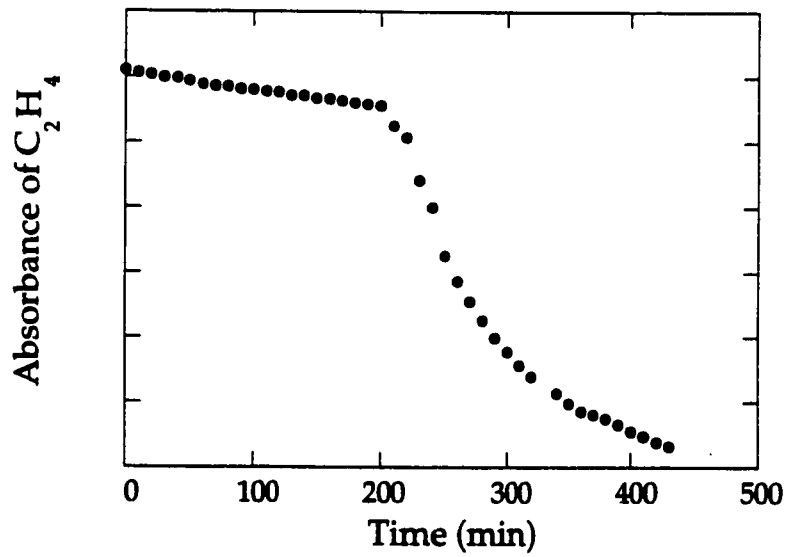

Figure 5.14 Time-resolved consumption of C_2H_4 during polymerization starting with $(\equiv SiO)_2Cr(CH_2C(CH_3)_3)_2$, **3a**, at 0.89 wt.% Cr loading. The temperature at time = 0 was 20°C and increased to 69°C over the course of the reaction.

5.8 Catalyst Recycling

The "livingness" of ethylene polymerization catalyzed by **4a** was studied. A slightly modified procedure was developed for the repeated introduction of the same pressure of ethylene into the reactor. The IR cell was connected to a vacuum line through which C_2H_4 was transferred. C_2H_4 first trapped in a side-arm tube (1.5 cm O.D., 15 cm length) immersed in liquid N_2. The breakseal containing the catalyst was broken then the cold trap was removed. The kinetics were recorded as described previously.

The reactions were carried out at 21°C with a Cr loading of 0.99 wt.%. Three sequential additions of 67, 69 and 65 Torr C_2H_4 gave polymerizations which all exhibited pseudo-first-order behavior. The kinetic curves are shown in Figure 5.15. The apparent rate constants are listed in Table 5.6. The apparent rate constants are virtually identical in subsequent polymerizations. The catalyst therefore is not deactivated during polymerization.

Table 5.6 Apparent first-order rate constants for C_2H_4 polymerization catalyzed by $(SiO)_2Cr{=}CHCMe_3$ in successive additions of C_2H_4 at 21°C

	P (C_2H_4) Torr	k_{app}/ min^{-1} [a]
first addition of ethylene	67	0.139 ± 0.006
second addition of ethylene	69	0.136 ± 0.005
third addition of ethylene	65	0.131 ± 0.004

[a] Errors are from non-linear least squares fit to a single exponential function

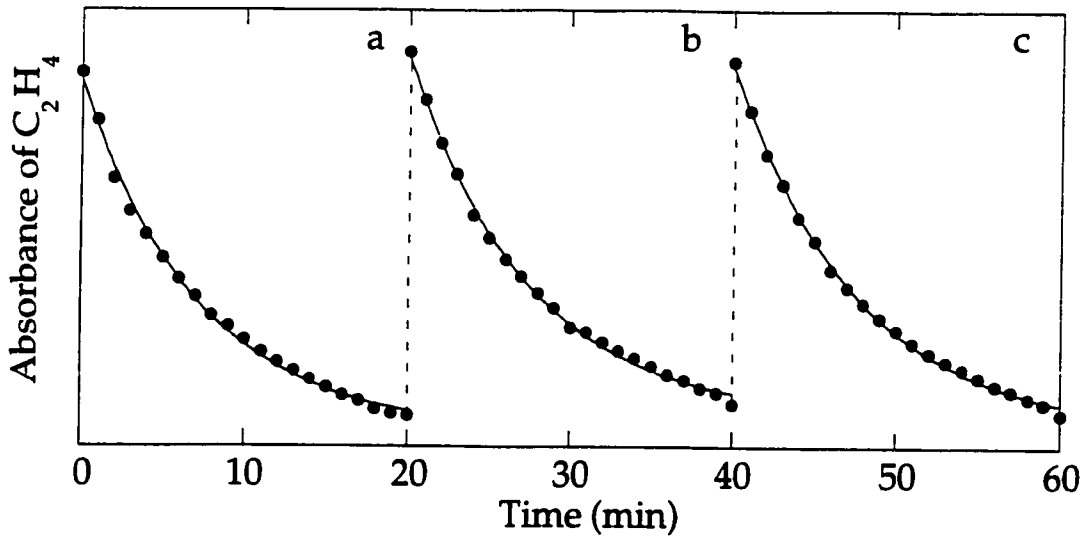

First addition $A = A_{\infty}+(A_0 - A_{\infty})\exp(-k_{app}t)$		
	Value	Error
A_{∞}	26.826	0.627
A_0	70.986	0.540
k_{app}	0.139	0.006

Second addition $A = A_{\infty}+(A_0 - A_{\infty})\exp(-k_{app}t)$		
	Value	Error
A_{∞}	28.707	0.490
A_0	74.239	0.403
k_{app}	0.136	0.005

Third addition $A = A_{\infty}+(A_0 - A_{\infty})\exp(-k_{app}t)$		
	Value	Error
A_{∞}	27.001	0.416
A_0	72.959	0.320
k_{app}	0.131	0.004

Figure 5.15 Time-resolved consumption of ethylene in three subsequent addition (a) 67, (b) 69 and (c) 65 Torr ethylene. The catalyst was $(\equiv SiO)_2Cr{=}CHC(CH_3)_3$, **4a**, with 0.99 wt.% Cr loading at 21°C. Solid curves are three-parameter single exponential fits to the first-order integrated kinetic rate equation.

5.9 Effect of H_2

H_2 is known to moderate the molecular weights of polymers produced by supported Cr catalysts. CrO_3/SiO_2 catalysts are thought to respond to H_2 by increasing the rate of chain transfer, although the response is much smaller than that of the Cp_2Cr/SiO_2 catalyst. Therefore the effect of H_2 on the kinetics of ethylene polymerization by **4a** was studied. The reactions were carried out at 21°C with different Cr loadings ranging from 0.62 - 0.99 wt.% Cr. A mixture of 10 Torr H_2 and 47 Torr C_2H_4 was added to a sample of **4a** and the decrease in intensity in the gas phase IR spectrum of C_2H_4 was monitored as a function of time. The polymerization exhibited pseudo-first-order behavior, Figure 5.16. The apparent rate constants are listed in Table 5.7. The magnitude of k_{app} shows a linear dependence on the mass of Cr present, Figure 5.17. The observed second-order rate constant at 21°C is (0.0303 ± 0.0008) min^{-1} (μmol Cr)$^{-1}$.

Table 5.7 Apparent first-order rate constants for C_2H_4 polymerization catalyzed by $(SiO)_2Cr{=}CHCMe_3$ in the presence of H_2 at 21°C

wt.% Cr	m_{Cr} / mg	k_{app} / min^{-1} [a]
0.56	0.479	0.307 ± 0.002
0.81	0.739	0.407 ± 0.002
1.27	1.10	0.639 ± 0.003

[a] Errors are from non-linear least squares fit to a single exponential function

The presence of a small amount of H_2 (0.18 mol%) therefore causes the rate of polymerization of ethylene to accelerate by a factor of 3.2. An increase in the termination rate alone will not explain this result. One possible reason for the

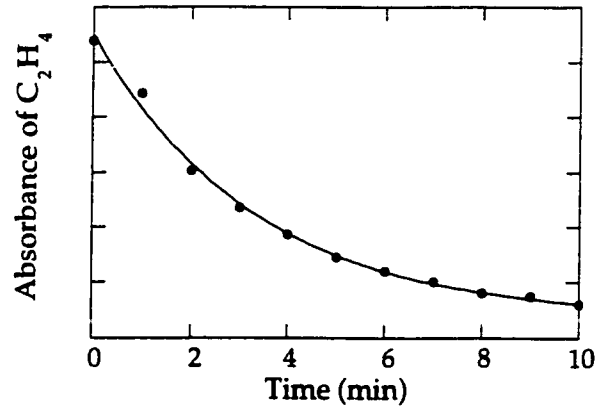

$A = A_\infty + (A_0 - A_\infty)\exp(-k_{app}t)$		
	Value	Error
A_∞	3.781	1.176
A_0	54.988	1.089
k_{app}	0.307	0.002

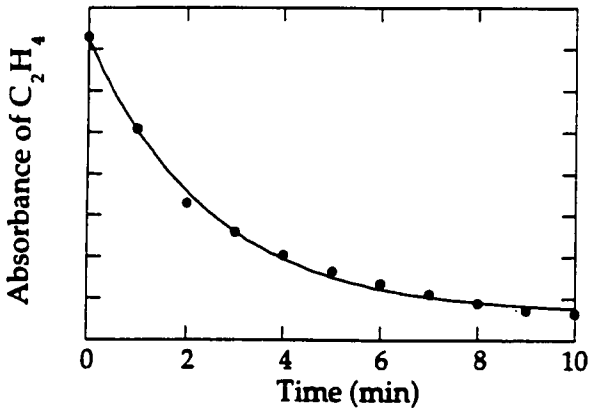

$A = A_\infty + (A_0 - A_\infty)\exp(-k_{app}t)$		
	Value	Error
A_∞	16.398	0.953
A_0	82.45	1.305
k_{app}	0.407	0.002

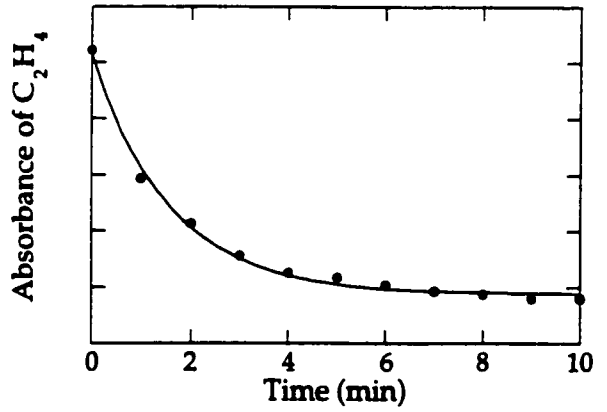

$A = A_\infty + (A_0 - A_\infty)\exp(-k_{app}t)$		
	Value	Error
A_∞	28.749	0.469
A_0	71.507	0.980
k_{app}	0.639	0.003

Figure 5.16 Time-resolved consumption of C_2H_4 during polymerization in the presence of H_2 with $(\equiv SiO)_2Cr{=}CHC(CH_3)_3$, **4a**, at 21°C. (a) 0.56 (b) 0.89 and (c) 1.27 wt.% Cr loading. Solid curves are three-parameter single exponential fits to the first-order integrated kinetic rate equation.

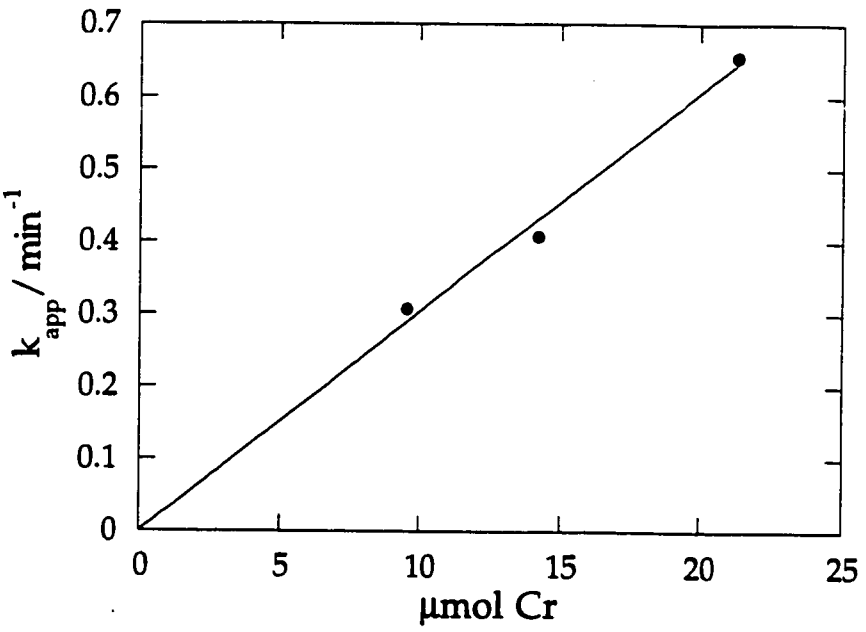

Figure 5.17 Dependence of k_{app} for ethylene polymerization catalyzed by $(SiO)_2Cr{=}CHCMe_3$ in the presence of H_2 at 21°C on the quantity of Cr.

increased activity of **4a** in the presence of H_2 is the reactivation of "non-participating" propagation sites by hydrogenating some of their ligands (for example, π-allyl) and replacing them with Cr-H.[33] We will discuss the effect of H_2 on the polymer molecular weight later in this chapter.

5.10 Kinetics of 1-Hexene Polymerization

In order to increase the amount of chain branching in commercial polyethylene, 1-hexene is often added to the ethylene/H_2 mixture. Therefore the kinetics of polymerization of 1-hexene catalyzed by **4a** were studied, using the procedure described for C_2H_4. The reactions were followed at 21°C with Cr loadings in the range of 0.52 - 0.99 wt.%. Approx. 0.5 mL 1-hexene was introduced via a breakseal, giving a pressure of ca. 200 Torr 1-hexene in the reactor. The consumption of 1-hexene is pseudo-first-order, Figure 5.18. The apparent rate constants are shown in Table 5.8. They depend linearly on the amount of Cr, Figure 5.19. The observed second-order rate constant at 21°C is (0.0023 ± 0.0001) min^{-1} μmol $(Cr)^{-1}$.

Table 5.8 Apparent first-order rate constants for 1-hexene polymerization catalyzed by $(SiO)_2Cr{=}CHCMe_3$ at 21°C

Wt.% Cr	m_{Cr} / mg	k_{app} / min^{-1} [a]
0.52	0.268	0.0118 ± 0.0004
0.77	0.390	0.0162 ± 0.0003
0.81	0.516	0.0211 ± 0.0010
0.99	0.761	0.0333 ± 0.0009

[a] Errors are from non-linear least squares fit to a single exponential function.

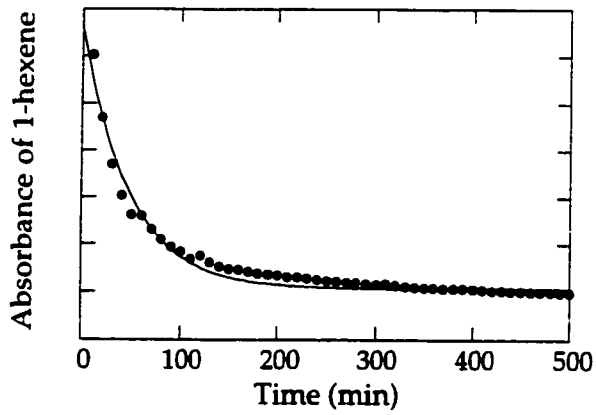

a

$A = A_{\infty}+(A_0-A_{\infty})\exp(-k_{app}t)$		
	Value	Error
A_{∞}	1.356	0.007
A_0	2.493	0.023
k_{app}	0.0118	0.0004

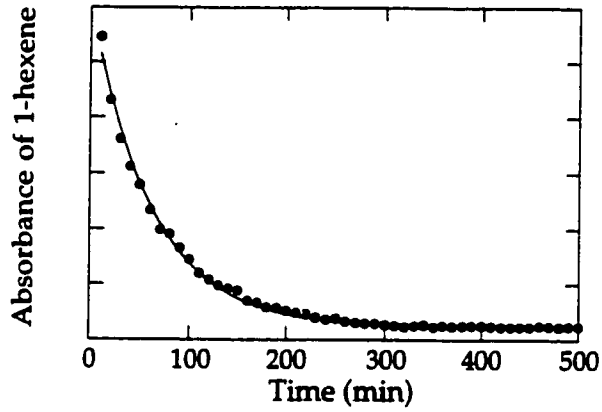

b

$A = A_{\infty}+(A_0-A_{\infty})\exp(-k_{app}t)$		
	Value	Error
A_{∞}	10.532	0.001
A_0	10.59	0.001
k_{app}	0.0162	0.0003

Figure 5.18 Time-resolved consumption of 1-hexene during polymerization with $(\equiv SiO)_2Cr{=}CHC(CH_3)_3$, **4a**, at 21°C. (a) 0.52 (b) 0.77 wt.% Cr loading. Solid curves are three-parameter single exponential fits to the first-order integrated kinetic rate equation.

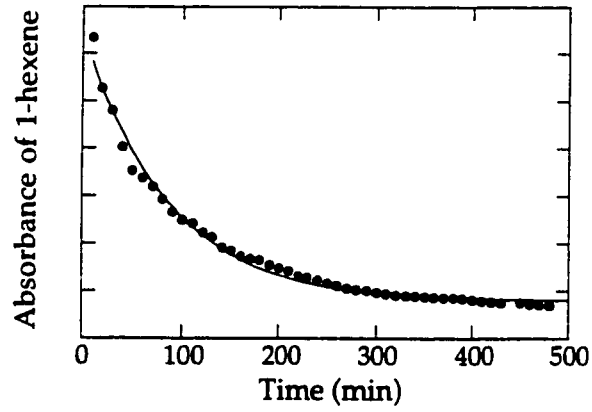

a

$A = A_{\infty} + (A_0 - A_{\infty})\exp(-k_{app}t)$		
	Value	Error
A_{∞}	0.107	0.002
A_0	0.663	0.018
k_{app}	0.0211	0.0010

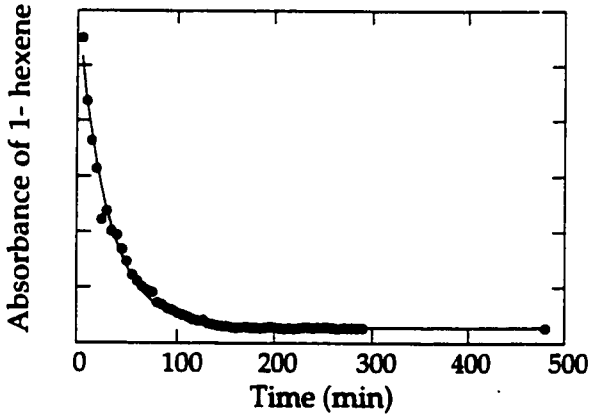

b

$A = A_{\infty} + (A_0 - A_{\infty})\exp(-k_{app}t)$		
	Value	Error
A_{∞}	8.033	0.001
A_0	8.090	0.001
k_{app}	0.0330	0.0010

Figure 5.18 (continued); Time-resolved consumption of 1-hexene during polymerization with $(\equiv SiO)_2Cr{=}CHC(CH_3)_3$, **4a**, at 21°C. (c) 0.81 (d) 0.99 wt.% Cr loading. Solid curves are three-parameter single exponential fits to the first-order integrated kinetic rate equation.

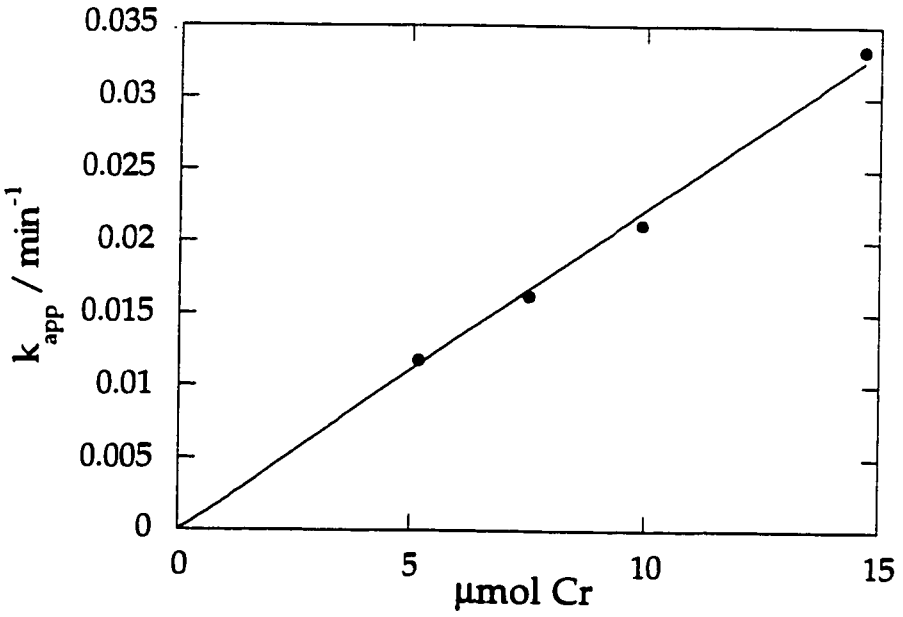

Figure 5.19 Dependence of the observed rate constant k_{app} for 1-hexene polymerization catalyzed by $(SiO)_2Cr{=}CHCMe_3$ on the quantity of Cr, in the range 0.52 - 0.99 wt.% Cr loading.

The rate of homopolymerization of 1-hexene is therefore 4.8 times slower than the homopolymerization of ethylene. However, since the catalyst generates ethylene oligomers (1-butene, 1-hexene, etc, see below) during homopolymerization, their subsequent incorporation into the growing chain is a plausible explanation for the low levels of chain branching observed in high density polyethylene. The binding constants for substituted olefins are usually less than for ethylene. For example, propylene binds 150 times weaker than ethylene to Cp_2^*NbH.[23] However propylene inserts 342 times faster than ethylene into Nb-H.[23] The slower polymerization of 1-hexene catalyzed by **4a** relative to ethylene therefore reflects weaker substrate binding, which is partially compensated by faster migratory insertion.

5.11 Kinetics of Ethylene-1-Hexene Copolymerization

In order to determine the selectivity for insertion of 1-hexene versus ethylene, the kinetics of copolymerization of a C_2D_4/1-hexene mixture were undertaken. The kinetics were performed with 50 Torr C_2D_4 and 200 Torr 1-hexene at 21°C and Cr loadings of 0.58 - 0.85 wt.%. The consumption of 1-hexene was determined by monitoring the change in absorbance in the ν(C-H) region of the gas phase IR spectrum, while the consumption of C_2D_4 was simultaneously analyzed by monitoring the loss of ν(C-D) intensity. Both are pseudo-first-order, as shown by the exponential curves in Figures 5.20 and 5.21. Both sets of values of k_{app} are proportional to the amount of Cr, Table 5.9.

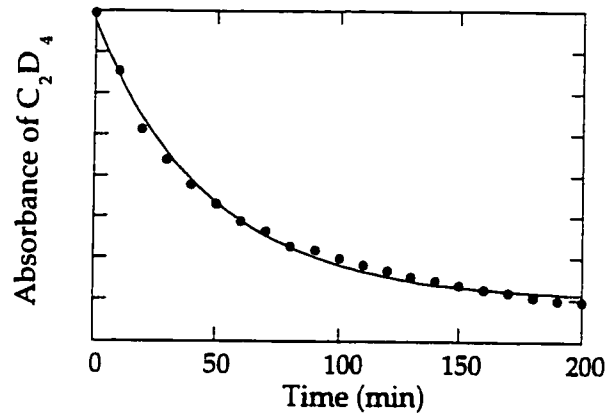

$A = A_\infty + (A_0 - A_\infty)\exp(-k_{app}t)$		
	Value	Error
A_∞	10.025	0.656
A_0	77.441	1.180
k_{app}	0.0211	0.0009

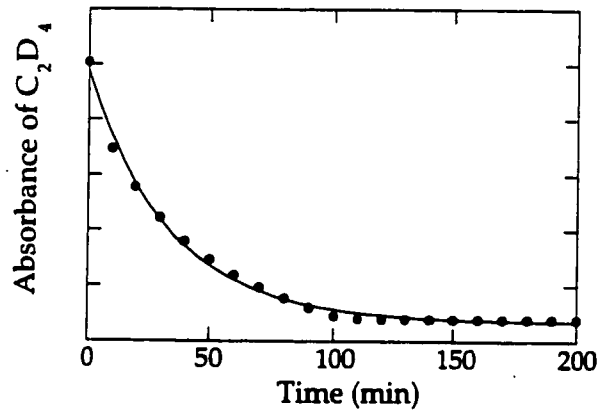

$A = A_\infty + (A_0 - A_\infty)\exp(-k_{app}t)$		
	Value	Error
A_∞	23.452	0.297
A_0	68.882	0.756
k_{app}	0.0299	0.0010

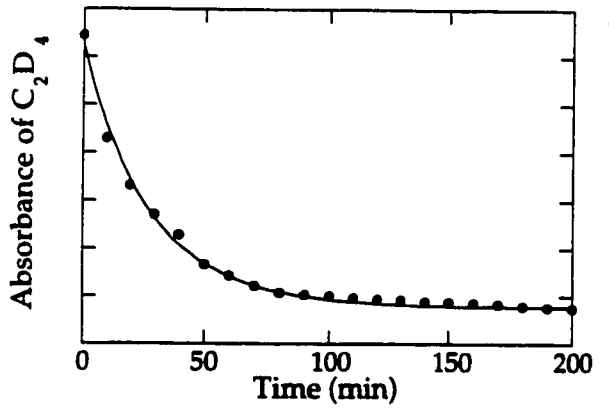

$A = A_\infty + (A_0 - A_\infty)\exp(-k_{app}t)$		
	Value	Error
A_∞	37.684	0.220
A_0	92.428	0.882
k_{app}	0.0359	0.0011

Figure 5.20 Time-resolved consumption of C_2D_4 during copolymerization with 1-hexene with $(\equiv SiO)_2Cr{=}CHC(CH_3)_3$, **4a**, at 21°C. (a) 0.56 (b) 0.89 and (c) 0.99 wt.% Cr loadings. Solid curves are three-parameter single exponential fits to the first-order integrated kinetic rate equation.

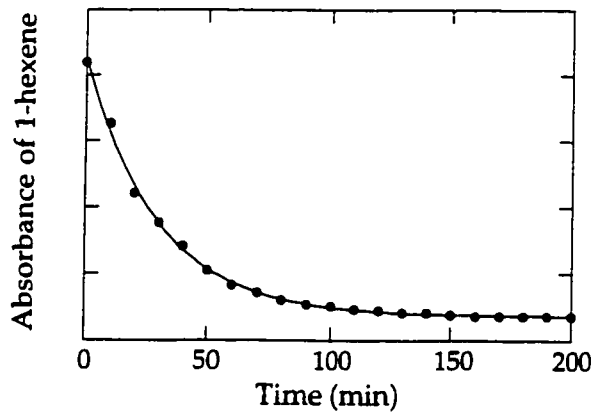

$A = A_\infty + (A_0 - A_\infty)\exp(-k_{app}t)$		
	Value	Error
A_∞	0.0718	0.003
A_0	0.850	0.009
k_{app}	0.0340	0.0008

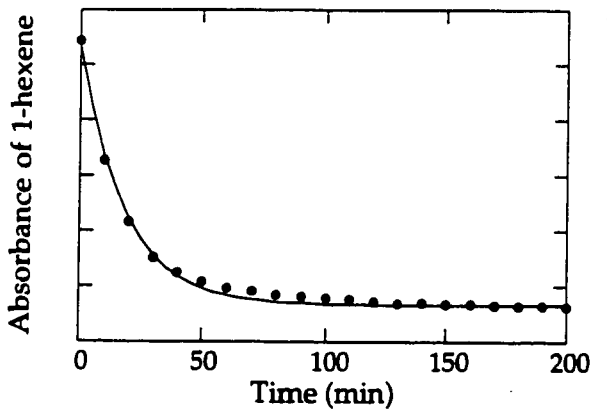

$A = A_\infty + (A_0 - A_\infty)\exp(-k_{app}t)$		
	Value	Error
A_∞	2.732	0.0032
A_0	3.672	0.015
k_{app}	0.0548	0.0017

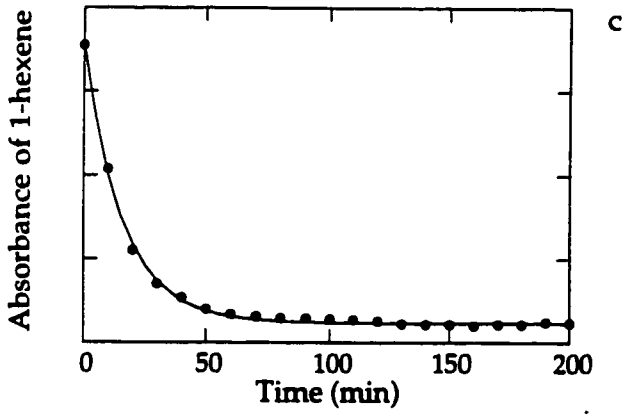

$A = A_\infty + (A_0 - A_\infty)\exp(-k_{app}t)$		
	Value	Error
A_∞	3.362	0.001
A_0	3.528	0.002
k_{app}	0.0626	0.0013

Figure 5.21 Time-resolved consumption of 1-hexene during copolymerization with C_2D_4 with $(\equiv SiO)_2Cr{=}CHC(CH_3)_3$, **4a**, at 21°C. (a) 0.56 (b) 0.89 and (c) 0.99 wt.% Cr loadings. Solid curves are three-parameter single exponential fits to the first-order integrated kinetic rate equation.

Table 5.9 Apparent first-order rate constants for copolymerization of C_2D_4/1-hexene mixtures, catalyzed by $(SiO)_2Cr{=}CHCMe_3$ at 21°C

wt.% Cr	m_{Cr} / mg	k_{app} / min^{-1} [a]	
		C_2D_4	1-hexene
0.56	0.494	0.0211 ± 0.0009	0.0340 ± 0.0008
0.89	0.813	0.0299 ± 0.0010	0.0548 ± 0.0017
0.99	0.965	0.0359 ± 0.0011	0.0626 ± 0.0013

[a] Errors are from non-linear least squares fit to a single exponential function.

The monomers ethylene and 1-hexene compete for the open coordination site on the supported Cr catalyst. The copolymerization mechanism is shown in eqs 5.15 and 5.16.

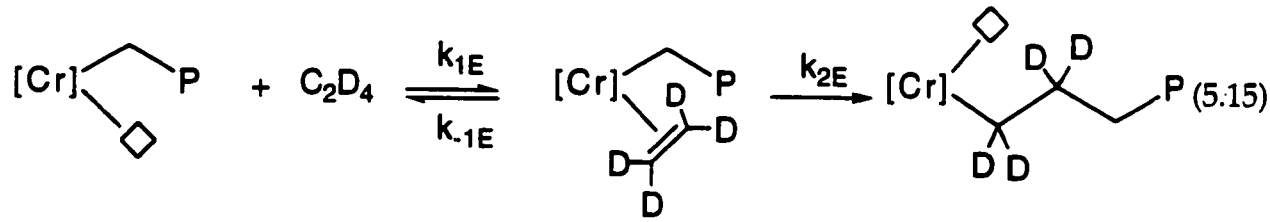

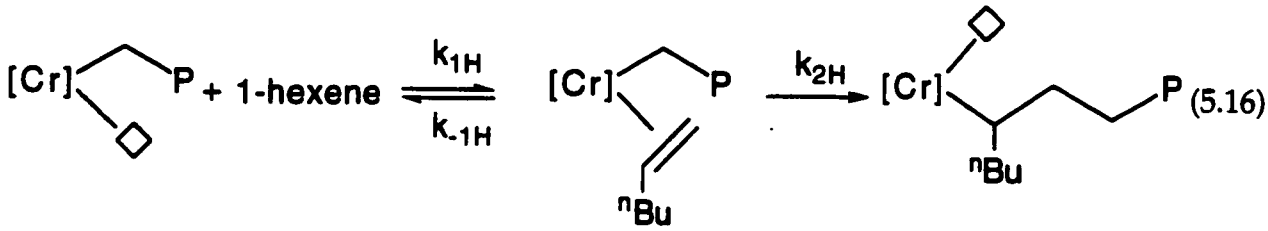

The Michaelis-Menton rate laws for competing substrates are shown in eqs 5.17 and 5.18.

$$-\frac{dP_{C_2D_4}}{dt} = \frac{\frac{k_{1E}}{k_{-1E}} k_{2E} m_{Cr} P_{C_2D_4}}{1 + \frac{k_{1E}}{k_{-1E}} P_{C_2D_4}} \tag{5.17}$$

$$-\frac{dP_{1-hexene}}{dt} = \frac{\frac{k_{1H}}{k_{-1H}} k_{2H} m_{Cr} P_{1-hexene}}{1 + \frac{k_{1H}}{k_{-1H}} P_{1-hexene}} \tag{5.18}$$

As the value of each denominator approaches 1, the kinetics will be first order with respect to each substrate, eqs 5.19 and 5.20. Since this behavior is indeed observed, the olefin binding constants must be small, such that each substrate behaves as if the other is absent.

$$\frac{dP_{C_2H_4}}{dt} = \frac{k_{1E}}{k_{-1E}} k_{2E} m_{Cr} P_{C_2H_4} = k_{Eapp} P_{C_2H_4} \tag{5.19}$$

$$\frac{dP_{1-hexene}}{dt} = \frac{k_{1H}}{k_{-1H}} k_{2H} m_{Cr} P_{1-hexene} = k_{Happ} P_{1-hexene} \tag{5.20}$$

The observed second-order rate constants k_E' for C_2D_4 and k_H' for 1-hexene are derived from plots of k_{app} versus m_{Cr}, Figure 5.22. The constants are tabulated in Table 5.10. C_2D_4 is polymerized four times slower in the presence of 1-hexene than in its absence, whereas the polymerization of 1-hexene is 50% faster in the presence of C_2D_4 relative to the homopolymerization rate.

According to the rate laws in eqs 5.19 and 5.20, the simultaneous presence of ethylene and 1-hexene cannot affect the forward and reverse rate constants for

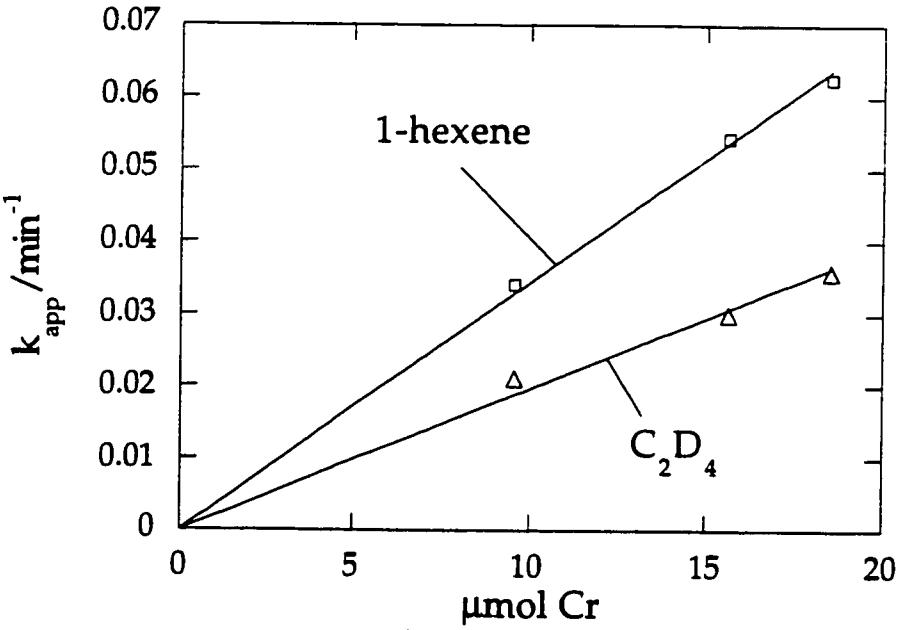

Figure 5.22 Dependence of the observed rate constant k_{app} for copolymerization of C_2D_4 and 1-hexene catalyzed by $(SiO)_2Cr{=}CHCMe_3$ on the quantity of Cr, in the range 0.56 - 0.99 wt % Cr loading.

Table 5.10 Summary of composite second-order rate constants for olefin polymerization catalyzed by $(SiO)_2Cr=CHCMe_3$ at 21°C

olefin	k′ / min^{-1} (μmol Cr)$^{-1}$
C_2H_4	0.0107 ± 0.0003
C_2D_4	0.0082 ± 0.0002
$C_2H_4 + H_2$	0.0303 ± 0.0008
1-hexene	0.0023 ± 0.0001
C_2D_4 + 1-hexene	C_2D_4: 0.0020 ± 0.0001 1-hexene: 0.0034 ± 0.0001

olefin binding. The observed difference in k′ values for homopolymerization and copolymerization must therefore be due to variations in the insertion rate constants, k_2. When deuterated ethylene inserts into a polymer chain containing butyl branches, its insertion rate constant will be slower (due to steric hindrance) compared to homopolymerization. For 1-hexene, the inverse phenomenon is observed, because the copolymer chain will have fewer butyl branches than poly(1-hexene). Therefore the rate constant for 1-hexene insertion increases. Under our chosen conditions ($P_{1\text{-hexene}} > P_{C_2H_4}$), the consumption of 1-hexene is actually faster than the consumption of C_2D_4. All the polymerization rate constants measured in this project are summarized in Table 5.10.

A plot of all the composite rate constants k_{app} at 21°C vs m_{Cr} is shown in Figure 5.23. It is obvious from the Figure that the fastest polymerization is that of ethylene in the presence of H_2 while the slowest is that of ethylene in the presence of 1-hexene.

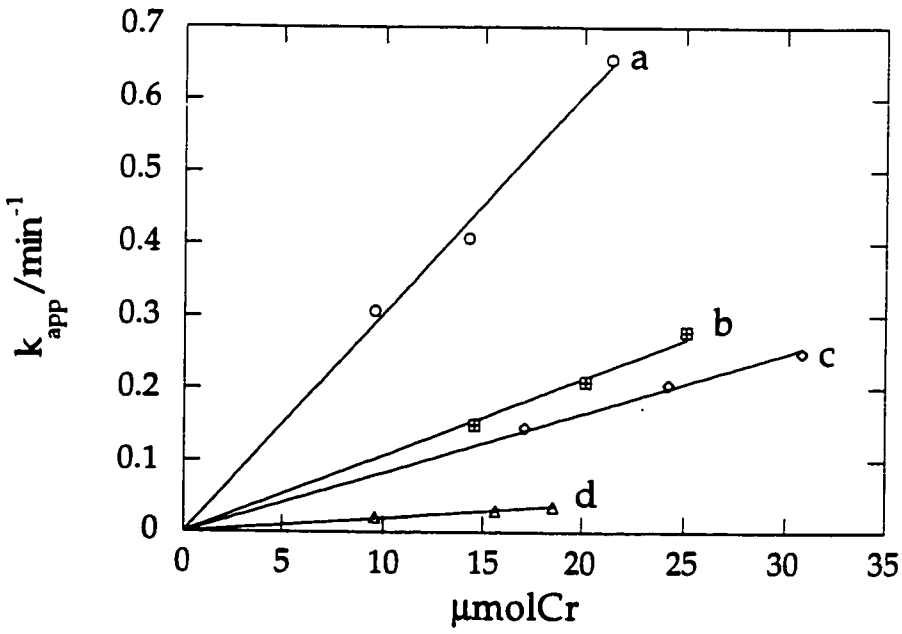

Figure 5.23 Dependence of the observed rate constants k_{app} for polymerization of (a) $C_2H_4 + H_2$, (b) C_2H_4, (c) C_2D_4, (d) C_2D_4 in the presence of 1-hexene, catalyzed by $(SiO)_2Cr{=}CHCMe_3$, on the quantity of Cr, in the range 0.33 - 1.27 wt.% Cr loading at 21°C.

5.12 Catalytic Activity

Catalytic activity tests were performed under commercial batch operating conditions at Nova Chemicals' Research and Technology Centre (Calgary) and Union Carbide's Catalyst Skills Center (Charleston, WV).

A variety of catalysts were tested by Dr. Qinyan Wang of Nova Chemicals. Her results show that the nature of the supported catalyst affects the polymerization activity, Table 5.11. The silica-supported catalyst **4a** exhibits the highest activity towards ethylene compared to **3a** and **4b**. The lower activity of **3a** was expected, since a significant fraction of the run time (1 hour) will be spent in the thermal transformation of **3a** to **4a**, as shown in Figure 5.14. Both preformed alkylidenes **4a** and **4b** are expected to show no induction period, so their activities are correspondingly higher. Although **4b** is thermally the more stable of the two alkylidene complexes,[11] it shows lower polymerization activity. The reason may be a difference in the fraction of active sites.

The absence of the triethylaluminum scavenger caused a dramatic decrease in activity, run 4. It is already established (chapter 4) that the catalyst **4a** is very sensitive to moisture and other impurities which may be present in the ethylene. Since these tests were performed in a reactor for large amounts of organoaluminum cocatalysts impurities were not scrupulously removed. The influence of H_2 was also tested, run 5. The presence of H_2 caused a small increase in activity but the molecular weight distribution, M_w/M_n, was virtually unchanged. All of the runs gave polymers with very high polydispersities, similar to the behavior of the commercial catalyst for which PD's range from 20-30.[33]

Further tests of the activity of **4a** were undertaken at Union Carbide by Dr. Tim Wenzel. His results are shown in Table 5.12. The presence of 50% more Et_3Al scavenger (run 2) caused the activity to decline substantially, implying that

Table 5.11 Activity tests for batch polymerization of ethylene and analysis of the resulting polymer performed at Nova Chemicals. Conditions: 0.5 L hexane, 200 psi C_2H_4, 1 hr, 90°C.

Run	Catalyst	mass of catalyst mg	µmol Cr	Activity g PE/ g Cr/ hr	Yield g PE	M_w	M_n	PD
0	Standard[a,b]	500	0.0348	32604	59	-	-	-
1	**3a**[b]	145	0.0269	1271	2.7	241 000	8 100	29.8
2	**4a**[b]	250	0.0468	15548	19	256 000	9 500	27.1
3	**4b**[b]	160	0.0139	3708	4.6	281 000	8 800	32.0
4	**4a**[c]	235	0.0437	786	0.9	158 000	8 100	19.6
5	**4a**[b,d]	155	0.0280	24725	18	240 000	8 900	27.0

[a] American Polymer Standards Catalyst.

[b] 250 mg of Et_3Al (4 wt %) on silica was used as scavenger.

[c] Run performed without scavenger.

[d] 25 mol/L H_2 added to the reactor.

Table 5.12 Batch polymerization of ethylene with $(\equiv SiO)_2Cr{=}CHC(CH_3)_3)_2$ and analysis of the resulting polymer performed at Union Carbide. Conditions: 0.5 L hexane, 85°C, 400 psi C_2H_4, 50 µL Et_3Al (1 M) were used as scavenger, 85°C.

Run	Mass of catalyst g	µmol Cr	Time min	Activity g PE/ g Cr/ hr	Yield g PE	M_n	M_w	PD
standard	0.1659	15.3	30	244123	97.2	-	-	-
1	0.0428	6.67	30	32853	5.7	-	-	-
2[b]	0.1046	16.29	120	21959	37.2	15031	266374	17.7
3[c]	0.0666	10.37	120	50557	54.5	10187	285950	28.1
4[d]	0.0682	10.6	120	8243	9.1	12165	248299	20.4
5[c,d]	0.0247	3.84	120	31250	12.5	7652	249725	32.6

[a] American Polymer Standards Catalyst B-375.

[b] 75 µL Et_3Al (1 M)

[c] 60 psi H_2 added to the reactor.

[d] 43 mL hexene added to the reactor.

the scavenger is potentially non-innocent in its interaction with the catalyst. (Note that all of our kinetics studies were performed without scavenger and that the commercial Cr-catalyzed polyethylene process does not use alkylaluminums.) As in the Nova tests, the addition of H_2 caused the activity to increase, but at Union Carbide the molecular weight distribution also broadened considerably, from 17.7 to 28.1. The addition of 1-hexene resulted in a significant loss of activity, both with and without H_2 (runs 4 and 5). This effect is at first surprising in light of the kinetics reported in the previous section. However, at a total pressure of 400 psi, 1-hexene is likely condensed on the catalyst and may actually present a diffusion barrier to ethylene binding at the active sites. It is also possible that the addition of 1-hexene introduces impurities which may inactivate some of the propagation centres, despite the presence of scavenger.

5.13 Polyethylene Characterization

5.13.1 Infrared Spectroscopy

The infrared spectrum of a thin self-supporting disk of **4a**, upon exposure to ethylene (60 Torr, RT), shows new bands in the ν(C-H) region at 2924 and 2850 cm^{-1}, due to the asymmetric and symmetric CH_2 stretching modes of polyethylene,[34] Figure 5.3. The methylene bending mode was observed at 1471 cm^{-1} with a shoulder at 1466 cm^{-1}. The band at 1471 cm^{-1} is characteristic of the crystalline phase of linear polyethylene.[34-37]

In the spectral "window" region on silica between 850 and 650 cm^{-1}, two new bands at 718 and 730 cm^{-1} were observed and are assigned to the methylene rocking mode.[38] A splitting of this mode is observed in the IR spectrum of crystalline PE, consequently a measure of the relative intensities of the bands at 718 and 730 cm^{-1} can be used to estimate the relative crystallinity of the polyethylene. For our polymer, the extent of crystallinity is 76 %.[39]

All other peaks in the region 3000-2800 cm^{-1} were attributed to surface t-butyl groups derived from **4a**. When **4a** was exposed to deuterated ethylene, the IR spectrum of the deuterated polymer showed the expected $(2)^{1/2}$ shift in (CH_2) stretching frequencies to 2180 and 2080 cm^{-1}, Figure 5.24. The vibrations of the undeuterated ν(C-H) modes of the catalyst decreased by one third in intensity during the polymerization of deuterated ethylene. In addition, two new bands appeared in the infrared spectrum at 2218 and 2158 cm^{-1}, attributed to asymmetric and symmetric stretches, respectively, of a CD_3 group.[37,39] These methyl vibrations are much more prominent for perdeuteropolyethylene than for unlabeled polyethylene.

The bands at 2218 and 2058 cm^{-1} are likely the result of chain transfer during polymerization. Since the observed propagation rate constant k′ for C_2D_4 polymerization is slower than k′ for C_2H_4, more chain transfer and more methyl end groups are expected for the deuterated polymer. This may explain why the CD_3 vibrations are so intense. β-D elimination would give rise to CD_3-terminated polymer chains upon insertion of C_2D_4 into the new Cr-D bond. However, β-D elimination is expected to be slower than β-H elimination giving rise to fewer (rather than more) methyl groups in the D-labeled polymer. Chain transfer to monomer is an alternate termination mechanism which might have an inverse kinetic isotope effect and hence enhance the number of methyl end groups.

No peaks attributable to unsaturation in the polymer were observed by *in situ* IR. However, when the unlabeled polymer was melted and pressed into a thin (0.002″) film, Figure 2.25, or when the catalyst was removed from the polymer with aqueous hydrofluoric acid (which dissolves the silica),[35] and the polymer was pressed with KBr into pellet, the IR spectrum showed clearly the methyl deformation mode at 1377 cm^{-1} as well as a weak band at 908 cm^{-1} which has been assigned to terminal vinyl groups.[40,41]

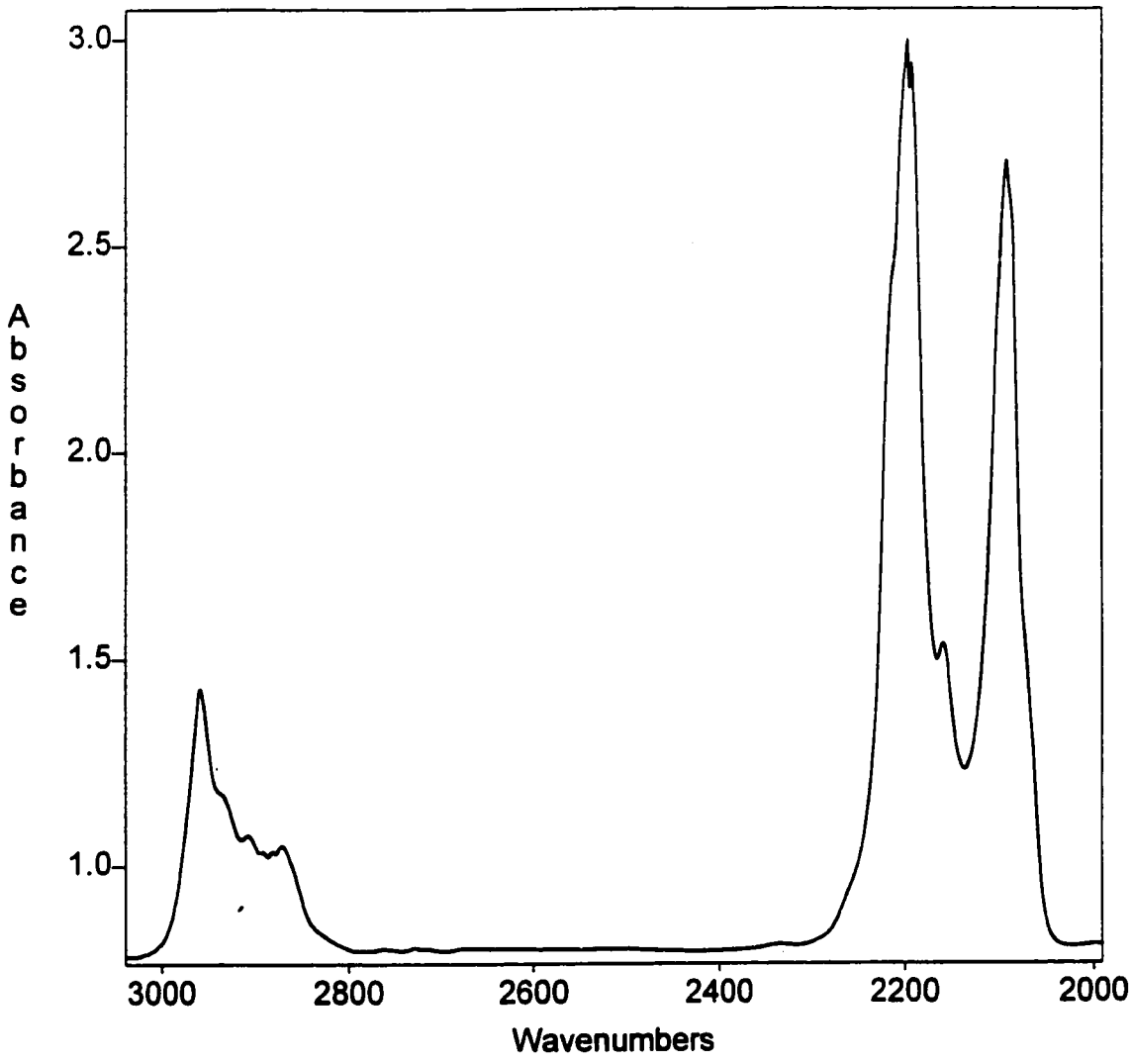

Figure 5.24 Transmission infrared spectrum of $(\equiv SiO)_2Cr{=}CHC(CH_3)_3$ after addition of C_2D_4 at room temperature.

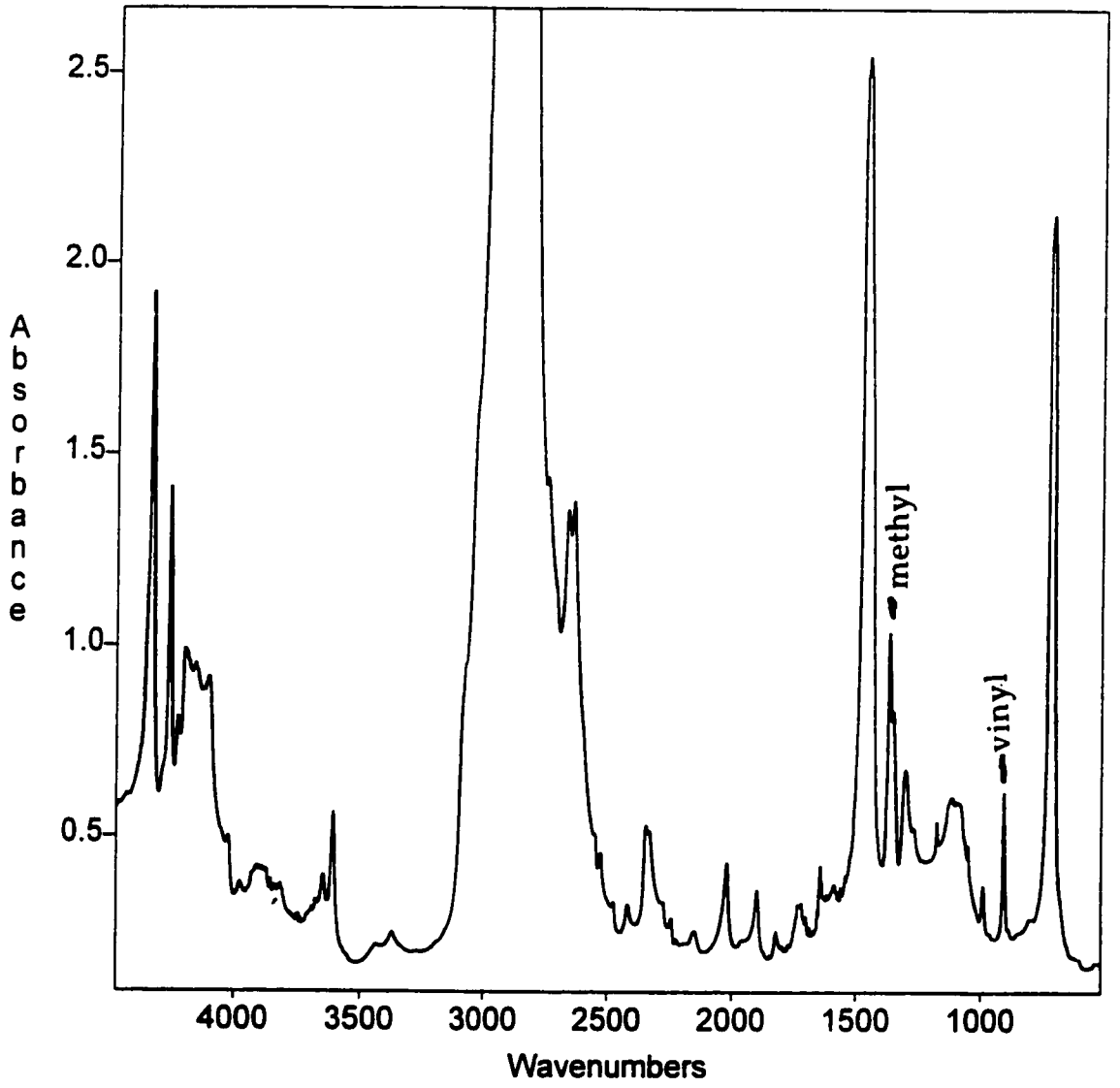

Figure 5.25 Transmission IR spectrum of polyethylene film showing bands due to methyl and vinyl end groups at 1377 and 908 cm^{-1}, respectively.

5.13.2 NMR Spectroscopy

NMR can be a useful tool in the characterization of polymers, but paramagnetic chromium had to be extracted with aqueous base prior to NMR analysis. The polymer was then dissolved in hot 1,2,4-trichlorobenzene (125°C). The ^{1}H NMR spectrum shows a single intense resonance at 1.33 ppm due to the methylene groups of the polymer, while the ^{13}C NMR spectrum shows a signal at 30.13 ppm for the secondary carbons of the CH_2 units.[40]

^{13}C NMR analysis of short chain branching was performed on polyethylene made with **4a** at Union Carbide. The spectrum contains small peaks in the region 10 to 40 ppm whose chemical shifts are characteristic of alkyl branches. Integrations in this region give quantitative information about the nature and number of short chain branches present. The results are summarized in Table 5.13. Only even-numbered branches (ethyl, butyl) gave signals above the detection limit (the terminal methyl groups were not detected). The relationship between branching frequency and mole fraction of branches is the following. The branching frequency per 1000 C is equivalent to the mole fraction divided by 2 (since a mole of monomer is counted in units of "C_2") and multiplied by 1000. The result in run 2 is consistent with an essentially linear homopolymer containing very few branches, on average just 1.7/1000 C. For comparison, the total short chain branching for polyethylene produced by supported organochromium compounds such as $Cr_4(CH_2SiMe_3)_8$, $Cr_2(CH_2SiMe_3)_8$[40] and $Cr_4(DMPD)_8$ (DMPD is 2,4-dimethylpentadienyl)[42] is 1 to 5 per 1000 C.

In the presence of H_2, run 3, the branching frequency increases slightly, to 3.3/1000 C. Copolymerization with 1-hexene causes a significant increase in the number of butyl branches, runs 4 and 5.

Table 5.13 Determination of short chain branching by ^{13}C NMR

run[a]	mole fraction of branches				branching frequency per 1000 C			
	ethyl	butyl	butyl +	total	ethyl	butyl	butyl +	total
2	0.0013	0	0.0021	0.0034	0.63	0	1.06	1.69
3[b]	0.0012	0	0.0053	0.0065	0.62	0	2.66	3.28
4[c]	0.0014	0.0059	0.0032	0.0105	0.71	2.96	1.62	5.29
5[b,c]	0	0.0036	0.0037	0.0073	0	1.81	1.87	3.68

[a] Run numbers refer to batch experiments conducted at Union Carbide, as described in Table 5.12.

[b] H_2 was added during the ethylene polymerization reaction.

[c] Polymerization of ethylene in the presence of 1-hexene.

5.13.3 Gel Permeation Chromatography (GPC) Analysis

The average molecular number (M_n) and the average molecular weight (M_w) of the polymer were determined by size exclusion chromatography. From Table 5.11, the average molecular weight obtained with catalyst **4b** was slightly higher than with **4a**, as was the polydispersity. In Table 5.12, we see that H_2 causes M_n to decrease while M_w increases, resulting in larger PD values. Broad molecular weight distributions are common for Cr-based catalysts,[8] and usually ascribed to heterogeneity of the active sites.

5.13.4 Thermal Analysis

Useful information about the polymer can be obtained from thermal

property measurements such as the temperature of the phase transition which converts microcrystalline polymer to liquid at the melting temperature, T_m, and the accompanying enthalpy and entropy changes. DSC measurements were performed at Union Carbide. The DSC curve is displayed as a profile of the instantaneous rate of change of heat flow versus temperature, reflecting changes in the heat capacity of the sample. A DSC thermogram of polyethylene, Figure 5.26, does not show the glassy transition T_g, which is generally below room temperature. The sharp trough corresponds to endothermic melting of the crystallites. The melting temperature T_m for run 1 (ethylene homopolymer) is 410 K and the enthalpy change for melting, ΔH_m, is 55.81 cal g^{-1}. The entropy change ΔS_m is $\Delta H_m/T$, or 0.14 cal g^{-1} K^{-1}. For comparison, literature data for HDPE report T_m = 414 K, with corresponding ΔH_m = 68.35 cal $g^{-1}$and ΔS_m = 0.17 cal g^{-1} K^{-1}.[43] The results of DSC analysis of polyethylene are summarized in Table 5.14. These values confirm that our polyethylene is high density, with significant crystallinity and chain stiffness due to structurally regular chains with very few, small branch points.[43,44]

In the presence of hydrogen, run 3, the value of T_m decreases slightly compared to run 2. The presence of H_2 and 1-hexene reduces the hardness of the polymer as indicated by decrease in T_m of the homopolymer.

DSC can also be used to determine quantitatively the extent of branching in the polymer. The total number of side branches and end groups A per 1000 C atoms is obtained from the melting temperature according to the formula A = 131 - 0.97 (T_m - 273).[37] The results are shown in Table 5.14. The number of branches and end groups range from to 0 to 2 per 1000 C atoms, which means that the polymer chain is only slightly branched, consistent with the results in Table 5.13. The polymer chain is less branched in the absence of H_2 than in its presence. In the presence of 1-hexene and H_2, the number of side

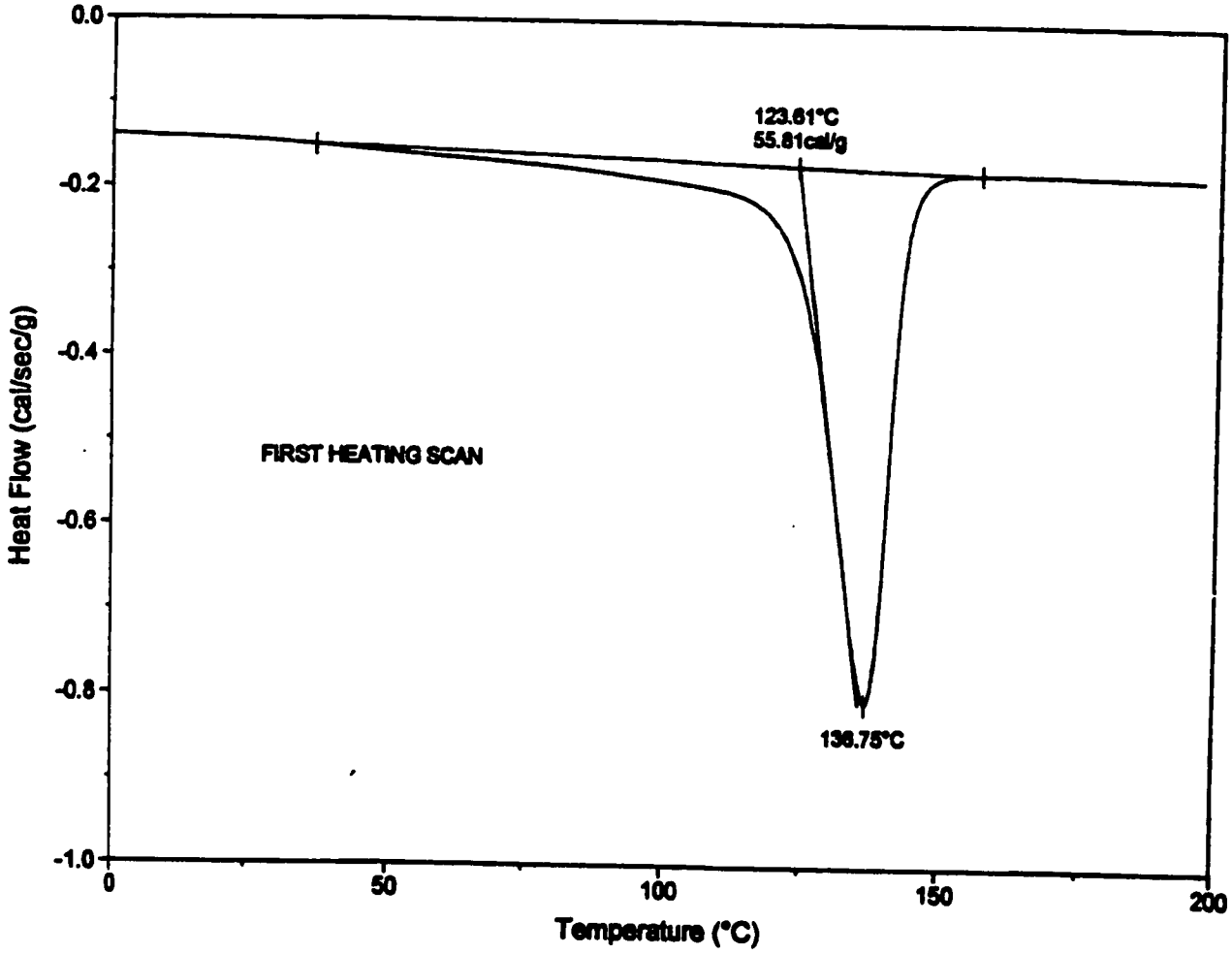

Figure 5.26 DSC of polyethylene produced by $(\equiv SiO)_2Cr{=}CHC(CH_3)_3$

Table 5.14 DSC analysis of polyethylene produced by $(\equiv SiO)_2Cr=CHC(CH_3)_3)_2$

Runs[a]	T_m (K)	ΔH_m cal/ g	ΔS_m cal/g*K	A[c]
literature[b]	414	68.35	0.165	0
2	409.75	55.81	0.136	0
3	409.14	55.64	0.136	0
4	408.13	49.32	0.121	0
5	405.78	51.64	0.127	2.2

[a] Run numbers correspond to polymer samples from Union Carbide, prepared under the conditions described in Table 5.12.

[b] High density polyethylene literature reference.[37]

[c] Total side branches and end groups per 1000 C.[37]

branches is estimated to be 2. Note that this method of calculating the number of branches is less sensitive than ^{13}C NMR analysis.

5.14 Polypropylene Characterization

5.14.1 Infrared Spectroscopy

Exposure of **4a** to 10 Torr propylene causes the appearance of new bands in the ν(C-H) region at 2971, 2945, 2916, 2872 and 2839 cm^{-1}, due to the asymmetric and symmetric CH_3 and CH_2 stretching modes of polypropylene, and at 1459, 1380 cm^{-1} due to the methyl and methylene deformation modes, Figure 5.4.[45]

5.14.2 NMR Spectroscopy

The polypropylene was dissolved in 1,2,4-trichlorobenzene at 125°C. The ^1H NMR spectrum shows three resonances at 0.85 ppm (s, 3H, CH_3), 1.25 ppm (s, 1H, CH) and 1.60 ppm (s, 2H, CH_2). The ^{13}C NMR spectrum shows three signals

at 21.9 ppm (s, CH_3), 28.6 ppm (s, CH) and 46.3 ppm (s, CH_2), Figure 5.27a.[45] The presence of a single sharp methyl signal in both spectra is consistent with the formation of isotactic propylene.[46]

The number of ^{13}C NMR CH_3 signals in polypropylene are determined by the polymer microstructure, which can be described in stereochemical notation.[47] The ^{13}C NMR shift of each methyl group is determined by the configurations in its neighbouring repeat units. The relative configurations of the methyl substituents in neighboring units are designated *m* for meso and *r* for racemo, shown below in a Fischer-type projection of the polymer backbone.[48] Each CH_3 is defined by a particular pentad pattern, represented by four consecutive m or r units and framed by them. Ten possible pentads can be drawn. They are mm-centered, mr-centered and rr-centered, Scheme 5.7.

Scheme 5.7 The ten possible stereochemical pentads of polypropylene

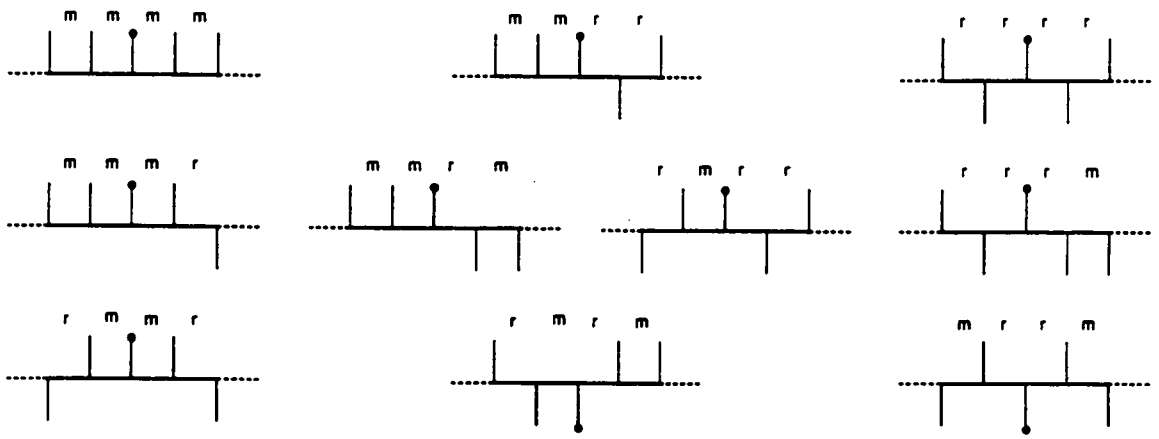

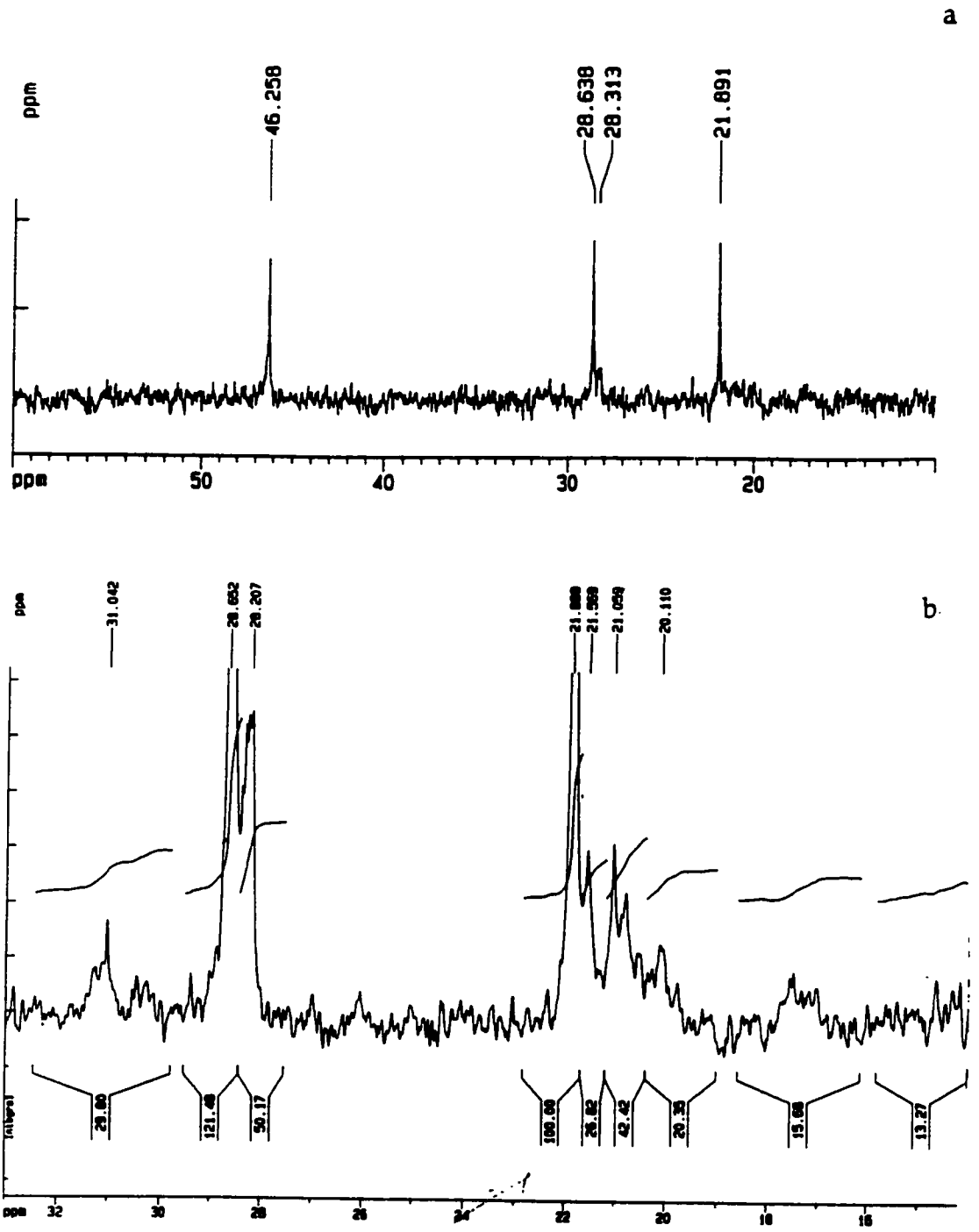

Figure 5.27 ^{13}C NMR spectra of polypropylene produced by $(\equiv SiO)_2Cr{=}CHC(CH_3)_3$, (a) CH_2, CH, CH_3 regions, (b) CH_3 region with [mmmm] = 53%.

All ten pentads are observed for the randomly configured repeat units of atactic polypropylene. Only the *mmmm* signal is observed for completely isotactic polypropylene.

The degree of isotacticity of polypropylene can be determined by ^{13}C NMR in the methyl region, and is expressed as the ratio of the *mmmm* pentad integral to the integral sum of all pentad signals observed. The ratio obtained with our catalyst **4a** operating at room temperature is 53%. Typical isotactic polypropylene produced by heterogeneous Ziegler-Natta catalysts is highly stereoregular with an *mmmm* fraction greater than 95%.[49]

5.15 Polystyrene Characterization

5.15.1 Infrared Spectroscopy

The admission of styrene vapor to either silica-supported alkylidene complex **4** causes a change in the IR spectrum. In the ν(C-H) region, new bands were observed at 3086 - 3029 cm^{-1} due to aromatic C-H stretching modes, and at 2962 and 2820 cm^{-1}, assigned to the asymmetric and symmetric C-H stretching modes of the methyl group of polystyrene, Figure 5.2. The methylene bending modes were observed at 1498 cm^{-1} and 1449 cm^{-1}, characteristic of the asymmetric and symmetric deformations, respectively. A deformation mode of the aromatic ring was observed at 1611 cm^{-1}.

5.15.2 NMR Spectroscopy

The ^1H NMR spectrum of polystyrene dissolved in $CDCl_3$ shows peaks at 1.20 ppm (s, CH_2), 1.50 ppm (s, CH) and 7.1 ppm (aromatic CH), characteristic of polystyrene. The ^{13}C NMR spectrum revealed five bands at 41.3 ppm (s, $\underline{C}H_2CHC_6H_5$), 42.4 ppm (s, $CH_2\underline{C}HC_6H_5$), 126.4 ppm (s, para carbon of the aromatic ring $\underline{C}_6H_5$), 128.8 ppm (s, meta and ortho carbons of the aromatic ring

$\underline{C}_6H_5$), 146.4 ppm (s, quaternary carbons of the aromatic ring $\underline{C}_6H_5$), Figure 5.28, also characteristic of polystyrene.[50]

5.16 Poly-1-hexene Characterization

5.16.1 Infrared Spectroscopy

The admission of 1-hexene vapor to the silica-supported **4a** causes a change the IR spectrum. In the ν(C-H) region, new bands were observed at 2965, 2920, 2876 and 2857 cm^{-1}, assigned to the asymmetric and symmetric C-H stretching modes of poly-1-hexene, Figure 5.5. Bending modes were observed at 1468, 1454 cm^{-1} and 1379 cm^{-1}.[45]

5.16.2 NMR Spectroscopy

The ^1H NMR spectrum showed broad peaks at 0.90 ppm (s, CH_3), 1.35 ppm (s, CH_2) and 1.65 ppm (s, CH). The ^{13}C NMR spectrum, Figure 5.29 shows peaks, at 14.5 ppm (s, $\underline{C}H_3$ in C_1), 23.9 ppm (s, $\underline{C}H_2$ in C_2), 29.2 ppm (s, $\underline{C}H_2$ in C_3), 33.0 ppm (s, $\underline{C}H_2$ in C_4), 35 ppm (s, $\underline{C}H_2$ in C_α and 41.7 ppm (s, methine carbon) characteristic of poly-1-hexene.[45] The carbon numbering scheme of poly-1-hexene is shown in Scheme 5.8.

Scheme 5.8 Carbon numbering in poly-1-hexene for ^{13}C NMR.

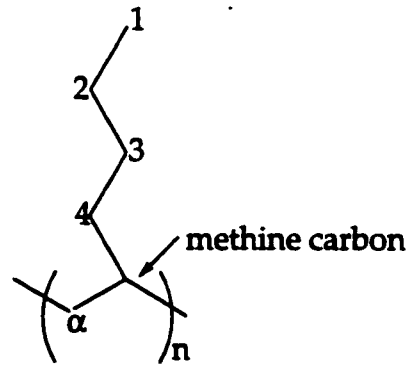

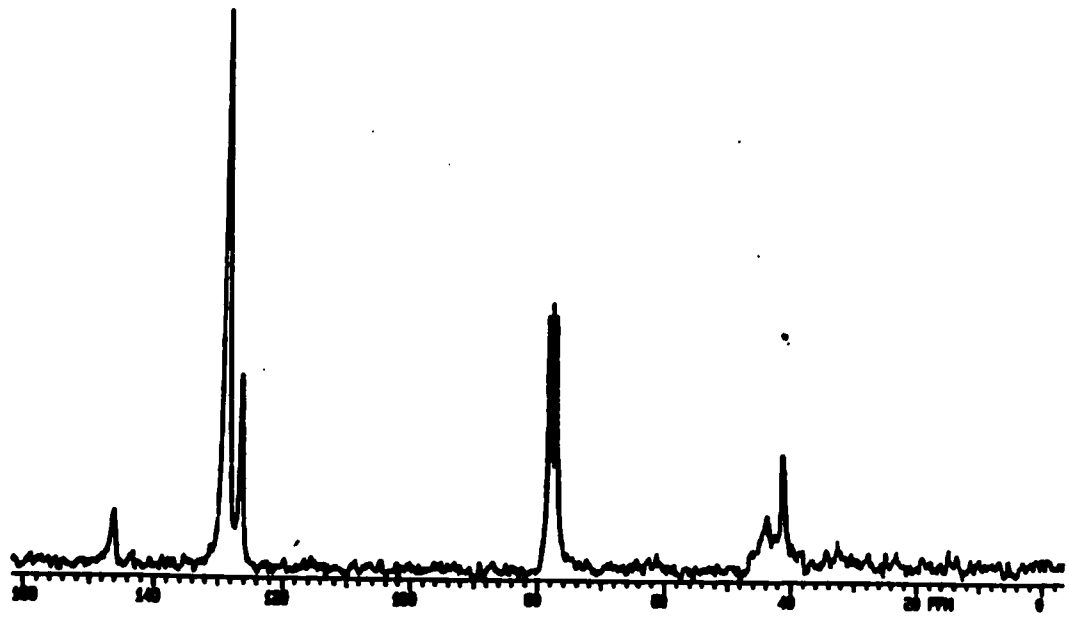

Figure 5.28 ^{13}C NMR of polystyrene produced by $(\equiv SiO)_2Cr{=}CHC(CH_3)_3$

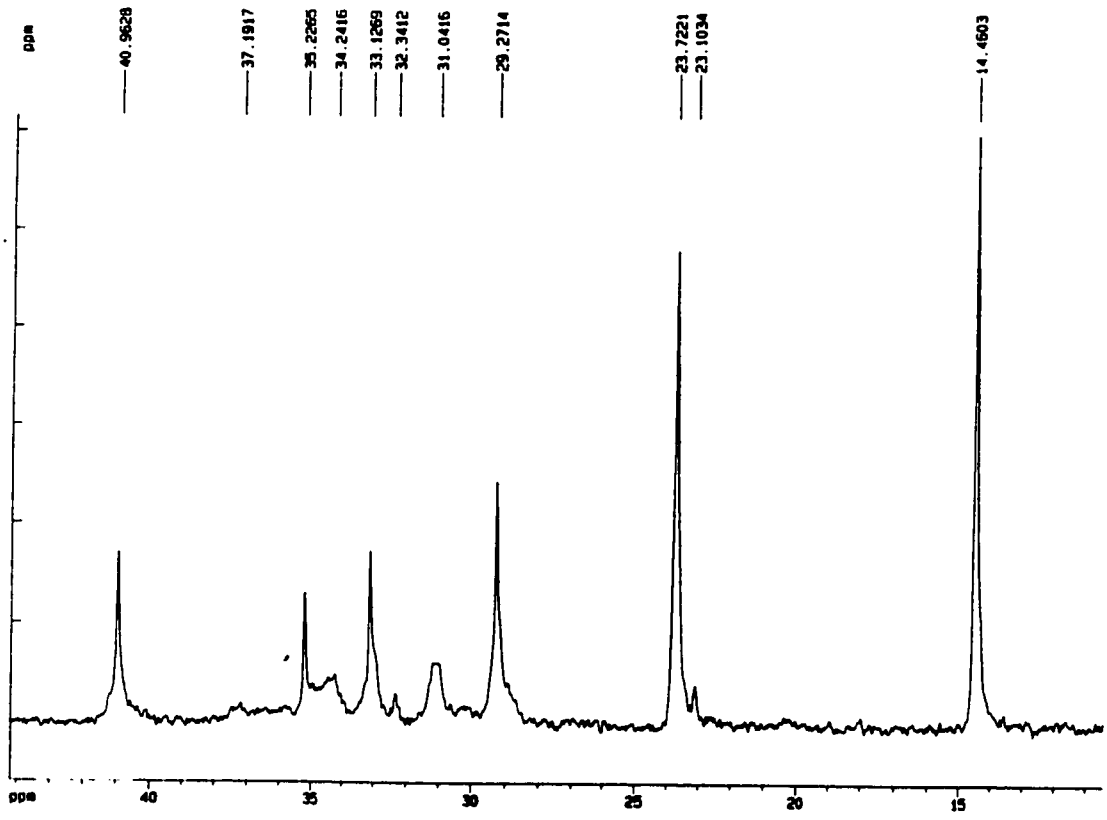

Figure 5.29 ^{13}C NMR of poly-1-hexene produced by $(\equiv SiO)_2Cr{=}CHC(CH_3)_3$

5.17 Proposed Mechanism for Polymerization of Ethylene

The silica-supported bis(neopentyl)Cr(IV) complex **3a** does not react with ethylene at room temperature. We presume this is due to steric hindrance by the bulky neopentyl ligands, which prevent ethylene binding and/or migratory insertion at Cr (*vide infra*). However, gentle thermolysis at 70°C suffices to induce an α-H elimination in one of the neopentyl ligands, leading to the reductive elimination of the second neopentyl ligand as neopentane. The silica-supported neopentylidene Cr(IV), **4a**, initiates polymerization of ethylene at room temperature. In order to identify the adsorbed ligands and the short-lived intermediates during polymerization of ethylene, we decided to study in detail the mechanism of polymerization at low ethylene pressures (0.1 to 0.3 Torr). Evidence for the first and second ethylene insertions was sought by analysis of the volatile products upon treatment of **4a** with ca. one equivalent of ethylene.

The fraction of active chromium sites at low ethylene pressures is approx. 20% from poisoning experiments (*vide supra*). The products observed upon treating **4a** with 1.2 mol ethylene/mol active Cr were a variety of linear and branched, terminal and internal olefins, Figure 5.30. Their possible origin is described below.

Some volatile products contain the neopentylidene fragment which was originally part of the neopentylidene ligand of **4a**. All the neopentylidene-derived olefins have odd carbon numbers. Upon reaction of **4a** with 1.2 equiv. ethylene, the ν(C-H) intensity in the *in situ* IR spectrum of the silica pellet decreased by one-third, suggesting that these products arise by elimination of the neopentylidene ligands from the *active* Cr sites. Three such olefins were identified by their mass spectra: 4,4-dimethyl-1-pentene, 4,4-dimethyl-2-pentene and 2,3,3-trimethyl-1-butene, Table 5.15. All are heptene isomers composed of a neopentylidene fragment plus one ethylene. Nonenes and undecenes containing

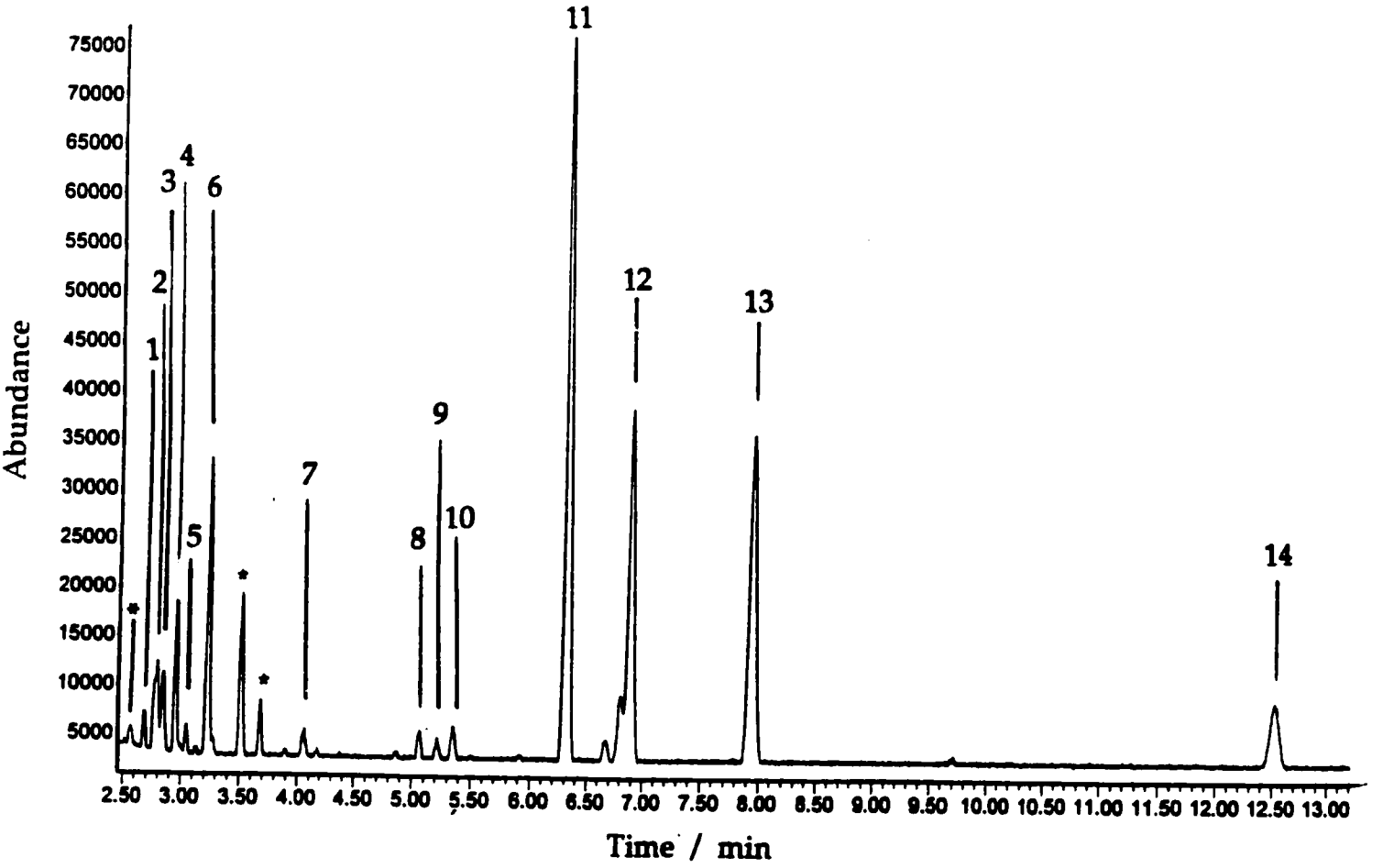

Figure 5.30 GC-MS of volatile reaction products upon treatment of **4a** with 0.1 Torr ethylene. Peaks marked * are known syringe contaminants. The peak marked * is neopentane, from catalyst decomposition.

Table 5.15 Volatiles formed upon reaction of **4a** with 0.1 Torr ethylene

peak number	retention time (min)	major ion fragments	formula	structure
1	2.68	84, 69, 56	C_6H_{12}	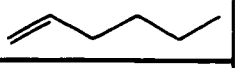
2	2.79	84, 69, 55	C_6H_{12}	
3	2.85	83, 67, 57	C_7H_{14}	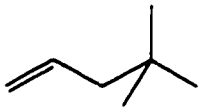
4	2.95	98, 83, 55	C_7H_{14}	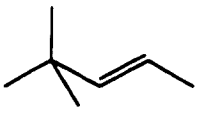
5	3.05	98, 83, 55	C_7H_{14}	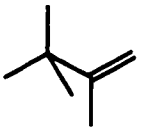
6	3.23	91, 83, 78, 70,55	C_8H_{16}	
7	5.07	111, 83, 69, 55	C_9H_{18}	
8	5.21	112, 69, 55	C_8H_{16}	
9	5.35	83, 70, 56	unidentified	
10	6.32	140, 125, 97, 83, 69, 55	$C_{10}H_{20}$	
11	6.88	126, 111, 70, 57	C_9H_{18}	
12	7.94	127, 85, 71, 57	$C_{11}H_{22}$	
13	12.5	154, 98, 83, 69, 57	$C_{11}H_{22}$	

the neopentylidene fragment were also detected. These products are presumably formed by insertion of two and three ethylenes, respectively. Unfortunately, we were not able to identify the specific isomers by library searching of mass spectra.

We also observed olefins with even carbon numbers which do not contain the neopentylidene fragment, for example, 1-hexene, 2-hexene, octene and decene, Table 5.15. (1-Butene and 2-butene were detected in previous experiments.)

For comparison, the analysis of volatiles from the reaction of **4a** with a higher pressure of ethylene (48 Torr) was also undertaken, Figure 5.31. The results of analysis of these gaseous reaction products is given in Table 5.16. At this pressure, only two heptenes were identified: 4,4-dimethyl-2-pentene and 2,3,3-trimethyl-1-butene. One C_9H_{18} and one $C_{11}H_{22}$ isomer were also observed. Surprisingly, no hexenes were detected. The most abundant olefins are C_8H_{16} and $C_{10}H_{20}$.

In order to explain the appearance of these products, we propose that the initiation step is a [2+2] cycloaddition of ethylene to **4a**, forming a metallacyclobutane, **5a**, Scheme 5.9. This reaction has been shown by DFT calculations to be very exothermic (by ca. 40 kcal/mol) and to have almost no activation barrier.[25] At high pressures of ethylene, **5a** likely undergoes a second ethylene insertion to generate a metallacyclohexane (which is exothermic by about 30 kcal/mol due to relief of ring strain).[25] However, at the low pressure of a near-stoichiometric experiment, we suggest that **5a** undergoes β-H elimination, generating one of two allylhydridoCr(IV) complexes, **6a** or **6b**. A similar elimination has been suggested for a titanacyclobutane derived from the reaction of a neopentylidene complex with ethylene.[51]

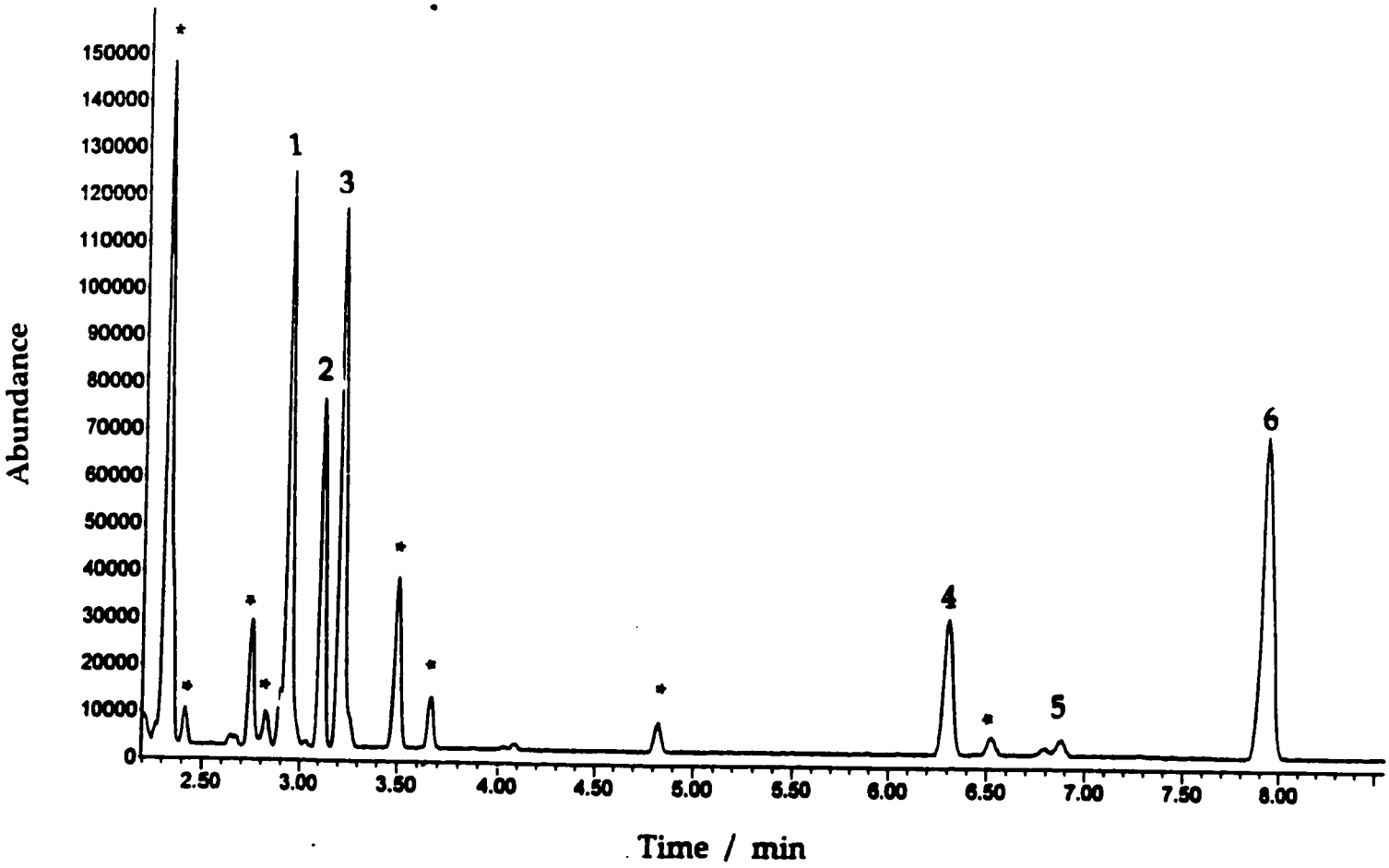

Figure 5.31 GC-MS of volatile reaction products upon treatment of **4a** with 48 Torr ethylene. Peaks marked * are known syringe contaminants.

Table 5.16 Volatile reaction products upon treatment of **4a** with 48 Torr ethylene

peak number	retention time (min)	major ion fragments	formula	structure
1	2.95	98, 83, 55	C_7H_{14}	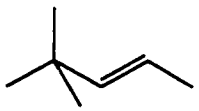
2	3.05	98, 83, 55	C_7H_{14}	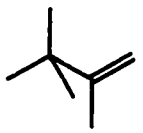
3	3.23	91, 83, 78, 70,55	C_8H_{16}	
4	6.32	140, 125, 97, 83, 69, 55	$C_{10}H_{20}$	
5	6.88	126, 111, 70, 57	C_9H_{18}	
6	7.94	127, 85, 71, 57	$C_{11}H_{22}$	

Scheme 5.9 Proposed origin of heptene isomers during early stages of ethylene polymerization

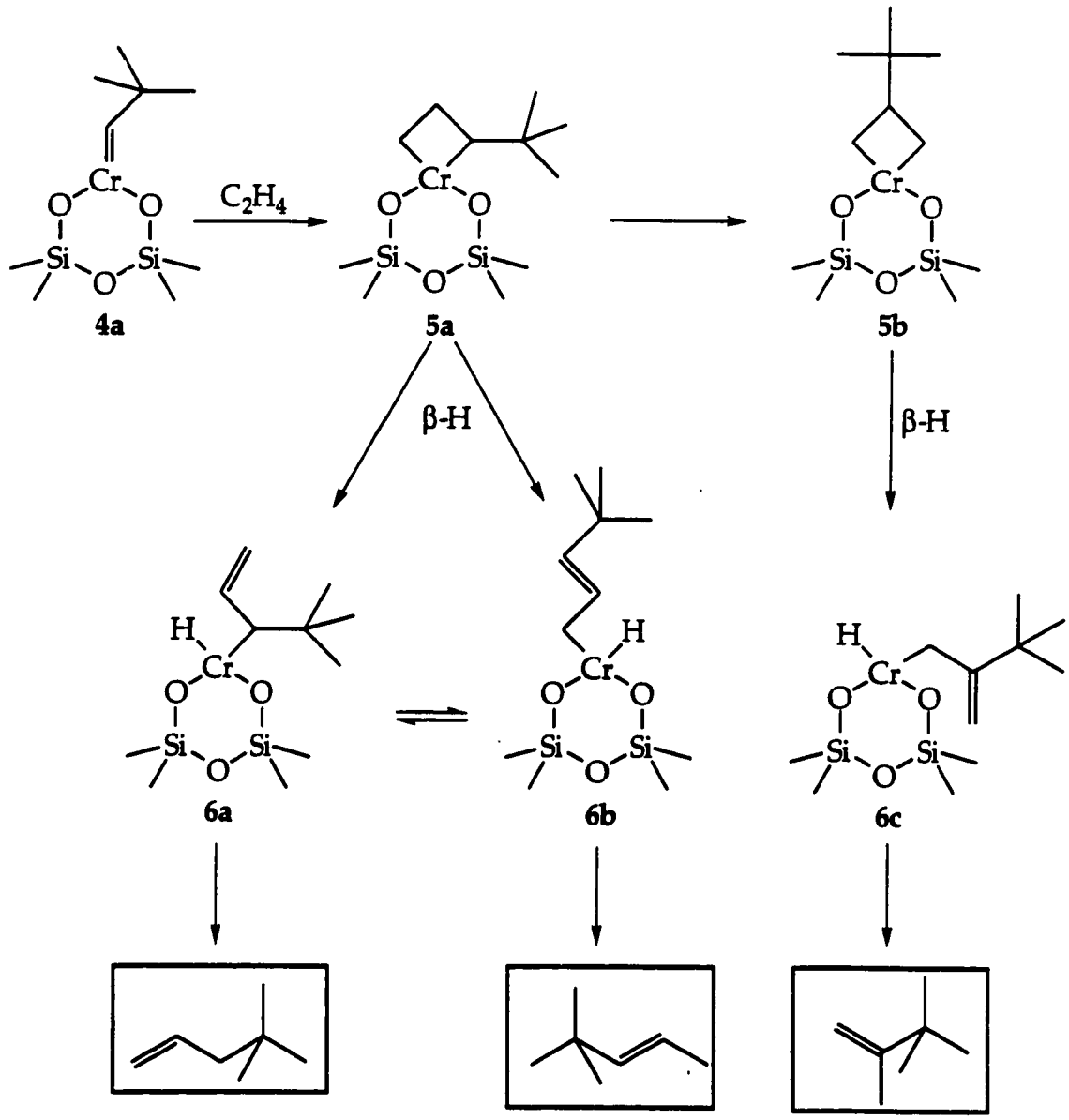

Reductive elimination liberates either 4,4-dimethyl-1-pentene from **6a** or trans-4,4-dimethyl-2-pentene from **6b**.

Isomerization of metallacyclobutane **5a** to **5b** (possibly by deinsertion of neohexene, rotation and readdition to the chromium methylidene) is proposed to lead to the third heptene isomer, 2,3,3-dimethyl-1-butene via the intermediate **6c**.

Nonene and undecene isomers may originate via a similar β-H elimination pathway from a metallacyclohexene intermediate (formed by ethylene insertion into **5a**).

Polymerization of C_2D_4 yielded heptene-d_4, which we deduce from its GC retention time and mass spectral fragmentation pattern to be $(CH_3)_3CCH{=}CDCD_3$, Figure 5.32. This deuterium-substitution pattern is consistent with the mechanism shown in Scheme 5.9 in which β-D elimination followed by reductive elimination produces an olefin composed of a neopentylidene fragment and a perdeuteroethylidene fragment.

After reductive elimination of the olefin containing the neopentylidene fragment, the supported chromium ion is formally Cr(II), as in $(\equiv SiO)_2Cr$. If ethylene induces reductive elimination, then the product could be any of the ethylene-Cr(II) complexes described in Scheme 1.3. These are propably the sites which generate linear 1- and 2-olefin oligomers of ethylene. Even-numbered olefins were detected from C_4 to C_{10}.

Thus after initiation of polymerization, our well-defined catalyst has become very similar to the proposed structure of active sites on the heterogeneous Phillips catalyst. The result is, in retrospect, a predictably broad molecular weight distribution, low response to H_2 and low comonomer incorporation. Although we succeeded in preparing a well-defined catalyst precursor, which could have been a single-site catalyst, the system generated its own heterogeneity in the initial stages of the polymerization.

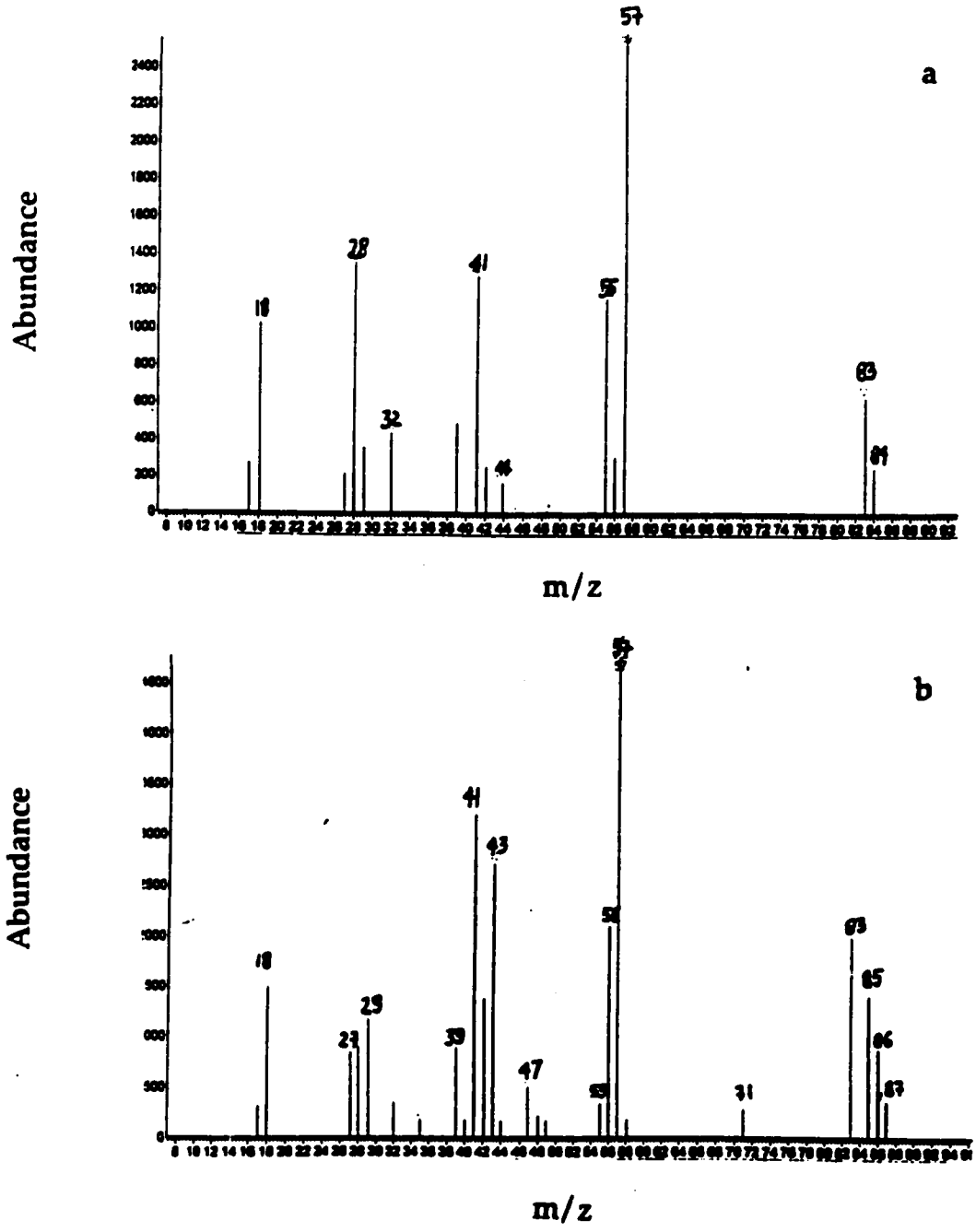

Figure 5.32 Mass spectra of 4,4-dimethyl-2-pentene formed by reaction of **4a** with (a) C_2H_4, and (b) C_2D_4.

5.18 Proposed Mechanism for Polymerization of Propylene

The silica-supported complex **4a** also initiates the polymerization of propylene at room temperature, forming somewhat isotactic polypropylene. At an initial pressure of 10 Torr propylene, various olefin oligomers were liberated and detected by GC-MS, Figure 5.33. The volatiles were identified by their mass spectra as dimers and trimers of C_3H_6, Table 5.17. No olefins containing any neopentylidene fragments were detected, unlike the experiments on ethylene polymerization.

The observation of three C_6H_{12} and three C_9H_{18} isomers suggests that there is no strong stereochemical preference in the first few propylene insertions. This result is not unexpected, since the catalyst is not initially asymmetric. We suggest that the isotacticity in the polypropene formed over this catalyst must develop after these first few insertions. In Scheme 5.10, we see that following β-H elimination two σ-allylhydrido complexes are generated, **10a** and **10b**, one of which is α-substituted. This steric bulk close to the chromium may lead to stereochemical preference in the growing polymer chain, since insertion into Cr-H will be directed to the side opposite the α-substituent.

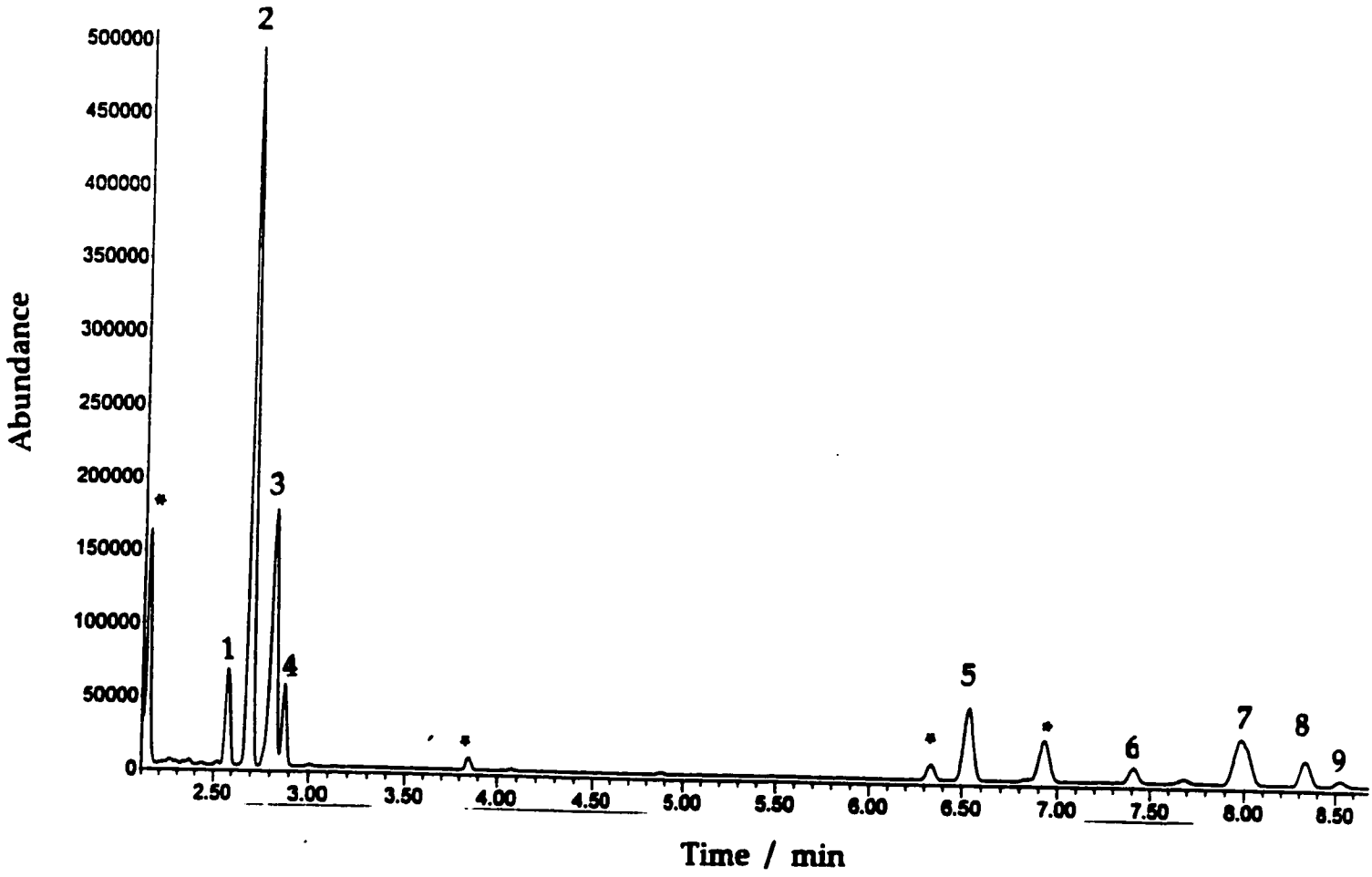

Figure 5.33 GC-MS of volatile reaction products upon treatment of **4a** with 10 Torr propylene. Peaks marked * are known syringe contaminants. The peak marked * is neopentane, from catalyst decomposition.

Table 5.17 Volatile reaction products upon treatment of **4a** with 10 Torr propylene

peak number	retention time (min)	major ion fragments	formula	structure
1	2.57	84, 69, 41	C_6H_{12}	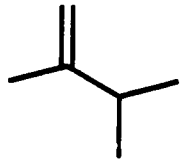
2	2.69	84, 69, 56	C_6H_{12}	
3	2.81	84, 69, 55, 41	C_6H_{12}	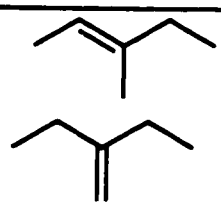
4	2.87	84, 69, 55	C_6H_{12}	
5	6.56	83, 70, 55	undefined	
6	7.40	126, 83, 69, 55	C_9H_{18}	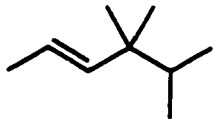
7	7.99	126, 83, 70, 55	C_9H_{18}	
8	8.31	126, 83, 69, 55	C_9H_{18}	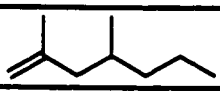
9	8.34	126, 83, 70, 55	C_9H_{18}	

Scheme 5.10 Mechanism for initiation of propylene polymerization

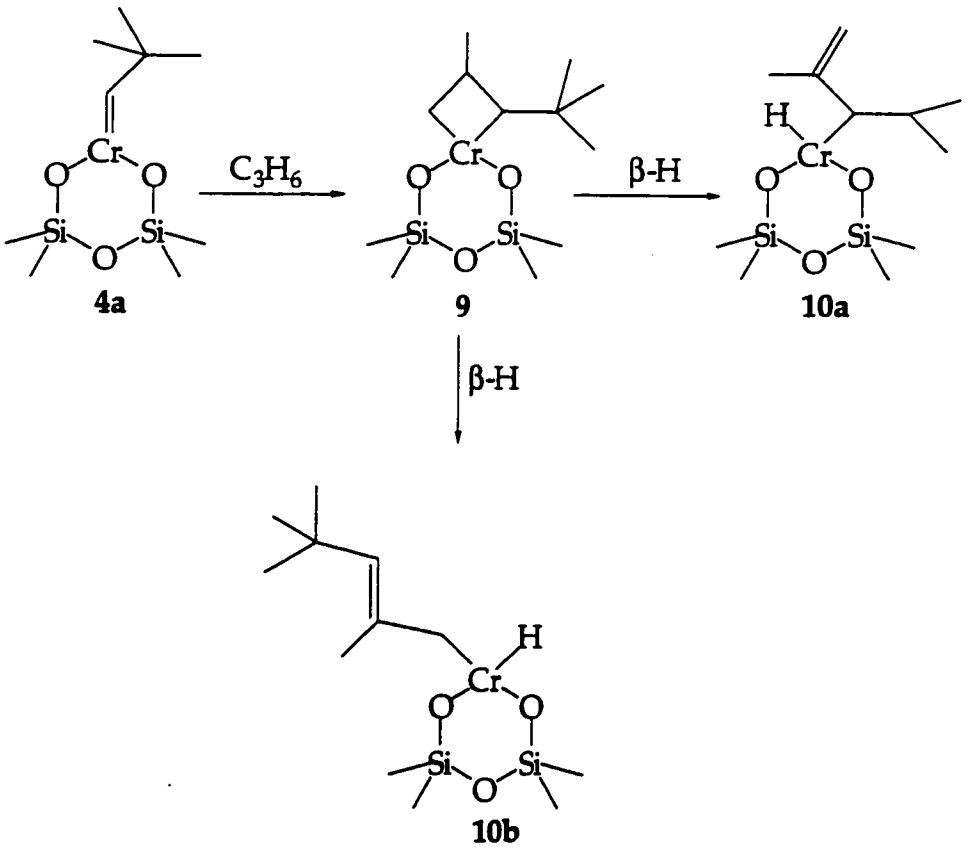

4a **9** **10a** **10b**

5.19 Conclusion

We have discovered a silica-supported chromium(IV) alkylidene catalyst that initiates polymerization of α-olefins. The catalyst exhibits a remarkable activity of 32 000 g PE/g Cr/hr at 85°C. The average oxidation state of the chromium remains (IV) even after polymerization, and the catalyst is active upon subsequent addition of ethylene.

The reaction of the surface alkylidene with ethylene to form a metallacyclic intermediate is, at low pressures, followed by β-H elimination to give a variety of low molecular weight oligomers. The observation of butenes and hexenes suggests that the incorporation of higher α-olefins into the growing polymer chain is responsible for low levels of chain branching. The very broad molecular weight distribution confirms the heterogeneity of the catalyst, despite its well-defined starting point.

5.20 References

1) Cossee, P. *J. Catal.* **1964**, *3*, 80.

2) Ivin, K. J.; Rooney, J. J.; Stewart, C. D.; Green, M. L. H.; Mahtab, R. *J. Chem. Soc., Chem. Commun.* **1978**, 604-606.

3) Dawoodi, Z.; Green, M. L. H.; Mtetwa, V. S. B. *J. Chem. Soc, Chem. Commun.* **1982**, 1410-1411.

4) Laverty, D. T.; Rooney, J. J. *J. Chem. Soc. Farad. Trans. 1* **1983**, *79*, 869-878.

5) Brookhart, M.; Green, M. L. H. *J. Organomet. Chem.* **1983**, *250*, 395-408.

6) Brookhart, M.; Green, M. L. H.; Wong, L. L. *Prog. Inorg. Chem.* **1988**, *36*, 1-124.

7) Grubbs, R. H.; Coates, G. W. *Acc. Chem. Res.* **1996**, *29*, 85-93.

8) McDaniel, M. P. *Adv. Catal.* **1985**, *33*, 47-98.

9) Hogan, J. P. *J. Polym. Sci.: A-1* **1970**, *8*, 2637-2652.

10) Amor Nait Ajjou, J.; Scott, S. L. *J. Am. Chem. Soc.* **1998**, *120*, 415-416.

11) Amor Nait Ajjou, J.; Rice, G.; Scott, S. L. *J. Am. Chem. Soc.* **1998**, *120*, 13436-13443.

12) Clark, A. *Catal. Rev.* **1970**, *3*, 145-173.

13) Wang, S.; Tait, P. J. T.; Marsden, C. E. *J. Mol. Catal.* **1991**, *65*, 237-252.

14) Kaminsky, W.; Sinn, H. *Transition Metals and Organometallics as Catalysts for Olefin Polymerization*; Springer-Verlag: New York, 1988.

15) Yermakov, Y.; Zakharov, V. *Catal. Rev.-Sci. Eng.* **1979**, *19*, 67.

16) Eden, C.; Feilchenfeld, H.; Haas, Y. *J. Catal.* **1968**, *11*, 263.

17) Yermakov, Y. I.; Zakharov, V. A. *Adv. Catal.* **1975**, *24*, 173-219.

18) Fu, S. L.; Rosynek, M. P.; Lunsford, J. H. *Langmuir* **1991**, *7*, 1179-1187.

19) Natta, G.; Pasquon, I. *Adv. Catal.* **1959**, *11*, 1.

20) Gillespie, R. D.; R. L. Burwell, J.; Marks, T. J. *Langmuir* **1990**, *6*, 1465-1477.

21) Mowat, W.; Shortland, A.; Yagupsky, G.; Hill, N. J.; Yagupsky, M.; Wilkinson, G. *J. Chem. Soc., Dalton Trans.* **1972**, 533-542.

22) Amor Nait Ajjou, J.; Scott, S. L. *Organometallics* **1997**, *16*, 86-92.

23) Doherty, N. M.; Bercaw, J. E. *J. Am. Chem. Soc.* **1985**, *107*, 2670.

24) Espenson, J. H. *Chemical Kinetics and Reaction Mechanisms*; McGraw-Hill: New York, 1981.

25) Schmit, R.; Ziegler, T. *Can. J. Chem.* in press

26) Groeneveld, C.; Wittgen, P. P. M. M.; Lavrijsen, J. P. M.; Schuit, G. C. A. *J. Catal.* **1983**, *82*, 77-91.

27) Karol, F. J.; Brown, G. L.; Davison, M. J. *J. Polym. Sci.* **1973**, *11*, 413-424.

28) Zakharov, V. A.; Yermakov, Y. I. *Catal. Rev.-Sci. Eng.* **1979**, *19*, 67-103.

29) Berger, M. N.; Grieveson, B. M. *Makromol. Chem.* **1965**, *83*, 80.

30) Badin, E. J. *J. Am. Chem. Soc.* **1958**, *80*, 6545.

31) Chien, J. C. W. *J. Am. Chem. Soc.* **1959**, *11*, 1.

32) Prosenc, M. H.; Janiak, C.; Brinzinger, H. H. *Organometallics* **1992**, *11*, 4036-4041.

33) Smith, P. D.; McDaniel, M. P. *J. Polym. Sci. A: Polym. Chem.* **1990**, *28*, 3587-3601.

34) Ghiotti, G.; Garrone, E.; Zecchina, A. *J. Mol. Catal.* **1988**, *46*, 61-77.

35) Bade, O. M.; Blom, R.; Dahl, I. M.; Karlsson, A. *J. Catal.* **1998**, *173*, 460-469.

36) Painter, P. C.; Coleman, M. M.; Koenig, J. L. *The Theory of Vibrational Spectroscopy and its Application to Polymeric Materials*; Wiley: New York, 1982.

37) Groeneveld, C.; Wittgen, P. P. M. M.; Swimmen, H. P. M.; Wernsen, A.; Schuit, G. C. A. *J. Catal.* **1983**, *83*, 346-361.

38) Koenig, J. L. *Chemical Microstructure of Polymer Chains*; Wiley: New York, 1980.

39) Koenig, J. L. *Spectroscopy of Polymers*; Wiley: Washington, DC, 1992.

40) Smith, P. D.; McDaniel, M. P. *J. Polym. Sci.: A: Polym. Chem.* **1990**, *28*, 3587-3601.

41) Blom, R.; Follestad, A.; Noel, O. *J. Mol. Catal.* **1994**, *91*, 237-249.

42) Freeman, W. J.; Wilson, D. R.; Ernst, R. D.; Smith, P. D.; Klendworth, D. D.; McDaniel, M. P. *J. Polym. Sci. Polym. Chem. Ed.* **1987**, *25*, 2063.

43) Campbell, I. M. *Introduction to Synthetic Polymers*; Oxford University Press: Oxford 1994.

44) Cowie, J. M. G. *Polymers; Chemistry and Physics of Modern Materials*; Blackie: London, 1991.

45) Weiss, K.; Krauss, H. L. *J. Catal.* **1984**, *88*, 424-430.

46) Locatelli, P.; Sacchi, M. C.; Tritto, I.; Zannomi, G.; Zambelli, A.; Piscitelli, V. *Macromolecules* **1985**, *18*, 627-630.

47) Bovey, F. A. *High Resolution NMR of Macromolecules*; Academic Press: New York, 1972.

48) Randall, J. C. In *NMR and Macromolecules*; Compagny, P. P., Ed.; American Chemical Society: Washington, D.C., 1984; pp. 55-65.

49) Kashiwa, N. *Polymer* **1980**, *12*, 603.

50) Ammendola, P.; Tancredi, T.; Zambelli, A. *Macromolecules* **1986**, *19*, 307-310.

51) van Doorn, J. A.; van de Heijden, H.; Orpen, A. G. *Organomet.* **1995**, *14*, 1278.

Synthesis of Silica-supported Amido and Alkoxo Complexes of Chromium(IV)

6.1 Introduction

The selective oxidation of primary and secondary alcohols to the corresponding carbonyl compounds is a key reaction in organic synthesis.[1] Traditionally such transformations have been performed with stoichiometric amounts of Cr(VI) reagents.[2-4] However, because of serious environmental problems associated with chromium-containing effluent, attention has been focused on the use of catalytic amounts of soluble chromium compounds in conjunction with more benign primary oxidants such as tert-butylhydroperoxide (TBHP),[5,6] peroxyacetic acid[7] and other hydrogen peroxide derivatives.[8]

Chromium dispersed on the surface of inorganic oxides constitutes an important class of catalytically active materials for oxidations.[9] There is an increasing interest in the highly specific oxidations afforded by organic derivatives of chromium. However, knowledge about the structure of the active sites is still rudimentary. The use of heterogeneous catalysts in the liquid phase offers several advantages over homogeneous ones, namely, ease of recovery, recycling and enhanced stability. For example, chromium(III)-impregnated Nafion K (a perfluorinated sulfonic acid resin) was shown to be an efficient catalyst for chemoselective oxidation of a variety of unsaturated alcohols using TBHP as oxidant.[5] Redox pillared clays[10] constitute another attractive type of heterogeneous catalyst. Choudary and co-workers[11,12] reported that chromia-, vanadia, titania-pillared montmorillonite catalyze the oxidation of various alcohols with either 30% aqueous H_2O_2 or TBHP, claiming unusually high regio-, shape- and enantioselectivities.

A problem associated with the chromium-catalyzed oxidation of alcohols is low efficiency in the use of primary oxidants, because chromium is a good catalyst not only for the oxidation of alcohols via an oxometal pathway but also for the homolytic decomposition of organic hydroperoxides. Thus to obtain high yields of carbonyl compounds from alcohols, a large excess of oxidant is required.[6] On the other hand, the chromium-catalyzed decomposition of organic hydroperoxides via a free radical mechanism may be advantageous with regard to the use of O_2 as a co-oxidant, since the resulting alkoxy radicals are good initiators for generating other alkylhydroperoxides in the presence of an active substrate and O_2. Furthermore, the alkylhydroperoxides so formed can reoxidize Cr(IV) to Cr(VI), while the peroxides themselves are converted to the desired products and water.

Another approach for creating heterogeneous oxidation catalysts is to incorporate redox-active metal ions into the lattice of molecular sieves such as zeolites, aluminophosphates and silicoaluminophosphates. Recently, Chen *et. al.* reported that Cr-substituted aluminophosphates (CrAPOs) catalyze the selective oxidation of alcohols by tert-butylhydroperoxide.[13] The proposed mechanism involves reduction of Cr(VI) to Cr(IV) by the alcohol, followed by reoxidation of Cr(IV) by the peroxide. In contrast, the mechanism for the catalytic oxidations of hydrocarbons using CrAPO[14] and Cr-substituted clays[12] was suggested to involve an alkylperoxochromium(VI) active site, whose oxidation state does not change during the reaction.

The Ti(IV)/SiO_2 catalyst developed by Shell, Scheme 6.1, is an effective heterogeneous catalyst for chemo-, regio- and stereo-selective epoxidations, but is highly water-sensitive.[10] Zeolite-based catalysts such as titanium silicalite-1 (denoted TS-1) are less active but are hydrolytically stable, presumably due to restricted access of water to the active site.[10] Aluminophosphate-based redox

molecular sieves possess hydrophilic cavities and are strongly inhibited by water, which renders them unsuitable for reactions with aqueous H_2O_2.[15] In contrast, they are suitable for oxidations with alkylhydroperoxides or O_2 as oxidant.[10]

Scheme 6.1 A proposed structure for the active site of the Ti(IV)/SiO_2 catalyst, developed by Shell.[10]

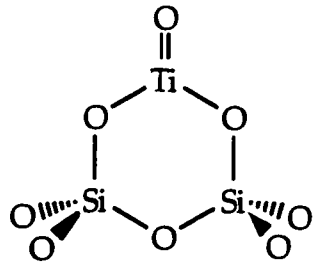

Catalytic oxygen transfer involves reaction of an oxygen donor with an organic substrate in the presence of a metal catalyst.

$$M + XOY + S \rightarrow M + SO + XY \qquad (6.1)$$

where XOY is an oxygen donor, S is the substrate and M is the catalyst. Two pathways for oxygen transfer are commonly invoked for transition metals. The active oxidant in these processes may be an oxometal or a peroxometal species, Scheme 6.2. Metals that are strong oxidizing agents in their high oxidation states (e.g., Ru(VIII), Cr(VI), Ce(IV)) react via oxometal pathways while weakly oxidizing metal ions (e.g., Mo (VI), W(VI), Zr(VI), Ti(IV)) generate peroxometal species in the key oxidation reaction. Some metals (e.g., vanadium) can, depending on the substrate, operate via either mechanism.

Scheme 6.2 Peroxometal (upper) and oxometal (lower) pathways for catalytic oxidation reactions

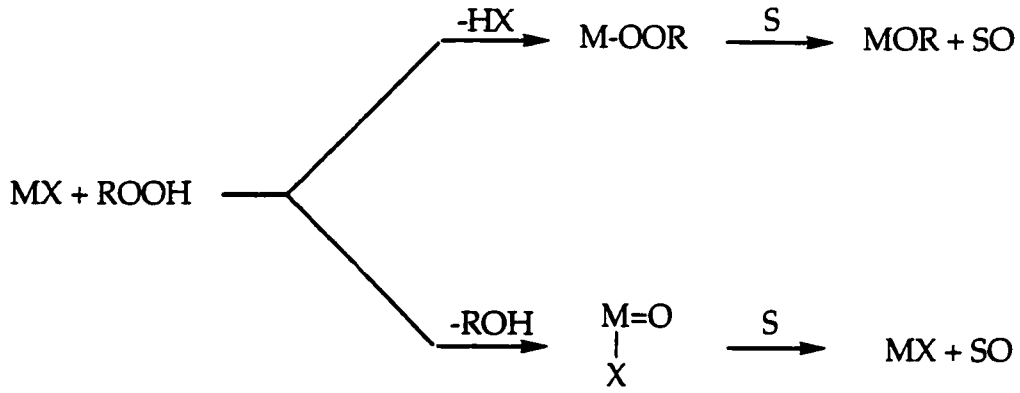

Since (IV) is an intermediate oxidation state for Cr, it is not clear *a priori* by which mechanism it will oxidize alcohols. In order to study oxidations by oxide-supported inorganic Cr(IV), it was necessary to devise a preparative method. The incipient wetness impregnation method is unfortunately not feasible, since the lifetime of the aquachromium(IV) ion is very short ($t_{1/2}$ ca. 30 s).[16] We therefore decided to approach the problem by preparing and characterizing silica-supported Cr(IV) coordination complexes.

Our objective was to prepare $(\equiv SiO)_2Cr=O$. Our first attempt was to study the reaction of $(\equiv SiO)_2CrNp_2$ with O_2. We hoped to obtain $(\equiv SiO)_2Cr(ONp)_2$, by analogy with the reaction reported for the comparable Zr complex.[17] The thermolysis of such a species could lead to a silica-supported oxo Cr complex via elimination of dineopentylether. However, the reaction of $(\equiv SiO)_2CrNp_2$ with O_2 turned out to be complicated (see Chapter 3). Next, we focused our efforts on the reaction of $Cr(NEt_2)_4$ with silica followed by exchange of the amido ligands with alcohols.

As stated in Chapter 3, the density of accessible surface hydroxyl groups on silica decreases with increasing dehydroxylation temperature. Also, we have

shown that the stoichiometry of the reaction of CrR_4 with the silica surface depends on the density of these hydroxyl groups. Therefore it was necessary to first establish how $Cr(NEt_2)_4$ reacts with silica.

6.2 Reaction of $Cr(NEt_2)_4$ with Silica-200

When $Cr(NEt_2)_4$ is sublimed onto a pellet of silica-200, a reaction proceeds with a color change of the solid from colorless to green. $HNEt_2$ is the exclusive gas-phase product detected by IR spectroscopy, GC, and GC-MS.

6.2.1 Infrared Spectroscopic Characterization

The reaction of $Cr(NEt_2)_4$ with silica-200 at room temperature was followed by infrared spectroscopy. Before reaction, the spectrum of a self-supporting disk of silica-200 contains a sharp band at 3747 cm^{-1}, attributed to non-hydrogen-bonded surface hydroxyl groups, with a broad low frequency shoulder assigned to hydroxyl groups that are perturbed by hydrogen bonding. After 3 h of reaction, the IR spectrum of the modified silica showed complete disappearance of the IR vibration at 3747 cm^{-1} due to the isolated surface hydroxyl groups, and appearance of new bands characteristic of the alkyl groups, Figure 6.1a. A band characteristic of the diethylamide ligands[18] is clearly visible at 991 cm^{-1}, Figure 6.1b, assigned to the stretching mode $\nu_s(N\text{-}C_2)$, Table 6.1.

6.2.2 Electronic Spectroscopy

The diffuse absorbance UV-visible spectrum of the modified silica contains bands which are dramatically red-shifted compared to those of the molecular precursor. The spectrum of $Cr(NEt_2)_4$ supported on silica has a peak at 547 nm with a minimum at 420 nm, Figure 6.2, whereas in pentane $Cr(NEt_2)_4$ has a peak at

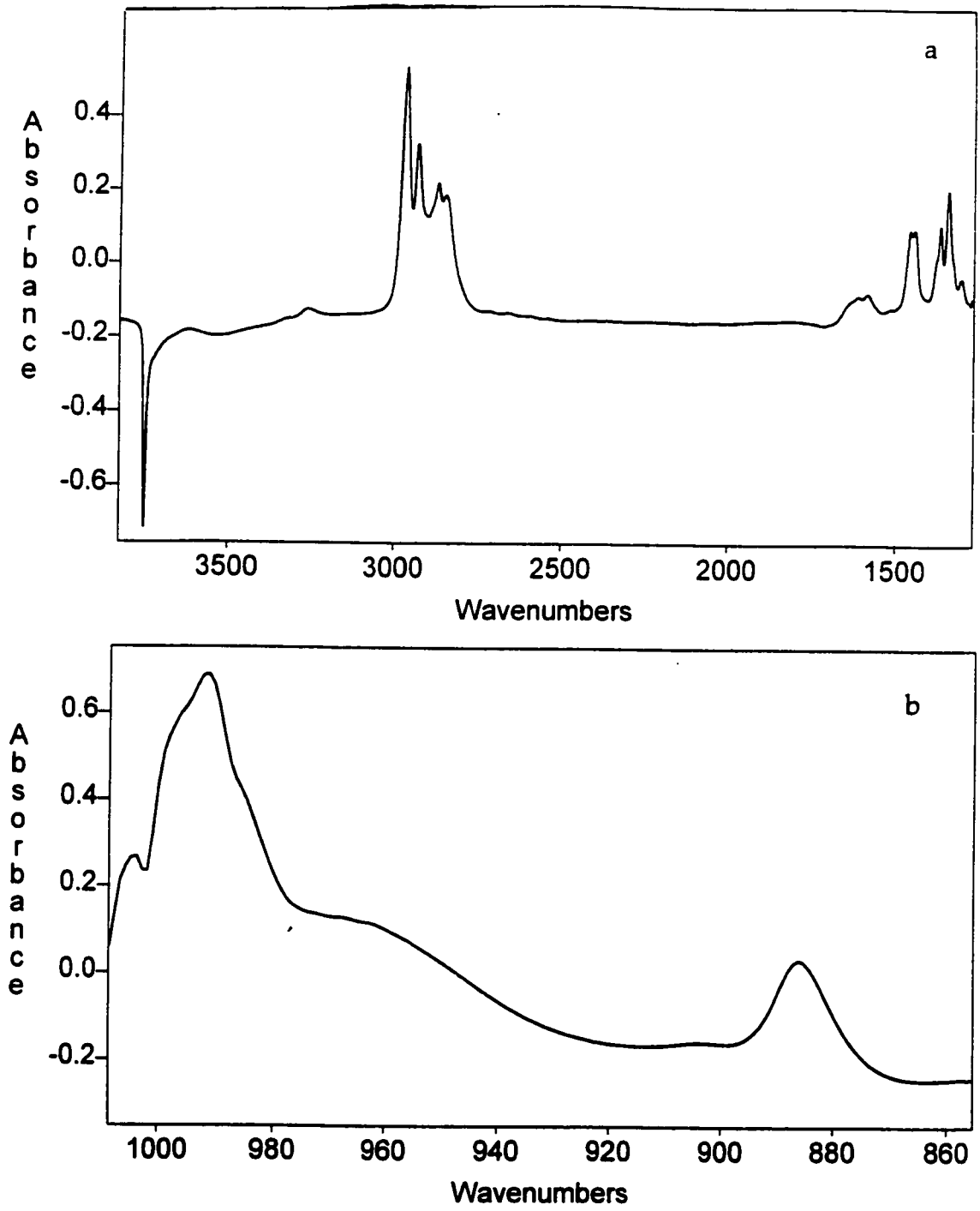

Figure 6.1 In situ IR difference spectra of a self-supporting disk of silica-200 treated with $Cr(NEt_2)_4$. The reference spectrum of silica-200 has been subtracted such that negative peaks correspond to the vibrations which are no longer present on the silica surface after reaction. (a) Region 4000 - 1300 cm^{-1}, and (b) region 1000 - 800 cm^{-1}.

Table 6.1 Infrared frequencies (cm^{-1}) on silica modified by $Cr(NEt_2)_4$

$(\equiv SiO)_nCr(NEt_2)_{4-n}$	Assignement[18]
2968	$\nu_{as}(CH_3)$
2932	$\nu_{as}(CH_2)$
2872	$\nu_s(CH_3)$
2850	$\nu_s(CH_2)$
1460	$\delta_{as}(CH_3)$
1447	$\delta_{as}(CH_2)$
1370	$\delta_s(CH_3)$
1346	$\delta_s(CH_2)$
991	$\nu_s(N\text{-}C_2)$
885	$\delta(Cr\text{-}N\text{-}C)$

737 nm and a well-defined minimum at 516 nm.[19] Nevertheless the color of the supported complex is green, like $Cr(NEt_2)_4$.

6.2.3 Stoichiometry of the Reaction of $Cr(NEt_2)_4$ with Silica

When $Cr(NEt_2)_4$ is sublimed onto silica and allowed to react at room temperature with the surface hydroxyl groups, a chemical reaction takes place in which adsorbed chromium species are formed, with concurrent liberation of protonated ligands as $HNEt_2$ as the only gaseous product, eq 6.2.

$$n \equiv SiOH + Cr(NEt_2)_4 \rightarrow (\equiv SiO)_nCr(NEt_2)_{4-n} + n\ HNEt_2 \qquad (6.2)$$

After desorption of unreacted $Cr(NEt_2)_4$, the amount of chemisorbed chromium was determined by extraction. The value of n was evaluated by comparing the

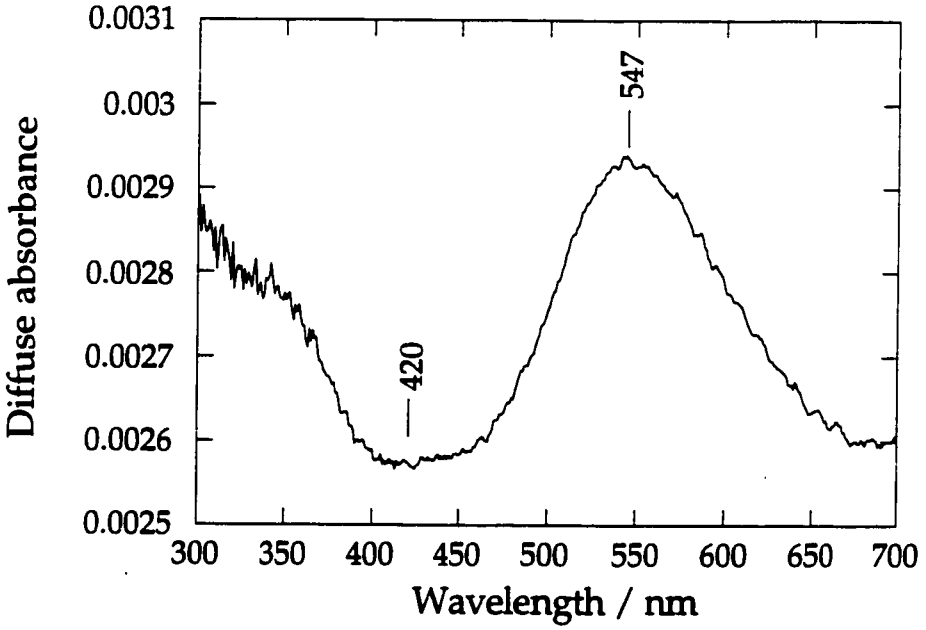

Figure 6.2 UV-visible spectrum of silica-200 modified with $Cr(NEt_2)_4$

amount of extracted chromium at the end of the experiment to the amount of diethylamine liberated upon grafting. $HNEt_2$ was quantified by IR spectroscopy.

Based on the average of 6 experiments, summarized in Table 6.2, on silica-200 the amount of chemisorbed chromium after complete reaction of the surface hydroxyl groups is 1.95 ± 0.02 wt.%, which corresponds to 0.44 Cr/≡SiOH. Also 1.97 ± 0.01 mol $HNEt_2$ are liberated per mol of grafted Cr. These results suggest the following stoichiometric reaction, eq 6.3:

$$2\,{\equiv}SiOH + Cr(NEt_2)_4 \rightarrow ({\equiv}SiO)_2Cr(NEt_2)_2 + 2\,HNEt_2 \qquad (6.3)$$

The number of amido groups coordinated to each chemisorbed chromium was confirmed by ligand exchange with an excess of t-butanol, described in the next section.

6.2.4 Reactions of $(\equiv SiO)_2Cr(NEt_2)_2$ with Alcohols

The reactivity of $(\equiv SiO)_2Cr(NEt_2)_2$ with an excess of either tert-butyl alcohol or trimethylsilanol was studied.

6.2.4.1 With *tert*-butanol

When tert-butyl alcohol was introduced into the reactor containing $(\equiv SiO)_2Cr(NEt_2)_2$, a color change from green to blue occurred. After 3h, nearly complete displacement of the amido ligands as $HNEt_2$ was observed, eq 6.4.

$$({\equiv}SiO)_2Cr(NEt_2)_2 + 2\,t\text{-}BuOH \rightarrow ({\equiv}SiO)_2Cr(O^tBu)_2 + 2\,HNEt_2 \qquad (6.4)$$

The amount of $HNEt_2$ liberated upon the exchange reaction with t-butanol was quantified by gas-phase IR spectroscopy to be 1.91 ± 0.01 per Cr. The results are shown in Table 6.2.

Table 6.2 Quantitative product analysis for the reaction of $Cr(NEt_2)_4$ with SiO_2-200

products of grafting					products of ligand exchange with ^tBuOH	
wt.% Cr	mmol Cr[a]	Cr/OH[b]	mmol $HNEt_2$[a]	$HNEt_2$/Cr	mmol $HNEt_2$[a]	$HNEt_2$/Cr
1.97	0.379	0.441	0.743	1.96		
1.95	0.375	0.436	0.743	1.98	0.713	1.90
1.94	0.373	0.434	0.734	1.97	0.712	1.91
1.93	0.371	0.431	0.735	1.98		
1.95	0.375	0.436	0.735	1.96		
1.96	0.377	0.438	0.743	1.97	0.724	1.92
average 1.95 ± 0.02		average 0.437 ± 0.004		average 1.97 ± 0.01		average 1.91 ± 0.01

a All quantities are reported normalized per g of silica

b Ratio of the amount of chemisorbed Cr to the initial amount of surface hydroxyl groups, 0.86 mmol OH/g silica-200.

In the IR spectrum of $(\equiv SiO)_2Cr(NEt_2)_2$ treated with $(CD_3)_3COD$, the ν(C-H) vibrations of the diethylamido ligands decreased in intensity by 95%, Figure 6.3a, while new bands were observed at 2235, 2135, 2076 and 2054 cm^{-1}, assigned to the ν(C-D) vibrations of perdeuterio-*tert*-butyl groups which are strongly chemisorbed, Figure 6.3b. The supported complex $(\equiv SiO)_2Cr(O^tBu\text{-}d_9)_2$ was then exposed to $(CH_3)_3COH$ vapor. Deuterated t-butanol was observed in the gas phase, and the IR spectrum of the pellet showed that 79% of the perdeuterio-hydrocarbon modes disappeared from the surface due to the displacement of the perdeuterio-*tert*-butoxo ligands, Figure 6.3c.

The ^2H MAS NMR spectrum of the product of reaction of $Cr(NEt_2)_4$ with silica-200 after exchange with $^tBu\text{-}d_9\text{-}OD$ is shown in Figure 6.4a. The central resonance was identified as the only real signal; all other bands are spinning side bands whose position shifted when the spin rate was varied. The central peak is therefore assigned to the supported complex, $(\equiv SiO)_2Cr(O^tBu\text{-}d_9)_2$. The stationary ^2H NMR spectrum (powder spectrum) of $(\equiv SiO)_2Cr(O^tBu\text{-}d_9)_2$ is a broad Pake doublet with inner singularities separated by 14 kHz and a splitting at the shoulders of 28 kHz, Figure 6.4b. This shape is characteristic of the C_3' and C_3 motions of a ^{t}butyl fragment and a methyl group, respectively.

By definition, the rotation of the methyl groups about a threefold axis is denoted C_3 motion and rotation of the entire $(CH_3)_3$-C group about its threefold axis is denoted C_3' motion. In the ^2H NMR spectrum of a ^{t}butyl fragment, three kinds of rotational motion may be distinguished. If there is no mobility whatsoever, the splitting between the inner singularities is ca. 128 kHz, and the splitting at the shoulders is 256 kHz. If only methyl rotation occurs, the inner and the shoulder splittings are diminished to 42 and 84 kHz, respectively. When the ^{t}butyl and methyl fragments rotate concertedly, the observed inner and shoulder splittings are 14 and 28 kHz, respectively.[20] The last case is consistent with our

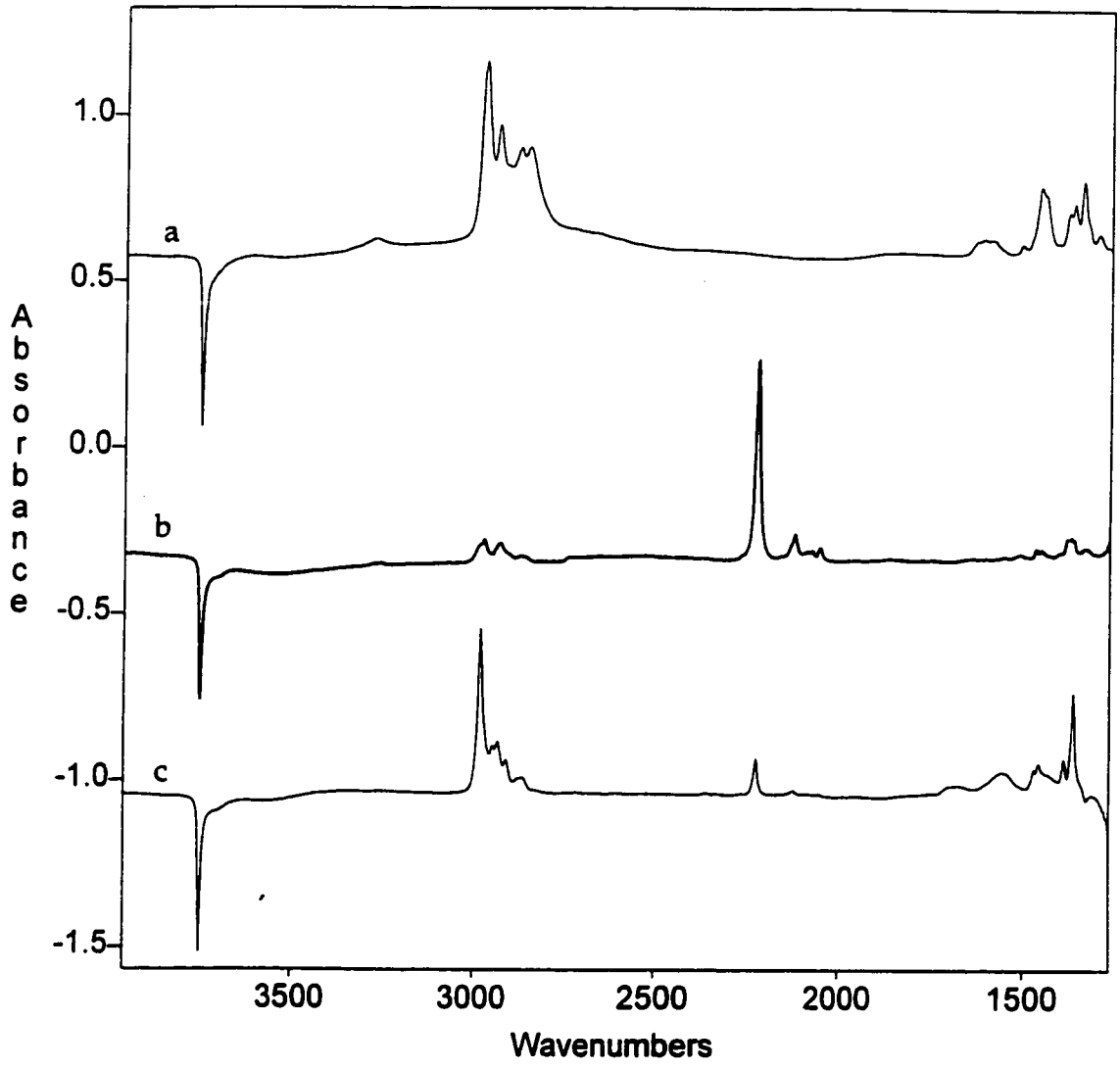

Figure 6.3 In situ IR difference spectra of a self-supporting disk of (a) $(\equiv SiO)_2Cr(NEt_2)_2$, followed by (b) addition of $(CD_3)_3COD$ to give $(\equiv SiO)_2Cr(O^tBu\text{-}d_9)_2$, followed by (c) addition of $(CH_3)_3COH$ to give $(\equiv SiO)_2Cr(O^tBu)_2$. The reference spectrum of silica-200 has been subtracted.

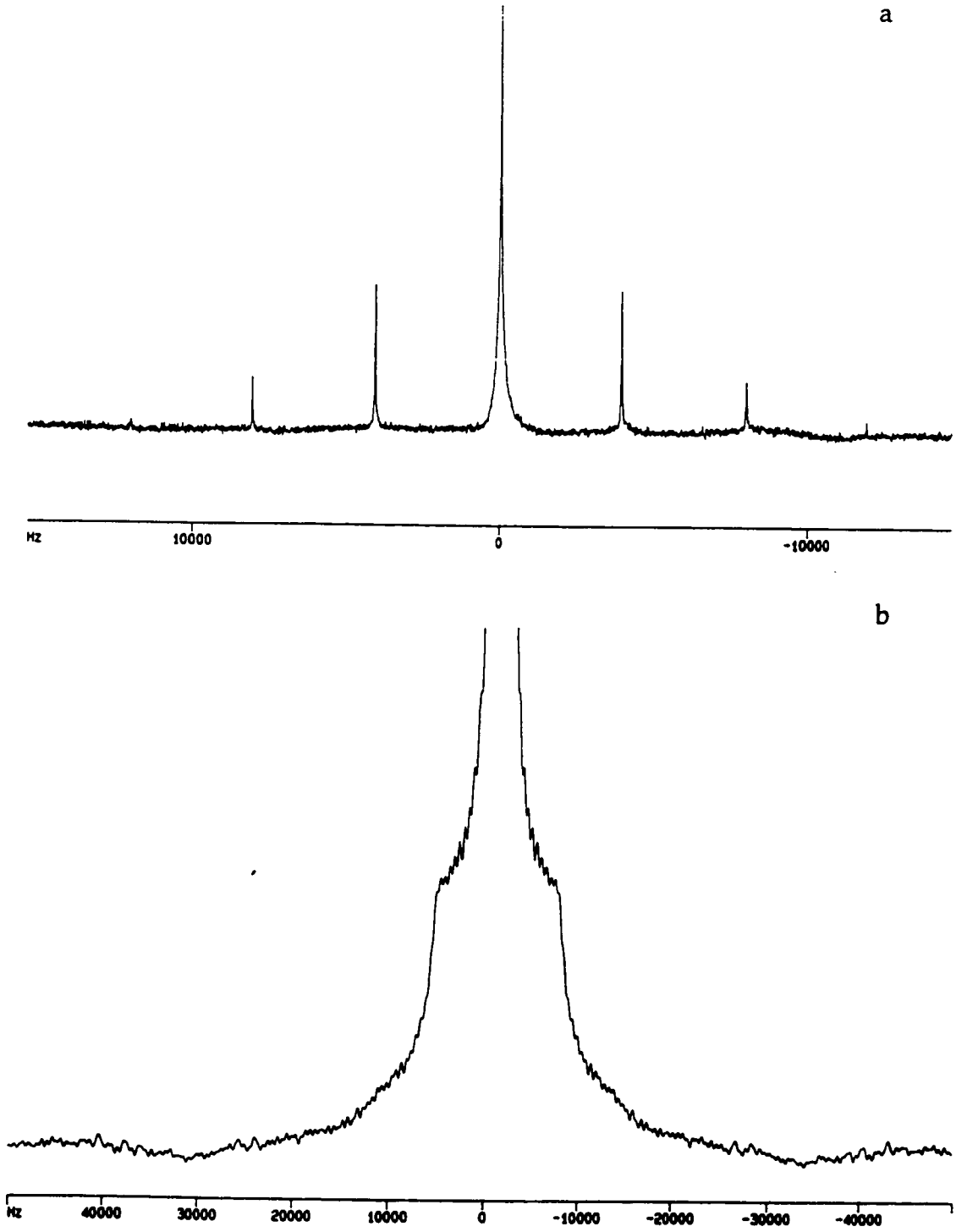

Figure 6.4 (a) ^{2}H MAS NMR spectrum at a spin rate of 4 kHz, and (b) stationary ^{2}H NMR spectrum of $(SiO)_2Cr(O^tBu)_2$

results. The ^2H NMR spectra confirm that simple ligand exchange has occurred between the supported chromium amido complex and ^{t}butanol. If the deuterated t-butoxocomplex were no longer chemically bound to the silica surface, a single sharp peak would have been observed in the static ^2H NMR spectrum of the solid sample. We conclude that alcohols are not capable of leaching chromium from the silica support.

6.2.4.2 With Trimethylsilanol

$(CH_3)_3SiOH$ vapor was prepared just before use in a Schlenk tube containing powdered $(CH_3)_3SiONa$. 1.3 Torr HCl was added and the Schlenk reactor was shaken. Volatile $(CH_3)_3SiOH$ was transferred directly into the IR cell containing $(\equiv SiO)_2Cr(NEt_2)_2$. When $(\equiv SiO)_2Cr(NEt_2)_2$ was exposed to excess $(CH_3)_3SiOH$, the color of the pellet changed from green to blue. The reaction was nearly complete after 3 hours, and diethylamine was observed in the gas phase. The IR spectrum of the surface species shows new bands in the ν(C-H) region at 2954, 2904 and 2869 cm^{-1}, assigned to vibrations of the trimethylsilyl groups. The CH_3 deformation modes appear at 1454 and 1411 cm^{-1}. The exchange reaction is shown in eq 6.5.

$$(\equiv SiO)_2Cr(NEt_2)_2 + 2\,(CH_3)_3SiOH \rightarrow (\equiv SiO)_2Cr(OSi(CH_3)_3)_2 + 2\,HNEt_2 \qquad (6.5)$$

6.3 Direct Reaction of $Cr(O^tBu)_4$ with Silica

Admission of $Cr(O^tBu)_4$ vapor at room temperature to the *in situ* IR cell containing a self supporting disk of silica led to an immediate color change of the colorless silica pellet to blue.

6.3.1. Infrared Spectroscopic Characterization

When $Cr(O^tBu)_4$ vapor reacts with silica at room temperature in a closed reactor with an initial pressure of 10^{-4} Torr, an irreversible chemisorption takes place over a period of 2 h. The volatile organic product liberated into the gas phase was identified as t-butanol by IR, GC and GC-MS. The IR spectrum of the modified silica confirms that the intense ν(SiO-H) mode of silica at 3747 cm^{-1} disappears, indicating complete reaction of the surface hydroxyl groups. At the same time, new bands were observed in the C-H stretching region at 2978, 2933, 2904 and 2874 cm^{-1}, assigned to vibrations of *tert*-butyl groups, Figure 6.5. The methyl deformation modes appear as in-phase and out-of-phase doublets at 1469 and 1458 cm^{-1} (δ_{as}) and 1374 and 1367 cm^{-1} (δ_s). The low frequency vibrations include a band at 947 cm^{-1} corresponding to ν(C-O).[21] The results are listed in Table 6.3.

Table 6.3 Infrared frequencies (cm^{-1}) of silica-200 modified by $Cr(O^tBu)_4$

$(\equiv SiO)_nCr(O^tBu_2)_{4-n}$	Assignment[21]
2978	$\nu_{as}(CH_3)$
2933	$\nu_{as}(CH_2)$
2904	$\nu_s(CH_3)$
2874	$\nu_s(CH_2)$
1469,1458	$\delta_{as}(CH_3)$
1373,1367	$\delta_s(CH_3)$
927	$\nu_s(C\text{-}O)$

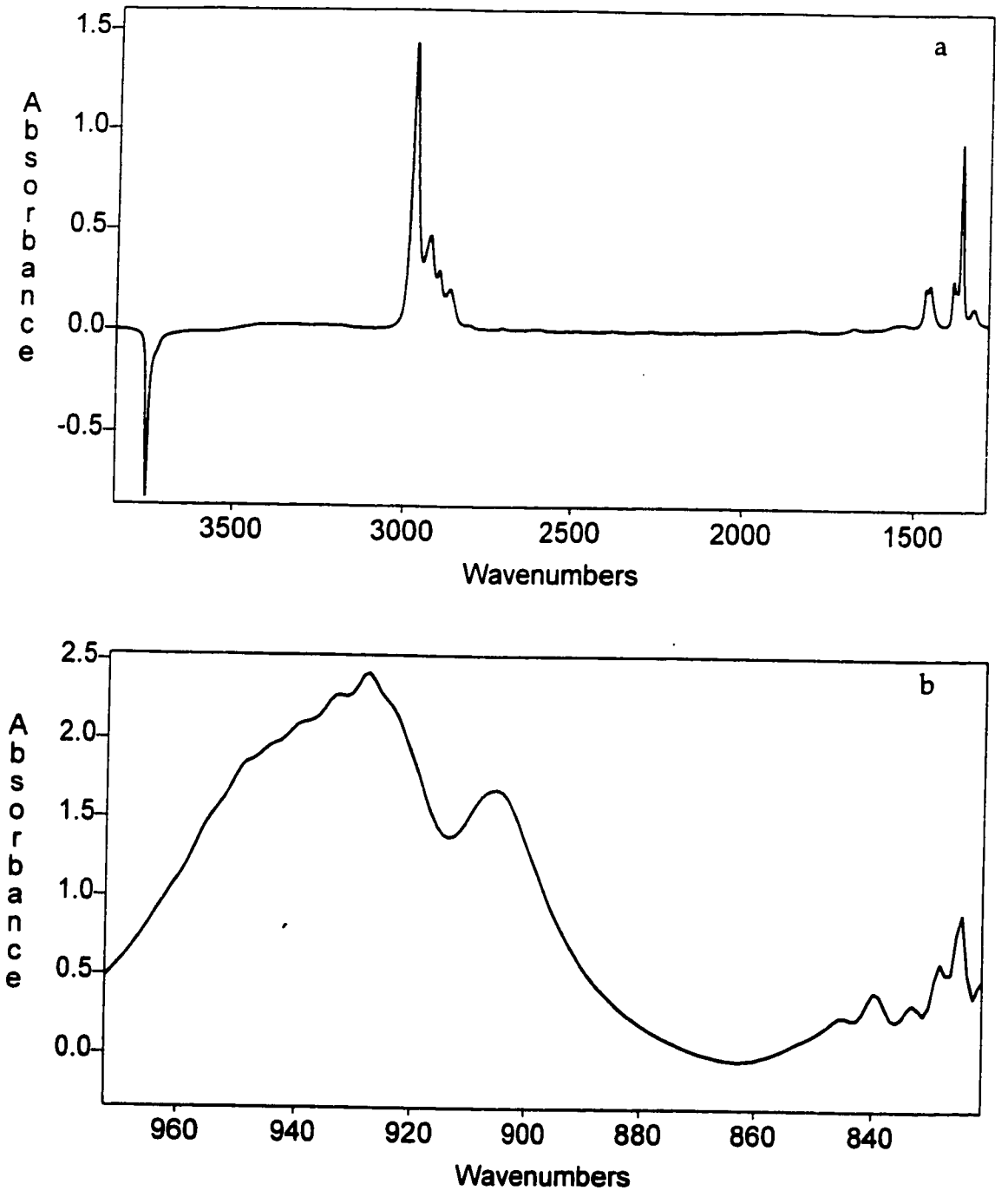

Figure 6.5 In situ IR difference spectra of a self-supporting disk of silica-200 treated with $Cr(O^tBu)_4$. The reference spectrum of silica-200 has been subtracted such that negative peaks correspond to the vibrations which are no longer present on the silica surface after reaction. (a) Region 4000 - 1300 cm^{-1}, and (b) region 1000 - 800 cm^{-1}.

6.3.2 Stoichiometry of the Reaction of $Cr(O^tBu)_4$ with Silica

When $Cr(O^tBu)_4$ vapor at room temperature contacts the surface hydroxyl groups of silica, a chemical reaction takes place in which adsorbed chromium species are formed with concurrent liberation of ^{t}BuOH as only volatile product, eq 6.6.

$$n \equiv SiOH + Cr(O^tBu)_4 \rightarrow (\equiv SiO)_nCr(O^tBu)_{4-n} + n\ ^t BuOH \qquad (6.6)$$

After desorption of unreacted $Cr(O^tBu)_4$, the amount of chemisorbed chromium was determined by extraction. The value of n was evaluated by determining the amount of ^{t}BuOH liberated by quantitative gas phase IR spectroscopy. The value of n was then confirmed by quantifying the ^{t}BuOH liberated upon protonolysis with HCl of the chemisorbed chromium complex. In addition to quantitative release of ^{t}BuOH, the addition of HCl leads to a dramatic color change from blue to yellow-green. Based on average of 7 experiments listed in Table 6.4, 1.97 ± 0.02 equivalents of ^{t}BuOH are evolved per chemisorbed Cr during grafting, which means n=2, consistent with the stoichiometry shown in eq 6.7.

$$2 \equiv SiOH + Cr(O^tBu)_4 \rightarrow (\equiv SiO)_2Cr(O^tBu)_2 + 2\ ^t BuOH \qquad (6.7)$$

The product $(\equiv SiO)_2Cr(O^tBu)_2$ retains an average of two alkoxo ligands per Cr, confirmed by protonolysis with 10 Torr HCl(g) to give 1.96 ± 0.01 ^{t}BuOH/Cr, eq 6.8.

$$(\equiv SiO)_2Cr(O^tBu)_2 + xs\ HCl \rightarrow \text{“}(\equiv SiO)_2CrCl_2\text{”} + 2\ ^t BuOH \qquad (6.8)$$

The results are summarized in Table 6.4. On silica-200, the average formula is therefore $(\equiv SiO)_2Cr(O^tBu)_2$.

Table 6.4 Quantitative product analysis for the reaction of $Cr(O^tBu)_4$ with SiO_2-200

products of grafting					products of protonolysis	
wt.% Cr	mmol Cr[a]	Cr/OH[b]	mmol ^{t}BuOH[a]	^{t}BuOH/Cr	mmol ^{t}BuOH[a]	^{t}BuOH/Cr
1.96	0.377	0.438	0.743	1.97	0.739	1.96
1.97	0.379	0.441	0.743	1.96	0.747	1.97
1.95	0.375	0.436	0.746	1.99		
1.92	0.369	0.429	0.731	1.98		
1.94	0.373	0.434	0.735	1.97	0.727	1.95
1.97	0.379	0.441	0.743	1.96		
1.96	0.377	0.438	0.743	1.97		
average 1.95 ± 0.02		average 0.437 ± 0.004		average 1.97 ± 0.02		average 1.96 ± 0.01

a All quantities are reported normalized per g of silica

b Ratio of the amount of chemisorbed Cr to the initial amount of surface hydroxyl groups, 0.86 mmol OH/g silica-200.

6.3.3. Electronic Spectroscopy

The diffuse absorbance UV-visible spectrum of $Cr(O^tBu)_4$ supported on silica consists of a peak at 400 nm with a minimum at 586 nm, Figure 6.6, whereas in pentane $Cr(O^tBu)_4$ has a peak at 400 nm.[19] The UV-visible spectra of the molecular and the grafted complexes are therefore very similar. The blue color of the grafted complex is due to a band centred above 800 nm, which is not reported in the literature for $Cr(O^tBu)_4$ (although the molecular complex is also blue).

6.4 Thermolysis of Supported Alkoxo/Siloxo Chromium(IV) Complexes

Supported alkoxo and siloxo complexes were heated in an effort to induce the formation of a chromyl (Cr=O) species via ligand elimination. The desired reaction is that shown in eq 6.9.

$$(\equiv SiO)_2Cr(OR)_2 \xrightarrow{\Delta} (\equiv SiO)_2Cr{=}O + ROR \qquad (6.9)$$

6.4.1 Thermolysis of $(\equiv SiO)_2Cr(O^tBu)_2$

The supported species $(\equiv SiO)_2Cr(O^tBu)_2$ was heated at 80°C for 12 hours. The IR spectrum showed that the ν(C-H) intensity decreased by 77%, and isobutene and t-BuOH appeared in the gas phase. These products are consistent with eq 6.10.

$$(\equiv SiO)_2Cr(O^tBu)_2 \xrightarrow{\Delta} (\equiv SiO)_2Cr{=}O + {}^tBuOH + (CH_3)_2C{=}CH_2 \qquad (6.10)$$

After evacuation, no new bands were apparent in the IR spectrum of the silica disk in the region above 1200 cm^{-1}. The expected ν(Cr=O) mode of $(\equiv SiO)_2Cr{=}O$ will likely be masked by the intense absorbance of the silica below 1200 cm^{-1}. Spectral subtraction revealed no weak band in the region 2100 - 2000 cm^{-1} which could be assigned to the overtone 2ν(Cr=O).

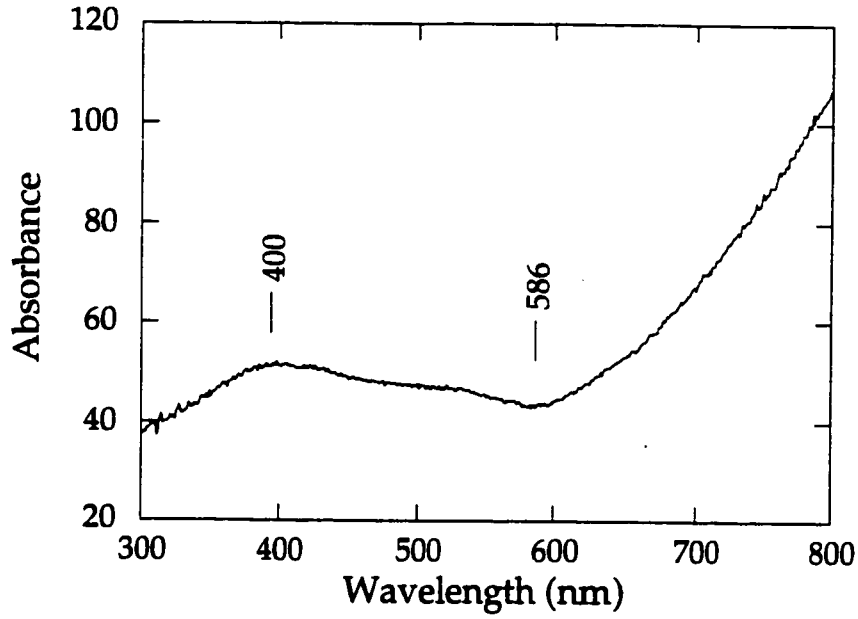

Figure 6.6 UV-visible spectrum of silica-200 modified with $Cr(O^tBu)_4$

6.4.2 Thermolysis of $(\equiv SiO)_2Cr(OSi(CH_3)_3)_2$

$(\equiv SiO)_2Cr(OSi(CH_3)_3)_2$ was heated at 75°C for 6 hours. In the IR spectrum of the pellet, the intensity in the ν(C-H) region decreased by 43%. Hexamethyldisiloxane was liberated into the gas phase, and detected by GC and GC-MS. This product is consistent with eq 6.11.

$$(\equiv SiO)_2Cr(OSi(CH_3)_3)_2 \xrightarrow{\Delta} (\equiv SiO)_2Cr{=}O + (CH_3)_3SiOSi(CH_3)_3 \qquad (6.11)$$

However, no characteristic band for "Cr=O" was observed in the IR spectrum.

6.4.3 Reactivity towards Various Alcohols

In order to test for the presence of Cr=O (which proved difficult to identify by IR spectoscopy), the thermolysis product of eq 6.10 was allowed to react with readily oxidizable alcohols.

6.4.3.1 Towards Allylic Alcohol

Upon addition of allylic alcohol vapor to thermolyzed $(\equiv SiO)_2Cr(O^tBu)_2$, t-butanol was released into the gas phase. However, the color of the pellet remained blue. The intensities of the bands in the aliphatic ν(C-H) region of the IR spectrum decreased by a further 80%, while new bands appeared in the region 3200-2800 cm^{-1}. The latter are characteristic of allylic ν(C-H) modes. The reaction of allylic alcohol appears to give simple ligand exchange without oxidation to acrolein, since no carbonyl vibrations were observed.

6.4.3.2 Towards Benzyl Alcohol

The reaction of thermolyzed $(\equiv SiO)_2Cr(O^tBu)_2$ with benzyl alcohol vapor, under similar conditions, caused the near total disappearance of t-butoxo

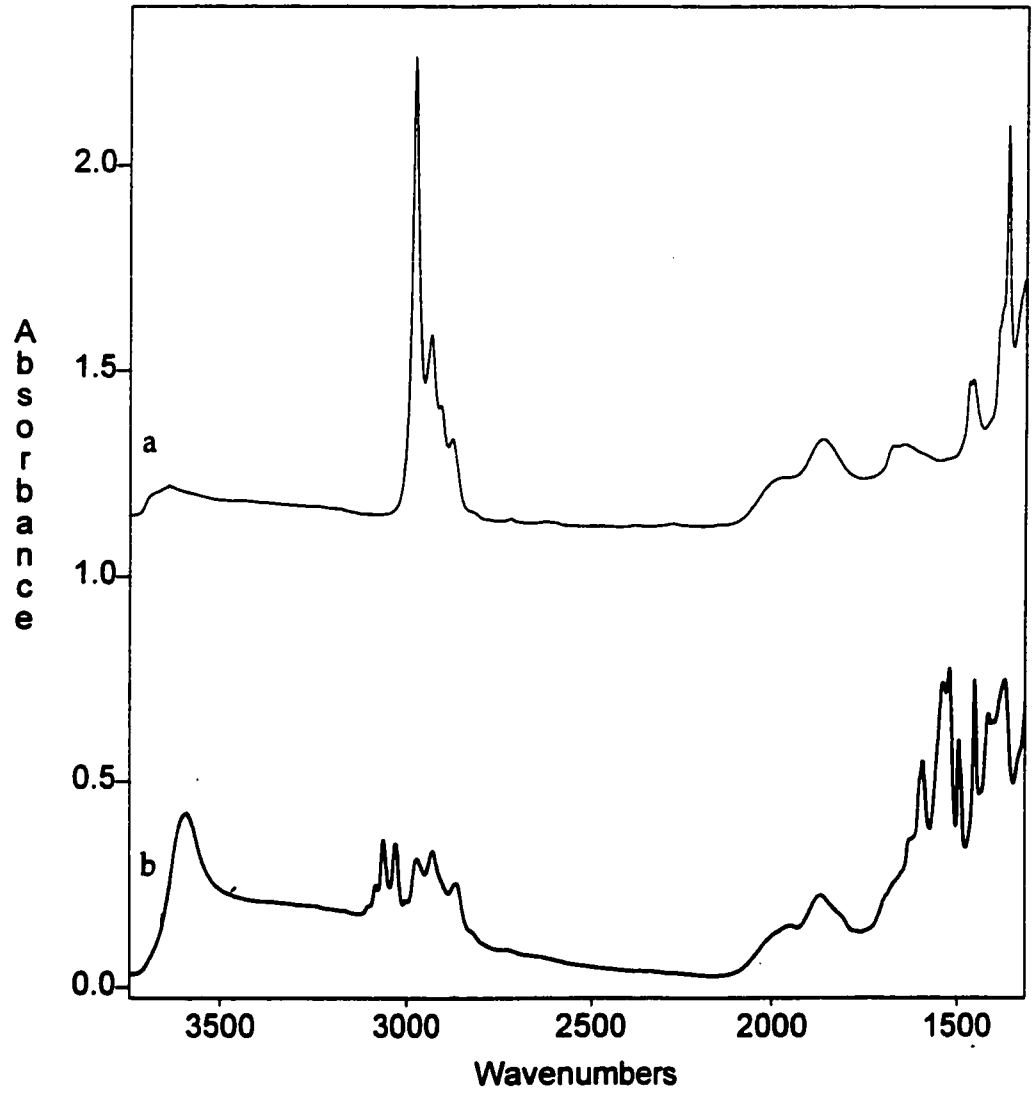

Figure 6.7 In situ IR difference spectra of a self-supporting disk of (a) thermolyzed $(\equiv SiO)_2Cr(O^tBu)_2$, followed by (b) the reaction with benzyl alcohol.

ligand vibrations, accompanied by the appearance of t-butanol in the gas phase. In this case, however, the appearance of new bands characteristic of benzoic acid were also observed, Figure 6.7.

6.5 Conclusions

The room temperature reactions of the molecular complexes $Cr(NEt_2)_4$ and $Cr(O^tBu)_4$ with the partially dehydroxylated surface of silica-200 give chemisorbed $(\equiv SiO)_2Cr(NEt_2)_2$ and $(\equiv SiO)_2Cr(O^tBu)_2$, respectively. Our characterization of these materials by IR and ^2H MAS NMR demonstrates how these two techniques provide complementary information about the coordination sphere and mobility of surface species.

Thermolysis of $(\equiv SiO)_2Cr(OR)_2$, where R is ^{t}Bu or $SiMe_3$, lead to elimination of (^{t}BuOH + isobutene) and $Me_3SiOSiMe_3$, respectively.

The reaction of the thermolyzed species from $(\equiv SiO)_2Cr(O^tBu)_2$, tentatively assigned as $(\equiv SiO)_2Cr{=}O$, with benzyl alcohol leads to the formation of benzoic acid as detected by IR spectroscopy. However the $\nu(Cr{=}O)$ vibration was not observed. Clearly more experiments will be needed to demonstrate the nature of the oxidation active site.

6.6 References

1) Sheldon, R. A.; Kochi, J. K. *Metal-Catalyzed Oxidations of Organic Compounds*; Academic Press: New York, 1981.

2) Wiberg, K. B. In *Oxidation in Organic Chemistry, Part A*; Academic Press: New York, 1965; pp. 69.

3) Cainelli, G.; Cardillo, G. *Chromium Oxidations in Organic Chemistry*; Springer- Verlag: Berlin, 1984.

4) Cainelli, G.; Cardillo, G.; Orena, M.; Sandri, S. *J. Am. Chem. Soc.* **1976**, *25*, 6737.

5) Kanemoto, S.; Saimoto, H.; Oshima, K.; Nozaki, H. *Tetrahedron Lett.* **1984**, *25*, 3317.

6) Muzart, J. *Chem. Rev.* **1992**, *92*, 113-140.

7) Corey, E.; Barrette, E. P.; Magriotis, A. P. *Tetrahedron Lett.* **1985**, *26*, 5855.

8) Kanemoto, S.; Oshima, K.; Matsubara, S.; Takai, K.; Nozaki, H. *Tetrahedron Lett.* **1983**, *24*, 2185.

9) Weckhuysen, B. M.; Wachs, I. E.; Schoonheydt, R. A. *Chem. Rev.* **1996**, *96*, 3327-3349.

10) Sheldon, R. A.; Dakka, J. *Catal. Today* **1994**, *19*, 215-246.

11) Choudary, B. M.; Durgaprasad, A.; Valli, V. L. K. *Tetrahedron Lett.* **1990**, *40*, 5785-5788.

12) Choudary, B. M.; Durgaprasad, A.; Bhuma, V.; Swapna, V. *J. Org. Chem.* **1992**, *57*, 5841-5844.

13) Chen, J. D.; Lempers, H. B. E.; Sheldon, R. A. *J. Chem. Soc., Farad. Trans.* **1996**, *92*, 1807-1813.

14) Chen, J. D.; Sheldon, R. A. *J. Catal.* **1995**, *153*, 1-8.

15) Chen, J. D.; Dakka, J.; Neeleman, E.; Sheldon, R. A. *J. Chem. Soc. Chem. Commun.* **1993**, 1379.

16) Scott, S. L.; Bakac, A.; Espenson, J. H. *J. Am. Chem. Soc.* **1991**, *113*, 7787-7788.

17) Quignard, F.; Lecuyer, C.; Bougault, C.; Lefebvre, F.; Choplin, A.; Olivier, D.; Basset, J.-M. *Inorg. Chem.* **1992**, *31*, 928.

18) Bradley, D. C.; Gitlitz, M. H. *J. Chem. Soc. (A)* **1969**, 980-984.

19) Basi, J. S.; Bradley, D. C.; Chisholm, M. H. *J. Chem. Soc. (A)* **1971**, 1433-1436.

20) Ripmeester, J. A.; Ratcliffe, C. I. *J. Chem. Phys.* **1985**, *82*, 1053-1054.

21) Barraclough, C. G.; Bradley, D. C.; Lewis, J.; Thomas, I. M. *J. Chem. Soc.* **1961**, 2601-2605.

Chapter 7

General Conclusions

By designing and then implementing experiments on the surface chemistry of complex organometallic fragments of chromium, we have attempted to relate the structures of surface species to their reactivity. Towards this goal, we have prepared silica-supported organochromium(IV) complexes whose relatively high uniformity makes them essentially homogeneous in nature, despite their superficial resemblance to heterogeneous catalysts.

By grafting homoleptic CrR_4 complexes via sublimation onto partially dehydroxylated silica, we synthesized mononuclear surface organometallic fragments. We showed that tris(alkyl) and bis(alkyl) complexes are predominant on silica-500 and silica-200, respectively. We also proved that the chemisorbed Cr species retain the oxidation state and nuclearity of their parent molecular precursors. The silica-supported complexes $\equiv SiOCrR_3$ and $(\equiv SiO)_2CrR_2$ show little reactivity except towards O_2.

We demonstrated by kinetic studies, isotope labeling experiments and mass balances that the silica-supported bis(alkyl)chromium(IV) complexes are transformed to alkylidenes by thermal α-H elimination in reactions which resemble known cases in homogeneous chemistry. This interesting thermal transformation represents an entry point to more reactive supported organochromium fragments. The alkylidene complexes undergo metathesis and are highly efficient low-pressure α-olefin polymerization catalysts.

The catalytic polymerization is pseudo-first-order with rate constants which are linearly dependent on the amount of catalyst present, regardless of the level of chromium loading on silica. The activation parameters $\Delta H^{\ddagger}_{obs}$= (8 ± 1) kcal/mol and $\Delta S^{\ddagger}_{obs}$= (-23 ± 2) cal K^{-1} mol^{-1} were measured for the propagation steps of ethylene polymerization, consisting of olefin binding followed by migratory

insertion. Evidence for an α-agostic interaction was found in the kinetic isotope effect for polymerization of D-labeled ethylene. The kinetics of copolymerization of ethylene and 1-hexene were undertaken in order to define the selectivity of the catalyst, which favours ethylene only slightly.

Despite its initially homogeneous nature, the number of active sites on the catalyst is only ca. 20 - 30% at low ethylene pressures. During and even after polymerization, the average oxidation state of the chromium remains (IV), and the catalyst retains its high activity for subsequent additions of ethylene. We formulated a initiation mechanism involving formation of a metallacyclic intermediate, followed by β-H elimination to give a variety of Cr(IV) alkyl hydrides. The initially well-defined catalyst thus generates its own heterogeneity, which is reflected in the breadth of the polyethylene molecular weight distribution.

Finally, we have prepared chemisorbed $(\equiv SiO)_2Cr(NEt_2)_2$ and $(\equiv SiO)_2Cr(O^tBu)_2$, by reaction of $Cr(NEt_2)_4$ and $Cr(O^tBu)_4$, respectively, with the partially dehydroxylated surface of silica. These complexes were characterized by IR and ^2H MAS NMR, which give complementary information about the coordination sphere and mobility of surface species. Treatment of $(\equiv SiO)_2Cr(NEt_2)_2$ and $(\equiv SiO)_2Cr(O^tBu)_2$ with trimethylsilanol and t-butyl alcohol leads to ligand-exchange reactions. Mild thermolysis of silica-supported bis(alkoxo)chromium(IV) may lead to the supported chromyl (Cr=O) fragment, which is a suggested intermediate in oxidation catalysis.

List of Publications

1. Reactions of Tetraalkylchromium(IV) with Silica: Mechanism of Grafting and Characterization of Surface Organometallic Complexes
   Amor Nait Ajjou, J.; Scott, S. L. *Organometallics* **1997**, *16*, 86-92

2. Synthesis and Characterization of Silica-stabilized Chromium(IV) Alkylidene Complexes
   Amor Nait Ajjou, J.; Scott, S. L. *J. Am. Chem. Soc.* **1998**, *120*, 415-416

3. Kinetics and Mechanisms of Thermally-induced Alkane Eliminations from Silica-supported Bis(alkyl)chromium(IV) and -vanadium(IV) Complexes.
   Amor Nait Ajjou, J.; Rice, G.; Scott, S. L. *J. Am. Chem. Soc.* **1998**, *120*, 13436-13443

4. Kinetics of Olefin Polymerization by a Silica-supported Cr(IV) Alkylidene
   Amor Nait Ajjou, J.; Scott, S. L. Manuscript in preparation.

5. Mechanism of Olefin Polymerization over a Heterogeneous Cr/SiO_2 Catalyst.
   Amor Nait Ajjou, J.; Scott, S. L. Manuscript in preparation.

Claims to Original Research

This thesis contributes to the basic understanding of heterogeneous ethylene polymerization catalysts by reporting the composition and reactivity of silica-supported chromium(IV) complexes. By controlling the hydroxyl density of the silica surface and working under rigorously anaerobic conditions, we have been able to isolate tris(alkyl)chromium(IV) fragments and bis(alkyl)chromium(IV) fragments on the surface. The latter undergo clean α-H elimination to give unusual chromium(IV) alkylidene fragments, which are without precedent in the molecular chemistry of chromium.

Through kinetics studies, isotope labeling experiments and mass balances, we have demonstrated that it is possible to prepare well-defined silica-supported organometallic fragments which can serve as models for the active sites of heterogeneous catalysts. We have shown that Cr(IV) is a highly active oxidation state in olefin polymerization. The reaction can be initiated on alkylidene sites, likely via formation of metallacyclic intermediates.

The polymerization mechanism was investigated by kinetic analysis and product studies. We found evidence for a migratory insertion propagation mechanism for Cr, assisted by α-agostic interactions. The transformation of our well-defined catalyst precursor into a heterogeneous working catalyst suggests that some solid catalysts, in particular the Phillips catalyst, spontaneously generate the active site inhomogeneity during the reaction. The result is a broad molecular weight distributions for polyolefins.